

REPORT DOCUMENTATION PAGE

Form Approved
OMB No. 0704-0188

Public reporting burden for this collection of information is estimated to average 1 hour per response, including the time for reviewing instructions, searching existing data sources, gathering and maintaining the data needed, and completing and reviewing the collection of information. Send comments regarding this burden estimate or any other aspect of this collection of information, including suggestions for reducing this burden, to Washington Headquarters Services, Directorate for Information Operations and Reports, 1215 Jefferson Davis Highway, Suite 1204, Arlington, VA 22202-4302, and to the Office of Management and Budget, Paperwork Reduction Project (0704-0188), Washington, DC 20503

1. AGENCY USE ONLY (Leave blank)		2. REPORT DATE 10/16/97	3. REPORT TYPE AND DATES COVERED Technical Report, May 96 - Sept. 97	
4. TITLE AND SUBTITLE Electrochemical Atomic Layer Epitaxy			5. FUNDING NUMBERS G-N-00014-19-J-1919 96 Pro - 2855 R&T 4133036	
6. AUTHOR(S) John L. Stickney				
7. PERFORMING ORGANIZATION NAME(S) AND ADDRESS(ES) Department of Chemistry University of Georgia Athens, GA 30602-2556			8. PERFORMING ORGANIZATION REPORT NUMBER Technical Report #29	
9. SPONSORING / MONITORING AGENCY NAME(S) AND ADDRESS(ES) Office of Naval Research Chemistry Division 800 North Quincy Street Arlington, VA 22217-5660			10. SPONSORING / MONITORING AGENCY REPORT NUMBER	
11. SUPPLEMENTARY NOTES				
12a. DISTRIBUTION / AVAILABILITY STATEMENT Approved for public release and sale: its distribution is unlimited			12b. DISTRIBUTION CODE	
13. ABSTRACT (Maximum 200 words) This is a review of work performed in the P.I.'s laboratory concerning development of the method of electrochemical atomic layer epitaxy. It includes an introduction covering compound semiconductor electrodeposition, with a table containing about 400 references. It contains a chapter on thin layer electrochemical studies, which are frequently used to get an initial idea of the conditions that should be used in an automated deposition cycle. There is a section on the development of the automated flow deposition system, and the growth of thin films of CdTe. There is a section on the atomic level characterization of these films using surface analytical methods. There is a section on the inverse of electrochemical ALE, digital etching. In those studies atomic layers are removed one at a time. There is also a conclusions section describing here we feel these techniques are going.				
14. SUBJECT TERMS atomic layer epitaxy, underpotential deposition, UPD, ALE, ECALE, CdTe, review			15. NUMBER OF PAGES 200	
			16. PRICE CODE	
17. SECURITY CLASSIFICATION OF REPORT Unclassified	18. SECURITY CLASSIFICATION OF THIS PAGE Unclassified	19. SECURITY CLASSIFICATION OF ABSTRACT Unclassified	20. LIMITATION OF ABSTRACT UL	

DTIC QUALITY INSPECTED 2

Office of Naval Research
Grant N00014-91-J-1919
R&T Code 4133036
96PRO-2855

Technical Report No. 29

Electrochemical Atomic Layer Epitaxy

By John L. Stickney

Prepared for Publication in Electroanalytical Chemistry, Ed. A.J. Bard, Marcel Dekker

Department of Chemistry
University of Georgia
Athens, GA 30602-2556

October 15, 1997

Reproduction in whole or in part is permitted for any purpose of the United States Government

This document has been approved for public release and sale; its distribution is unlimited.

Accepted "Electroanalytical Chemistry," Ed. A.J. Bard, Marcel Dekker

Electrochemical Atomic Layer Epitaxy

John L. Stickney

Department of Chemistry

University of Georgia

Athens, GA 30602-2556

(706) 542-1967

FAX (706) 542-9454

Stickney@sunchem.chem.uga.edu

19971028 169

Table of Contents:

I.	Introduction	3
II.	Thin Layer Electrochemical Cell Studies	21
III.	Thin Film Formation Using ECALE	32
IV.	Surface Chemistry in the ECALE Cycle	46
V.	Digital Electrochemical Etching	62
VI.	Directions	70
VII.	References	75
VIII.	Figures	102

I. Introduction

The formation of electronic grade compound semiconductor thin films is generally performed using techniques based on vacuum or gas phase reactors. Such methods include: chemical vapor deposition (CVD) (1- 4) and molecular beam epitaxy (MBE) (5-11). In addition, methods based on sputtering or evaporation are frequently used. The work being performed in this author's laboratory seeks to answer the question: can electronic grade compound semiconductor thin films be formed electrochemically? The work described in this chapter is directed towards understanding the basic limits to electrodeposition as a method for forming high quality compound thin films.

Electrodeposition has a number of possible advantages, including: low temperature deposition (near room temperature); relatively low cost hardware; coverage measurements via coulometry; uniform coverage on odd shapes; more tractable waste issues (12); and increased selectivity, thus lower impurity levels in some systems (12-15). For the formation of large area photovoltaics, the cost factors are inviting, while, in the formation of electro-optical devices, low temperature deposition is generally desirable.

Possible drawbacks to electrodeposition in the formation of compound semiconductors include: the need for a conductive substrate, the need for some level of conductivity in the deposits themselves, and the fact that a condensed deposition medium is used and may result in increased levels of some impurities.

This chapter describes the current state and progress in the development of electrochemical ALE (ECALE), an electrodeposition methodology that may provide the control necessary to produce electronic grade thin films. ALE stands for atomic layer epitaxy, a technique involving the formation of thin films one atomic layer at a time (7-11, 16-20, 21).

Generally, a cycle is used where atomic layers of the individual elements are deposited independently and alternately. The idea being that if surface limited reaction are used to form each atomic layer, three dimensional growth modes will never be initiated and epitaxial deposits will result. ECALE is the application of electrochemical surface limited reactions, underpotential deposition (UPD) (22, 23), to ALE. Ideally, in a solution containing an ion of an element that can be electrodeposited, there is a potential beyond which a bulk deposit of the element remain stable. That a monolayer, or so, of the element frequently deposits on a second element at a potential prior to (under) that potential, has been known for over 80 years (24, 25), and is generally referred to as UPD:



One way to view UPD is as formation of a surface compound. That is, deposition of the first atomic layer of an element on a second element involves a larger deposition driving force than subsequent layers, as it benefits from the ΔG of compound formation. For deposits formed at underpotential, once the substrate is covered the deposition stops, as the reaction is surface limited. No more of the substrate element is available to react, unless it can quickly diffuse to the surface through or around the initially deposited monolayer (an example would be amalgam formation at a mercury electrode surface). Subsequent deposition is then only observed when the bulk deposition potential has been exceeded.

UPD generally involves the reductive deposition of an atomic layer of one element on a second. It has clearly been shown, however, that if there is a preadsorbed atomic layer of a third element, the UPD process may involve reactions with both the substrate and the preadsorbed layer. For example, the voltammogram in Figure 1 depicts Ag UPD on an I coated Pt(111) electrode (26). There are three features that can be attributed to the UPD of Ag, and each results in the formation of a new structure on the surface, as indicated by the LEED patterns diagrammed in the circles. It was concluded in that work that UPD involved more than a single monolayer of

Ag. Ag depositing at underpotential reacted with the Pt substrate as well as with the adsorbed I atom layer. It is also interesting to note that Ag underpotentially deposited in Figure 1, reacted with the adsorbed atomic layer of I atoms to form a monolayer of the I-VII compound AgI on the Pt surface.

ECALE is then ALE where the elements are deposited by controlling the substrate's electrochemical potential, so that atomic layers are formed at underpotentials (Eq. 1). The underpotentials are used in order to obtain surface limited deposition reactions. Compounds are deposited using a cycle, where a first solution containing a precursor to one of the elements is introduced to the substrate and an atomic layer is electrodeposited at its underpotential. The cell is then rinsed, a solution containing a precursor to the second element is introduced, and an atomic layer is electrodeposited at its underpotential. An ECALE cycle thus involves the use of separate solutions and potentials to deposit atomic layers of each of the elements, to sequentially form a monolayer of the compound.

Electrodeposition is by its nature a condensed phase process, whereas most studies of ALE have been performed using gas phase or vacuum methodologies, CVD or MBE. A solution phase deposition methodology related to ALE has been developed in France by Nicolau et al. (27-32) (Figure 2), in which adsorbed layers of elements are formed by rinsing a substrate in aqueous solutions containing ionic precursor for the desired elements, sequentially, in a cycle. After exposure to each precursor, the substrate is copiously rinsed and then transferred to a solution containing the precursor for the next element. The method is referred to as successive ionic layer adsorption and reaction (SILAR). Reactivity in SILAR appears to be controlled by the rinsing procedure, solution composition, pH and specifically by the activities of the reactant species. It might be thought of as a kind of chemical bath (33-37) ALE.

A number of different methods have been and are being used to form compound semiconductor thin films electrochemically (See Table 1). Most of the previous work has

involved formation of various II-VI and related compounds. In general, other electrodeposition methodologies appear to be inherently faster than ECALE, but result in deposits with less than ideal structure and morphology. Most compound electrodeposition methodologies lack sufficient control over deposit structure to form electronic grade deposits, and require post deposition annealing before reasonable X-ray diffraction patterns can be obtained. However, some recent advances have been very encouraging (38, 39).

One of the major benefits of the ECALE methodology is that it breaks compound electrodeposition into a series of identical cycles, and each cycle into a set of individual steps. Each step is examined and optimized independently, resulting in increased control over deposit structure, composition, and morphology. Better understanding of the individual steps in the deposition mechanism should allow the electrochemical formation of high quality thin films of compound semiconductors.

The remainder of this introduction will involve a brief discussion of previous work in the area of semiconductor electrodeposition. The focus will be on the strengths and limitations of the various electrodeposition methods with regards to controlling deposit structure, composition and morphology. Most of this work has been well reviewed by others (13, 40-44).

The methodology most practiced is referred to here as codeposition: where a single solution contains precursors for all the elements being deposited, and is reduced at a fixed potential or current density. The earliest report appears to be that by Gobrecht et al., and was published in 1963 (45). Two anodes were used in the study, one of Se and one of Cd (or Ag), to form selenite and cadmium ions respectively. CdSe was then formed by co-reduction of both species at the cathode. Reports of the formation of GaP (1968) (46) and ZnSe (1975) (47) via codeposition were subsequently published, and both involved molten salt electrolysis.

Table 1: Compound Electrodeposition Studies

Compound	Mechanism	Solvent	Characterization	Substrates	Reference
	codeposition				(41)
	codeposition		theory		(48)
	codeposition		theory		(49)
	codeposition		review		(40)
			review		(50)
	codeposition		review		(51)
	codeposition		review		(52)
	codeposition, pulse plate		theory		(53)
Bi ₂ S ₃	codeposition	DMSO, DMF, EG	Con, XRD	Pt,Au,SS,Ni,Zn	(54)
Bi ₂ S ₃	precipitation	1 M KOH	RRDE	Cd, Bi	(55)
Bi ₂ S ₃	precipitation	base	RDE, PEC	Cd, Bi	(56)
CdBiS	codeposition			ITO	(57)
CdS			OS, Raman, XRD		(58)
CdS	ECALE		Raman	Au, on Si	(59)
CdS	ECALE		STM, EC	Au(111)	(60)
CdS	ECALE	pH 5,9, pH 9	TLE,	Au	(61)
CdS	ECALE	pH 9-10	EC, STM	Au(100)	(62)
CdS	codeposition		J-V	SnO ₂	(63)
CdS	codeposition		J-V,	ITO, CdS	(64)
CdS	codeposition	1 M NaOH	SEM, XRD, EDX, XPS,DP, PEC	Cd	(65)
CdS	codeposition	DEG	EC	Pt, Au	(66)
CdS	codeposition	DEG:H ₂ O, 10:1	Hall, XRD, SEM, Con	Mo	(67)
CdS	codeposition	DMSO	EC,	Pt	(68)
CdS	codeposition	DMSO	EC, DME	Hg, Pt, Au	(69)
CdS	codeposition	DMSO	EC, PEC,	Au	(70)
CdS	codeposition	DMSO	PEC, OS	Pt	(71)
CdS	codeposition	DMSO	SEM, XRD, RBS,	Pt, Au	(72)
CdS	codeposition	DMSO	XRD, SEM. AES, Photocon	ITO	(73)
CdS	codeposition	DMSO, DMF, EG	Con, XRD,	Pt,Au,SS,Ni,Zn,	(54)
CdS	codeposition	DMSO, EG	TEM, XRD, PEC, OS, ED	Au	(43)
CdS	codeposition	DMSO, PC	XRD, EDX, OS	SS, SO	(74)
CdS	codeposition	EG, LiClO ₄	SEM, OS,	ITO	(75)
CdS	codeposition	LiCl-KCl	XRD, SEM,	GC	(76)
		eutectic			
CdS	codeposition	LiCl-KCl	XRD, SEM, RHEED	Ag, Cu	(77)
		eutectic			
CdS	codeposition	NH ₃ buffer	PEC, J-V	Ti	(78)
CdS	codeposition	PC	EC	Au, Pt	(79)
CdS	codeposition	PC	EDX, EC,	Ti	(80)
CdS	codeposition	PC	PEC, SEM, XRD, OS	Ti, CdS, ITO,	(81)
CdS	codeposition	aqueous	Con	ITO	(82)
CdS	codeposition	pH 1, H ₂ SO ₄	SEM, OS	ITO	(57)
CdS	codeposition	pH 1.6	EC, AA, OS, J-V, XRD	ITO, ITO/CdS	(27)

CdS	codeposition	pH 1.6	SEM, EDX, J-V	ITO/CdS	(83)
CdS	codeposition	pH 2	I-V, SEM, Cap	ITO	(84)
CdS	codeposition	pH 2, pH 1.8	i-T, i-V	ITO,	(85)
CdS	codeposition	pH 2.3	XRD, SEM, EC, Cap	Pt, Mo, Al	(86)
CdS	codeposition	pH 2.3	XRD, SEM, EDX, EC, ED, OS	Al	(87)
CdS	codeposition	pH 2.5, pH 2	I-V, CAP	ITO	(88)
CdS	codeposition	pH 2.5, pH 2	XRD, SEM, I-V, CAP	ITO	(89)
CdS	codeposition	pH 2.8	XRD, SEM, EC, Cap, EPMA, RDE	Pt	(90)
CdS	codeposition	pH 4	CV, EC,	Pt, ITO	(91)
CdS	codeposition	pH 8, DEG, PC	Hall, Con	ITO	(92)
CdS	codeposition, pulse plate		OS, con	ITO	(93)
CdS	codeposition, pulse plate	pH 2	XRD, J-V, CAP	FTO	(15)
CdS	precipitation		PEC, elip., SNMS, EC	HgCdTe	(94)
CdS	precipitation		Raman, EC	Cd	(95)
CdS	precipitation	1 M KOH	RRDE	Cd, Bi	(55)
CdS	precipitation	1 M NaHCO ₃	AC, modeling	Hg, Cd(Hg)	(96)
CdS	precipitation	1 M NaHCO ₃	EC, Mott, AC,	Cd	(97)
CdS	precipitation	1 M NaHCO ₃	PEC, SEM	Cd	(98)
CdS	precipitation	1 M NaOH	Raman,	Cd	(99)
CdS	precipitation	base	RDE, PEC	Cd, Bi	(56)
CdS	precipitation	pH 14	EC, modeling	Cd	(100)
CdS	precipitation	pH 7-13	RRDE, Cap, AES-DP	Cd	(101)
CdS	precipitation	pH 9	EC		(102)
CdS	precipitation	pH 9, carbonate buffer	PEC, Mott, CAP, RRDE	Cd	(103)
CdSSe	codeposition	DMSO	SEM, XRD, OS,	ITO	(104)
CdSSe	codeposition	DMSO, 0.1 M H ₂ SO ₄	XRD, SEM, RBS, PEC	Pt on glass	(105)
CdSSe	codeposition	LiCl-KCl eutectic	XRD, SEM,	GC	(76)
CdSe	ECALC		LEED, AES, STM	Au(111)	(106)
CdSe	ECALC		LEED, AES, STM,	Au, single crys	(107)
CdSe	ECALC	sulfite	TLEC,	Au	(108)
CdSe	SMD	.5M HCl, 25M H ₂ SO ₄	XRD, SEM, EC, EDX	Ni, Ti	(109)
CdSe	SMD	0.25 H ₂ SO ₄	SEM, EDX map, J-V, XRD	Ni	(110)
CdSe	SMD	0.25 M H ₂ SO ₄	PEC, EC,	ITO	(111)
CdSe	Two Stage, Selenization	pH 9	SEM, EDAX		(112)
CdSe	codeposition				(42)
CdSe	codeposition		Carrier type determination	ITO	(113)
CdSe	codeposition		RHEED, XRD, MBE	InAs	(114)
CdSe	codeposition		TEM, ED	Au	(115)
CdSe	codeposition		TEM, ED,	Ti	(116)
CdSe	codeposition	0.5 M H ₂ SO ₄	EC, PEC	GC,	(117)
CdSe	codeposition	0.5 M H ₂ SO ₄	EC, XRD	Ti	(118)
CdSe	codeposition	0.5 M H ₂ SO ₄	PEC, SEM, AES,	Ti	(119)
CdSe	codeposition	0.5 M HCl	PEC	Ti	(120)

CdSe	codeposition	0.5M H ₂ SO ₄	SEM, PL, Raman, AES	Ti	(121)
CdSe	codeposition	1 M H ₂ SO ₄	RRDE, PEC	Ti,	(122)
CdSe	codeposition	1 M NH ₄ Cl	PEC,	Ti, Ni	(123)
CdSe	codeposition	1 M NaOH	SEM, XRD, EDX, XPS, DP, PEC	Cd	(65)
CdSe	codeposition	DEG, PC	P, PEC, OS, J-V, SEM,	Ti, ITO	(124)
CdSe	codeposition	DMSO	TEM, ED	Au(111)	(125)
CdSe	codeposition	DMSO	TEM, ED,	Au(111)	(115)
CdSe	codeposition	DMSO	TEM, ED,	Au(111)	(125)
CdSe	codeposition	DMSO, 0.1 M H ₂ SO ₄	XRD, SEM, RBS, PEC	Pt on glass	(105)
CdSe	codeposition	DMSO, DMF, EG	Con, XRD,	Pt, Au, SS, Ni, Zn,	(54)
CdSe	codeposition	DMSO, EG	TEM, XRD, PEC, OS, ED	Au	(43)
CdSe	codeposition	H ₂ SO ₄	PL, EL	Ti	(126)
CdSe	codeposition	KCN	EC, PEC, J-V, XRD	Ti	(127)
CdSe	codeposition	acid, base(NaCN)	SEM, XRD, PEC,	Ti	(128)
CdSe	codeposition	acidic sulfate	PEC, XRD, EDX?, J-V	Ti	(129)
CdSe	codeposition	aqueous	XPS-DP	Ti	(130)
CdSe	codeposition	pH 0.7	PEC,	Ti	(131)
CdSe	codeposition	pH 1-2			(45)
CdSe	codeposition	pH 10	RRDE, J-V, PEC,	Ti, Au, Cd	(132)
CdSe	codeposition	pH 2	J-V, OS	ITO	(133)
CdSe	codeposition	pH 2 - 7	EC, Pourbaix, XPS-DP, PEC,	Ti, Pt, GC	(134)
CdSe	codeposition	pH 2.2	XRD, EDAX, SEM, TEM, OS	Ti	(135)
CdSe	codeposition	pH 2.2	XRD, SEM, EDAX, PEC, OS	tin oxide	(136)
CdSe	codeposition	pH 2.2	XRD, SEM, EDX, RDE, OS, PEC,	Ni	(137)
CdSe	codeposition	pH 2.7	AES DP, PEC,		(138)
CdSe	codeposition	pH 3-4	QCM, EC	Au	(139)
CdSe	codeposition	pH 4	SEM, XRD, OS, I-V,	Ti, ITO?	(140)
CdSe	codeposition	pH 7?	Hall, resistivity	ITO, + Se, Cd	(141)
CdSe	codeposition	pH 8	EC, PEC	Ti	(142)
CdSe	codeposition	pH 8	EC, RBS, SEM, XRD, P	Ti	(143)
CdSe	codeposition	pH 8	SEM, EDX, PEC	Ti	(144)
CdSe	codeposition	pH 8, DEG, PC	Hall, Con	ITO	(92)
CdSe	codeposition	pH 9	RBS, SEM, PEC, EC	Ti	(145)
CdSe	codeposition	pH 9	Reflectance	Ti, SS, Si,	(146)
CdSe	codeposition	pH 9, 1 M H ₂ SO ₄	SEM, Reflectance	Ti on Si wafers	(147)
CdSe	codeposition, pulse plate	aqueous	XRD, SEM, EDX, EC	Ti, GC	(148)
CdSe	precipitation	1 M KOH	PEC	Cd, Cd on Fe, SS	(149)
CdSe	precipitation	1 M KOH	PEC,	Cd	(150)
CdSeTe	codeposition	1 M H ₂ SO ₄	PL, XRD, PEC,	Ti	(151)
CdSeTe	codeposition	1 m H ₂ SO ₄	PEC, Con, J-V	Ti	(152)

CdSeTe	codeposition	KCN	EC, PEC, J-V, XRD	Ti	(127)
CdSeTe	codeposition	acid, base(NaCN)	SEM, XRD, PEC,	Ti	(128)
CdSeTe	codeposition	pH 1-2.5	PEC, XRD, EDX, AES-DP, OS	Ti	(153)
CdSeTe	codeposition	pH 2.2	XRD, EDAX, SEM, TEM, OS	Ti	(135)
CdSeTe	codeposition	pH 2.2	XRD, SEM, EDX, RDE, OS, PEC,	Ni	(137)
CdSeTe	codeposition	pH 9.6	PEC, RRDE, XRD,	Au, Ti	(154)
CdSeTe	codeposition, pulse plate	aqueous	XRD, SEM, EDX, EC	Ti, GC	(148)
CdTe	ECALE	20 mM H ₂ SO ₄	EC, Pourbaix, AES, LEED, STM	Au-SC	(155)
CdTe	ECALE	aqueous		Au	(156)
CdTe	ECALE	aqueous	EC, AES, LEED	Au-SC	(157)
CdTe	ECALE	aqueous	EC, EPMA, ICP-AES, SEM	Au	(158)
CdTe	ECALE	aqueous	STM, EC	Au-SC	(159)
CdTe	ECALE	pH 2.9 and pH 1.3	TLE, review	Au-SC	(160)
CdTe	ECALE	pH 4.6 and pH 2.2	TLE, LEED, AES	Au	(161)
CdTe	ECALE	pH 4.7 and pH 2.1	AES, LEED, EC,	Au-SC	(162)
CdTe	ECALE	pH 5.2 and pH 2.9	EC, TLE, EPMA, SEM, STM	Au	(44)
CdTe	SMD	0.25 H ₂ SO ₄	SEM, EDX map, J-V, XRD	Ni	(110)
CdTe	Two stage	aqueous	XRD, EPMA	Mo	(163)
CdTe	codeposition		AES-DP, J-V	ITO/CdS	(164)
CdTe	codeposition		Con	ITO	(165)
CdTe	codeposition		J-V	SnO ₂	(63)
CdTe	codeposition		J-V,	ITO, CdS	(64)
CdTe	codeposition		PEC, SEM, EDS	Si	(166)
CdTe	codeposition		Theory		(167)
CdTe	codeposition	0.1 M H ₂ SO ₄	EC	VC	(168)
CdTe	codeposition	0.1 M H ₂ SO ₄	QCM, EC	Au	(169)
CdTe	codeposition	0.5 M H ₂ SO ₄	EC	GC	(170)
CdTe	codeposition	0.5 M H ₂ SO ₄	EC, PEC	GC,	(117)
CdTe	codeposition	0.5 M H ₂ SO ₄	RDE, DSC	Pt, Ti	(171)
CdTe	codeposition	0.5 M H ₂ SO ₄	RRDE	Pt, Te on Pt	(172)
CdTe	codeposition	1 M H ₂ SO ₄	RDE, AA	Ti	(173)
CdTe	codeposition	1 M NaOH	Pourbaix, XPS, AES, SEM,	Cd	(174)
CdTe	codeposition	1 M NaOH	SEM, XRD, EDX, XPS,DP, PEC	Cd	(65)
CdTe	codeposition	DMSO	ED, EDX, SEM	SnO ₂	(175)
CdTe	codeposition	DMSO	con, TEM, SEM, ED,	ITO	(176)
CdTe	codeposition	EG	SEM, EC	Ni	(177)
CdTe	codeposition	EG	XPS-DP, SEM, PEC, XRD	Ni	(178)
CdTe	codeposition	EG	XPS-DP, SEM, XRD,	Ni	(179)
CdTe	codeposition	EG, LiClO ₄	SEM, OS,	ITO	(75)

CdTe	codeposition	H ₂ SO ₄	AES-DP, XRD, EPMA	Cu,Ti,SS,ITO	(180)
CdTe	codeposition	H ₂ SO ₄	EDS, PEC, PL, Raman, SEM, XRD	ITO	(181)
CdTe	codeposition	H ₂ SO ₄	PEC,	Ti	(182)
CdTe	codeposition	H ₂ SO ₄	PL,	ITO-CdS	(183)
CdTe	codeposition	H ₂ SO ₄	XRD, SEM, EC, EPMA	Ni, Te on Ni	(184)
CdTe	codeposition	LiCl-KCl molten salt	XRD, SEM,	GC	(185)
CdTe	codeposition	PC	Con, Hall, SEM,	ITO	(186)
CdTe	codeposition	PC	Con, SEM	ITO	(187)
CdTe	codeposition	PC	EC, XRD, SEM, PEC	Ti	(188)
CdTe	codeposition	PC	P, EC, SEM, PEC	ITO, Ti	(189)
CdTe	codeposition	PC	PEC, SEM, XRD, OS	Ti, CdS, ITO,	(81)
CdTe	codeposition	PC	con, depth profil, Hall, XPS,	ITO	(190)
CdTe	codeposition	PC, LiClO ₄	Hall,	ITO	(191)
CdTe	codeposition	aqueous	Cap, Con	Ti	(192)
CdTe	codeposition	aqueous	Con	ITO	(82)
CdTe	codeposition	aqueous	EC, XPS, optical microscopy	GC	(193)
CdTe	codeposition	pH 0	PEC	Ti	(194)
CdTe	codeposition	pH 0.5	EC, XRD, SEM, EDX,	Si n-type	(195)
CdTe	codeposition	pH 1.4	AES-DP, XRD,	Ti	(196)
CdTe	codeposition	pH 1.4	EC, PEC, XRD	Ti, Ni,	(197)
CdTe	codeposition	pH 1.4	PEC, XRD, AES	Ti, Ni	(198)
CdTe	codeposition	pH 1.4	XRD, AES, Con	Ti, Ni	(199)
CdTe	codeposition	pH 1.5	RDE, Pourbaix	SnO ₂	(200)
CdTe	codeposition	pH 1.5 - 2.0	RDE, EC, Theory	VC, SS	(201)
CdTe	codeposition	pH 1.6	EC, AA, OS, J-V, XRD	ITO, ITO/CdS	(202)
CdTe	codeposition	pH 1.6-2	SEM, EDAX, XRD,	Ni	(203)
CdTe	codeposition	pH 1.6-2	SEM, XRD, EDAX, OS,	SnO ₂	(204)
CdTe	codeposition	pH 1.7	XRD, SEM,	GaAs	(205)
CdTe	codeposition	pH 1.8	XRD, DSC, XPS, EC, ellipsometry, RBS	n- p- Si	(206)
CdTe	codeposition	pH 1.8	in situ ellipsometry, raman, EDAX, DSC	MCT	(207)
CdTe	codeposition	pH 2	I-V, SEM, Cap	ITO	(84)
CdTe	codeposition	pH 2	J-V, OS	ITO	(133)
CdTe	codeposition	pH 2	SEM, XRD,	CdS/SnO ₂ /glass	(208)
CdTe	codeposition	pH 2	SIMS, AA, SEM, XRD, NAA, PIXE, AES	ITO, CdS, Ni, Ti	(13)
CdTe	codeposition	pH 2	XRD, RHEED,	InP-CdS	(39)
CdTe	codeposition	pH 2, pH 1.8	i-T, i-V	ITO,	(85)
CdTe	codeposition	pH 2-3	XRD, V-J	Ni	(209)
CdTe	codeposition	pH 2.0-3.5	Con, XRD	SS, ITO	(210)
CdTe	codeposition	pH 2.2	AC, RDE,	Ni	(211)
CdTe	codeposition	pH 2.2	EC, XRD, SEM, OS, PEC	SnO ₂	(212)
CdTe	codeposition	pH 2.2	SEM, J-V, OS,	Cu, Steel, Ni, Cd	(213)
CdTe	codeposition	pH 2.2	SEM, XRD, XPS, OS,	SnO ₂	(214)

CdTe	codeposition	pH 2.2	PEC XRD, EDAX, SEM, TEM, OS	Ti	(135)
CdTe	codeposition	pH 2.2	XRD, SEM, EDAX, PEC, OS	tin oxide	(136)
CdTe	codeposition	pH 2.2	XRD, SEM, EDX, RDE, OS, PEC,	Ni	(137)
CdTe	codeposition	pH 2.2	XRD, SEM, RHEED, EDS	Ni, Ti	(215)
CdTe	codeposition	pH 2.5	EPMA, AES-DP, V-J, XRD	ITO, Mo	(216)
CdTe	codeposition	pH 2.5	Theory	C, Pt, etc.	(217)
CdTe	codeposition	pH 2.5	XRD, OS, PEC,	TO-CdS	(38)
CdTe	codeposition	pH 2.5, pH 2	I-V, CAP	ITO	(88)
CdTe	codeposition	pH 2.5, pH 2	XRD, SEM, I-V, CAP	ITO	(89)
CdTe	codeposition	pH 2.5-3	XRD, SEM, EDX, EC, Pourbaix, Con-type	Ni, SnO ₂ :Sb	(218)
CdTe	codeposition	pH 2.5-3.0	PEC, XRD, OS, SEM, EC, EDX	Ti, Nesatron	(219)
CdTe	codeposition	pH 2.5-3.0	SEM, AES-DP, EPMA, J-V, Mott	ITO, Mo	(220)
CdTe	codeposition	pH 8, DEG, PC	Hall, Con	ITO	(92)
CdTe	codeposition, pulse plate		Theory		(221)
CdTe	codeposition, pulse plate	0.3 M H ₂ SO ₄	SEM, RDE, PEC	Cd	(222)
CdTe	codeposition, pulse plate	aqueous	XRD, SEM, EDX, EC	Ti, GC	(148)
CdTe	codeposition, pulse plate	pH 2	XRD, J-V, CAP	FTO	(15)
CdTe	precipitation	1 M CdSO ₄ , 1 M ZnSO ₄	PEC, EC	Te	(223)
CdTe	precipitation	pH 4.5	EC, AA,	Te, Cd	(224)
CdZnS					(57)
CdZnS	codeposition				(57)
CdZnS	codeposition	DMSO	SEM, XRD, OS,	ITO	(104)
CdZnS	codeposition	pH 2	XPS, XRD, SEM, AES depth profile	Ti, Pt, ITO	(225)
CdZnSe	codeposition	pH 2 - 7	EC, Pourbaix, XPS- DP, PEC,	Ti, Pt, GC	(134)
CdZnSe	codeposition	pH ?	AC, I-V	Ti	(226)
CdZnTe	Two stage	1 M H ₂ SO ₄	SEM, XRD, J-V, OS	ITO, SnO ₂	(227)
CoS	codeposition	DMSO, DMF, EG	Con, XRD	Pt, Au, SS, Ni, Zn	(54)
Cu ₂ S	codeposition	DMSO, DMF, EG	Con, XRD	Pt, Au, SS, Ni, Zn	(54)
Cu ₂ Se	codeposition	pH 2.9, 3.28, 3.7	XRD, SEM, EDX, OS	Ti, Ni	(228)
Cu ₉ In ₄	codeposition	pH 2.9, 3.28, 3.7	XRD, SEM, EDX, OS	Ti, Ni	(228)
CuISe ₃	codeposition	4 M HI	J-V	ITO	(229)
CuIn ₅ S ₈	codeposition, Two stage	pH 2	SEM, PEC, EPMA, XRD, AES	Ti	(230)
CuInS ₂	codeposition, Two stage	pH 2	SEM, PEC, EPMA, XRD, AES	Ti	(230)
CuInS ₂	codeposition, two				(12)

CuInSe ₂	stage				(231)
CuInSe ₂	Two stage				(232)
CuInSe ₂	Two stage		SEM, XRD, depth profil	Mo,	(232)
CuInSe ₂	Two stage		XRD, XPS,	Mo, ITO	(233)
CuInSe ₂	codeposition		AC, Con	Mo	(234)
CuInSe ₂	codeposition		J-V	Mo	(235)
CuInSe ₂	codeposition		J-V, XRD	Mo	(236)
CuInSe ₂	codeposition		PEC, Mott		(237)
CuInSe ₂	codeposition		SEM, XRD, J-V, SIMS, EPMA	Mo, W	(238)
CuInSe ₂	codeposition	0.4 citric acid	AA, XRD, EDX	Mo	(239)
CuInSe ₂	codeposition	4 M HI	J-V	ITO	(229)
CuInSe ₂	codeposition	pH 1	RRDE, PEC, Pourbaix	GC	(240)
CuInSe ₂	codeposition	pH 1	SEM, ED, OS, Pourbaix, EDX, J-V	Ti	(241)
CuInSe ₂	codeposition	pH 1	XRD, PEC	SnO ₂ :F	(242)
CuInSe ₂	codeposition	pH 1.6-1.7	RRDE, SEM, XRD, EDX, PEC	Ti, Ni, Mn, Cu	(243)
CuInSe ₂	codeposition	pH 2.9, 3.28, 3.7	XRD, SEM, EDX, OS	Ti, Ni	(228)
CuInSe ₂	codeposition, Two stage	pH 2	SEM, PEC, EPMA, XRD, AES	Ti	(230)
CuInSe ₂	codeposition, pulse plate	pH 2.3	SEM, XRD, EC	Ti	(244)
CuInSe ₂	codeposition, pulse plati		XRD, SEM,		(245)
CuInSe ₂	codeposition, two stage				(12)
CuInSe ₂	two stage	H ₂ SO ₄	XRD, SEM, EPMA	W/C	(246)
CuInTe ₂	codeposition	pH 2.0, pH 8-9	EC, EDX, XRD	Ti	(247)
CuIn _x Se _y I _z	codeposition	4 M HI	J-V	ITO	(229)
CuS	?		RHEED, OS, J-V	Ag-Cr/CdS	(248)
CuS	codeposition	pH 3-5	OS	CdS	(249)
CuSe	Two Stage, Selenization	pH 9	SEM, EDAX		(112)
CuSe	codeposition		RRDE, PEC, Pourbaix	GC	(240)
CuSe	codeposition	melt, LiCl added		Al oxide	(250)
FeS ₂	Two Stage	pH 10, pH ?	EQCM, EC	Au	(251)
GaAs	ECALE	aqueous	EC, AES, LEED	Au-SC	(157)
GaAs	ECALE	pH 1.9 and pH 4.0	TLE, AES, LEED, Pourbaix	Au-SC	(252)
GaAs	ECALE	pH 2.7 and pH 3.2	AES, EC, LEED, STM	Au(100), (110)	(253)
GaAs	codeposition		PEC		(254)
GaAs	codeposition	B ₂ O ₃ , NaF, molten salt	XRD	GaAs, Ni	(14)
GaAs	codeposition	KGaCl ₄ molten salt	XRD, EC,	Au on Ni	(255)
GaAs	codeposition	pH < 3, pH > 12	SIMS, AES depth profile, EDAX, XRD,	Ti, Si, Pb, Sn, C	(256)
GaAsSb	Two stage	5 M KOH, 7 M HCl	XRD, EDX, SEM	Ti, Ni/Cu, VC	(257)
GaP	codeposition	NaPO ₃ , NaF	SEM, XRD, J-V, Laue, ES	GrC, Si-SC	(46)

GaP	codeposition	NaPO ₃ , NaF,	SEM, Laue	GrC, Si, GaP	(258)
GaSb	Two stage	5 M KOH, 1.6 M H ₂ SO ₄ -HCl	XRD, EC, SIMS, EDX	Ni plated Cu	(259)
HgCdTe	codeposition	H ₂ SO ₄	I-V, PEC	Ti	(182)
HgCdTe	codeposition	PC	XRD, OS, AA, PIXE	ITO	(260)
HgCdTe	codeposition	pH 1.6	EC, AA, OS, J-V, XRD	ITO, ITO/CdS	(202)
HgCdTe	codeposition	pH 1.6	SEM, EDX, J-V	ITO/CdS	(83)
HgCdTe	codeposition	pH 1.6	XRD, OS, PEC	ITO	(261)
HgCdTe	codeposition	pH 1.6	XRD, SEM, EDX, PEC	Ti	(262)
HgCdTe	codeposition	pH 2, H ₂ SO ₄	EDS, OS, PEC, XRD	Ti	(263)
HgCdTe	codeposition	H ₂ SO ₄	PEC	Ti	(182)
HgS	codeposition	DMSO, DMF, EG	Con, XRD,	Pt,Au,SS,Ni,Zn,	(54)
HgS	precipitation	1 M NaHCO ₃	EC	DME	(264)
HgSe	precipitation	0.1 M HClO ₄	EC, PEC	DME, Hg pool	(265)
HgTe	precipitation	pH 4.5	EC, AA,	Te, Cd	(224)
InAs	Two Stage	7M HCl, pH 2	XRD, EDX, EC	Ni	(266)
InAs	codeposition / two stage	citric acid	XRD, EC, PEC, AC, Mott	Ti	(267)
InGaSb	Two stage	5M KOH, pH 1.5-2, pH 0	XRD, SEM, EDX, SIMS, EC	Ni,Pt,Sb,InSb	(268)
InP	codeposition	DMF	XRD, EDS, Con	Ti	(269)
InP	codeposition	NaPO ₃ /NaF molten salt	EC, SEM	CdS, InP(111)	(270)
InP	codeposition	pH 2	XRD, EDS, OS	Ti	(271)
InP	codeposition / two stage	citric acid	XRD, EC, PEC, AC, Mott	Ti	(267)
InSb	Two stage	1 M H ₂ SO ₄	EC, XRD,	Sb	(272)
InSb	Two stage	5M KOH, pH 1.5-2, pH 0	XRD, SEM, EDX, SIMS, EC	Ni,Pt,Sb,InSb	(268)
InSb	codeposition / two stage	citric acid	XRD, EC, PEC, AC, Mott	Ti	(267)
InSe	Two Stage, Selenization	pH 9	SEM, EDAX		(112)
In ₂ Se ₃	codeposition	pH 3.45	XRD, CV, OS	SnO ₂ ,Mo on glass	(273)
InSe	codeposition	pH 1	SEM, EPMA, XRD	Ti	(274)
NiS	codeposition	DMSO, DMF, EG	Con, XRD	Pt,Au,SS,Ni,Zn	(54)
PbS	codeposition	DMSO	EC, DME	Hg, Pt, Au	(69)
PbS	codeposition	DMSO, DMF, EG	Con, XRD	Pt,Au,SS,Ni,Zn,	(54)
PbS	precipitation	0.1 M Na ₂ S	EC	Hg(Pb)	(275)
PbS	precipitation	pH 9-14	EC	Pb	(276)
SnS	codeposition/pulse	EG	SEM, XRD, SPX, EPMA, AES, PEC, Pourbaix	ITO	(277)
SnSe	codeposition	pH 3, DMF	XRD, O, Con, EMPA	ITO	(278)
Tl ₂ S	codeposition	DMSO, DMF, EG	Con, XRD	Pt,Au,SS,Ni,Zn,	(54)
ZnMgSeTe	codeposition		RHEED,XRD,MBE	InAs	(114)
ZnS	ECALC		TLEC, EC	Au	(279)
ZnS	codeposition	pH 2.5	XRD, OS	ITO	(280)

ZnS	codeposition	pH 8-10	SEM, EC, OS	Ti, SS, SnO ₂	(281)
ZnS	codeposition	DMSO	EC, DME	Hg, Pt, Au	(69)
ZnSe		pH 2	EC, XRD,	Ti, SS, SnO ₂	(282)
ZnSe	ECALE		TLEC, EC	Au	(279)
ZnSe	codeposition		AC, PEC	Ti	(283)
ZnSe	codeposition	0.5 M H ₂ SO ₄	EC, PEC	GC,	(117)
ZnSe	codeposition	KCl + LiCl, eutectic	XRD, ED, SEM	Ge(111), Si(111)	(47)
ZnSe	codeposition	aqueous	XPS-DP	Ti	(130)
ZnSe	codeposition	pH 2 - 7	EC, Pourbaix, XPS- DP, PEC,	Ti, Pt, GC	(134)
ZnSe	codeposition	pH 2-6	AC, PEC	Ti	(284)
ZnSeTe	codeposition	pH 2.3 - 3	PEC, EC	Ti	(285)
ZnTe	ECALE		TLEC, EC	Au	(279)
ZnTe	ECALE	pH 5.2 and pH 2.9	EC, TLE, EPMA, SEM, STM	Au	(44)
ZnTe	codeposition	pH 4.5	XRD, SEM, EPMA, OS	Ti, Ni, SnO ₂	(286)
ZnTe	codeposition		RHEED, XRD, MBE		(114)
ZnTe	codeposition	pH 4	XPS, XPS depth profile, EC, PEC, Cap	MCT	(287)
ZnTe	precipitation	1 M CdSO ₄ , 1 M ZnSO ₄	PEC, EC	Te	(223)
ZnTe	precipitation	pH 4.5 or less	XRD, Gravimetry	homogenous	(288)

Analytical techniques: AA = Atomic adsorption; AC = ac impedance; AES = Auger electron spectroscopy; Cap = capacitance; Con = conductivity measurements; DME = dropping mercury electrode; DP = depth profiling; DSC = differential scanning calorimetry; EC = electrochemical analysis; ED = electron diffraction; EDX = energy dispersive X-ray analysis; EL = electroluminescence; EPMA = electron probe microanalysis; ES = emission spectroscopy; ICP-AES = inductively coupled plasma - atomic emission spectroscopy; J-V = current voltage curves; LEED = low energy electron diffraction; Mott = Mott-Schottky; NAA = neutron activation analysis; OS = optical spectroscopy; P = polarography; PEC = photoelectrochemical cells; PIXE = photon induced X-ray emission; PL = photoluminescence; QCM = quartz crystal microbalance; RBS = Rutherford backscattering; RDE = rotating disk electrode; RHEED = reflection high energy electron diffraction; RRDE = rotating ring disk electrode; SEM = scanning electron microscopy; STM = scanning tunneling microscopy; TEM = transmission electron microscopy; TLE = thin layer electrochemistry; VPD = van der Pauw; XPS = X-ray photoelectron spectroscopy; XRD = X-ray diffraction.

Reactants: BPS = tri(n-butyl)phosphine selenide; BPT = tri(n-butyl)phosphine teluride; NTA = nitrilotriacetate complex ion; SeCN = selenocyanide; SOS = selenosulfite; STS = sodium thiosulfate; TeCN = Tellurocyanide; TFMS = Trifluoromethane sulfanate; TSS = triphenylstibine sulfide.

Solvents: aq = aqueous; DEG = diethylene glycol; EG = ethylene glycol; PC = propylene carbonate.

Substrates: DME = dropping mercury electrode; FTO = Fluorine doped tin oxide; G = graphite; GC = glassy carbon; GrC = graphitic carbon; ITO = indium tin oxide coated glass; SC = single crystals; SS = stainless steel; TCO = transparent conducting oxide; VC = vitreous carbon;

Miscellaneous: ECALE = electrochemical atomic layer epitaxy; ED = electrodeposition; ML = monolayer; RT = room temperature; SMD = sequential monolayer deposition; V = vacuum.

In 1976 a paper published by Hodes, Manassen, Cahen described the codeposition of CdSe using a solution made by dissolving CdSO₄ and SeO₂ in sulfuric acid (129). This appears to be the first of a large number of similar studies where II-VI compounds were formed from aqueous solutions by co-reduction of Cd⁺² and HSeO₃⁻ (or HTeO₂⁺, as performed in the classic study by Panicker, Knaster, Kroger (218)).

Codeposition produces some of the better II-VI electrodeposits and, as can be seen in Table 1, has been used and studied extensively. Aqueous codeposition of CdTe serves as a good example of the method. The deposition is usually performed at an underpotential for Cd. At a potential where the Cd deposits exclusively on previously deposited Te. Te, on the other hand, is more noble than Cd and is thus deposited at an overpotential. The tellurite concentration, however, is kept far below that of the Cd⁺², so there is a large excess of Cd⁺². As soon as Te deposits, Cd quantitatively underpotentially deposits on top, providing control over deposit stoichiometry.

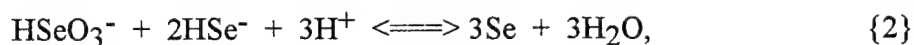
One of the exciting aspects of the early work in this area, was the observation that both n- and p-type semiconductors could be formed from the same bath, simply by adjusting the deposition potential (Figure 3) (218). At the more positive deposition potentials, where p-type behavior was observed, Cd is less reactive, and small amounts of excess Te may be present. On the other hand, n-type behavior was observed at more negative potentials, where excess Cd may have been present. Type conversion, from n- to p-, was also frequently achieved by annealing deposits near 350° (218).

The down side to the codeposition methodology is that the chalcogenide is generally deposited at overpotential and it is not clear that the chalcogenide atoms necessarily deposit in optimal sites. It is expected that significant surface diffusion of the chalcogenide is required in order to avoid high defect densities. The use of higher deposition temperatures has been observed to improve deposit structure significantly (Figure 4), in line with the need for adequate surface diffusion. In addition, post-deposition annealing generally improved deposit crystallinity.

The case in which both elements are deposited at underpotentials, simultaneously, from a

single bath, has been considered by Engelken (49). A deposition potential that did not exceed the reversible potential for either element could be used if both elements have similar UPD potentials. The elements could induce the UPD of each other, possibly forming a higher quality deposit than those where one element is deposited at an overpotential.

In the case of CdSe formation using the codeposition methodology, a problem was encountered early on, and studied by Skylas Kazacos and Miller (122). It concerned the formation of selenide ions and their reaction with the selenite starting material to form elemental Se:



an example of conproportionation. The net results were CdSe deposits that required thermal treatments to obtain optimal photoactivity due to the presence of elemental Se (129). The initial solution to this problem was to search for a Se precursor in a lower oxidation state, such as selenosulfite, SeSO_3^{2-} (132). The nominal oxidation state of Se in this species is zero, as it is formed by the reaction of elemental Se with sulfite:



Use of selenosulfite in combination with EDTA complexed Cd^{+2} , eliminated the elemental Se contamination and improved the photoresponse of the as formed deposits (132). A second method for avoiding conproportionation, also suggested by Skylas-Kazacos, was to use a cyanide solution to dissolve elemental Se (or Te) and high concentrations of CdCl_2 (127). Again, the Se was felt to be in the zero oxidation state.

A major modification of the codeposition methodology was the introduction of nonaqueous solvents by Baranski and Fawcett (54, 72). The nonaqueous solvent allowed the use of elemental chalcogenides, again avoiding conproportionation. High quality films were observed in those studies, although some were prone to cracking. Another advantage of using the nonaqueous solvents was the ability to deposit films at higher temperatures, which in general

improved deposit quality.

As indicated previously, the state of the art in codeposition appears to be the work of Lincot et al. (38, 39). They have shown that the optimal deposition potential is around 5 mV positive of the reversible potential for Cd^{+2}/Cd . In addition, they have incorporated a feedback step in the deposition to correct for the increasing resistance of the films as they grow (289). The resulting deposits have shown a remarkable degree of epitaxy, observed with reflection high energy electron diffraction (RHEED) and XRD pole patterns. Their results offer great promise for the formation of high quality compound semiconductor thin films.

A second major methodology for electrochemically forming compound semiconductors, investigated by a number of workers (Table 1), involves the dissolution of a substrate in a solution containing a species that will react with the dissolving ions. This methodology is referred to here as the precipitation method, as it can be thought of as electrochemically initiated precipitation at the electrode surface. The first example appears to be work performed by Panson (288), where ZnTe was deposited by forming Te^{2-} ions electrochemically, and then precipitating them using a zinc salt. Similar studies were performed a few years later by Miles and McEwan (224) in the formation of CdTe and HgTe, where a tellurium cathode was used to form telluride ions and a cadmium anode was used to form Cd^{2+} ions. Attempts were made to use a Hg anode to form Hg^{2+} ions in solution but much better results were obtained using a mercury (II) salt. Use of a solution containing a salt of one of the ions proved important, as it localized the precipitation to one of the electrodes, resulting in much better films.

In 1976 Miller and Heller used a solution of sulfide ions, and formed Cd^{2+} ions from a Cd anode and Bi^{3+} ions from a Bi anode (56), precipitating the corresponding sulfides. Reasonably photoactive deposits of the sulfides were formed on both the Cd and the Bi anodes. Subsequently, extensive studies of the growth of CdS by this method were published by Miller, Menezes, and Heller (55) and by Peter (97, 98) in 1978.

Advantages of the precipitation methodology were simplicity and good adhesion of the

deposits to the substrate. There are inherent deficiencies, however, such as the lack of control over deposit structure. Deposit growth by the precipitation mechanism requires the transport of ions from solution to the substrate-compound interface, or from the substrate to the compound-solution interface. The process is analogous to formation of passive films during corrosion. It is not clear how control over the structure and morphology of the depositing material could be significantly improved.

Another group of methods, associated with the electrodeposition of compounds, are referred to here as two stage methods. This designation covers deposits where the elements are deposited in a first stage, and then a reaction is initiated to form the compound in a second stage. Both stages are not necessarily electrochemical in nature, and thus these techniques are not strictly electrodeposition methodologies. Several examples have been included in Table 1, however, for completeness. A good example of a two stage method is delineated in the patent by Kapur, Choudary, and Chu (290), where thin films of the two component elements, of the compound to be formed are first electrodeposited individually, from separate solutions, one on the other. The second stage is then a heat treatment, or anneal, resulting in interdiffusion and reaction of the component elements. A variation on this scenario was developed by Hodes et al. in 1985 (12), where CuInS_2 and CuInSe_2 were formed by first electrodepositing a Cu-In alloy, and then heating the deposits in the presence of H_2S or H_2Se gases, to form the respective ternary compounds. Other scenarios include formation of a layer of Cd on an inert substrate (via electrodeposition, vapor deposition...), and then use of the precipitation methodology, oxidation in a sulfide, selenide or telluride solution to form the corresponding II-VI compounds electrochemically (112). A completely electrochemical two stage method has recently been described by Rajeshwar et al. (251), where a layer of sulfur was first electrodeposited and then transferred to a solution containing cations of the desired metal, in that case Fe^{2+} . The metal was then reduced into the sulfur layer forming a thin films of the corresponding sulfide.

One of the advantages of the two stage methods is control over the deposited amounts. If all the elements are electrodeposited prior to thermal annealing, for instance, coulometry can be

used to account for the amounts deposited, and thus help control the stoichiometry of the resulting film. The annealing step can be a problem, as mentioned previously, when inter-diffusion at heterojunctions is not desirable. It is interesting to note that the annealing temperatures used to form compounds by the two stage method (290) are similar to those used to post anneal deposits formed by other electrodeposition methodologies, possibly indicating that the quality of many of the as deposited films listed in Table 1 were not much better than a deposit consisting of segregated domains of the component elements.

There are a number of electrodeposition methods described in the literature based on potential programs, of which pulse plating is a good example (53, 222, 244, 277, 290). One of these methodologies, sequential monolayer electrodeposition (SMED), developed by Sailor et al., is a more atomic level approach to the formation of compounds electrochemically, and may provide the control needed to form high quality deposits (109, 110). The method was developed in order to avoid the traces of elemental Se that are generally incorporated in deposits of CdSe formed by codeposition from a solution containing selenite species (Eq. 2). SMED involves a potential program which starts low in order to deposit both sub-monolayer quantities of CdSe and several monolayers of bulk Cd. Under those low potential conditions, it is assumed that all the available Se reacts with Cd. The next step in the cycle involves oxidative removal of the bulk Cd using a potential where only the CdSe is stable and remains behind. In the original studies, a fast cyclic potential program was used to form the CdSe deposits (Figure 5).

Given the diversity of results described in the papers listed in Table 1, the future importance of electrodeposition in the formation of compound semiconductor thin films is not clear. ECALE is suggested as a means for examining limits to compound semiconductor electrodeposition. The rest of this chapter, then, describes studies of ECALE, and has been organized as follows: Section II describes the use of manual thin layer electrochemical cells (TLECs) to investigate the potentials and solutions needed for an ECALE cycle. Section III

describes the formation of thin films of a number of compounds using an automated flow cell electrodeposition system. Section IV describes studies of the nucleation and growth of the individual atomic layers, while section V describes the inverse of electrochemical ALE, electrochemical digital etching (where a cycle is used to remove atomic layers of the elements constituting a compound, one at a time). Finally, Section VI describes possible new and future directions for ECALE related work.

II: Thin Layer Electrochemical Cell Studies

The development of ECALE in our group was directly stimulated by work and discussions with M.L. Norton (Huntington University, WV) (291). Those studies involved the use of a TLEC to investigate the deposition of Cd and Te on a series of metal electrodes (Cu, Au, and Pt) and of Cd and Te on atomic layers of each other (291). TLECs were used for a number of reasons, such as that they provide a clean defined environment for the electrode. In the TLECs used in these studies, the electrodes and deposits were exposed to only a few microliters of solution instead of the 10s of mLs used in corresponding thick layer cells. The decreased amount of solution results in a corresponding decrease in the amounts of solution-born contaminants exposed to the electrode. Another advantage of these TLECs is that they allowed careful control of the amounts of reactant exposed to the electrode. The volumes of the TLECs used in these studies were easily determined to within 1-2%, using a standard solution of an electroactive species (Figure 6). Thus if the concentration of the reactant solution is known, the total number of moles exposed to the electrode surface are easily determined. Additionally, accurate coulometry can be performed with TLECs (292, 293), due to minimal and reproducible background currents. The most important reason for using a TLEC in these studies, however, was the ease with which solutions could be exchanged without exposing the surface to air. Application of a small over pressure of N₂ gas on the inside of the TLEC (Figure 6), results in expulsion of the solution aliquot through the two pin holes at the tip of the cell. The TLEC can then be dipped into a new solution and after relief of the N₂ over pressure, an aliquot of the solution in contact with the tip wicks in via capillary action.

Figures 7B and C display voltammetry for the deposition of Cd and Te, respectively, on a polycrystalline Au electrode. In Figure 7B, Cd UPD is clearly evident as a broad peak centered at -0.15 V (all potentials are listed vs. Ag/AgCl (1 N NaCl)). The resulting Cd coverage corresponded to about ½ monolayer (ML), where 1 ML corresponds to the deposition of one atom for each substrate surface atom. Figure 7C displays the deposition of Te from a tellurite

solution (HTeO_2^+). Two features are evident, a UPD peak at 0.32 V followed by a small bulk deposition feature at 0.0 V, accounting for the remainder of the tellurite aliquot.

The next step was to alternate the deposition of Cd and Te. As Te is more noble than Cd, various amounts of Te were first deposited, and then exposed to a Cd^{+2} ion solution at underpotential. Figure 8 is a graph of the Cd coverages observed to form on a Cu electrode initially coated with various amounts of Te. The slope of the graph is 0.95 (the Cd/Te ratio), which is consistent with the Cd reacting 1:1 with the Te. Similar results were observed for deposits formed on Pt and Au electrodes. The graph indicates that the Cd reacted at underpotential quantitatively with the Te, even when multiple atomic layers of Te were present.

Deposition of the first ML of CdTe was straightforward, the problem with development of an electrochemical ALE cycle for CdTe was forming the second ML of CdTe. That is, UPD of a less noble element on the UPD of a more noble element appears to work well. However, in the second cycle, use of the same conditions for UPD of the more noble element is a thermodynamically untenable arrangement, as it must form on the deposit of the less noble element (Figure 9). Figures 9A and B are Pourbaix diagrams for Cd and Te, respectively, and the nobility of Te relative to Cd is evident.

The Pourbaix diagrams in Figures 9A and B do not, however, take into account the fact that the two elements are forming a compound. When the free energy of compound formation is considered, the origins of UPD become clear (155). Figure 9C is a Pourbaix diagram describing the stability of CdTe, where the free energy for CdTe formation has been included in the calculations. Figure 9D is a combination of Figures 9A, B and C. The differences in stability between the elements and the compound are clearly evident, and can be equated to underpotentials.

Also evident from examination of the Pourbaix diagram shown in Figure 9B, is the equilibrium between Te and Te^{2-} :



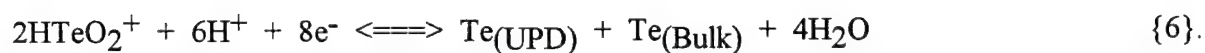
It was the realization that the equilibrium in Eq. 4 might be used to form atomic layers of Te, that allowed development of the first workable ECALE cycle for CdTe. From Figure 9D it can be seen that Te UPD can be performed oxidatively from a telluride solution:



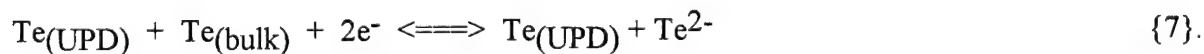
The vast majority of previous UPD studies (22, 23) have involved “reductive” UPD of a less noble metal on a more noble one. “Oxidative” UPD is not unprecedented, however. Some evidence for oxidative UPD has been shown for S (61, 294), Se (295), Te (160, 161, 291), and even O (296). In addition, the adsorption of halides from solution on metal surfaces can be thought of as UPD: Cl (297), Br (298-300), and I (299, 301-304). Normally, UPD is considered a precursor to the formation of a bulk deposit of an element. Bulk deposits of the halides are generally soluble, but the first atomic layer is formed at an underpotential. Recent studies have indicated that oxidative UPD of As can be performed as well (252, 253).

At present, it appears that one of the criteria for construction of an ECALE cycle for a compound, is whether atomic layers of one of the compound's elements can be formed using an equilibrium analogous to Eq. 5: oxidative UPD. As indicated above, the elements that can be deposited using oxidative UPD are mostly non-metals such as the halides, chalcogenides, and pnictides.

Some telluride compounds, such as K_2Te , are available commercially, however black specks and/or a deep purple color (dependent on the pH of the solution) are frequently observed when they are dissolved in the presence of traces of oxygen. The black specks are elemental Te, while the purple color has been attributed to Te_2^{2-} ions (305). The apparent lack of stability of such solutions makes them undesirable for use in an ECALE cycle. The equilibrium shown in Eq. 5 can still be used to form Te atomic layers, however the deposition is generally run as a stripping experiment. A small amount of bulk Te is first formed from a solution of $HTeO_2^+$, which is more tractable:



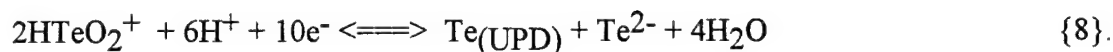
The excess (bulk) Te is then be reduced off the surface as Te^{2-} ions at a potential just below that where bulk Te is stable:



These two steps can then be used to form Te atomic layers in an ECALE cycle that works for the formation of more than one monolayer.

In the first TLEC studies of CdTe formation, a one step variation on the reactions in Eq. 6 and 7 was used to form the Te atomic layers (160, 161). In those studies, an aliquot of a 0.3 mM $HTeO_2^+$ solution was first rinsed into the TLEC. Given the low concentration, and low volume of the cell, a total of a little over one ML of Te was initially present in the cell. A potential of

-1.1 V was then applied, and used to reduce most of the HTeO_2^+ aliquot all the way to Te^{2-} , while leaving about $\frac{1}{2}$ ML of Te on the surface:



The resulting Te^{2-} was then flushed from the cell, leaving the Te atomic layer.

Deposition of atomic layers of Te in this way, allowed multiple cycles of alternated Cd and Te deposition to be performed, with each cycle producing another monolayer of CdTe. The total amounts of deposited Cd and Te were subsequently determined using stripping coulometry. Figure 7E displays a typical stripping voltammogram after two cycles of CdTe deposition. The peak centered at -0.3 V corresponds to oxidative stripping of the Cd from the CdTe deposit, while the twin peaks at 0.3 and 0.5 V correspond to oxidation of the remaining Te. As the electrodes were cylindrical and difficult to take apart after each deposition in these early studies, the only analysis performed on the deposits was coulometric stripping.

At present, TLEC studies of the ECALE deposition of a number of II-VI compounds have been performed, including: CdS (61), CdSe (106), CdTe (155-157, 160, 161), ZnTe (279), ZnSe (279) and ZnS (279). In addition, ECALE deposition of the III-V compound GaAs (157, 252, 253) has been reported. Other compounds that should be amenable to deposition by ECALE include IV-VI compounds such as PbS, and the family of ternary compounds exemplified by CuInSe_2 (306).

In the rest of this section, studies of the deposition of Zn based II-VI compounds will be discussed in more depth, as an example of how TLECs have been used to develop initial ECALE cycles for a number of compounds. Figure 10 is a series of thin-layer voltammograms showing the deposition of the chalcogenides (S, Se, and Te) on polycrystalline Au. Prior to each voltammogram, a series of oxidation and reduction cycles were performed in H_2SO_4 to clean the

electrode, followed by recording a voltammogram. Clean electrodes produced voltammetry equivalent to that shown in Figure 7A. The TLEC was then immersed into the chalcogenide solution and an aliquot rinsed in. Figure 10A is the voltammogram for an aliquot of HTeO_2^+ , and displays two reduction peaks, at 0.2 and -0.1 V, correspond to Te UPD and bulk Te deposition, respectively. The peaks are fairly broad for a couple of reasons, one is that the Au electrode is polycrystalline and the oxidation reduction cycles used to clean the electrode also cause surface roughening (307-309). In addition, the peaks are broadened by significant changes in the HTeO_2^+ activity in the cell during the deposition.

At potentials just below -1.0 V, a reversible couple corresponding to reduction of bulk Te to Te^{2-} (Eq. 7), is clearly visible. As the Te^{2-} was formed inside the TLEC, it was trapped and quantitatively reoxidized to Te during the subsequent anodic scan. No corresponding reduction feature for the atomic layer of Te on the Au was observed, under any of the conditions investigated, indicating the dramatic stability of the first atomic layer.

An atomic layer of Te can be formed by deposition through the UPD peak in the HTeO_2^+ solution (at 0.0 V). The excess HTeO_2^+ can then be rinsed from the cell with an aliquot of pure electrolyte. Alternatively, the whole HTeO_2^+ aliquot can first be deposited (at -0.5 V), and then the potential can be shifted to -1.0 V, to reduce the bulk Te. The resulting Te^{2-} can be rinsed out of the cell with an aliquot of fresh electrolyte, to leave an equivalent Te atomic layer. This latter case is more consistent with the procedure used in an ECALE cycle.

Figure 10B is a corresponding voltammogram for the deposition of Se from a solution of HSeO_3^- . The voltammograms in 10A and B are very similar, with the main differences being that the potentials for Se features are shifted positively from the corresponding features for Te. The largest shift being for bulk Se reduction, which occurs at -0.4 V, over half a volt positive of the corresponding Te feature (Eq. 7).

As mentioned previously, Te^{2-} solutions are not generally stable, and Se^{2-} are similarly hard to work with. Na_2S solutions, however, are stable and, in principle, should make the oxidative UPD of S a straight forward process. Figure 10C is the voltammetry of an aliquot of a Na_2S solutions. Two cycles are displayed, the first initiated at -1.2 V and scanned up to -0.6 V and reversed. The oxidative UPD of S on Au is evident at -0.8 V. On the second cycle, the potential was scanned to 0.3 V, and reveals a very large feature for the oxidation of the remaining S^{2-} in the aliquot, forming bulk S. Above 0.3 V, the current began to increase again, as the deposited S converts to sulfate (61).

Voltammetry such as that in Figure 10 was used to determine potentials for formation of chalcogenide atomic layers, as a first step in development of ECALE cycles for forming the zinc chalcogenides. For instance, the first atomic layer of Te was easily produced by depositing between 0.0 and 0.1 V, while that for Se was formed at 0.2 V, and the S atomic layers were formed oxidatively between -0.6 and -0.7 V. Generally, deposits were given two minutes to form before the reactant solutions were flushed from the cell. Several rinses with the corresponding blank solutions were performed and then the ZnSO_4 solution was introduced.

Figure 11 is a series of voltammograms for the deposition of Zn on atomic layers of Te, Se, and S. A definite trend in the Zn UPD peak potentials is evident, going up the periodic table. Zn is hardest to deposit on the Te atomic layer, where deposition is not initiated till -0.7 V. A well defined Zn UPD peak is evident on the Se layer, initiated near -0.5 V, while Zn deposition on the S atomic layer begins near -0.3 V. These numbers are consistent with differences in the free energies of formation of the three compounds: -115.2, -173.6, and -200.0 kJ/mole for ZnTe , ZnSe , and ZnS respectively (310). For a two electron process, these differences in the stabilities of the compounds correspond to 0.30 V and 0.14 V respectively, in line with the shifts observed in Figure 11.

Subsequent studies of Zn chalcogenide deposition, using the TLEC, involved coulometric stripping of deposits to characterize elemental coverages/cycle as a function of cycle conditions, specifically: deposition potentials and solution compositions. Those experiments proved tedious, with each cycle requiring about 12 steps (Figure 12), but worthwhile. Figure 13 displays stripping curves for deposits of ZnTe, ZnSe, and ZnS, each formed from four ECALE cycles. The same trend in Zn stability, observe in the deposition scans (Figure 11) is seen here in Figure 13. That is, that Zn is easier to strip from ZnTe than from ZnSe than from ZnS, in line with the free energies of formation. Examination of Figure 13 also reveals that there are generally two Zn stripping features in each scan. This is seen most clearly for ZnTe (Figure 13A) where the low potential peak (-0.7 V) grows in first as a function of the number of cycles performed, but does not significantly increase in size after the second cycle. Instead, the higher potential stripping feature (-0.3 V) starts to grow. As the number of cycles is increased further, this second peak grows and shifts to still higher potentials. A simple explanation would be that the first peak represents the top layer(s) of Zn atoms, those not completely coordinated to Te, while the second peak results from stripping the more highly coordinated interior Zn atoms. Studies where the first peak is stripped and then the potential held for 5 minutes, just prior to the potential needed to strip the second peak, evidenced the full second stripping feature, when the stripping scan was resumed. This may suggest a thermodynamic effect, as opposed to a problem with the kinetics of transporting interior Zn atoms or ions out of the Te matrix.

Another trend in Figure 13 involves the size of the valley between the Zn and chalcogenide stripping features, where that for ZnTe > ZnSe > ZnS. The width of the valley in each case shrinks as the number of cycles is increased, due to the tendency of the Zn stripping feature to broaden to higher potentials as the coverage increases. As the Zn feature continues to broaden, it eventually runs into the chalcogenide stripping feature, and it becomes difficult to independently determine the coverages of the two elements coulometrically. In the present studies, clear

problems were encountered after 16 cycles of ZnTe, after 10 cycles of ZnSe, and after only 4 cycles of ZnS (Figure 13).

In the next series of graphs, the number of monolayers of an element deposited per cycle is plotted as a function of the potential used to deposit one of the compound's elements, with other cycle conditions held constant. The coverage nomenclature used here can be a little confusing. The discussion is based on a simple model for the deposition of the elements on a polycrystalline Au substrate. The model states that it takes about $\frac{1}{2}$ monolayer (ML) of each element (where a ML would be that amount of an element required to deposit one atom on each Au surface atom), to form one monolayer of the compound. That a $\frac{1}{2}$ ML of each element should be deposited each cycle is based on the idea that a compound monolayer is equivalent to a half unit cell thick slab of the compound in the zinc blende structure. This model is very simplistic, and based on a large number of assumptions. In addition, the coverages should not be taken too literally either, as their measurements were made with a number of assumptions, such as the actual number of Au surface atoms and the background correction used in the coulometry. Given the above statements, the data does provide an idea of the trends in growth that can be expected for a given variable, and of the conditions that might be used for subsequent flow cell studies, such as described in the next section.

Figure 14 is a graph of the Zn and S coverages/cycle resulting from ZnS formation. Each point was determined after execution of three ECALE cycles, as a function of the S deposition potential. The Zn deposition potential was held constant at -0.9 V. The Zn and S curves clearly parallel each other, but do not coincide well. One possible explanation for the deviation is that there was a problem calculating the elemental coverages. Recall Figure 13C, where the Zn stripping feature overlapped significantly with the S oxidation feature after only four cycles. If some of the Zn was, in fact, stripping with the S feature, the Zn coverages would be seen as lower than expected. There would, however, be little change in the calculated S coverage as S oxidation to sulfate is a six electron process:



while Zn oxidation is a two. A second explanation for the discrepancy would be that there is something about the structure of the initial few monolayers that is not adequately explained as being $\frac{1}{2}$ ML of S on $\frac{1}{2}$ ML of Zn. Regardless of the discrepancy between the Zn and S coverages in these initial TLEC studies, the trends appear valid. Ideal ALE behavior is frequently represented by an "S" curve (17-21). That is, for deposits formed as a function of a given variable, at one extreme the coverage will be too high, while at the other extreme the coverage will be too low. In-between, ALE behavior is frequently signified by the presence of a plateau, where the coverages are independent of the particular variable, and the growth is truly controlled by surface limited reactions alone. In Figure 14, at the most negative potentials, below -1.1 V, insufficient S is being deposited with each cycle, and since the Zn requires the presence of S to deposit, both coverages begin to drop. At potentials above -0.9 V, both coverages start to increase, as some bulk S begins to deposit. Those increases, however, start to drop off at potentials above -0.7 V as it becomes difficult to hold the Zn on the surface while the S is depositing. The conclusion drawn from this study is that S should be deposited at potentials between -1.1 and -0.9 V, where there is a small plateau corresponding to surface limited control over the deposition.

Given the results shown in Figure 14, the Zn potential dependence was investigated while holding the S deposition potential at -1.0 V (Figure 15). The dependence on the Zn potential is not dramatic, but it again shows some "S" curve behavior. At low potentials the Zn coverage builds up as the bulk deposition potential is exceeded, and the corresponding S coverage stays one for one. At higher potentials, the Zn coverage falls off, followed by the S coverage. A Zn potential of -0.9 V was used in Figure 14, resulting in significant differences between the Zn and S coverages at all potentials. It appears from Figure 15 that use of -1.0 V for Zn deposition may result in deposits closer to the desired $\frac{1}{2}$ ML/cycle of each element.

Figure 16 is a graph of Zn and Se coverages/cycle for ZnSe deposits, as a function of the Zn potential. The Se deposition was carried out by first depositing a two monolayers at -0.9 V, and then reducing off the excess at -0.9 V. The drop in coverage above -0.8 V is due to decreased stability of the Zn (Figure 11). A plateau in both the Zn and Se coverages is evident between -1.2 and -0.9 V, however the Zn coverage/cycle is nearly 3/4 of a ML, while the Se remains at 1/2 ML. The standard potential for Zn deposition is about -1.0 V (vs. Ag/AgCl), and given that a mM solution of ZnSO_4 was used, bulk deposition would not be expected until -1.1 V. The reason for the disparity between the Zn and Se in the plateau region is not clear. It is interesting to note that in Figure 16 it is the metal coverage that is high, not the chalcogenide, as was observed for ZnS (Figure 14). It is probable that the conditions used to form the Se atomic layers were not optimized and needed more study. Given the data in Figure 16, however, the optimal Zn deposition potential appears to be between -0.9 and -0.7 V, with -0.8 V looking best.

Figure 17 is a graph of the Zn and Te coverages/cycle as a function of the Zn deposition potential. Atomic layers of Te were formed by first depositing a little more than a monolayer of Te at -0.8 V, and reducing off the excess Te at -1.1 V, in a blank electrolyte solution. The Te coverage/cycle looks low, about 1/3 ML per cycle at all potentials. This is not the expected 1/2 ML behavior, and indicates that the dependence of Te coverage on its deposition conditions needs more study. There is a short plateau between -1.1 and -1.0 V, similar to that seen in Figure 16 for ZnSe formation, where again the Zn coverage is significantly higher than the corresponding chalcogenide. However, between -0.95 and -0.8 V the coverages/cycle for Zn and Te coincide at about 1/3 ML, per cycle. Above -0.8 V, the coverage of Zn falls off as expected. It is not clear why the Te coverage remains high at -0.7 V, when the Zn coverage is decreasing. It does point out the need to better understand the Te atomic layer formation part of the ECALE cycle. This problem with the Te atomic layers is probably at fault for the low CdTe coverages observed with the automated system, discussed in the next section. Given the data in Figure 17, a Zn deposition potential of near -0.9 V is probably a good starting point for subsequent studies.

Finally, given the starting conditions determined from Figures 14-17, the dependence of coverages on the number of cycles performed was studied (Figure 18). A linear dependence is expected for an ALE process, twice the number of cycles should result in twice the coverage. Linear behavior is evidenced in each of the graphs in Figure 18, given the error inherent in the measurements. The slopes in the graphs of ZnSe and ZnS formation are very close to the expected $\frac{1}{2}$ ML per cycle. In the case of ZnTe the slope is a little low, in line with the low Te atomic layer coverages discussed previously with regards to Figure 17. In all three graphs, there is some negative deviation from the line at the higher number of cycles. This may be due to problems in quantifying stripped amounts as the peaks start to overlap. It may also be a problem with operator error, as each cycle involves 12 steps (Figure 12), and the more steps performed, the more chances for mistakes.

The deviations from ideality evident in the studies above may be very important and real, or they may be a result of problems with the operator, with quantification, or with the experimental set up. They do, however, provide a direction, for an initial ECALE cycle to be used in the next stage: an automated deposition system to form thin films that can be analyzed with techniques other than coulometric stripping.

III. THIN FILM FORMATION USING ECALE

In considering the limits to the quality of deposits that may be formed electrochemically, a number of issues come up, including the quality of the reagents used: reactants, electrolytes, solvents and substrates. Most of the reagents presently used in the formation of thin films of these same compounds by other commercial methods, can be used in the formation of thin films electrochemically. Some of the same substrates used to form deposits via CVD or MBE can also be used for electrodeposition. Reactant precursors used in an electrochemical method are generally ionic, and thus differ from the volatile species used in a metal organic chemical vapor

deposition (MOCVD) reactor, but the absolute amounts used in the two cases can be very similar. In addition, if electronic grade metals are the basis for the CVD precursors, then the same grade metals can serve as the basis for the ionic precursors used in an electrodeposition method, generated by electrochemical dissolution.

Another frequently raised concern about purity involves the fact that electrodeposition takes place in a condensed phase, a solvent in contact with the substrate and deposit. The solvent used for the present studies is water, and water is used copiously in the processing of compounds and devices. The electronics industries are well aware of how to obtain very high purity water.

The point is that the purity issues in an electrodeposition method are the same issues being addressed in presently used methodologies. There does not appear to be anything inherently dirty about electrodeposition.

A second factor controlling the absolute quality that can be achieved electrochemically, is the mechanism. As discussed in the introduction, there may be fundamental flaws in the precipitation and codeposition methodologies (although, as mentioned, there have been some surprisingly good quality films produced recently by codeposition (38, 39)). In an ideal ECALE cycle, each element should be deposited under equilibrium conditions, from a separately optimized solution. In addition, the deposition process can be thought of as decomposed into a series of steps, each step being a variable in the cycle, and thus an adjustable parameter. This provides a large parameter space to work with, and the cycle can serve as a window into the mechanisms of compound electrodeposition in general. Most other electrodeposition methodologies are more limited (Table 1).

The logistics of forming thin films using ECALE revolve around alternating the solutions and potentials in a cycle. As stated earlier, manually forming deposits with much over 10 cycles proved tedious. Some work in this area has thus necessarily focused on development of an automated deposition system, where each cycle can be performed reproducibly.

Initially, a thin layer flow cell (Figure 19) was used in this group, to study the ECALE formation of compounds (158) and in studies of electrochemical digital etching (312, 313). Wei and Rajeshwar (130) used a flow cell system to deposit compound semiconductors as well, however the major intent of that study was to form superlattices by modulating the deposition of CdSe and ZnSe. Their study appears to be the first example of the use of a flow electrodeposition system to form a compound semiconductor superlattice.

Besides the electrochemical flow cells just mentioned, other hardware for sequential solution deposition scenarios has been developed to form deposits by the SILAR method (Figure 2), described in the introduction (28-32). Related hardware has also been used by workers concerned with the construction of magnetic superlattices, of Cu and Ni (314, 315). One method for forming Cu-Ni superlattices is referred to as the two bath method, and it involves using separate baths for depositing the individual layers, and alternately exposing the substrate to the two baths. The two bath instruments were not designed to deposit atomic layers necessarily, but alternate 1 nm or thicker films of Cu and Ni. One particularly interesting two bath instrument, made use of a rotating deposition cell, where the substrate was rotated over two distinct deposition zones, with rinsing stations in between. Thus, in a single cycle, a full period of the superlattice was produced (314). An analogous system might be made to work for the formation of deposits using ECALE, if sufficient control over deposition potentials and rinsing conditions can be achieved.

As mentioned above, initial work in automating ECALE involved use of a thin-layer flow cell deposition system. A thin layer cell was chosen as it allowed very small amounts of solution to be used in each step, minimizing the total volume of solution used to form a deposit. Development of an automated thin layer flow deposition system began early on and proceeded by a long sequence of incremental improvements (Figure 19) (158).

The hardware consisted of a set of low volume pumps, attached to Pyrex glass solution reservoir. Two solution reservoirs were used for each element, one for the reactant precursor and

one for a corresponding blank solution, to rinse the system. The pumps fed a valve which selected the solution to be sent to the cell. The cell consisted of two plates (Figure 19) between which the substrate and a gasket were sandwiched. A small slot cut in the gasket material was used to define the deposition cavity. A variety of gasket materials were used, including: Teflon, silicone rubber, and Viton rubber. Teflon is inert, but does not seal as well as the other two materials. The cell plates were compressed in a steel vice, reproducibly tightened using a torque wrench. The plates were plumbed in a number of different patterns, but were generally tapped 1/4"-28 so that conventional low pressure Peek fittings and tubing could be used. The basic design involved solution flowing in one side of the cavity and out the other. Additionally, a small compartment housing the reference and auxiliary electrodes was attached. Several positions for the compartment were investigated, however it was generally placed down stream of the cell so that products from the auxiliary and leakage from the reference would not encounter the substrate. The major drawback to the down stream placement of the compartment appears to be IR drops associated with the thin layer. A second position for the compartment was in the center of the slot in the face-plate. This position cut down on IR drop problems, but required a porous Vycor plug be inserted into the face plate. The plug may have resulted in some cross contamination, from ions trapped in the Vycor.

A typical program, used in forming these deposits is shown in Figure 20. The top of the figure shows the aliquots of solution being introduced into the flow cell, and times involved. The bottom half of the figure shows the potentials applied to the cell, and the times. In Figure 20, the initial step was to introduce 5 aliquots of the Te deposition solution while the potential was at open circuit. Open circuit was used during the introduction so that the Te did not deposit differentially across the substrate surface, such as at the cell entrance. The Te deposition solution was then held in the cell at -0.8 V for 60 sec, while all the Te was deposited. Open circuit was then used again to introduce the Te blank solution, so that excess Te solution in the tubing could be flushed through the cell, without it depositing differentially across the surface. Next, the Te

blank was held quiescent in the cell at -1.25V, while excess Te was reduced to Te^{2-} . The resulting Te^{2-} was flushed from the cell with more Te blank, again at open circuit. Next, the Te blank was then replaced with a Cd blank, at -0.6 V, and then 5 aliquots of the Cd^{2+} solution were introduced at open circuit. Finally, the Cd^{2+} solution was held quiescent in the cell for 60 sec at -0.6 V, and then flushed from the cell using the Cd blank and then the Te blank to end the cycle.

The principle of ALE is that deposits are formed one atomic layer at a time, using surface limited reactions. That appears to be the case with ECALE. The name electrochemical atomic layer epitaxy, however, suggests that the deposits should be epitaxial, and the first 100 cycle deposits appeared anything but epitaxial (Figure 21A). These initial deposits looked like they were composed of a large number of particles which fell out of solution.

There turned out to be several reasons for the particles, the first being conproportionation. As described in the introduction, conproportionation has been a problem with the codeposition of Se containing compounds for a long time (Eq. 2) (122, 132), as the deposition potentials used were sufficiently negative to result in some Se^{2-} formation. As both Se^{2-} and HSeO_3^- were present in solution at the same time, conproportionation resulted in the formation of traces of elemental Se in the deposits. Since Te is reduced to Te^{2-} at a significantly more negative potential than Se is to Se^{2-} (Figure 10), conproportionation was not a significant problem during codeposition studies of CdTe (Table 1).

The initial program, used to deposit the CdTe film shown in Figure 21a, involved a couple of cycle steps that were different than those shown in Figure 20. Initially, the HTeO_2^+ aliquot was held at a potential where the atomic layer of Te was formed directly. That is, a more negative deposition potential was used so that the atomic layer would form, and all the excess HTeO_2^+ would then be reduced to Te^{2-} in a single step (Eq. 8). That procedure, however, resulted in both HTeO_2^+ and Te^{2-} being present in the cell at the same time and thus conproportionation. It appears that a large number of the particles shown in Figure 21A were the

result of forming Te nuclei by conproportionation, which subsequently settled out on the surface and were coated with successive monolayers of CdTe.

The solution to the conproportionation problem was adoption of the program shown in Figure 20, where the Te atomic layers were deposited using the two steps described in the last section: initial deposition of several atomic layers worth of Te at a potential sufficiently positive that no Te^{2-} is formed (Eq. 6), and then reductive dissolution of excess Te to Te^{2-} at a second more negative potential in the Te blank solution (Eq. 7). The result of this program change was formation of the deposit shown in Figure 21B, for 100 cycles.

In addition to conproportionation, there were indications that some of the particles shown in Figure 21A resulted from cross contamination. There were several problems with the pumps, valves and cell design which appear to have resulted in some cross contamination. Homogeneous precipitation of CdTe should result any time Te^{2-} ions mix with Cd^{2+} . The most significant cross contamination problem came from a solenoid actuated Teflon distribution valve, used to select the solution sent to the cell. The internal construction of the valve (Figure 22A) resulted in a significant amount of intermixing. That valve was subsequently replaced by a rotating distribution valve (Figure 22B) which eliminated the intermixing. After several changes in valves, pumps and plumbing, cross contamination was decreased significantly, as can be seen from the deposit shown in Figure 23. Figure 23 is a deposit made with 100 cycle in a system using the rotating distribution valve, and a program very close to that shown in Figure 20. There are still a number of obvious defects and particles in the deposit, but a majority can be attributed to the commercial polycrystalline Au foil used in the early studies, which had a very high defect density to begin with.

The decision on which substrates to use is continuing. The surface chemistry of Au in solution is relatively well known. The Au foil was rugged and could be reused, the problem was the surface finish. Polishing, etching, and electropolishing were all investigated, but resulted in too much variation from piece to piece. There are a large number of reports in the literature that

high quality Au surfaces can be formed on mica (316-319) and studies were performed. The problem was that the Au would frequently lift off during long runs due to the large number of rinses performed. The best solution, so far, has been the use of polished Si(100) wafers coated with Au, with a thin layer of Ti to promote adhesion. Switching from foil to these wafers greatly enhanced reproducibility, as variations in the substrate were no longer a significant factor. Not that the substrates are perfect, or that they do not affect the quality of the deposit, but under visual inspection, the resulting deposits appear reproducible.

The images in Figure 24 were all run on Au on Si wafers using the thin layer flow cell deposition system. The Figure in 24A is an optical micrograph of one of the best deposits formed with the thin layer flow cell system.

In addition to the problems discussed above, there were several others associated specifically with using a thin layer flow cell deposition system, including: edge effects (Figure 24B), effect of bubbles (Figure 24C), and IR drop problems. The bubbles appeared to result from small amounts of gas that either leaked in through the fittings, became entrained in the solution, or that were dissolved in the solutions to begin with. The bubbles appeared during the deposition and significantly interfered with the fluid flow (Figure 24B and C). The edges of the gasket also cause problem with fluid flow, that showed up as decreased deposition near the deposit edges (Figure 24C). IR drop problems in the cell were always suspected, due to the dimensions of the cavity. Measured values of the IR drop were around 1 k Ω , depending on the configuration and solution composition. However, to investigate the importance of the IR drop, deposits were formed with the auxiliary/reference electrode compartment positioned in the center of the cell face-plate, and both at the outlet and the inlet, with no obvious change in the deposits.

Overall, the main problem with the thin layer flow cell studies was reproducibility. It was nearly impossible to produce equivalent deposits, two days in a row. The investigations became an endless series of tests to figure out how to improve the substrate, get rid of bubbles, get the right gasket material, and deal with possible IR drop problems. Although some problems were

solved and some deposits formed, very little progress was made towards a better understanding the mechanism of compound electrodeposition, or ECALE (158).

The best solution to the bubble, edge, and IR drop problems was to switch to a larger cell (Figure 25), to get rid of the thin layer configuration (Figure 19). The two obvious drawbacks are that more solution is needed for every rinse, and that potential control is lost between each rinse, using the cell design shown in Figure 25. The solution volume problems have not been addressed as yet. So far, the problem with loss of potential control with each rinse does not appear to be a big problem. However, there are several cell designs being considered that allow potential control during solution exchange. The design in Figure 25 is simple and straightforward, consisting of an H-cell with a small rectangular portion at the bottom for the substrate. The compartment for the reference and auxiliary electrodes is attached across from the deposit, via a fine glass frit. At the bottom of the H-cell, the distribution valve is attached using capillary tubing. The valve is used to both fill and drain the cell. Having the frit in the cell is somewhat problematic, in that some ions get held up in the frit, resulting in cross-contamination. At present this does not appear to be a major problem. The rest of the hardware is very similar to that used for the thin layer flow cell system (Figure 19). Each solution reservoir has a separate pump feeding into the distribution valve. The computer is used to select the solution to be delivered via the pumps and distribution valve. The control program is essentially the same as that shown in Figure 20, except that the aliquot sizes are larger.

Immediate benefits of switching to the larger volume cell (Figure 25), include the formation of larger area deposits, 2-3 cm², verses the 0.1-0.2 cm² deposits obtained using the thin layer flow cell. The thicker layer of solution eliminated problems with IR drops, bubbles and edge effects, except at the top of the deposit. Some non-uniformity at the top of the deposit resulted from small variations in the levels of different solutions pumped into the cell. Rinse solution levels, for instance, were always raised to a slightly higher level then the reactant solutions, in order to make sure that the reactants were completely removed after each deposition.

Given reproducibility from run to run, the dependencies of deposit composition and structure on various ECALE cycle variables were investigated, including: deposition potentials, deposition times, temperature, solution compositions, rinsing procedures, substrate dependence, annealing, and photo-effects. CdTe serves as a test compound in these studies, as it was the first compound studied by this group and it is the compound about which the most has been learned. Initial TLEC studies of CdTe formation, similar to those described in the last section for the formation of the Zn chalcogenides, involved manually performing 1-10 cycles and stripping the deposits to determine the total amounts of Cd and Te (160, 161). Some thin films were formed as well using the thin layer flow cell deposition system described above (158). In addition, UHV-EC studies of the formation of the first few monolayers of CdTe on Au electrodes were performed (159, 162, 320).

One of the most significant benefits of having these larger deposits, is that an array of analytical techniques can be used to investigate the deposits. The first analysis, however, is always made visually. Visual inspection of deposits formed with from 50-200 cycles can be used to get a clear idea of the homogeneity, as a good deposit will have a homogeneous color, except at the very top, discussed above, and on some deposits at the bottom, where drops of solution sometimes hang up. These interference colors are quite striking, and a very good indicator of deposit thickness. The deposits with the H-cell are visually evident after only 15 cycles, brown after 50, mauve after 100, purple after 150, and dark blue after 200 cycles. Our standard deposits are formed with 200 cycles, and the dark blue colored deposits appeared to be the best quality formed under these conditions.

The potential used to deposit Cd in the formation of CdTe is an important factor in determining deposit morphology and composition. Figure 26A is a graph of the relative coverages of Cd and Te in deposits formed using different Cd deposition potentials. The coverages were measured using electron probe microanalysis (EPMA). Absolute coverages by this technique are difficult to determine, as the thin CdTe films constitute only a small portion of

the sampled volume. The 30 kV electron beam stimulates X-ray emission from up to several μm deep in the substrate. However, for the thin films, the Cd and Te signals are directly proportional to their coverages, having been corrected for the elemental sensitivity factors determined using a single crystal of CdTe. A sigmoid curve is apparent in Figure 26, suggesting that reactivity over a large potential range is controlled by a surface limited reaction. Figure 27 displays the stoichiometry of the deposits, the Cd/Te ratio, as a function of potential. At -0.5 V, and above, the coverages of Cd and Te are down, as well as the Cd/Te, indicating the potential is too positive for the Cd to deposit. Between -0.55 and -0.65 V, there is a short plateau in the coverage (Figure 26A), where the Cd/Te ratio is 1. The ratio remains 1 up to -0.75 V (Figure 27), even though there is a significant increase in both the Cd and Te coverages between -0.65 and -0.75 V. Between -0.75 and -0.85 V, the coverages continue to rise, with the Cd rising faster than the Te, and the Cd/Te ratio becoming 1.5. Below -0.85 V the coverage of Cd increases still more rapidly, as bulk Cd is deposited.

X-ray diffraction (XRD) has also been used to study the deposits used in Figures 26 and 27. Figure 28 is a set of XRD patterns for which the Cd deposition potential had been adjusted. A thin film attachment was used with a Sintage diffractometer so that glancing incident XRD patterns could be obtained. It was determined experimentally that Au and Si substrate features could be essentially eliminated using an incident angle near 0.25° . As expected, use of a Cd deposition potential of -0.4 V resulted in no CdTe deposit. However, a strong feature corresponding to zinc blende CdTe(111) planes was evident near 24° for deposits formed using a Cd deposition potential of -0.55 V or below. In addition, two significantly smaller peaks, characteristic of the CdTe(220) and (311) planes, were observed near 40° and 47° respectively. Clearly, the deposits show a predominance of (111) oriented crystallites. Hexagonally oriented deposits are expected, given that the Au on Si substrates used had a predominance of (111) surface facets. However, recent work using single crystal Au substrates oriented to the (111), (100), and (110) planes, all showed the same preference for forming CdTe(111) planes

[ref.(311)]. Also evident in Figure 28, for deposits formed below -0.85 V, is an array of peaks assignable to Cd, indicating that the potential for bulk Cd deposition was exceeded.

By simply adjusting the Cd deposition potential, a broad range of deposit compositions and morphologies were formed. The fact that no deposits formed when the Cd potential was too high, clearly indicates the dependence of Te deposition on the previously deposited Cd. Using slightly lower potentials, where Cd UPD does occur, there is a 0.2 V plateau (Figure 27) where stoichiometric deposits were formed, however in Figure 26A only a 0.1 V plateau in coverage is evident. At present, the best deposits made with this cell appear to be those formed using Cd deposition potentials in that 0.1 V window, between -0.55 and -0.65 V.

Ideally, a coverage of one monolayer of CdTe should be formed with each cycle. Recently, studies were performed where the deposits used to perform the EPMA investigations (Figures 26A and 27) were dissolved and used to run investigations of the total amounts of Cd and Te, using ICP-MS. Those results, for deposits formed at different Cd UPD potentials, are shown in Figure 26B. As discussed above, the plateau between -0.55 and -0.65 V result in what looks to be the best deposits. The ICP-MS results give absolute coverages, and from Figure 26B it is evident that the optimal deposits are not 1 ML/cycle, but more like 0.4 ML/cycle (311, 321).

That other than 1 ML/cycle appears to be the optimal deposition rate is not unusual for ALE, however (17-21). The reasons for this low growth rate in the present studies are not yet clear. Similar studies in the formation of CdSe have been shown to result in growth rates of 0.8 ML/cycle. As described in the next section, the lattice match of CdSe with Au is much better than that of CdTe with Au, suggesting that lattice matching may be a controlling factor. There are, however, significant differences in the potentials that can be used to deposit the chalcogenides in these two cycles, and they may be the controlling factors (311, 321). The rinsing steps are presently under study as well.

CdTe deposits formed using Cd potentials between -0.65 and -0.75 V appear to have the best morphology after 200 cycles. SEM micrographs for some of these 200 cycle deposits (Figure 29) show changes in surface morphology on the 10 μm scale as a function of the Cd deposition potential. For the most part, the deposits corresponding to the plateau between -0.55 to -0.65 V look very flat, with a few small white specks scattered across the surface. The larger feature, observed in Figure 29B (-0.6 V), was used by the SEM operator to focus the microscope, and is probably a dust particle. For deposit formed at -0.7 V, the number of small particles has increased significantly, and suggests the beginning of three dimensional nucleation and growth, clearly outside ideal ALE conditions. The flowery deposits obtained with Cd potentials below -0.8 V are consistent with the formation of some crystalline Cd. Figure 30 shows two images taken with a high resolution field emission SEM. The first image shows the clean Au on Si substrate. Evident is a series of little bumps, and Figure 31 is a scanning tunneling micrograph (STM) of the same surface. From Figure 31, and others, it is apparent that the substrates being used are optically flat, yet they are covered with 40-50 nm wide bumps that are about 20 nm in height. Higher resolution STM images have shown these bumps to be crystallographically ordered, but to have a very high density of short terraces. That is, atomically resolved images of the terraces show them to be well ordered and (111) oriented. The second field emission SEM image (Figure 30B) shows an equivalent substrate on which 200 cycles of CdTe deposition has been performed, using a Cd potential of -0.6 V. The similarity of the two images is encouraging, as it is consistent with epitaxial deposition. The deposits have essentially the same morphology; on the scale of the micrograph, however, the image of the deposit (Figure 30B) is a little less clear than that of the clean substrate (Figure 30A). The difference might be a simple focus problem. Alternatively, it could be a charging problem or a difference in the electron scattering characteristics of the two surfaces, due to the presence of the compound. However, given the morphology evident in Figure 31, a high substrate induced defect density is expected in the deposits. The difference between the images in Figure 30 may result from the presence of a large number of small CdTe crystallites induced by the lattice mismatch with the Au and substrate step

density. A problem with the CdTe deposits matching up with the highly stepped surface could help account for the low growth rate described above. Work is underway to switch substrates. In the case of Au substrates, it is well known that Au on mica can have very large terraces, as can Au on glass under certain sets of conditions.

As previously discussed, Te atomic layer formation in the present cycle is a two step process. The first being deposition of a few monolayers of bulk Te, while the second involves reduction of excess Te from the surface in a blank solution at fairly negative potentials. The dependence of the deposit composition on the potential used to form the first few monolayers of bulk Te, is graphed in Figure 32. At potentials above -0.7 V, the coverage per cycle of both Cd and Te drop off. The potentials are well within the range for bulk Te deposition, so the decrease is not a problem with depositing Te. The problem is more likely that Cd is being lost while the Te is being deposited, as the potentials are sufficiently positive that the Cd may not be stable. Deposits formed in the plateau region, between -0.8 V and -0.7 V, were equivalent to the optimal deposits previously formed. Using potentials more negative than -0.8 V, introduced problems with conproportionation again (Eq. 2), as evidenced by the decrease in the Cd/Te ratio (Figure 33), as some Te^{2-} is formed at these low potentials which then reacts with the HTeO_2^+ to form Te particles. Alternatively, the decreased Cd/Te ratio may simply result from too much Te deposition, so that the resulting Te layers are not completely reduced under the condition used in Figures 32 and 33.

The second step in the formation of atomic layers of Te is the reduction of the excess Te. Figure 34 shows, at least for the first Te atomic layer on Au, that bulk Te is reduced from the surface at potentials below -0.8 V. The reduction is rapid, occurring within a few seconds, for a reduction potential of -1.4 V (Figure 35). The graph in Figure 36 shows the coverages of Cd and Te for a series of deposits made with 200 cycle each, as a function of the potential used to reductively remove the excess Te. At potentials above -1.0 V the coverage per cycle goes up, as expected, since not all the bulk Te deposited in the previous step is stripped. The corresponding

Cd/Te ratio also drops (Figure 37) as the Cd is not reacting quantitatively with the excess Te. Stripping the Te at potentials below -1.1 V results in optimal deposits. The plateau in Figure 36 is large, stretching to below -1.4 V. It might be expected that even the Te bound to Cd could be stripped, given a sufficiently negative stripping potential. The fact that the coverage does not drop is an indication of the stability of the Te bound up as CdTe. In addition, the electrode is somewhat non-polarizable, due to solvent decomposition in the borate solution, preventing the substrate potential from adjusting sufficiently negative to reduce Te bound to Cd.

One of the attributes of an ALE growth mode, is that the number of cycles determines the thickness of the deposit. Double the number of cycles and you double the thickness of the deposit. Figure 38A is a graph of the relative coverages of Cd and Te as a function of the number of cycles. The graph is linear as expected, passing through the origin. The stoichiometry of the 1000 cycle deposit is a little Te rich, however. XRD of this deposit showed that elemental Te was clearly present, suggesting that the conditions developed to deposit 200 cycles may not have been optimal for the deposition of 1000, that the optimal conditions can change as the deposit grows thicker. Similar studies of CdSe deposition show linear growth as a function of the number of cycles (Figure 38B). For CdSe (Figure 38B), the 1000 cycle deposit shows no elemental Se with XRD but does show a slight excess of Se with EPMA. Very few 1000 cycle deposits have been formed so far, and further studies are needed to understand these changes in deposit composition.

These changes in composition could simply require fine tuning of the deposition cycle for the thicker deposits. Alternatively, the conditions needed to grow optimal layers may change as the deposits get thicker. One of the nice things about using the automated deposition system is that the program could be easily modified so that a small change is made in a particular step in the deposition cycle, with each cycle as the deposit is formed. The Cd potential could be changed a mV each cycle as the semiconducting film grows. There have been some interesting reports describing the co-deposition of CdTe, where the open circuit potential was checked every few

minute during the codeposition of CdTe, and the deposition conditions were adjusted accordingly during the deposition (289). An analogous feedback procedure might be incorporated into an ECALE deposition cycle if some measurement step can be devised.

Presently, work is continuing on formation of CdTe thin films in an effort to understand the dependence of the deposit composition and structure on the cycle variables. Recent work involving changes in the cell design, and deposition program has resulted in 0.95 monolayers of CdTe being deposited with each cycle, and publication of those results will be forth coming. In addition, work is being performed on the deposition of ZnS, ZnSe, CdS and CdSe.

Raman studies of CdS films formed using ECALE have been performed by Shannon et al. (59). Those studies concluded that good quality bulk CdS was being formed and in a layer by layer manner.

IV: SURFACE CHEMISTRY IN THE ECALE CYCLE

The macroscopic approach to investigating ECALE, forming thin films and analyzing them, was discussed in the last section. In this section, studies designed to provide an atomic level description of the growth of atomic layers in an ECALE cycle is be described.

As mentioned, coverage is defined as the ratio of the number of deposited atoms relative to the number of substrate surface atoms. In the studies presented in the previous two sections, polycrystalline Au electrodes were used. Most of the work described in the present section has been performed using Au single crystal electrodes. Each low index plane of Au has a different atomic surface density so that 1/2 coverage corresponds to a different number of atoms/cm² for each plane. Each compound studied has a number of possible orientations which can be adopted at the deposit-substrate interface. Some compounds have multiple possible crystal structures,

CdSe for instance can crystallize in the Zinc Blende or Wurtzite structure. Deposition of a "monolayer" of a compound on Au is thus a relative term. In addition, there are questions concerning the dimensions and quality of the interface: is there compression or expansion of the deposit structure to account for a lattice mismatch with the substrate? What are the densities of steps and defect sites? How clean is the substrate? How good is the assumption that each element is nucleating and growing two dimensionally, that no three dimensional growth is taking place? It should be clear that when 1/2 ML coverage on a polycrystalline substrate is discussed, it is an approximation. To say more requires detailed studies, such as described below, of the individual atomic layers on single crystal substrates. The structure, composition and morphology of the substrate and individual atomic layers of each of the elements making up the compound are being investigated with the intent of understanding their influence on deposit quality.

Studies carried out in this group concerning surface chemistry in an ECALE cycle have involved ultra high vacuum-electrochemical (UHV-EC) techniques (322), and scanning tunneling microscopy (323-329). The point of the UHV-EC techniques is to study the structure and composition of electrodes using surface sensitive electron spectroscopes such as Auger electron spectroscopy (AES) and X-ray photoelectron spectroscopy (XPS or ESCA), as well as low energy electron diffraction (LEED). LEED provides diffraction information for surface unit cells, while elemental coverages can be determined using AES. In addition, AES is very helpful in identifying any contamination problems, i.e., the presence of C or O signals. A carbon signal indicates that something was not clean, while an oxygen signal can indicate that some electrolyte has been "emersed" (withdrawn from solution) with the sample or that the surface has been oxidized. XPS provides information on the surface elemental composition, as does AES, but is generally slower. XPS has the advantage, however, that it can provide information on the oxidation states of surface species, and is used mostly to answer question concerning the bonding environment of elements on the surface (330, 331).

The idea of UHV-EC is to perform electrochemical experiments inside an antechamber attached to a UHV surface analysis instrument, so that substrates can be examined using the above techniques both prior to and after electrolysis, without their leaving the instrument or being exposed to air (Figure 39). The challenge is to perform experiments where the surfaces studied closely resemble those that existed under potential control in solution, and thus gain information on nature and mechanisms of interfacial process. There are significant limitations, however, and careful work and controls must be applied for the resulting data to be meaningful. For instance, if an adsorbed species is to be examined, it must be covalently, or ionically, bounded to the surface, as physisorbed species (ΔH less than 10 kcal/mole) are easily pumped away when the substrates are transferred to UHV for analysis. UHV-EC is thus a method best suited for examining specifically adsorbed species, or electrodeposits. In addition, there are problems associated with studies in some potential regimes. Electrodes emerged from aqueous solutions at potentials below the formal potential for hydrogen, stand a good chance of undergoing spontaneous oxidation upon loss of potential control. Indications of this are the appearance of a surface oxide where a reduced surface should have existed in solution, or the dissolution of deposits that would otherwise be stable in solution, under potential control (332). Another general problem with UHV-EC studies is that the concentrations of reactants and electrolytes in the solutions must be kept low, generally below mM, as when the substrate is emerged from solution it brings with it a layer of solution, referred to as an "emersion layer." Upon evacuation, a layer of reactant or electrolyte can be left behind on the surface, depending on the viscosity of the solution, the geometry of the electrode emersion process, the hydrophobicity of the substrate surface and the volatility of the species. The pump down process generally helps to get rid of most of the emersed layer, as the solution layers explode when vacuum is applied, spraying small amounts the solution around the inside of the antechamber and minimizing the amount left on the crystal. Experience has shown that most problems associated with emersed species go away if the total concentration is kept below mM, while problems are generally encountered when the total

concentration exceeds 10 mM. Tricks like rinsing the electrode work in some situations, however they can obscure the meaning of any results obtained.

STM studies give unparalleled atomic scale structural information, in air, in-situ (in solution and underpotential control) and in vacuum. Each environment has advantages. Imaging in air is the simplest. The drawbacks to imaging in air involve contamination, oxidation, humidity and that you can only look at "snapshots" of the deposition process. That is, the deposition takes place in solution, at some potential and must be emersed for imaging in air. If the deposits are stable in air, then good images may be possible (159, 333, 334). Images taken in-situ can be "movies," where the conditions are adjusted on the fly, providing a sequence of images of the deposition taking place. Problems with imaging in-situ imaging are mostly associated with the tip, in that the tip must be insulated and compatible with the solution. The coating process is another step in the production of a tip, lowering the chances of producing one capable of atomic resolution. With respect to solution compatibility, both the insulating coating and the tips must be stable in solution. In in-situ studies, the tips are electrodes and have their own potential dependent reactivity with the solution. W tips are quite popular for achieving atomic resolution images, however, they can oxidize at potentials above 0 mV. Se deposition, for example, normally takes place at potentials above 0 mV, so that W does not work well, as the tip must be held at a still higher potential to prevent bulk Se from depositing on it. STM studies in UHV are advantageous because UHV is clean and oxygen free, allowing less stable surfaces to be investigated, as well as ready access to other surface sensitive techniques such as LEED and AES. As with studies in air, however, only snapshots of the surface are obtained, making it difficult to follow the deposition sequence.

The first surface studies of ECALE cycle chemistry focused on CdTe deposition (159, 162, 320). The structures of the first atomic layers of Te deposited on Au single crystal surfaces were studied (320), as were the structures of the deposits after subsequent deposition of atomic layers of Cd, to form CdTe monolayers (159, 162). UHV-EC studies of Cd atomic layer

formation on Au were attempted, but generally resulted in surfaces displaying diffuse LEED patterns and variable amounts of Cd and O. This is consistent with the problems, previously mentioned, of depositing reactive species, at potentials negative of the formal potential for hydrogen. It was difficult to emerge the Cd coated Au substrates without the Cd spontaneously oxidizing. The emerged crystal is at least momentarily encased in a layer of liquid at open circuit, prior to evacuation. Te, on the other hand, was quite stable and well behaved, displaying a sequence of ordered atomic layers on each of the Au low index planes (320).

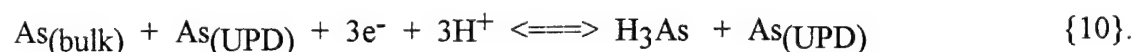
The influence of the initial Te atomic layer structure on the resulting CdTe monolayer was also investigated (159, 162). A series of experiments were performed where Te atomic layers of various coverages and structures were first deposited, and then Cd UPD was performed on top. Ordered CdTe deposits were formed on each of the low index planes. What was interesting was that the initial Te structure or coverage had very little to do with the structure of the resulting CdTe monolayers. That is, the LEED patterns observed for the CdTe deposits did not change appreciable as a function of coverage or structure of the initial Te atomic layer.

On Au(100), for instance, a $c(2 \times 2)$ -CdTe structure was observed (Figure 40). This structure ideally consists of $1/2$ MLs of both Cd and Te (159, 162). The CdTe LEED pattern was not a function of the initial Te coverage, or even the subsequent Cd coverage, only the clarity of the pattern changed with coverage. For instance, in the case where Cd was deposited on the $1/3$ coverage Te structure, such as the Au(100)($2 \times \sqrt{10}$)-Te, there should only be enough Te for the resulting CdTe structure to cover $2/3$ of the surface (Figure 41A). The remaining $1/3$ of the surface should be covered by Cd UPD. The $2/3$ of the surface covered with CdTe produces a $c(2 \times 2)$ pattern, while the $1/3$ covered with Cd UPD contributes diffuse intensity, as it spontaneously oxidizes upon emersion, resulting in disordered domains. On the other hand, if the initial Te structure contained $2/3$ ML of Te, only $1/2$ ML is needed to form the first monolayer of CdTe. The excess Te may have contributed to the formation of a partial second layer, and the formation of CdTe islands (Figure 41C). Island formation is a form of surface roughing which

also contributes to diffuse scattering in LEED patterns, depending on the number and sizes of the islands. This helps explain why the LEED patterns become diffuse if too much Te is present in the initial layer. Studies have shown that the Cd can react completely with the Te, even if multiple monolayers of Te are present initially (291).

From the above results it is clear that the amount of Te deposited in the first atomic layer on the Au surface is critical but not structure controlling. Control over the coverage of Te in subsequent cycles should not be as critical, as it should be naturally controlled by the previously deposited Cd atomic layer. The first Te layer, however, involves the reaction of Te with the Au substrate to form a Au-Te surface compound, not CdTe. The coverages of the Te atomic layer structures formed on Au have nothing to do with the formation of stoichiometric CdTe. A homogeneous atomic layer of Te on Au at the correct coverage (1/2 ML on Au(100)) (Figure 41B), with no pits or islands, should produce the lowest defect density in the subsequently formed CdTe film, according to the structure proposed in Figure 40

Similar studies of the formation of the first monolayer of GaAs have also been performed (157, 252, 253). The chemistry of arsenic facilitates the ECALE cycle, as it is easily reduced to H₃As at negative potentials (Figure 42):



UPD of As on Au single crystals resulted in well ordered atomic layers, as observed with LEED. In addition, subsequent UPD of Ga results in formation of an ordered GaAs monolayer. The structure of the monolayer is similar to that for CdTe, in that it consists of a 1/2 ML each of Ga and As, on Au(100). The observed LEED pattern, however, was not a c(2X2), but a p(2X2) structure (Figure 43). This larger unit cell has been proposed to result from dimer formation in the top layer (Figure 44), which is consistent with previous UHV studies of GaAs single crystal surfaces (335-339). Those results concerned mostly the formation of a single monolayer of GaAs, as the deposition of multiple layers proved difficult since, at that time, the hardware

resulted in deposits being left at open circuit, briefly, during each solution change. In the case of the CdTe deposits described above, Cd oxidized spontaneously when emersed in the absence of Te (Figure 45B), but did not oxidize if Te was present as well (Figure 45D and E). It was concluded that the Cd did not oxidize because it was stabilized by bonding to the Te. In the present case, the Ga did not appear to be sufficiently stabilized by bonding with the As to keep it from oxidizing under open circuit conditions. Deposition hardware in which potential control is not lost with each rinse should facilitate the formation of thicker GaAs deposits, however, and those studies are planned.

The nature of the material that results after the first few ECALE cycles has been questioned by some, whether the surface is covered with separate domains or islands of Cd and of Te, or with a monolayer of CdTe, for instance. The electrochemical results are fairly definitive on this point, in that if there were islands of Cd present on the surface, bulk Cd would be expected to strip from the surface at potentials below -0.7 V, which is not observed. No Cd stripping was observed below -0.6 V from the CdTe deposits. Additionally, Figure 46 is a set of XPS spectra of the 3d transitions of Te. Figure 46B is from a Te UPD layer on Au, while Figure 46D is from bulk Te, and they show essentially the same chemical shift. The spectrum in Figure 46C is of a Te atomic layer after deposition of an atomic layer of Cd on top, and displays a shift of 0.4 eV to lower binding energy, indicating destabilization of the Te electrons, consistent with the formation of CdTe (340).

The early surface studies described above indicated that compounds were probably being formed with the first cycle and that the deposits had some degree of order. LEED, however is an averaging technique. A surface can have significant amounts of disorder, relatively small domains, and still give a reasonable LEED pattern. STM was also used in those studies of compound monolayers, however the images collected were generally of very small areas of the deposits, 5 - 15 nm on a side. Those STM studies did provide information on the atomic arrangements in the unit cells identified with LEED, but did not address how much of the surface

they covered, or involve investigation of other features present on the surface such as: steps, pits and islands. One of the last images taken in those studies is Figure 47. The image clearly shows the $c(2\times 2)$ structure described in Figure 40, but the presence of steps, pits, islands, and a series of phase boundaries, are evident as well. Given that one cycle of CdTe displays so many defect features, it is hard to envision epitaxial deposits after 50 cycles.

A study designed to better understand and remove many of the defects evident in Figure 47 was performed (309). With a single crystal, the step density is generally controlled by the misalignment. As delivered single crystals are frequently mis-oriented by several degrees, so the first step to decreasing the substrate defect density was to reorient the crystal to within a fraction of a degree of the Au(100) plane. The crystal was then repolished mechanically with successively finer grades of polishing cloth, finishing with an electropolish (341, p. 62). The standard cleaning procedure used for the substrate in Figure 47 involved an initial flame annealing and water quenching, followed by a number of oxidation-reduction cycles (ORCs) in acid. Figure 48 is an STM image of the resulting clean Au surface and displays a large number of monoatomically high Au islands. Islands such as these have been observed by a number of workers after ORC treatments. One explanation of the origin of these islands involves the reconstructions that take place when Au(100) is reduced. A corrugated hexagonal over layer structure (307, 308, 342-344) is formed on Au(100) at low potentials, which contain 20-24% more surface atoms than the unreconstructed surface (345-347). When the electrode potential is switched positive, the reconstruction is relaxed, releasing the extra Au atoms to form Au islands. The more ORCs performed, the more islands formed.

The need for ORCs to clean the surface was not necessary in the STM studies, as the electrodes were flame annealed prior to each experiment. Flame annealing does not, however, leave a perfect surface under most conditions, although it is generally much better than that resulting from ORCs (348, 349). There have been several studies showing that electrode surfaces can be atomically leveled, or annealed, using an electrochemical treatment (347, 350, 351). In the

case of Au, halide solutions appear to promote the leveling, either by increasing the mobility of the surface Au atoms (347, 351) or by a small amount of etching (309). Use of dilute KI solutions by this group have resulted in complete removal of the islands formed during ORCs and formation of 300X300 nm atomically flat terraces (Figure 49). These surfaces, however, are coated with an atomic layer of I atoms (301, 352-356).

There are a couple of ways to remove an atomic layer of I atoms. It can be reduced off:



but the low potentials needed also results in reconstruction of the surface and then island formation upon lifting of the reconstruction. Alternatively, the I atom layers can be oxidatively removed, converted to iodate:



The oxidation, however, occurs commensurate with Au oxide formation, and oxidation can result in roughening of electrode surfaces, as occurs for Pt (357). A third method that is more compatible with the formation of chalcogenide atomic layers and that avoids roughening the substrate, involves deposition of a chalcogenide layer on top of the halide layer (309). Figure 50 shows voltammetry for the deposition of Te from a HTeO_2^+ solution, on clean Au(100) (Figure 50A) and on I coated Au(100) (Figure 50B). Two Te reductive UPD features are evident on the clean Au (0.325 and 0.0 V), as well as a bulk Te deposition feature (below 0.0 V). On the I coated Au(100) electrode, the first Te UPD feature is gone and the second has been noticeably suppressed. The subsequent oxidative Te stripping features in Figures 50A and B are essentially

the same, indicating that there is very little difference between the resulting Te layers. Studies following the surface composition with AES indicated that the I atom layer is completely displaced by the depositing Te atoms (Figure 51). However, the resulting Te layer generally contains more than a monolayer of Te, which can be removed either by oxidation at 0.400 V, or reduction below -0.900 V, to produce a Te atomic layer. The layers appear well ordered and with a significantly lower defect densities than those formed on substrates subjected to ORC cleaning.

More recent work, concerning surface chemistry in an ECALE cycle, centers on the formation of the first few monolayers of CdSe. Again, the chalcogenide serves as the first atomic layer, due to Cd instability upon emersion. Figure 52C is the Auger spectrum for a Au(100) crystal covered with Cd UPD, while Figure 52D is the spectrum for Cd UPD on the crystal precoated with an atomic layer of Se. As in the case of CdTe formation (Figure 45), the Cd Auger transition at 375 is accompanied by one at 500 eV, for oxygen, when no other chalcogenide is present (Figure 52C). The oxygen signal is nearly absent from Figure 52D, where the Cd has reacted with previously deposited Se.

Se forms a number of different atomic layer structures on each of the Au low index planes (as does Te), as a function of time and potential. The following discussion of Se deposition will concentrate on just the (100) face (295, 334), although similar results have been observed for Au(111) and to a lesser extent Au(110) (333). As a function of coverage, the structures formed on Au(100) were: a p(2X2)-Se at 1/4 coverage, a (2X $\sqrt{10}$)-Se at 1/3 coverage, a c(2X2)-Se at 1/2 coverage, and a (3X $\sqrt{10}$)-Se at 8/9 coverage (295, 334). LEED patterns, STM images and proposed structures are displayed in Figures 53, 54, and 55, respectively. The low coverage p(2X2)-Se and (2X $\sqrt{10}$)-Se structures are direct analogs of structures formed by Te on Au(100) (162, 320), and a S structure similar to the higher coverage (3X $\sqrt{10}$)-Se has been observed to form on Au(111) (358-360).

As previously mentioned, the first atomic layer, in contact with the substrate, appears to be the most critical. Electrochemically, there are three different ways to form the first atomic layer of Se and graphs depicting each are displayed in Figure 56. The first method is straightforward, the direct reductive deposition of Se atomic layers from a HSeO_3^- solution. The voltammetry for Se deposition is shown in Figure 57 and displays two features, C_1 and C_2 . C_1 could be thought of as a "UPD" feature, as it corresponds to the deposition of less than a monolayer of Se. C_2 appears to also result from a surface limited reaction, but corresponds to over two ML of Se. These features show up as small plateaus in Figure 56A, which is a graph of the coverage observed after sitting for 2 minutes at the indicated deposition potential. Examination of the voltammetry alone might lead to the conclusion that UPD results in a single $1/2$ ML structure. The second, larger, feature (C_2) results in a coverage considerably higher than is normally associated with UPD. That is, UPD results from stabilization of a deposit via proximity to the substrate (22, 23), and there are instances where a second monolayer does show some stabilization (26, 361), however in the present case (peak C_2), a coverage of over two Se monolayers is observed. It is interesting to note that the measured equilibrium potential for Se in this solution is about 0.4V, positive of even C_1 . Evidently, even the "UPD" feature has been deposited at an over-potential. Features in the reduction voltammetry (Figure 57) appear to be very much a function of slow kinetics, and will be discussed later.

There are two other methods of producing atomic layers of Se, and both involve two steps. The first step in both methods is the deposition of about 1.25 ML of Se, while the second step involves stripping off the excess Se to leave the desired atomic layer. Figure 56B shows the resulting Se coverages left after oxidative stripping at various potentials. A broad plateau is visible at $3/4$ ML coverage, and there is some indication of a halt near $1/4$ ML. A similar graph is shown in Figure 56C for the reductive stripping of excess Se in a borate solution, leaving an atomic layer. The same plateaus observed in Figure 56B for oxidative stripping are observed in

Figure 56C for reductive stripping: one near $3/4$ coverage and the other between $1/3$ and $1/4$ coverage (295).

A first atomic layer of Se can be formed by any one of the three methods. In construction of an ECALE cycle, however, the second and successive atomic layers of Se must be formed by the reductive stripping method (Figure 56C), as use of a positive deposition or stripping potential would result in loss of the previously deposited group II element, as discussed previously.

The structures diagrammed in Figure 55 can be formed by any one of the three methods described above; however kinetics play a very important role in determining the homogeneity of the surface (333, 334). The fact that each of the structures shown in Figure 55 can be formed at the same overpotentials (feature C₁ in Figure 57) makes it difficult to isolate one, to the exclusion of others. The low coverage structures: p(2X2), (2X $\sqrt{10}$) and c(2X2), are all difficult to form homogeneously over the surface. Deposition of less than $1/4$ ML of Se generally resulted in no discernible structure, probably due to a high Se atom surface mobility at such a low coverage. Similar studies on Au(111) evidenced the same problem imaging the low coverage Se unless higher resistance conditions were employed, whereupon some very interesting clustering of Se was observed, at coverages below $1/4$ ML (333). As the Se coverage increased to a $1/4$ ML on Au(100), the p(2X2) structure (Figure 54A) was imaged, but was frequently found to coexist with domains of the (2X $\sqrt{10}$) (Figure 54B). In Figure 54C, at $1/3$ coverage, domains of the (2X $\sqrt{10}$) clearly coexist within domains of the c(2X2) and some S₈ rings are present, as well.

At coverages above $1/2$ ML, the number of S₈ rings increase (Figure 54D). Present understanding of the rings is that they consist of a square arrangement of eight Se atoms, and appear to be bound to the Au substrate in the first Se layer. STM height measurements show height differences of 0.05 to 0.1 nm, not the 0.25 nm expected if the rings represented a second layer of Se. As the number of rings increased still further they began to coalesce into a close packed structure, some domains of which are visible in Figure 54D. It is interesting to note that the close packed rings are rotated 45° from the isolated rings. Sequential STM images of low

density Seg rings showed that they are mobile, at least under the imaging conditions. That is, they act like molecules, with structural integrity. Evidently, when they pack together, they rotate to achieve a better fit. Analogous Seg rings in crystalline Se adopt a chair conformation (362); however, bonding with the Au substrate appears to facilitate the planar configuration.

Coincident with the formation of Seg rings was the formation of pits on the surface (Figure 54D, E and F). Cross sections of the pits indicated them to be a single atom deep (about 0.3 nm), and to have the same Seg ring structure on their floor. Pit formation appears to be reversible, and connected to the appearance and disappearance of the ring structures on the surface. For well prepared Au surfaces, no pits are visible until the rings begin to form. If the Se coverage is decreased by oxidation, the rings appear to go away, as well. The pits account for about 10% of the total surface area at Se coverages near 1 ML. Similar pits are frequently observed on Au surfaces where long chain alkane thiols have been adsorbed (363-369). Those pits are usually a single atom deep as well, and have a similar distribution over the surface. Several explanations have been proposed, including contamination or defect sites (363, 364), small amounts of etching (366-369), and the idea of a surface reconstruction where the lateral extent of the surface Au atoms actually shrinks due to bonding with the thiols (365, 370). At present, the last two explanations fit most closely with the observations described here. A small amount of dissolution could easily account for the observed pits. Alternatively, for 10% of the surface to be covered with pits, a change of only 3% in the Au-Au distance would be required, which is difficult to rule out with STM. Elemental Seg rings naturally have a Se-Se bond distance of 0.233 nm (362), while the Se-Se distances in the square Seg ring structures on Au (Figure 54) appear to coincide more closely with the 1X1 arrangement on the Au surface, or a Se-Se distance of close to 0.29 nm. The increased Se-Se distance in the adsorbed Seg rings probably involves significant strain associated with forming a layer commensurate with the Au surface. This strain could in turn account for the compression of the surface Au atoms, and the observed pits.

Ideally, the starting point for the formation of CdSe deposits using an ECALE cycle would be formation of a homogeneous, stable, $1/2$ coverage Se structure, as described previously in the case of CdTe. Isolation of the pure $\text{Au}(100)\text{c}(2\times 2)\text{-Se}$ with a Se coverage of $1/2$, as described above, was difficult to achieve under all conditions investigated. Multiple structures were nearly always present simultaneously on the resulting surfaces, due to the sluggish kinetics of Se electrodeposition. However, as previously described in the case of CdTe formation, the structure of the chalcogenide atomic layer may not be as important as the overall chalcogenide coverage. The mobility of the chalcogenide during the subsequent deposition of the Cd then becomes very important. The Se atoms must move from areas of high coverage, such as where the Seg rings are formed, to areas with a lower Se coverage, such as domains of the $1/3$ coverage $(2\times\sqrt{10})\text{-Se}$ structure. If this mobility were not observed, domains of the Seg rings would probably result in islands of CdSe, more than a monolayer thick.

Voltammetry for Cd deposition on the Au "tri" crystal (a single crystal which has been oriented and polished on three faces, each to a different low index plane) is shown in Figure 58A. A very broad UPD feature, peaked at 0.0 V is evident. The Cd coverage of the UPD feature is a function of the low potential limit and the background corrections chosen for the integration, but is nominally about $1/3$ ML or less (371). The formal potential for Cd appears to be near -0.75 V, as similar scans to -0.8 V and below show a sharp stripping spike in the oxidative scan near -0.75 V. There is a gradual increase in the Cd deposition current beginning at -0.4 V (Figure 58A) as the potential is scanned negatively. Examination of the literature concerning Cd UPD indicates that alloying of Cd with the Au electrode (372) frequently takes place, which could account for this current. This alloy formation, also occurring at an underpotential, is not strictly a surface limited reaction as is the UPD. From the voltammetry (Figure 58A) it appears that most alloy formation can be avoided if the potential is kept above -0.5 V.

For the initial studies of Cd deposition on Se atomic layers, the $1/3$ coverage $\text{Au}(111)(\sqrt{3}\times\sqrt{3})\text{R } 30^\circ$, the $1/2$ coverage $\text{Au}(100)\text{c}(2\times 2)$, and the $2/3$ coverage $\text{Au}(110)(3\times 2)$

(Figures 59A, B and C respectively) were selected. For those structures the ideal coverages are 4.5×10^{14} , 5.8×10^{14} , and 5.5×10^{14} atoms/cm², respectively. Given the constraints of the Se deposition kinetics previously discussed, these Se adlattices were formed by scanning to just past the Se UPD peak (C₁ in Figure 57), where the potential was then held for 2 minutes. The Cd deposition voltammetry shown in Figure 58B was performed on the Au(100)c(2X2)-Se surface. The UPD feature is significantly increased, relative to Cd UPD on clean Au (Figure 58A), and has shifted negatively by 200 mV. The peak shift indicates that Cd at low coverages is more stable on clean Au than on the Se coated Au. At -0.3 V, the Cd coverage for deposition on clean Au vs. Se coated Au is 1/3 vs. 1/2 ML. As the potential is scanned to still more negative potentials, the current characteristic of alloy formation is again evident, regardless of the presence of the Se layer.

Ordered deposits were formed at -0.3 V on all three low index planes of Au precoated with the Se adlattices listed above. The clearest LEED patterns were observed for deposits formed on Au(111), which happens to be the plane for which ordered Se structures were seen most infrequently with LEED. The Au(100) surface, which evidenced the sequence of Se atomic layers diagrammed in Figure 55, showed the least tendency to form ordered CdSe deposits. This is further evidence that the structures of the II-VI compound monolayers are independent of the structures of the initial chalcogenide atomic layers. Given that the CdSe monolayers formed on Au(111) appear to be the most well ordered and understood, they will be described below.

Under the various Se deposition conditions studied, a $(\sqrt{3} \times \sqrt{3})R 30^\circ$ -Se structure was the only ordered structure observed on Au(111) (Figure 60). The $(\sqrt{3} \times \sqrt{3})R 30^\circ$ unit cell should correspond to a Se coverage of 1/3 or possibly 2/3 ML. The LEED pattern was observed for deposits emerged at the outset of the UPD feature (Figure 57), and was still evident for deposits emerged after conclusion of the UPD feature. Coulometry and Auger spectroscopy indicated a Se coverage of 1/3 (333), as did STM (Figure 61A). Figure 62A is the LEED pattern observed when a potential of -0.25 V (Figure 58B) was used to deposit Cd on the

Au(111)($\sqrt{3}\times\sqrt{3}$)R 30°-Se structure. The unit cell responsible for Figure 62A is a ($\sqrt{7}\times\sqrt{7}$)R 19.1°-CdSe. A proposed structure is shown in Figure 63A, and indicates a coverage of 3/7 for both Cd and Se. A similar structure was seen in the case of CdTe formation on Au(111) (159, 162). By depositing Cd at a more negative potential, below -0.45 V, a structure displaying a (3X3) unit cell was observed using LEED (Figure 62B). STM studies, such as those of Se structures in air, were unworkable with the CdSe layers, as the Cd did not show sufficient stability in air. Some in-situ STM results have been obtained where Se layers were first formed in a standard electrochemical H-cell, and then transferred to a custom electrochemical cell designed for use with a Nanoscope III (373) (Figure 64A). The Se structure shown in Figure 64A has domains of both the ($\sqrt{3}\times\sqrt{3}$)R 30°-Se structure at 1/3 coverage, and Seg domains at 8/9ths coverage. The over all Se coverage on the surface was probably close to 0.6 ML. The image was obtained at -0.1 V in the Cd²⁺ solution, where no Cd had yet deposited. The image shown in Figure 64B was taken on the same surface after shifting the potential to -0.4 V, where Cd had deposited. The image displays a surface which has an orientation and dimensions consistent with the (3X3) LEED pattern (Figure 62B). A proposed structure is shown in Figure 63B that suggests slightly higher Cd and Se coverages, 4/9 (0.444), vs. the 3/7 (0.429) in the ($\sqrt{7}\times\sqrt{7}$)R 19.1°-CdSe structure (Figure 63A). An equivalent structure has been reported by other workers using TEM in a study of electrodeposited CdSe nanoclusters on Au(111) substrates (115, 125). This increase in the Cd coverage to 0.444 has resulted in a structure closely resembling the hexagonal basal plane of CdSe (Wurtzite), and involves a lattice mismatch of only 0.6% between the CdSe and Au.

Also evident in Figure 64B are small light colored clusters, near 1/2 nm in size. At present, it appears that these clusters are extra CdSe formed because too much Se was present on the surface initially (Figure 64A). As mentioned above, the Se coverage prior to Cd deposition appeared close to 0.6 ML, significantly greater than the 0.44 needed for the structure diagrammed in Figure 63B. Studies have shown that Cd will react nearly stoichiometrically with up to several

monolayers of Se (107). These results are consistent with the discussions of CdTe formation in Figure 41C, where a second layer begins to form and results in island on the surface.

In the work described above concerning the formation of CdSe monolayers, the Se was the first atomic layer formed. Cd can be used as the first atomic layer, as well, although the structures of Cd UPD layers on Au are not well characterized. Subsequent Se deposition resulted in a structure with a (3X3) unit cell on Cd coated Au(111), very similar to that formed when the Se was deposited first (Figure 62B). There is some evidence that when the Se is deposited first, it remains under as the Cd is deposited, and conversely, that when the Cd is deposited first it remains on under subsequently deposited Se (333).

Progress on understanding the surface chemistry relevant to the formation of compound semiconductors is being made. One major issue is the genesis of defects that appear in deposits formed with the flow deposition system. Probable defect sources include the substrate quality, lattice mismatch problem, and problems associated with deposition of a compound on an elemental substrate (374-383). Many of these problems are related to the choice of Au as a substrate. The next section describes attempts to better understand the electrochemistry of compound surfaces. Given sufficient control of compound surface chemistry in aqueous solutions, it may be possible to use them as lattice matched substrates in subsequent deposition studies. Other efforts in this group concern the formation of other compounds, and an increased effort to investigate the deposition process an atomic layer at a time using in-situ STM.

V: Digital Electrochemical Etching

Au is an excellent electrode material. It is inert in most electrochemical environments, and its surface chemistry is moderately well understood. It is not, however, the substrate of choice for the epitaxial formation of most compounds. One major problem with Au is that it is not well

lattice matched with the compounds being deposited. There are cases where fortuitous lattice matches are found, such as with CdSe on Au(111), where the $\sqrt{3}$ times the lattice constant of CdSe match up with three times the Au (Figure 63B) (115, 125). However, there is still a 0.6 % mismatch. A second problem has to do with formation of a compound on an elemental substrate (Figure 65) (384-387). Two types of problems are depicted in Figure 65, in A, the first element incompletely covers the surface, so that when an atomic layer of the second element is deposited, anti-phase boundaries result on the surface between the domains. These boundaries may then propagate as the deposit grows. In Figure 65B, the presence of an atomically high step in the substrate is seen to also promote the formation of anti-phase boundaries. The first atomic layer is seen to be complete in this case, but when an atomic layer of the second element is deposited on top, a boundary forms at the step edge. Both of the scenarios in Figure 65 are avoided by use of a compound substrate.

For deposition of II-VI compounds, three scenarios for lattice matched compound substrates are readily available: deposition on the compound itself, homoepitaxy; deposition on a second II-VI compound that happens to be lattice matched, such as HgTe on CdTe; or deposition on a corresponding III-V compound. There are two problems with homoepitaxy, one is why? Most of the time there is no need to grow a layer of a compound on a substrate of the same compound. There are cases where the substrate is grown by a method which produces an inexpensive but inferior material, and a high quality "epi" layer of the same compound is grown on top. These epi layers can also be used to provide an independently doped layer, depending on the device structure. The second problem with homoepitaxy is that the ability to analyze the quality of the resulting material is decreased, as most techniques have trouble differentiating between the substrate composition or structure, and that of the deposit.

The use of a lattice matched II-VI compound as a substrate works if lattice matched substrates are available. However, even in the case of HgTe on CdTe, there is a slight mismatch. Frequently, the solution has been to alloy in a third element to adjust the lattice constant. For example: substrates used to make MCT detectors ($\text{Hg}_x\text{Cd}_{1-x}\text{Te}$) frequently have at least a very

thin buffer layer of CdTe alloyed with Zn to provide a better lattice match (388, 389).

A third lattice matching scenario is to use a corresponding III-V compound for a substrate. For instance, the lattice constants for CdTe and InSb are both listed as 0.648 nm (390), and similar lattice matches are found between the other II-VI and III-V compounds. As with the II-VI compounds, there are a number of situations where the lattice constants of the substrate can be incrementally adjusted by alloying with a third element. In addition, some high quality wafers of III-V compounds are available commercially, at reasonable prices.

The problem with all three of the above scenarios, is that they require an understanding of the surface chemistry of compound semiconductor in aqueous solutions. Much more is known about the surface chemistry and reactivity of Au in aqueous solutions. A prerequisite, then, to the use of a compound semiconductor as a substrate for compound electrodeposition, is to gain a better understanding of the substrate's reactivity under electrochemically relevant conditions. Our initial studies of compound reactivity in electrochemical environments involved CdTe single crystals (391). The electrochemistry of CdTe is reasonably well understood from electrodeposition studies (Table 1), and single crystals are commercially available.

For a compound semiconductor to be useful as a substrate in studies of electrodeposition, it is desirable that clean, unreconstructed, stoichiometric surfaces can be formed in solution, prior to electrodeposition. For CdTe, the logical starting point is the standard wet chemical etch used in industry, a 1-5% Br₂ methanol solution. A CdTe(111) crystal prepared in this way was transferred directly into the UHV-EC instrument (Figure 39) and examined (391). Figure 66B is an Auger spectrum of the CdTe surface after a three minute etch in a 1% Br₂ methanol solution. Transitions for Cd and Te are clearly visible at 380 and 480 eV, respectively, as well as a small feature due to Br at 100 eV. No LEED pattern was visible, however. As described previously, a layer of solution is generally withdrawn with the crystal as it is dragged (emersed) from solution (the emersion layer). After all the solvent has evaporated, the surface is left with a coating composed of the electrolyte initially contained in the emersion layer. In many cases, it can be rinsed away prior to analysis using a dilute solution. The spectrum shown in Figure 66C is for a

Br₂/methanol etched crystal after a rinse in dilute H₂SO₄. Both the Br and Cd signals have disappeared. Evidently, the Cd and Br were present as CdBr₂ salt, which was easily rinsed from the surface. The low Auger signal for Br in Figure 66B can be accounted for by its low Auger sensitivity factor (392). Again, no LEED pattern was observed for the resulting Te rich surface. That a Te layer was present is not surprising, as Cd is the less noble element and should be preferentially etched in the Br₂ solution. That the layer is disordered is consistent with having removed Cd atoms from the CdTe zinc blende lattice, leaving behind Te.

Figure 66D was obtained for the same CdTe(111) crystal after electrochemical reduction at -2.0 V for two minutes. Transitions for both Cd and Te are evident and the Cd/Te peak height ratio is similar to that observed by other workers for stoichiometric CdTe (393, 394). In addition, well ordered (1X1) LEED patterns (Figure 67) were observed on both the CdTe(111)-Cd and CdTe(111)-Te faces. This is in contrast to CdTe surfaces prepared by ion bombardment, where post bombardment annealing was required to produce a LEED pattern, and the annealing appeared to result in formation of a reconstructed surface. In summary, well ordered, clean, and unreconstructed CdTe surfaces have been produced using a wet etching/electrochemical treatment.

The results described above suggested that an electrochemical analog of digital etching might be achievable. Digital etching is a term used to describe methodologies where a material is decomposed an atomic layer at a time, in a cycle (395-399). It fits under the heading of atomic layer processing, along with ALE. The benefits are increased control over the etching process and etched depths. One obvious use for digital etching is where it is desirable to carefully and homogeneously remove some small number of monolayers, say 1-500. Historically, digital etching cycles have involved the alternated exposure of a substrate to first a gas source, and second to an energetic beam of electron, ions, photons, or neutrals. Examples of gases include the halides, hydrogen halides, or halide sources such as SF₆. An example scenario would be to expose a surface to a reactive gas, forming an adsorbed layer of the in a surface limited reaction. After pumping away the excess, the surface is exposed to an energetic beam, promoting the formation

of a volatile species composed of stoichiometric amounts of the adsorbed gas and the material being etched. The extent of etching is then limited by the amount of the previously adsorbed gas.

An electrochemical analog of digital etching can easily be envisioned, where first some reactant is adsorbed in a surface limited reaction, and then the potential is switched to one where a product species is produced, stoichiometric in the adsorbate and the substrate. The results of the CdTe etching study described above, suggested still another scenario, where no adsorbate is involved, just two electrochemical potentials. Figure 68 is a side view of a CdTe crystal. The structure is drawn such that the (100) plane of CdTe is the top, and we are looking down the [110] direction. The Figure has been drawn to suggest that the top layer of atoms are all Cd atoms. The premise of this electrochemical digital etching cycle is that there is a potential at which only the top layer of Cd atoms will be removed, as they are less stable than interior Cd atoms, less coordinated. Removal of the Cd atoms will expose a layer of Te atoms. From the above studies it appears that these under-coordinated Te atoms can be removed by electrochemical reduction, to reform the Cd terminated surface, completing removal of a single compound monolayer (44, 313, 400).

Studies of electrochemical digital etching, in this group (44, 313, 400), have taken two tracks, the first involving UHV-EC studies of CdTe single crystal surfaces such as those described above (391). The second track involved the use of atomic force microscopy (AFM) to follow etch depths on CdTe single crystals subjected to 150 cycles. Patterned photoresist coated crystals were used so that the etch depth could be accurately determined. Given 0.648 nm as the lattice constant for CdTe (zinc blende), and definition of a monolayer of CdTe as being one atomic layer of Cd and one of Te (Figure 68), a monolayer should be half the thickness of the unit cell in the [100] direction, or 0.328 nm thick. 150 cycles of etching should then remove 52.2 nm of CdTe.

Ideal substrates, for digital etching studies using the AFM, would start off atomically flat. However, preparation of an atomically flat CdTe surface is not a simple matter. Commercially polished CdTe has striations the size of the last grit used, unless a wet chemical etch is used as a last polishing step. The homogeneity and extent of leveling produced by the wet etch, especially

at an atomic level, is quite variable. Figure 69A is an AFM image of a CdTe crystal surface prior to electrochemical digital etching, after a Br₂/methanol etch. The roughness is considerable, as the experiment is only expected to remove 50 nm of CdTe. This surface was then coated with a commercial photo-resist and developed, so that it consisted of 2 micron wide lines of photoresist, 2 microns apart. This photo-resist covered surface was then subjected to 150 cycles of electrochemical digital etching, in a thin layer flow cell (44). The photo-resist was then removed and imaged again with AFM (Figure 69B). The measured height was close to that predicted above, but on the high side, indicating that under the conditions used, a little more than a monolayer of the compound was being removed each cycle.

In addition to studies using photo-resist covered substrates and AFM, atomic level studies were performed to help identify the nature of the surface limited reactions used to form the electrochemical digital etching cycle (313). In those studies the dependence of etched amounts on the potential used for Cd oxidation was investigated using a UHV-EC instrument (Figure 39).

Initial treatments of a zinc blende CdTe(100) crystal involved argon ion bombardment, followed by a brief anneal. The resulting LEED pattern was a (1X1), indicating an unreconstructed surface. The crystal was then immersed into 50 mM K₂SO₄, pH 5.6. A voltammogram showing the initial reduction of the crystal is depicted in Figure 70A, and exhibits no significant reduction features. Subsequent examination of the surface with Auger spectroscopy evidenced no change in the surface composition. No change was observed in the LEED pattern, as well. The conclusion drawn was that the surface resulting from ion bombardment and annealing, contained no excess (reducible) Te, and that the resulting surface was Cd terminated.

When an equivalently prepared surface was first scanned in the positive direction, Figure 70B was obtained. There appears to be two components to the oxidation feature, a peak at about 0.15 V, superimposed on a slowly increasing background. Auger spectra of the resulting surface showed a marked decrease in the signal for Cd, indicating that some had been removed. In addition, the (1X1) LEED pattern was no longer present, only diffuse intensity indicating that

some roughening of the surface resulted from the oxidation step.

Subsequent reduction of the surface, after the oxidation step, is shown in Figure 70C. A new reduction feature is clearly visible. After scanning through this feature, the Auger spectrum looks as it did after ion bombardment and annealing. In addition, a LEED pattern was again visible. It appears that the initial oxidation step results in a Te terminated surface, indicated by the presence of reducible Te, and that after its reduction, the Cd terminated surface is regenerated, suggesting that the digital etching cycle can be performed.

In order to gain a better understanding of the potential dependence of this process, a series of chronoamperograms were run (Figure 71). In each case, the crystal was pretreated the same, by ion bombardment and annealing. It was then stepped to the indicated potentials in the 50 mM K_2SO_4 solution and held. Two types of current appear to flow in the system. In the first 60 seconds, a transitory current flows, while in addition, a constant background current flows the whole time. The background current is a function of potential, increasing significantly, the more positive the oxidation potential used. On the other hand, the charge associated with the transitory current is about the same in all experiments run using potentials above -0.25 V. After each potential step, a corresponding potential step was carried out to reduce off any Te made available by removal of the Cd. This data is summarized in Figure 72.

In Figure 72, there appears to be a break at about -0.2 V. Below -0.2 V, the oxidation charge matches the subsequent Te reduction charge, as would be expected for a digital etching cycle. On the other hand, at potentials above -0.2 V, the total charge for oxidation goes up steeply, and corresponds to the oxidation of multiple monolayers, not the single atomic layer anticipated. This oxidation charge has been further broken down into its two components, the transient oxidation charge and the background oxidation charge. If just the transient charge is considered, it follows the subsequent Te reduction charge, as did the total charge at potentials below -0.2 V.

Assuming that the CdTe crystal starts with a Cd terminated surface, the data in Figures 70-72 suggests that at potentials below -0.2 V, the charge corresponds to the oxidation of just the

top Cd atomic layer, as does the peak at 0.15 V in Figure 70. However, as the potential is increased to above -0.2 V, a constant background current develops, and the total charge increases dramatically, to the point that it cannot be accounted for simply by removal of a Cd atomic layer. In addition, it does not appear reasonable that all the charge is due to Cd oxidation. If the increase in oxidation charge was all Cd, then significantly more Te would be available for reduction, which is not the case. The amount of Te subsequently reduced, actually goes down slowly at potentials above -0.2 V. The increasing charge for potentials above -0.2 V is best understood if it is considered to arise from both Cd and Te oxidation. Elemental Te, however, begins to oxidize at about 0.2 V in this solution. To account for this 0.4 V shift in the oxidation potential for Te, it is suggested that the Te present on the surface, after Cd has been electrochemically removed, is destabilized. That is, if the Cd atoms in Figure 68 were simply removed from the model, a network of doubly coordinated Te atoms would be left. These atoms might reconstruct to form elemental Te, etc., however, at room temperature it may be difficult, due to limited mobility. If they do not reconstruct, then they should show less significantly less stability than elemental Te, and might oxidize at a significantly lower potential. That is, at potentials above -0.2 V, where more than the top layer of Cd atoms is removed, the resulting destabilized Te atoms are oxidized as well, in what might be referred to as underpotential etching (UPE). UPE would then be oxidation of an element at a potential under that required to oxidize it in its elemental form.

The idea of electrochemical digital etching described in this section is similar to the methodology developed by Kohl and co-workers (401-406). Their studies involved the electrochemical photoetching of compound semiconductors such as InAs, InP, and GaAs, using a modulated potential. The main difference between the work described above and that of Kohl et al is the intent. In the work described above, the removal of a single monolayer of the compound each cycle was the express goal, and felt to be achievable via the application of surface limited reactions. The work of Kohl et al. was intended to perform macroscopic etching, and is in fact a much more generally applicable methodology. Their work examined an extensive set of

conditions, inclusive of those described above, and their studies have been useful in understanding some aspects of electrochemical digital etching. It is anticipated that these atomic level studies (313) will benefit the development of a digital etching cycle and will provide some insight into the photo-electrochemical etching performed by Kohl et al.

Future direction for this work will involve other compounds, such as the some of the III-Vs: InAs and InP. In addition, etching studies of the different low index planes of a compound and the dependence on cycle conditions are planned. It is anticipated that individual planes will etch differentially, as a function of the cycle conditions. Understanding this dependence may facilitate controlled anisotropic etching. It is also clear that the conditions for etching compounds differ, and that device structures composed of more than one compound could be selectively etched.

VI: DIRECTIONS

There are a number of methods available for the formation of compound semiconductors by electrodeposition (Table 1). Electrochemical ALE promises better control over the deposition process, by breaking it into a series of individual steps, with each step becoming a point of control. The questions raised include: what kind of deposit quality can be achieved? What compounds can be formed? What device structures can be formed? What niches will electrodeposition fill in the field of compound semiconductor device formation?

Possible advantages to an electrochemical deposition method include: that deposits can be formed near equilibrium, at room temperature; that the hardware required is cost efficient; that the waste produced consists of an aqueous solution with a low concentration of the reactant ions,

reasonably easy to treat, and relatively harmless unless consumed; that there are no poisonous gases; and that the hardware is easy to clean.

From the previous sections of this chapter, it should be clear that the substrate is very important and will continue to be a major area of study. Improvements in the quality of Au substrates can be made by switching to Au vapor-deposited on mica or glass. However, a very important direction of study will be towards using lattice matched compound semiconductor substrates, and that work is closely tied with studies of electrochemical digital etching (44, 312, 313, 400).

Cycles have been worked on for a number of different compounds, including: CdTe(44, 159-162, 311, 321), CdSe(106-108, 321), CdS(60-62, 321), ZnTe(44, 279), ZnSe(279), ZnS(279, 407), PbSe, CuSe(306), InSe(306), and CuInSe₂(306). However, thin films of reasonable quality have, so far, only been formed of CdTe (158, 311, 321), CdSe (321) and CdS (59, 321). The main problem is that there is a significant effort needed to get a flow deposition system up and running and producing deposits. Then there is a large variable space to be examined, so that it takes a significant amount of time to investigate and optimize a single compound. At present, then, the main limitation to the formation of more compounds is time.

Other compounds to be investigated include the III-V compounds such as InAs, InP, and GaAs (155, 157, 252, 253). The stability of these compounds in aqueous solutions is questionable, however, with relatively simple modifications in the hardware, a system where potential control is maintained during the whole deposition can be constructed. Work is underway to deposit the Zn based II-VI compounds as well (279), and initial work has been encouraging.

As mentioned in Section III, initially, a thin layer flow cell was used in the automated deposition systems, which proved problematic (158). Presently, a simple H-cell configuration is being used, with much better results (311, 321). There are a number of drawbacks to the present configuration, however, including the volumes of solution needed to fill the cell, and the fact that potential control is lost between each deposition step, when the solutions are drained from the cell. There appears to be significant room for improvement in the deposition hardware. One direction presently being investigated is the use of a flow cell. The new flow cell would not be considered a thin layer cell, however, a significantly thicker gap would be used between the electrode and the far side of the cell. It is anticipated that a cell of this geometry will have fewer problems with fluid flow, similar to the present H-cell configuration, yet potential control will not be lost with each rinse, allowing the formation of less stable compounds.

Studies of the dependence of deposit structure on cycle conditions are continuing. Most of the work along this line has been performed with CdTe (311). Optimizations of CdSe and CdS are continuing as well, and look promising (321). That is, it appears that significant improvements in deposit structure will be possible. Studies of this type, with most of the compounds mentioned above, represent the bulk of the studies needed to answer the questions raised at the beginning of this section. These studies involve the formation of thin film deposits under systematically varying conditions, followed by characterization.

Given that high quality deposits of a number of compounds can be formed, device structure formation should be pursued. Obvious structures include diodes, such as p-CdTe on CdS, which is an important photovoltaic structure (15, 39, 63, 64, 84, 85, 88, 89). Questions include, can high quality CdTe be formed on CdS? What will the structure of the CdS be if

grown on ITO? Can p-CdTe be formed on the CdS directly or will it be n-type, requiring an annealing step to convert it to p-type? Type conversion for electrodeposited CdTe has historically been achieved by annealing (164). One of the main benefits, however, of an electrochemical method is the low temperature that is needed to form films. It is desirable, then, to achieve p-type CdTe during the electrodeposition process, either by optimizing the deposition conditions or by an electrochemical doping scheme, and avoid annealing.

One natural direction for this work to go is towards the formation of superlattices. As very thin films can, in principle, be formed reproducibly, and at low temperatures, superlattices would be a logical application. There are significant problems in placing one compound on another in most deposition schemes, as they generally involve elevated substrate temperatures, promoting interdiffusion. Since electrodeposition is a low temperature technique, very little interdiffusion should occur. Rajeshwar et al. (130) have already performed some studies in this direction, when they used a flow deposition system to modulate between ZnSe and CdSe, forming a superlattice. Those studies showed that it could be done. The modulation period of those deposits were relatively large, however, compared with what should be possible using an ALE method for electrodeposition.

As mentioned, studies of substrates are closely connected with studies of digital electrochemical etching. At present, most work has been performed on CdTe substrates. There are a number of other suitable compounds that should be looked at, for various reasons. Kohl et al. (401-406) have shown that InP and GaSb can be photoelectrochemically etched using a modulated potential program. These compounds would be good candidates for digital etching studies.

Substrate orientation should be examined, to determine if some planes are preferentially etched. If there is preferential etching taking place, what is its dependence on the etching cycle conditions. The hardware being used for these studies should also be investigated. Very little has been done to optimize the flow cell. It is anticipated that a hydrodynamic electrode system, such as a rotating disk or wall jet should work, as well.

One of the most intriguing directions for electrochemical digital etching involves the selective etching of device structures composed of multiple layers of different compounds. That is, some compounds contain less noble elements that will be the first to oxidize, possibly using conditions that leave behind the compound containing the more noble element. While the other compound could contain an element which is more easily reduced, then the corresponding element in the other compound, so that that compound could be selectively removed by controlling the reductive step. It may then be possible to remove either compound in the presence of the other by controlling the cycle potentials used.

VII: References

1. W. A. Bryant, *J. Mat. Sci.* **12**, 1285 (1977).
2. K. K. Schuegraf, *Handbook of Thin-Film Deposition Processes and Techniques* (Noyes, Park Ridge, NJ, 1988).
3. W. Kern, in *Microelectronic Materials and Processes* R. A. Levy, Ed. (Kluwer Academic, Dordrecht, 1989).
4. F. S. Galasso, *Chemical Vapor Deposited Materials* (CRC Press, Boca Raton, 1991).
5. A. Y. Cho, J. R. Arthur, *Prog. Solid State Chem.* **10**, 157 (1975).
6. K. Ploog, *Ann. Rev. Mater. Sci.* **11**, 171 (1981).
7. A. Y. Cho, *Thin Solid Films* **100**, 291 (1983).
8. E. H. C. Parker, *The Technology and Physics of Molecular Beam Epitaxy* (Plenum Press, New York, 1985).
9. M. A. Herman, H. Sitter, *Molecular Beam Epitaxy: Fundamentals and Current Status* (Springer-Verlag, Berlin, 1989).
10. M. B. Panish, H. Temkin, *Ann. Rev. Mater. Sci.* **19**, 209 (1989).
11. J. Y. Tsao, *Materials Fundamentals of Molecular Beam Epitaxy* (Academic Press, Inc., Boston, 1993).

12. G. Hodes, D. Cahen, *Solar Cells* **16**, 245 (1986).
13. L. E. Lyons, G. C. Morris, D. H. Horton, J. G. Keyes, *J. Electroanal. Chem.* **168**, 101 (1984).
14. R. C. d. Mattei, D. Elwell, R. S. Feigelson, *J. Crystal Growth* **43**, 643 (1978).
15. S. K. Das, G. C. Morris, *Solar Energy Mater.* **30**, 107 (1993).
16. Suntula, T., Anson, J., . (United States, 1977).
17. C. H. L. Goodman, M. V. Pessa, *J. Appl. Phys.* **60**, R65 (1986).
18. S. P. DenBaars, P. d. Dapkus, *J. Cryst. Growth* **98**, 195 (1989).
19. A. Usui, H. Watanabe, *Annu. Rev. Mater. Sci.* **21**, 185 (1991).
20. Kuech, et al., Eds., *Atomic Layer Growth and Processing*, vol. 222 (Materials Research Society, Pittsburgh, 1991).
21. Bedair, S., Eds., *Atomic Layer Epitaxy* (Elsevier, Amsterdam, 1993).
22. Juttner, K., Lorenz, W.J., *Z. Phys. Chem. N. F.* **122**, 163 (1980).
23. Kolb, D.M., H. Gerischer, C. W. Tobias, Eds. (Wiley, New York, 1978), vol. 11, pp. 125.
24. G. V. Hevesy, *Physik. Z.* **13**, 715 (1912).
25. L. B. Rogers, D. P. Krause, J. C. Griess, Jr., D. B. Ehrlinger, *J. Electrochem. Soc.* **95**, 33 (1949).
26. J. L. Stickney, S. D. Rosasco, D. Song, M. P. Soriaga, A. T. Hubbard, *Surf. Sci.* **130**, 326 (1983).

27. Y. F. Nicolau, J. C. Menard, *J. Cryst. Growth* **92**, 128 (1988).
28. Y. F. Nicolau, J. C. Menard, *J. Cryst. Growth* **92**, 128 (1988).
29. V. V. Klechkovskaya, V. N. Maslov, M. B. Muradov, S. A. Semiletov, *Sov. Phys. Crystallogr.* **34**, 105 (1989).
30. Y. F. Nicolau, J. C. Menard, *J. Appl. Electrochem.* **20**, 1063 (1990).
31. Y. F. Nicolau, M. Dupuy, M. Brunel, *J. Electrochem. Soc.* **137**, 2915 (1990).
32. Y. F. Nicolau, J. C. Menard, *J. Col. Int. Sci.* **148**, 551 (1992).
33. P. K. Nair, M. T. S. Nair, H. M. K. K. Pathirana, R. A. Zingaro, E. A. Meyers, *J. Electrochem. Soc.* **140**, 754 (1993).
34. J. M. Dona, J. Herrero, *J. Electrochem. Soc.* **141**, 205 (1994).
35. M. Froment, M. C. Bernard, R. Cortes, B. Mokili, D. Lincot, *J. Electrochem. Soc.* **142**, 2642 (1995).
36. H. Cachet, H. Essaïdi, M. Froment, G. Maurin, *J. Electroanal. Chem.* **396**, 175 (1995).
37. H. Cachet, M. Froment, G. Maurin, *J. Electroanal. Chem.* **406**, 239 (1996).
38. A. Kampmann, P. Cowache, J. Vedel, D. Lincot, *J. Electroanal. Chem.* **387**, 53 (1995).
39. D. Lincot, et al., *Appl. Phys. Lett.* **67**, 2355 (1995).
40. G. F. Fulop, R. M. Taylor, *Ann. Rev. Mater. Sci.* **15**, 197 (1985).
41. G. Hodes, in *"Physical Electrochemistry"* I. Rubinstein, Ed. (1995) pp. 515.
42. T. Gruszecki, B. Holmstrom, *Solar Energy Materials and solar cells* **31**, 227 (1993).

43. G. Hodes, *Isr. J. Chem.* **3**, 95 (1993).
44. C. K. Rhee, B. M. Huang, E. M. Wilmer, S. Thomas, J. L. Stickney, *Mater. and Manufact. Proc.* **10**, 283 (1995).
45. H. Gobrecht, H. D. Liess, A. Tausend, *Ber. Bunsenges. Phys. Chem.* **67**, 930 (1963).
46. J. J. Cuomo, R. J. Gambino, *J. Electrochem. Soc.* **115**, 755 (1968).
47. A. Yamamoto, M. Yamaguchi, *Jpn. J. Appl.* **14**, 561 (1975).
48. F. A. Kroger, *J. Electrochem. Soc.* **125**, 2028 (1978).
49. R. D. Engelken, *J. Electrochem. Soc.* **135**, 834 (1988).
50. R. C. DeMattei, R. S. Feigelson, in *Electrochemistry of Semiconductors and Electronics, Processes and Devices* J. McHardy, F. Ludwig, Eds. (Noyes Publications, Park Ridge, NJ, 1992) pp. 1.
51. K. Rajeshwar, *Adv. Mater.* **4**, 23 (1992).
52. R. K. Pandey, S. N. Sahu, S. Chandra, *Handbook of Semiconductor Electrodeposition*. A. M. Hermann, Ed., Applied Physics, A series of Professional Reference Books (Marcel Dekker, Inc., New York, ed. 1st, 1996), vol. 5.
53. M. W. Verbrugge, C. W. Tobias, *J. Electrochem. Soc.* **132**, 1298 (1985).
54. A. S. Baranski, W. R. Fawcett, *J. Electrochem. Soc.* **127**, 766 (1980).
55. B. Miller, S. Menezes, A. Heller, *J. Electroanal. Chem.* **94**, 85 (1978).
56. B. Miller, A. Heller, *Nature* **262**, 680 (1976).

57. C. D. Lokhande, V. S. Yermune, S. H. Pawar, *J. Electrochem. Soc.* **138**, 624 (1991).
58. K. Shirai, Y. Moriguchi, M. Ichimura, A. Usami, M. Saji, *Jpn. J. Appl. Phys.* **35**, 2057 (1996).
59. B. E. Boone, C. Shannon, *J. Phys. Chem.* **100**, 9480 (1996).
60. U. Demir, C. Shannon, *Lang.* **10**, 2794 (1994).
61. L. P. Colletti, D. Teklay, J. L. Stickney, *J. Electroanal. Chem.* **369**, 145 (1994).
62. U. Demir, C. Shannon, *Lang.* **12**, 594 (1996).
63. A. K. Turner, et al., *Solar Energy Mater.* **23**, 388 (1991).
64. B. M. Basol, E. S. Tseng, R. L. Rod., *Pro. 16th IEEE Photovolt. Special. Conf. San Diego*, 805 (1982).
65. D. Ham, K. K. Mishra, K. Rajeshwar, *J. Electrochem. Soc.* **138**, 100 (1991).
66. A. S. Baranski, W. R. Fawcett, *J. Electrochem. Soc.* **131**, 2509 (1984).
67. A. S. Baranski, M. S. Bennett, W. R. Fawcett, *J. Appl. Phys.* **54**, 6390 (1983).
68. F. Mondon, *J. Electrochem. Soc.* **132**, 319 (1985).
69. A. S. Baranski, W. R. Fawcett, A. C. McDonald, *J. Electroanal. Chem.* **160**, 271 (1984).
70. D. K. Roe, L. Wenzhao, H. Gerisher, *J. Electroanal. Chem.* **136**, 323 (1982).
71. G. Hodes, I. D. J. Howell, L. M. Peter, *J. Electrochem. Soc.* **139**, 3136 (1992).
72. A. S. Baranski, W. R. Fawcett, A. C. McDonald, R. M. d. Nobriga, *J. Electrochem. Soc.* **128**, 963 (1981).

73. T. Edamura, J. Muto, *Thin Solid Films* **235**, 198 (1993).
74. E. Fatas, P. Herrasti, F. Arjona, E. G. Camarero, J. A. Medina, *Electrochim. Acta* **32**, 139 (1987).
75. A. Darkowski, M. Cocivera, *J. Electrochem. Soc.* **134**, 226 (1987).
76. H. Minoura, Y. Takeichi, H. Furuta, T. Sugiura, Y. Ueno, *J. Mater. Sci.* **25**, 472 (1990).
77. I. Markov, E. Valova, M. Ilieva, I. Kristev, *J. Crystal Growth* **65**, 611 (1985).
78. J. F. McCann, M. S. Kazacos, *J. Electroanal. Chem.* **119**, 409 (1981).
79. E. Fatas, P. Herrasti, *Electrochimica Acta* **33**, 959 (1988).
80. S. Preusser, M. Cocivera, *J. Electroanal. Chem.* **252**, 139 (1988).
81. J. v. Windheim, A. Darkowski, M. Cocivera, *Can. J. Phys.* **65**, 1053 (1987).
82. S. S. Ou, O. M. Stafsudd, B. M. Basol, *Thin Solid Films* **112**, 301 (1984).
83. B. M. Basol, E. S. Tseng, *Appl. Phys. Lett.* **48**, 946 (1986).
84. G. C. Morris, S. K. Das, P. G. Tanner, *J. Crystal Growth* **117**, 929 (1992).
85. S. K. Das, *Thin Solid Films* **226**, 259 (1993).
86. E. Fatas, R. Duo, P. Herrasti, F. Arjona, E. Garcia-Camarero, *J. Electrochem. Soc.* **131**, 2243 (1984).
87. E. Fatas, P. Herrasti, F. Arjona, E. Garcia-Camarero, M. Leon, *J. Mater. Sci. Lett.* **5**, 583 (1986).
88. S. K. Das, G. C. Morris, *J. Appl. Phys.* **73**, 782 (1993).

89. S. K. Das, G. C. Morris, *J. Appl. Phys.* **72**, 4940 (1992).
90. G. P. Power, D. R. Peggs, A. J. Parker, *Electrochim. Acta* **26**, 681 (1981).
91. S. Dennison, *Electrochim. Acta* **38**, 2395 (1993).
92. J. A. v. Windheim, H. Wynands, M. Cocivera, *J. Electrochem. Soc.* **138**, 3435 (1991).
93. G. C. Morris, R. Vanderveen, *Solar Energy Materials and Solar Cells* **27**, 305 (1992).
94. P. V. Elfick, L. E. A. Berlouis, S. M. M. Donald, S. Affrossman, P. Rocabolis, *J. Phys. Chem.* **99**, 15129 (1995).
95. N. R. d. Tacconi, K. Rajeshwar, *J. Phys. Chem.* **97**, 6504 (1993).
96. M. I. d. S. Pereira, L. M. Peter, *J. Electroanal. Chem.* **140**, 103 (1982).
97. L. M. Peter, *Electrochimica Acta* **23**, 165 (1978).
98. L. M. Peter, *Electrochimica Acta* **23**, 1073 (1978).
99. D. Ham, Y. Son, K. K. Mishra, K. Rajeshwar, *J. Electroanal. Chem.* **310**, 417 (1991).
100. V. I. Briss, L. E. Kee, *J. Electrochem. Soc.* **133**, 2097 (1986).
101. M. Krebs, M. I. Sosa, K. E. Heusler, *J. Electroanal. Chem.* **301**, 101 (1991).
102. J. Vedel, M. Soubeyrand, E. Castel, *J. Electrochem. Soc.* **124**, 177 (1977).
103. M. Krebs, K. E. Heusler, *Electrochimica Acta* **37**, 1371 (1992).
104. T. Edamura, J. Muto, *Thin Solid Films* **266**, 135 (1993).
105. A. S. Baranski, et al., *J. Electrochem. Soc.* **130**, 579 (1983).

106. T. E. Lister, J. L. Stickney, *Appl. Surf. Sci.* (1996).
107. T. E. Lister, J. L. Stickney, *Isr. J. Chem.* **accepted** (1997).
108. J. Jenkins, J. L. Stickney, (prep).
109. A. M. Kressin, V. V. Doan, J. D. Klein, M. J. Sailor, *Chem. Mater.* **3**, 1015 (1991).
110. J. D. Klein, et al., *Chem. Mater.* **5**, 902 (1993).
111. D. Liu, P. V. Kamat, *J. Electroanal. Chem.* **347**, 451 (1993).
112. A. C. Rastogi, K. S. Balakrishnan, A. Garg, *J. Electrochem. Soc.* **140**, 2373 (1993).
113. H. Wynands, M. Cocivera, *Solar Energy Mater.* **32**, 187 (1994).
114. M. T. Litz, et al., *J. Cryst. Growth* **159**, 54 (1996).
115. Y. Golan, L. Vargulis, I. Rubinstein, G. Hodes, *Lang.* **8**, 749 (1992).
116. A. Albu-Yaron, D. Cahen, G. Hodes, *Thin Solid Films* **112**, 349 (1984).
117. K. K. Mishra, K. Rajeshwar, *J. Electroanal. Chem.* **273**, 169 (1989).
118. A. T. Vasko, E. M. Tsikovdin, S. K. Kovach, *Ukrainskii Khimicheskii Zhurnal* **49**, 1070 (1983).
119. M. Tomkiewicz, I. Ling, W. S. Parsons, *J. Electrochem. Soc.* **129**, 2016 (1982).
120. G. J. Houston, J. F. McCann, D. Haneman, *J. Electroanal. Chem.* **134**, 37 (1982).
121. R. P. Silberstein, M. Tomkiewicz, *J. Appl. Phys.* **54**, 542 (1983).
122. M. Skylas-Kazacos, B. Miller, *J. Electrochem. Soc.* **127**, 869 (1980).

123. K. Colbow, D. J. Harrison, B. L. Funt, *J. Electrochem. Soc.* **128**, 547 (1981).
124. B. W. Sanders, M. Cocivera, *J. Electrochem. Soc.* **134**, 1075 (1987).
125. Y. Golan, L. Margulis, G. Hodes, I. Rubinstein, J. L. Hutchison, *Surf. Sci.* **311**, L633 (1994).
126. N. Muller, M. Abramovich, F. Decker, F. Iikawa, P. Motisuke, *J. Electrochem. Soc.* **131**, 2204 (1984).
127. M. Skylas-kazacos, *J. Electroanal. Chem.* **148**, 233 (1983).
128. G. Hodes, J. Manassen, S. Neagu, *Thin Solid Films* **90**, 433 (1982).
129. G. Hodes, J. Manassen, D. Cahen, *Nature* **261**, 403 (1976).
130. C. Wei, K. Rajeshwar, *J. Electrochem. Soc.* **139**, L40 (1992).
131. R. A. Boudreau, R. D. Rauh, *Solar Energy Mater.* **7**, 385 (1982).
132. M. Skylas-Kazacos, B. Miller, *J. Electrochem. Soc.* **127**, 2378 (1980).
133. B. M. Basol, *J. Appl. Phys.* **55**, 601 (1984).
134. V. Krishnan, D. Ham, K. K. Mishra, K. Rajeshwar, *J. Electrochem. Soc.* **139**, 23 (1992).
135. Z. Loizos, A. Mitsis, N. Spyrellis, M. Froment, G. Maurin, *Thin Solid Films* **235**, 51 (1993).
136. M. Bouroushian, Z. Loizos, N. Spyrellis, G. Maurin, *Thin Solid Films* **229**, 101 (1993).
137. Z. Loizos, N. Spyrellis, G. Maurin, D. Pottier, *J. Electroanal. Chem.* **269**, 399 (1989).
138. R. K. Pandey, A. J. N. Roosz, *J. Phys. D: Appl. Phys.* **19**, 917 (1986).

139. C. Wei, C. S. C. Bose, K. Rajeshwar, *J. Electroanal. Chem.* **327**, 331 (1992).
140. K. R. Murali, V. Subramanian, N. Rangarajan, A. S. Lakshmanan, S. K. Rangarajan, *J. Electroanal. Chem.* **368**, 95 (1994).
141. H. Wynands, M. Cocivera, *J. Electrochem. Soc.* **139**, 2052 (1992).
142. J. P. Szabo, M. Cocivera, *J. Electroanal. Chem.* **239**, 307 (1988).
143. J. P. Szabo, M. Cocivera, *J. Electrochem. Soc.* **133**, 1247 (1986).
144. N. Ardoin, J. Winnick, *J. Electrochem. Soc.* **135**, 1719 (1988).
145. M. Cocivera, A. Darkowski, B. Love, *J. Electrochem. Soc.* **131**, 2514 (1984).
146. F. Decker, N. G. Ferreira, M. Fracastoro-Decker, *J. Electrochem. Soc.* **134**, 1499 (1987).
147. F. Decker, J. R. Moro, J. L. S. Ferreira, *Ber. Bunsenges. Phys. Chem.* **91**, 408 (1987).
148. S. M. Babu, T. Rajalakshmi, R. Dhanasekaran, P. Ramasamy, *J. Crystal Growth* **110**, 423 (1991).
149. W. A. Gerrard, J. R. Owen, *Mat. Res. Bull.* **12**, 677 (1977).
150. B. Miller, et al., *J. Electrochem. Soc.* **124**, 1019 (1977).
151. M. Abramovich, et al., *J. Solid State Chem.* **59**, 1 (1985).
152. S. Licht, J. Manassen, *J. Electrochem. Soc.* **132**, 1076 (1985).
153. R. N. Bhattacharya, *J. Appl. Electrochem.* **16**, 168 (1986).
154. J. M. Rosamilia, B. Miller, *J. Electroanal. Chem.* **215**, 249 (1986).

155. D. W. Suggs, I. Villegas, B. W. Gregory, J. L. Stickney, *J. Vac. Sci. Technol. A* **10**, 886 (1992).
156. J. L. Stickney, B. W. Gregory, I. Villegas, in *U.S. Patent* . (University of Georgia, 1994), vol. 6, pp. 5320736.
157. D. W. Suggs, I. Villegas, B. W. Gregory, J. L. Stickney, *Mat. Res. Soc. Symp. Proc.* **222**, 283 (1991).
158. B. M. Huang, L. P. Colletti, B. W. Gregory, J. L. Anderson, J. L. Stickney, *J. Electrochem. Soc.* **142**, 3007 (1995).
159. D. W. Suggs, J. L. Stickney, *Surface Sci.* **290**, 375 (1993).
160. B. W. Gregory, J. L. Stickney, *J. Electroanal. Chem.* **300**, 543 (1991).
161. B. W. Gregory, D. W. Suggs, J. L. Stickney, *J. Electrochem. Soc.* **138**, 1279 (1991).
162. D. W. Suggs, J. L. Stickney, *Surface Sci.* **290**, 362 (1993).
163. I. Shih, C. X. Qiu, *Mater. Lett.* **3**, 446 (1985).
164. B. M. Basol, *J. Appl. Phys.* **58**, 3809 (1985).
165. J. v. Windheim, I. Renaud, M. Cocivera, *J. Appl. Phys.* **67**, 4167 (1990).
166. Y. Sugimoto, L. M. Peter, *J. Electroanal. Chem.* **386**, 183 (1995).
167. R. D. Engelken, T. P. V. Doren, *J. Electrochem. Soc.* **132**, 2910 (1985).
168. P. Carbonnelle, C. Labar, L. Lamberts, *Analisis* **15**, 286 (1987).
169. C. Wei, N. Myung, K. Rajeshwar, *J. Electroanal. Chem.* **347**, 223 (1993).

170. E. Mori, K. Rajeshwar, *J. Electroanal. Chem.* **258**, 415 (1989).
171. W. Lin, K. K. Mishra, E. Mori, K. Rajeshwar, *Anal. Chem.* **62**, 821 (1990).
172. W. J. Danaher, L. E. Lyons, *Aust. J. Chem.* **37**, 689 (1984).
173. W. J. Danaher, L. E. Lyons, *Aust. J. Chem.* **36**, 1011 (1983).
174. D. Ham, K. K. Mishra, A. Weiss, K. Rajeshwar, *Chem. Mater.* **1**, 619 (1989).
175. A. C. Rastogi, K. S. Balakrishnan, *J. Electrochem. Soc.* **136**, 1502 (1989).
176. K. S. Balakrishnan, A. C. Rastogi, *Solar Energy Materials* **23**, 61 (1991).
177. R. K. Pandey, G. Razzini, L. P. Bicelli, *Solar Energy Mater.* **26**, 285 (1992).
178. R. B. Gore, R. K. Pandey, S. K. Kulkarni, *Solar Energy Mater.* **18**, 159 (1989).
179. R. B. Gore, R. K. Pandey, S. K. Kulkarni, *J. Appl. Phys.* **65**, 2693 (1989).
180. J. Llabres, V. Delmas, *J. Electrochem. Soc.* **133**, 2580 (1986).
181. D. A. Fiedler, H. P. Fritz, *Electrochim. Acta* **40**, 1595 (1995).
182. J. K. You, et al., *J. Electroanal. Chem.* **405**, 233 (1996).
183. S. S. Ou, A. Bindal, O. M. Stafsudd, K. L. Wang, B. M. Basol, *J. Appl. Phys.* **55**, 1020 (1984).
184. J. H. Chen, C. C. Wan, *J. Electroanal. Chem.* **365**, 87 (1994).
185. H. Minoura, M. Kitakata, T. Sugiura, M. Murayama, *Bull. Chem. Soc. Jpn.* **60**, 2373 (1987).

186. J. A. v. Windheim, M. Cocivera, *J. Phys. D: Phys.* **23**, 581 (1990).
187. J. A. v. Windheim, M. Cocivera, *J. Electrochem. Soc.* **138**, 250 (1991).
188. A. Darkowski, M. Cocivera, *J. Electrochem. Soc.* **132**, 2768 (1985).
189. J. v. Windheim, M. Cocivera, *J. Electrochem. Soc.* **134**, 441 (1987).
190. L. Gheorghita, M. Cocivera, A. J. Nelson, A. B. Swartzlander, *J. Electrochem. Soc.* **141**, 529 (1994).
191. J. A. v. Windheim, M. Cocivera, *J. Phys. Chem. Solids* **53**, 31 (1992).
192. M. Takahashi, K. Uosaki, H. Kita, S. Yamaguchi, *J. Appl. Phys.* **60**, 2049 (1986).
193. S. Dennison, S. Webster, *J. Electroanal. Chem.* **333**, 287 (1992).
194. W. J. Danaher, L. E. Lyons, *Nature* **271**, 139 (1978).
195. Y. Sugimoto, L. M. Peter, *J. Electroanal. Chem.* **381**, 251 (1995).
196. M. Takahashi, K. Uosaki, H. Kita, *J. Appl. Phys.* **58**, 4292 (1985).
197. M. Takahashi, K. Uosaki, H. Kita, *J. Electrochem. Soc.* **131**, 2304 (1984).
198. K. Uosaki, M. Takahashi, H. Kita, *Electrochim. Acta* **29**, 279 (1984).
199. M. Takahashi, K. Uosaki, H. Kita, *J. Appl. Phys.* **55**, 3879 (1984).
200. C. Sella, P. Boncorps, J. Vedel, *J. Electrochem. Soc.* **133**, 2043 (1986).
201. A. Saraby-Reintjes, L. M. Peter, M. E. Ozsan, S. Dennison, S. Webster, *J. Electrochem. Soc.* **140**, 2880 (1993).

202. B. M. Basol, *Solar Cells* **23**, 69 (1988).
203. A. Pal, J. Dutta, D. Bhattacharyya, S. Chaudhuri, A. K. Pai, *Vacuum* **46**, 147 (1995).
204. J. Dutta, D. Bhattacharyya, A. B. Maitil, S. Chaudhuri, A. K. Pal, *Vacuum* **46**, 17 (1995).
205. P. Sircar, *Appl. Phys. Lett.* **53**, 1184 (1988).
206. J. M. Fisher, et al., *J. Crystal Growth* **138**, 86 (1994).
207. J. M. Fisher, L. E. A. Berlouis, B. N. Rospendowski, P. J. Hall, M. G. Astles, *Semiconductor Science and Technology* **8**, 1459 (1993).
208. B. Qi, D. Kim, D. L. Williamson, J. U. Trefny, *J. Electrochem. Soc.* **143**, 517 (1996).
209. V. Valvoda, J. Touskova, D. Kindl, *Cryst. Res. Technol.* **21**, 975 (1986).
210. J. Llabres, *J. Electrochem. Soc.* **131**, 464 (1984).
211. G. Maurin, O. Solorza, H. Takenouti, *J. Electroanal. chem.* **202**, 323 (1986).
212. P. Cowache, D. Lincot, J. Vedel, *J. Electrochem. Soc.* **136**, 1646 (1989).
213. G. Fulop, M. Doty, P. Meyers, J. Betz, C. H. Liu, *Appl. Phys. Lett.* **40**, 327 (1982).
214. L. Ndiaye, P. Cowache, M. Cadene, D. Lincot, J. Vedel, *Thin Solid Films* **224**, 227 (1993).
215. G. Maurin, D. Pottier, *J. Mater. Sci. Lett.* **6**, 817 (1987).
216. R. N. Bhattacharya, K. Rajeshwar, R. N. Noufi, *J. Electrochem. Soc.* **132**, 732 (1985).
217. R. D. Engelken, T. P. V. Doren, *J. Electrochem. Soc.* **132**, 2904 (1985).

218. M. P. R. Panicker, M. Knaster, F. A. Kroger, *J. Electrochem. Soc.* **125**, 566 (1978).
219. R. N. Bhattacharya, K. Rajeshwar, *J. Electrochem. Soc.* **131**, 2032 (1984).
220. R. N. Bhattacharya, K. Rajeshwar, *J. Appl. Phys.* **58**, 3590 (1985).
221. M. W. Verbrugge, C. W. Tobias, *Am. Inst. chem. Eng. J.* **33**, 628 (1987).
222. M. W. Verbrugge, C. W. Tobias, *J. Electrochem. Soc.* **134**, 3104 (1987).
223. H. J. Gerritsen, *J. Electrochem. Soc.* **131**, 136 (1984).
224. M. H. Miles, W. S. McEwan, *J. Electrochem. Soc.* **119**, 1188 (1972).
225. G. C. Morris, R. Vanderveen, *Solar Energy Mater.* **26**, 217 (1992).
226. K. Singh, A. K. Shukla, *Solar Energy Mater.* **30**, 169 (1993).
227. B. M. Basol, V. K. Kapur, M. L. Ferris, *J. Appl. Phys.* **66**, 1816 (1989).
228. D. Pottier, G. Maurin, *J. Appl. Electrochem.* **19**, 361 (1989).
229. S. Menezes, *Appl. Phys. Lett.* **61**, 1564 (1992).
230. G. Hodes, T. Engelhard, C. R. Herrington, L. L. Kazmerski, D. Cahen, *Progr. Cryst. Growth Charact.* **10**, 345 (1985).
231. B. M. Basol, *J. Vac. Sci. Technol. A* **10**, 2006 (1992).
232. C. Guillen, J. Herrero, *J. Electrochem. Soc.* **143**, 493 (1996).
233. C. Guillen, J. Herrero, *J. Electrochem. Soc.* **142**, 1834 (1995).
234. C. X. Qiu, I. Shih, *J. Appl. Phys.* **64**, 758 (1988).

235. I. Shih, C. X. Qiu, S. N. Qiu, J. F. Huang, *J. Appl. Phys.* **63**, 439 (1988).
236. C. X. Qiu, I. Shih, *Can. J. Phys.* **67**, 444 (1989).
237. R. P. Singh, S. L. Singh, *J. Phys. D: Appl. Phys.* **19**, 1759 (1986).
238. C. X. Qiu, I. Shih, *Can. J. Phys.* **65**, 1011 (1987).
239. C. Guillen, J. Herrero, *J. Electrochem. Soc.* **141**, 225 (1994).
240. K. K. Mishra, K. Rajeshwar, *J. Electroanal. Chem.* **271**, 279 (1989).
241. R. P. Singh, S. L. Singh, S. Chandra, *J. Phys. D: Appl. Phys.* **19**, 1299 (1986).
242. R. N. Bhattacharya, *J. Electrochem. Soc.* **130**, 2040 (1983).
243. W. Jiang-Shan, T. Zheng, M. Tian-Ying, S. Gong-Quan, *Sci. China (series B)* **35**, 281 (1992).
244. C. D. Lokhande, *J. Electrochem. Soc.* **134**, 1728 (1987).
245. S. Endo, Y. Nagahori, S. Nomura, *Jpn. J. Appl. Phys.* **35**, L1101 (1996).
246. T. L. Chu, S. S. Chu, S. C. Lin, J. Yue, *J. Electrochem. Soc.* **131**, 2182 (1984).
247. C. D. Lokhande, S. H. Pawar, *J. Phys. D* **20**, 1213 (1987).
248. A. M. Al-Dhafiri, P. C. Pande, G. J. Russell, J. Woods, *J. Crystal Growth* **86**, 900 (1988).
249. A. C. Rastogi, S. Salkalachen, *J. Appl. Phys.* **58**, 4442 (1985).
250. R. I. Kazhlaeva, A. I. Alekperov, Z. A. Aliyarova, K. V. Kirilyuk, *Electrokhimiya* **21**, 1197 (1985).

251. N. R. d. Tacconi, O. Medvedko, K. Rajeshwar, *J. Electroanal. Chem.* **379**, 545 (1994).
252. I. Villegas, J. L. Stickney, *J. Electrochem. Soc.* **139**, 686 (1992).
253. I. Villegas, J. L. Stickney, *J. Vac. Sci. Technol. A* **10**, 3032 (1992).
254. S. Chandra, N. Khare, *Semicond. Sci. Technol.* **2**, 220 (1987).
255. I. G. Dioum, J. Vedel, B. Tremillon, *J. Electroanal. Chem.* **139**, 329 (1982).
256. M. C. Yang, U. Landau, J. C. Angus, *J. Electrochem. Soc.* **139**, 3480 (1992).
257. P. Andreoli, S. Cattarin, M. Musiani, F. Paolucci, *J. Electroanal. Chem.* **385**, 265 (1995).
258. R. C. D. Mattei, D. Elwell, R. S. Feigelson, *J. Crystal Growth* **44**, 545 (1978).
259. F. Paolucci, G. Mengoli, M. M. Musiani, *J. Appl. Electrochem.* **20**, 868 (1990).
260. C. L. Colyer, M. Cocivera, *J. Electrochem. Soc.* **139**, 406 (1992).
261. M. Neumann-Spallart, G. Tamizhmani, C. Levy-Clement, *J. Electrochem. Soc.* **137**, 3434 (1990).
262. L. Jun, T. Zheng, M. Tian-Ying, *Sci. China (series B)* **33**, 1153 (1990).
263. J. Ramiro, E. Garcia, Camarero, *J. Mater. Sci.* **31**, 2047 (1996).
264. L. M. Peter, J. D. Reid, B. R. Scharifker, *J. Electroanal. Chem.* **119**, 73 (1981).
265. G. Mattsson, L. Nyhom, L. M. Peter, *J. Electroanal. Chem.* **347**, 303 (1993).
266. G. Mengoli, M. M. Musiani, F. Paolucci, *J. Electroanal. Chem.* **332**, 199 (1992).
267. J. Ortega, J. Herrero, *J. Electrochem. Soc.* **136**, 3388 (1989).

268. G. Mengoli, M. M. Musiani, F. Paolucci, *J. Appl. Electrochem.* **21**, 863 (1991).
269. S. N. Sahu, *J. Mater. Sci.* **3**, 102 (1992).
270. D. Elwell, R. S. Feigelson, M. M. Simkins, *J. Cryst. Growth* **51**, 171 (1981).
271. S. N. Sahu, *J. Mater. Sci. Lett.* **8**, 533 (1989).
272. M. C. Hobson, Jr., H. Leidheiser, Jr., *Trans. Metallurg. Soc. AIME* **233**, 482 (1965).
273. S. Massaccesi, S. Sanchez, J. Vedel, *J. Electroanal. Chem.* **412**, 95 (1996).
274. Y. Igasaki, T. Fujiwara, *J. Crystal Growth* **158**, 268 (1996).
275. K. M. Totland, D. A. Harrington, *J. Electroanal. Chem.* **274**, 61 (1989).
276. B. Scharifker, Z. Ferreira, J. Mozota, *Electrochimica Acta* **30**, 677 (1985).
277. K. Mishra, et al., *J. Electrochem. Soc.* **136**, 1915 (1989).
278. R. D. Engelken, A. K. Berry, T. P. V. Doren, J. L. Boone, A. Shahnazary, *J. Electrochem. Soc.* **133**, 581 (1986).
279. L. P. Colletti, S. Thomas, E. M. Willmer, J. L. Stickney, in *Electrochemical Synthesis and Modification of Materials* P. C. Searson, T. P. Moffat, P. C. Andricacos, S. G. Corcoran, J. L. Delplancke, Eds. (Materials Research Society, Pittsburgh, 1996).
280. T. Mahalingam, C. Sanjeeviraja, *Physica Status Solidi A* **129**, K89 (1992).
281. C. D. Lokhande, M. S. Jadhav, S. H. Pawar, *J. Electrochem. Soc.* **136**, 2756 (1989).
282. C. Natarajan, M. Sharon, C. Levy-Clement, M. Neumann-Spallart, *Thin Solid Films* **237**, 118 (1994).

283. J. P. Rai, *Solar Energy Mater.* **30**, 119 (1993).
284. J. P. Rai, K. Singh, *Ind. J. Chem.* **32**, 376 (1993).
285. K. Singh, R. K. Pathak, *Ind. J. Chem.* **32**, 55 (1993).
286. M. Neumann-Spallart, C. Konigstein, *Thin Solid Films* **265**, 33 (1995).
287. C. Wei, K. Rajeshwar, J. D. Luttmer, *J. Electrochem. Soc.* **140**, 829 (1993).
288. A. J. Panson, *Inorg. Chem.* **3**, 940 (1964).
289. J. Vedel, A. Kampmann, D. Lincot, , 188th meeting of the Electrochemical Society, Chicago (Electrochemical Society, 1995).
290. V. K. Kapur, V. Choudary, A. K. P. Chu, . (USA, 1986).
291. B. W. Gregory, M. L. Norton, J. L. Stickney, *J. Electroanal. Chem.* **293**, 85 (1990).
292. M. P. Soriaga, A. T. Hubbard, *JACS* **104**, 2742 (1982).
293. M. P. Soriaga, A. T. Hubbard, *JACS* **104**, 2735 (1982).
294. I. C. Hamilton, R. Woods, *J. Appl. Electrochem.* **13**, 783 (1983).
295. T. E. Lister, B. M. Huang, R. D. Herrick-II, J. L. Stickney, *J. Vac. Sci. Technol. B* **13**, 1268 (1995).
296. J. M. M. Droog, C. A. Alderliesten, P. T. Alserliesten, G. A. Gootsma, *J. Electroanal. Chem.* **111**, 61 (1980).
297. C. B. Ehlers, I. Villegas, J. L. Stickney, *J. Electroanal. Chem.* **284**, 403 (1990).
298. G. N. Salaita, et al., *Lang.* **2**, 1986 (1986).

299. N. J. Tao, S. M. Lindsay, *J. Phys. Chem.* **96**, 5213 (1992).
300. H. A. Gasteiger, N. M. Markovic, P. N. J. Ross, *Lang.* **12**, 1414 (1996).
301. B. G. Bravo, et al., *J. Phys. Chem.* **95**, 5245 (1991).
302. B. M. Ocko, G. M. Watson, J. Wang, *J. Phys. Chem.* **98**, 897 (1994).
303. S. Sugita, T. Abe, K. Itaya, *J. Phys. Chem.* **97**, 8780 (1993).
304. R. L. McCarley, A. J. Bard, *J. Phys. Chem.* **95**, 9618 (1991).
305. A. B. Ellis, S. W. Kaiser, J. M. Bolts, M. S. Wrighton, *JACS* **99**, 2839 (1977).
306. R. D. Herrick, II, J. L. Stickney, in *New Directions in Electroanalytical Chemistry* J. Leddy, M. Wightman, Eds. (The Electrochemical Society, Pennington, NJ, 1996), vol. 96-9, pp. 186.
307. D. M. Kolb, J. Schneider, *Electrochim. Acta* **31**, 929 (1986).
308. X. Gao, A. Hamelin, M. J. Weaver, *PRL* **67**, 618 (1991).
309. L. B. Goetting, B. M. Huang, T. E. Lister, J. L. Stickney, *Electrochimica Acta* **40**, 143 (1995).
310. A. Nasar, M. Shamsuddin, *Thermochim. Acta* **205**, 157 (1992).
311. L. P. Colletti, J. L. Stickney, (in prep).
312. Q. P. Lei, J. L. Stickney, in *Interface dynamics and growth* K. S. Liang, M. P. Anderson, R. F. Bruinsma, G. Scoles, Eds. (Materials Research Society, Pittsburg, 1992), vol. 237, pp. 335.

313. T. A. Sorenson, B. K. Wilmer, J. L. Stickney, in *Solid-Liquid Electrochemical Interfaces* G. Jerkiewicz, K. Uosaki, A. Wieckowski, Eds. (American Chemical Society, Washington, 1997), vol. 656, pp. Chp. 9.
314. C. A. Ross, L. M. Goldman, F. Spaepen, *J. Electrochem. Soc.* **140**, 91 (1993).
315. C. A. Ross, *Ann. Rev. Mat. Sci.* **24**, 159 (1994).
316. C. E. D. Chidsey, D. N. Loiacono, T. Sleator, S. Nakahara, *Surf. Sci.* **200**, 45 (1988).
317. E. Holland-Moritz, J. Gordon-II, G. Borges, R. Sonnenfeld, *Lang.* **7**, 301 (1991).
318. S. Buchholz, H. Fuchs, J. P. Rabe, *J. Vac. Sci. Technol. B* **9**, 857 (1991).
319. J. A. DeRose, T. Thundat, L. A. Nagahara, S. M. Lindsay, *Surf. Sci.* **256**, 102 (1991).
320. D. W. Suggs, J. L. Stickney, *J. Phys. Chem.* **95**, 10056 (1991).
321. L. P. Colletti, B. Flowers, J. L. Stickney, *J. Cryst. Growth* (in prep).
322. M. P. Soriaga, J. L. Stickney, in *Modern Techniques in Electroanalytical Chemistry* P. Vanysek, Ed. (Wiley & Sons, New York, 1996) pp. 1.
323. G. Binnig, H. Rohrer, C. Gerber, E. Weibel, *Phys. Rev. Lett.* **49**, 57 (1982).
324. G. Binnig, H. Rohrer, *Surf. Sci.* **126**, 236 (1983).
325. R. Sonnenfeld, B. C. Schardt, *Appl. Phys. Lett.* **49**, 1172 (1986).
326. R. Sonnenfeld, J. Schneir, P. K. Hansma, in *Modern Aspects of Electrochemistry* R. E. White, J. O. M. Bockris, B. E. Conway, Eds. (Plenum Press, New York,), vol. 12, pp. 1.
327. T. R. I. Cataldi, et al., *J. Electroanal. Chem.* **290**, 1 (1990).

328. D. A. Bonnell, Ed., *Scanning Tunneling Microscopy and Spectroscopy, Theory, Techniques and Applications* (VCH Publishing, 1993).
329. A. J. Stroscio, W. J. Kaiser, Eds., *Scanning Tunneling Microscopy*, vol. 27 (Academic Press, New York, 1993).
330. K. S. Kim, N. Winograd, R. E. Davis, *JACS* **93**, 6296 (1971).
331. B. M. Huang, T. E. Lister, J. L. Stickney, in *Handbook of surface imaging and visualization* A. T. Hubbard, Ed. (CRC Press, Boca Raton, 1995) pp. 77.
332. B. C. Schardt, et al., *Surf. Sci.* **175**, 520 (1986).
333. T. E. Lister, J. L. Stickney, *J. Phys. Chem.* **in press** (1997).
334. B. M. Huang, T. E. Lister, J. L. Stickney, *Surf. Sci.* (submitted).
335. M. D. Pashley, K. W. Haberern, W. Friday, J. M. Woodall, P. D. Kirchner, *PRL* **60**, 2176 (1988).
336. B. K. Biegelsen, L.-E. Swartz, R. D. Brigans, *J. Vac. Sci. Technol. A* **8**, 280 (1990).
337. P. K. Larsen, G. Meyer-Ehmsen, *Surf. Sci.* **240**, 168 (1990).
338. H. H. Farrell, M. C. Tamargo, J. L. d. Miguel, *Appl. Phys. Lett.* **58**, 355 (1991).
339. C. Deparis, J. Massies, *J. Cryst. Growth* **108**, 157 (1991).
340. J. F. Moulder, W. F. Stickle, P. E. Sobol, K. D. Bomben, *Handbook of X-ray Photoelectron Spectroscopy* (Perkin Elmer Corp., Eden Prairie, 1992).

341. W. J. M. Tegart, *The electrolytic and Chemical Polishing of Metals in Research and Industry* (Pergamon Press Ltd., Oxford, 1959).
342. A. Hamelin, *J. Electroanal. Chem.* **142**, 299 (1982).
343. J. Schneider, D. M. Kolb, *Surf. Sci.* **193**, 579 (1988).
344. D. M. Kolb, in *Structure of Electrified Interfaces* J. Lipkowski, P. N. Ross, Eds. (VCH Publishers, New York, 1993) pp. 65.
345. X. Gao, A. Hamelin, M. J. Weaver, *Phys. Rev. B* **46**, 7096 (1992).
346. P. Skoluda, D. M. Kolb, *Surf. Sci.* **260**, 229 (1992).
347. X. Gao, G. J. Edens, A. Hamelin, M. J. Weaver, *Surf. Sci.* **296**, 333 (1993).
348. A. Hamelin, X. Gao, M. J. Weaver, *J. Electroanal. Chem.* **323**, 361 (1992).
349. O. M. Magunssen, J. Hotlos, R. J. Behm, N. Batina, D. M. Kolb, *Surf. Sci.* **296**, 310 (1993).
350. X. Gao, M. J. Weaver, *J. Phys. Chem.* **97**, 8685 (1993).
351. I. Villegas, C. B. Ehlers, J. L. Stickney, *J. Electrochem. Soc.* **137**, 3143 (1990).
352. R. L. McCarley, A. J. Bard, *J. Phys. Chem.* **95**, 9618 (1991).
353. N. J. Tao, S. M. Lindsay, *J. Phys. Chem.* **96**, 5213 (1992).
354. W. Haiss, J. K. Sass, X. Gao, M. J. Weaver, *Surf. Sci.* **274**, L593 (1992).
355. X. Gao, M. J. Weaver, *Ber. Bunsenges. Phys. Chem.* **97**, 507 (1993).
356. B. M. Ocko, G. M. Watson, J. Wang, *J. Phys. Chem.* **98**, 897 (1994).

357. F. T. Wagner, P. N. Ross, *Surf. Sci.* **160**, 305 (1985).
358. X. Gao, Y. Zhang, M. J. Weaver, *J. Phys. Chem.* **96**, 4156 (1992).
359. R. L. McCarley, Y. Kim, A. J. Bard, *J. Phys. Chem.* **97**, 211 (1993).
360. L. P. Colletti, J. L. Stickney, . (unpublished results).
361. H. Siegenthaler, K. Juttner, E. Schmidt, W. J. Lorenz, *Electrochim. Acta* **23**, 1009 (1978).
362. N. N. Greenwood, A. Earnshaw, *Chemistry of the elements* (Pergamon Press, Oxford, 1984).
363. Y.-T. Kim, A. J. Bard, *Lang.* **8**, 1096 (1992).
364. T. Han, T. P. Beebe, *Lang.* **10**, 1096 (1994).
365. O. Chailapakul, L. Sun, C. Xu, R. M. Crooks, *JACS* **115**, 12459 (1993).
366. K. Edinger, A. Golizhauser, K. Demota, C. Woll, M. Grunze, *Lang.* **9**, 4 (1993).
367. C. Schonenberger, J. A. M. Sondag-Huethorst, J. Jorritsma, L. G. J. Fokkink, *Lang.* **10**, 611 (1994).
368. G. E. Poirier, M. J. Tarlov, *Lang.* **9**, 2853 (1994).
369. G. E. Poirier, M. J. Tarlov, H. E. Rushmeier, *Lang.* **10**, 3383 (1994).
370. C. A. M. Dermott, M. T. M. Dermott, J. B. Green, M. D. Porter, *J. Phys. Chem.* **99**, 13257 (1995).
371. J. C. Bondos, A. A. Gewirth, R. G. Nuzzo, *J. Phys. Chem.* **100**, 8617 (1996).
372. J. W. Schultze, F. D. Koppitz, M. M. Lohrengel, *Ber. Buns. Phys. Chem.* **78**, 693 (1974).

373. D. W. Suggs, A. J. Bard, *JACS* (1995).
374. R. F. C. Farrow, G. R. Jones, G. M. Williams, I. M. Young, *Appl. Phys. Lett.* **39**, 954 (1981).
375. T. H. Myers, Y. Lo, J. F. Schetzina, S. R. Jost, *J. Appl. Phys.* **53**, 9232 (1982).
376. S. Wood, et al., *J. Appl. Phys.* **55**, 4225 (1984).
377. H. A. Mar, N. Salansky, *J. Appl. Phys.* **56**, 2369 (1984).
378. S. K. Ghandhi, I. Bhat, *Appl. Phys. Lett.* **45**, 678 (1984).
379. Z. C. Feng, et al., *Appl. Phys. Lett.* **47**, 24 (1985).
380. G. M. Williams, C. R. Whitehouse, N. G. Chew, G. W. Blackmore, A. G. Cullis, *J. Vac. Sci. Technol. B* **3**, 704 (1985).
381. K. J. Mackey, P. M. G. Allen, W. G. Herrender-Harker, R. H. Williams, *Surf. Sci.* **178**, 124 (1986).
382. T. D. Golding, M. Martinka, J. H. Dinan, *J. Appl. Phys.* **64**, 1874 (1988).
383. I. B. Bhat, K. Patel, N. R. Taskar, J. E. Ayers, S. K. Ghandhi, *J. Cryst. Growth* **88**, 23 (1988).
384. N.-H. Cho, B. C. DeCooman, C. B. Carter, R. Fletcher, D. K. Wagner, *Appl. Phys. Lett.* **47**, 879 (1985).
385. K. Morizane, *J. Cryst. Growth* **38**, 249 (1977).
386. H. Kroemer, *J. Cryst. Growth* **81**, 193 (1987).

387. S. Strite, et al., *J. Vac. Sci. Technol. B* **8**, 1131 (1990).
388. S. B. Quadri, E. F. Skelton, A. W. Webb, J. Kennedy, *Appl. Phys. Lett.* **46**, 257 (1985).
389. J. L. Bell, S. Sen, *J. Vac. Sci. Technol. A* **3**, 112 (1985).
390. H. F. Wolf, *Semiconductors* (Wiley Interscience, New York,).
391. I. Villegas, J. L. Stickney, *J. Electrochem. Soc.* **138**, 1310 (1991).
392. L. E. Davis, N. C. MacDonald, P. W. Palmberg, G. E. Riach, R. E. Weber, *Hand book of Auger Electron Spectroscopy* (Physical Electronics Division, Perkin-Elmer Corporation, Eden Prairie, Minnesota, 1978).
393. V. Solzbach, H. J. Richter, *Surf. Sci.* **97**, 191 (1980).
394. Y.-C. Lu, R. S. Feigelson, R. K. Route, *J. Appl. Phys.* **67**, 2583 (1990).
395. T. Meguro, et al., *Appl. Phys. Lett.* **56**, 1556 (1990).
396. Y. Horiike, et al., *J. Vac. Sci. Technol. A* **8**, 1844 (1990).
397. T. Meguro, Y. Aoyagi, in *Atomic Layer Growth and Processing* T. F. Kuech, P. D. Dapkus, Y. Aoyagi, Eds. (Mater. Res. Soc., Pittsburgh, 1991), vol. 222, pp. 121.
398. H. Sakaue, et al., in *Atomic Layer Growth and Processing* T. F. Kuech, P. D. Dapkus, Y. Aoyagi, Eds. (Mater. Res. Soc., Pittsburgh, 1991), vol. 222, pp. 195.
399. P. A. Maki, D. J. Ehrlich, *Appl. Phys. Lett.* **55**, 91 (1989).
400. P. Lei, Choong, J. L. Stickney, . (University of Georgia, USA, 1995).
401. P. A. Kohl, F. W. J. Ostermayer, *Annu. Rev. Mater. Sci.* **19**, 379 (1989).

- 402. P. A. Kohl, D. B. Harris, J. Winnick, *J. Electrochem. Soc.* **137**, 3315 (1990).
- 403. P. A. Kohl, D. B. Harris, J. Winnick, *J. Electrochem. Soc.* **138**, 608 (1991).
- 404. E. K. Propst, K. W. Vogt, P. A. Kohl, *J. Electrochem. Soc.* **140**, 3631 (1993).
- 405. P. A. Kohl, D. B. Harris, *Electrochim. Acta* **38**, 101 (1993).
- 406. D. Harris, P. A. Kohl, J. Winnick, *J. Electrochem. Soc.* **141**, 1274 (1994).
- 407. L. P. Colletti, R. Slaughter, J. L. Stickney, *J. Soc. Info. Display* (1997).

VIII: FIGURES

1. Cyclic current-potential curves and LEED patterns: 10^{-4} M Ag^+ in 1M HClO_4 at the $\text{Pt}(111)(\sqrt{7} \times \sqrt{7})\text{R}19.1^\circ$ -I surface. Scan rate = 2 mV/s.
Reproduced from (26), with permission from North-Holland Publishing Co.
2. Detailed drawing of the circulation of fluids and of the immersion and rinsing vessels for a SILAR deposition system: (1) substrates, (2) tweezers, (3) moving crown, (4) immersion beakers, (5) rinsing beakers, (6) circulatory tray, (7) bottles, (8) pumps, (9) filters, (10) overflows, (11) magnetic stirrers, (12) electrodes, (13) rinsing vessels, (14) rotameters, (15) sieves, (16) electrogate, (17) draining pipe, (18) electrogate, (19) conductivity cell, (20) rotameter, (21) bubbler, (22) zinc (or cadmium) compartments, (23) Sulfur compartments.
Reproduced from (30), with permission from Chapman and Hall Ltd.
3. Current density vs. cathode voltage for deposition at 85°C from a 1.2 M CdSO_4 solution saturated with TeO_2 ; pH = 3.4, stirring rate 160 rpm.
Reproduced from (218), with permission from the Electrochemical Society.
4. X-ray diffraction patterns of films deposited on SnO_2 -covered glass from a solution of 1 M CdSO_4 , saturated with TeO_2 , pH \approx 2.7, with current density 0.5 mA/cm^2 ($E_{\text{rest}} =$

0.18V) at 22°C (a), 35°C (b), 65°C (c), and 90°C (d), and the pattern (e) of film (a) after annealing for 3.5 hr at 350°C in an argon atmosphere.

Reproduced from (218), with permission from the Electrochemical Society.

5. Current-voltage trace obtained during cyclic electrodeposition of CdSe onto a Ni rotating disk electrode (1000 rpm): (A) potential region where Se and CdSe are deposited; (B) deposition of bulk Cd; (C) stripping wave of excess Cd. Voltage scale is referenced to SCE. Negative potentials are to the left; cathodic (negative) currents are in the downward direction. Scan rate is 10 V/s.

Reproduced from (109), with permission from the American Chemical Society.

6. Diagram of thin-layer electrochemical cell (TLEC): (A) TLEC in conjunction with electrochemical H-cell; (B) enlarged diagram showing pinhole region.

Reproduced from (161), page 1280, with permission from the Electrochemical Society.

7. Current-potential curves of Au tricrystal: (A) clean Au in 10 mM H₂SO₄ (pH = 1.7); (B) in 1.0 mM CdSO₄ + a buffer consisting of 2.0 mM acetic acid and 1.0 mM CsOH (pH = 4.6), sweep rate = 2 mV/s; (C) in 0.40 mM TeO₂ + 10 mM H₂SO₄ (pH = 2.2), sweep rate = 1 mV/s; (D) Te UPD-covered Au in 1.0 mM CdSO₄ + a buffer consisting of 2.0 mM acetic acid and 1.0 mM CsOH (pH = 4.6), sweep rate = 2 mV/s; (E) stripping of two ECALE layers of CdTe from polycrystalline Au in a TLEC.

Reproduced from (161), page 1281, with permission from the Electrochemical Society.

8. Plot of Cd coverage vs. Te coverage on a polycrystalline Cu electrode. Slope = 0.95; x-intercept = 0.40.
Reproduced from (291), page 92, with permission from Elsevier Sequoia S.A., Lausanne.
9. Pourbaix diagrams describing (a) Cd, (b) Te, (c) CdTe, and (d) the underpotential deposition of Cd and Te on CdTe, in water. The diagrams were calculated using an activity of 10^{-3} M for all soluble species. The hatched areas in (d) represent the differences in potentials, UPD, associated with deposition on CdTe as opposed to deposition on the pure elements.
Reproduced from (155), page 887, with permission from the American Vacuum Society.
10. A) Clean Au electrode in 0.25 mM TeO_2 + 20 mM H_2SO_4 + 0.5 M Na_2SO_4 , pH = 9.2.
B) Clean Au electrode in 1.0 mM SeO_2 + 10 mM $\text{Na}_2\text{B}_4\text{O}_7$ + 1.0 M NaClO_4 , pH = 8.6.
C) Clean Au electrode in 2.5 mM Na_2S + 0.5 M NaClO_4 , pH = 11.
11. Zn deposition on a Au TLEC coated with an atomic layer of: A) Te, B) Se, and C) S.
12. Diagram of steps involved in a single ECALE cycle using a TLEC, for the deposition of ZnS.
13. Voltammetry showing the stripping of deposits of A) ZnTe, B) ZnSe, C) ZnS. Each deposit was the result of four ECALE cycles.

14. Coverages of zinc and sulfur per cycle, after three ECALE cycles, as a function of the potential used to deposit sulfur. The zinc deposition potential was held constant at -0.9 V.
15. Zinc and sulfur coverages per cycle, after three ECALE cycles, as a function of the potential used to deposit zinc. The sulfur deposition potential was held constant at -1.00 V.
16. Zinc and selenium coverages, per cycle, after four ECALE cycles, as a function of the potential used to deposit zinc. The Se atomic layers were formed by first depositing a couple of monolayers of Se at -0.9 V, and then reducing off the excess at -0.9 V, in the corresponding blank electrolyte solution.
17. Zinc and tellurium coverages, per cycle, after four ECALE cycles, as a function of the Zn deposition potential. Te atomic layers were formed by initial deposition of a couple of ML of Te at -0.8V, followed by reductive dissolution of the excess Te at -1.1V.
18. Graphs of total coverage, determined coulometrically as a function of the number of cycles. A) ZnS, B) ZnSe, and C) ZnTe.
19. Automated flow electrodeposition system, initial design. Thin layer cell design.
20. Program of potentials and solutions amounts in one ECALE cycle for CdTe deposition.
Reproduced from (44), page 292, with permission from Marcel Dekker, Inc.

21. SEM micrographs of two deposits, each formed with 50 cycles and the same deposition hardware, but with differing ECALE programs. The conditions are as follows: (A) deposit atomic layer of Te at -1.25 V directly; (B) deposit bulk Te at -0.8 V first, followed by rinsing out excess HTeO_2 , and subsequently stripping off the excess Te in the corresponding blank.

Reproduced from (158), page 3010, with permission from the Electrochemical Society.

22. Cross section of the distribution valves: (a) the solenoid driven valve (b) the inert rotatable valve. The former has a design which can cause cross contamination.

Reproduced from (158), page 3013, with permission from the Electrochemical Society.

23. An SEM micrograph of a deposit formed using 100 cycles, and the new hardware.

24. Optical micrographs of CdTe deposits formed using the thin layer flow cell, with 200 cycles. A) high quality deposit. B) showing effect of bubbles in the cavity. C) showing edge effects and some bubble effects.

25. Thick layer deposition cell for automated system.

26. A) Relative coverages of Cd and Te as a function of the Cd deposition potential. Each deposit was formed using 200 cycles. Coverages measured using EPMA. B) Absolute

coverages vs. the Cd UPD potential, measured by dissolving deposits and running ICP-MS on the resulting solutions.

27. Cd/Te ratio observed using EPMA for deposits formed using 200 cycles, as a function of the Cd deposition potential.
28. XRD spectra for CdTe films grown with 200 cycles, as a function of the Cd deposition potential. Omega had been optimized for increased surface sensitivity in each case.
29. SEM micrographs of CdTe deposits formed using 200 cycles, and adjusting the Cd deposition potential. A) -0.4 V, B) -0.6 V, C) -0.75 V, D) -0.90 V.
30. SEM micrographs taken with a microscope with a field emission tip. A) Clean Au on Si substrate; B) CdTe deposit formed using 200 cycles on a substrate equivalent to that shown in A.
31. STM micrograph of Au on Si substrate. The vertical range used in the image was 23 nm.
32. Relative coverages of Cd and Te in deposits formed using 200 cycles each, as a function of the potential used to form the first few monolayers of Te, as a first step in the formation of Te atomic layers. Data obtained using EPMA.

33. Cd to Te ratio for deposits formed using 200 cycles each, as a function of the potential used to form the first few monolayers of Te, as a first step in the formation of Te atomic layers. Data obtained using EPMA.
34. Graph of the Te coverage remaining on the surface after reductions at various potentials. Each point results from the initial deposition of 1.3 ML at -0.8 V, followed by the indicated reduction in the Te blank solution.
35. The Te coverage remaining after reductive dissolution, as a function of time, at -1.4 V on the Au(100) surface.
36. Graph of the coverages of Cd and Te, formed using 200 cycles, as a function of the potential used to reductively remove excess Te, as the second step in the formation of Te atomic layers.
37. Graph of the Cd/Te ratio for the same deposits shown in Figure 36. Deposits formed using 200 cycles, as a function of the potential used to reductively remove excess Te, as the second step in the formation of Te atomic layers.
38. A) Graph of Cd and Te relative coverages as a function of the number of cycles used to form the deposits. B) Graph of the Cd and Se relative coverages as a function of the number of cycles used to form the deposits.

39. Schematic diagram of UHV-EC instrument.
40. Proposed structure for CdTe monolayer formed on Au(100). The structure corresponds to a $c(2 \times 2)$, with a coverage of $1/2$ ML each of Cd and Te.
41. Schematic drawing of possible scenarios for CdTe deposits formed on increasing initial coverages of Te, A) $1/3$, B) $1/2$, C) $2/3$.
42. As coverage vs. deposition potential and pH in a Au TLEC.
Reprinted from (252), with permission from the Electrochemical Society.
43. Picture showing (2×2) LEED pattern from Au(100) surface supporting a monolayer of GaAs. Beam energy was 40 eV.
44. Proposed structure for Au(100) (2×2) - GaAs structure.
45. Auger spectrum for Au(100): (A) after ion bombardment and annealing, (B) after emersion following Cd UPD, (C) after emersion following first Te UPD, (D) after emersion following Cd UPD on first Te UPD, and (E) after emersion following Cd UPD on second Te UPD.
Reprinted from (162) with permission from Elsevier Pub. V.B.

46. XPS spectra of Au(100) after (A) ion bombardment and annealing, (B) first Te UPD, (C) Cd UPD on first Te UPD, and (D) deposition of bulk Te.
Reprinted from (331), page 81, with permission from CRC Press.
47. STM image of a monolayer of CdTe on Au(100). Image depicts the heterogeneity of the surface.
48. STM micrograph showing monoatomically high Au islands on a clean Au(100) surface, $V_b = 109.9$ mV, $i_t = 1.0$ nA, Z range = 5.0nm.
49. STM image of I coated Au(100) surface, showing large atomically flat terraces.
50. Current-potential curves in 0.2 mM TeO_2^+ , in 10 mM H_2SO_4
a) Te deposition on clean Au(100)
b) Te deposition on I-treated Au(100)
51. AES intensities for Te and I as a function of potential for the three low index planes. (a) Au(100); (b) Au(111); (c) Au(110).
52. Auger spectra for a Au(100) single crystal:
A) After cleaning.
B) Covered with an atomic layer of Se.
C) Covered with an atomic layer of Cd.

D) An atomic layer of Se covered with an atomic layer of Cd.

53. LEED patterns for Se adsorbed on Au(100).

A) $p(2 \times 2)$ -Se, 1/4 ML coverage, 36.7 eV.

B) $(2 \times \sqrt{10})$ -Se, 1/3 ML coverage, 33.5 eV.

C) $c(2 \times 2)$ -Se, 1/2 ML coverage, 32.9 eV.

D) $(3 \times \sqrt{10})$ -Se, 8/9 ML coverage, 33.3 eV.

Reproduced from (295) with permission from the American Vacuum Society.

54. STM micrographs of Se atomic layers on Au(100).

A) $p(2 \times 2)$ -Se, 1/4 coverage.

B) $(2 \times \sqrt{10})$ -Se, 1/3 coverage.

C) $c(2 \times 2)$ -Se, 1/2 coverage.

D) Increasing number of S_8 rings.

E) Close packed S_8 rings, $(3 \times \sqrt{10})$ -Se.

F) Pits formed at high Se coverages.

55. Diagram of structures proposed for Se atomic layers formed on Au(100).

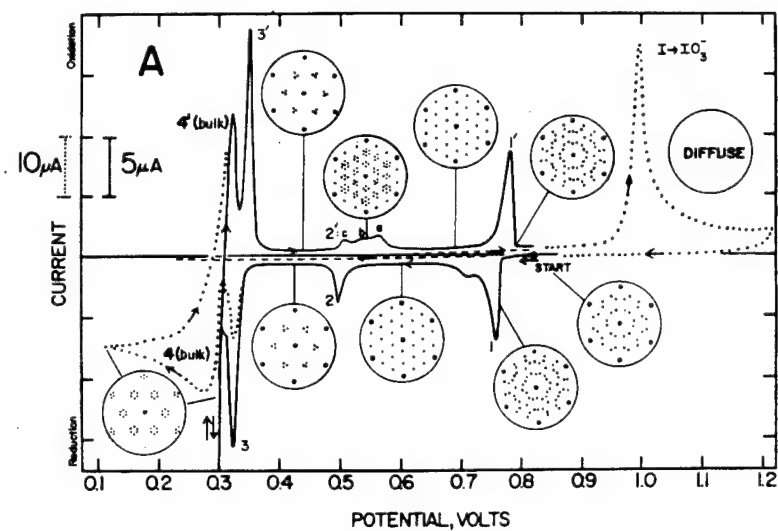
56. Se coverage vs. potential curves on Au(100). Coverage values were obtained by coulometry, using anodic stripping voltammetry of deposit. (a) Reductive deposition of Se. (b) Anodic stripping of bulk Se (bulk = ~ 1.25 monolayers). (c) Cathodic stripping of bulk Se (bulk = ~ 1.25 monolayers).

Reproduced from (295) with permission from the American Vacuum Society.

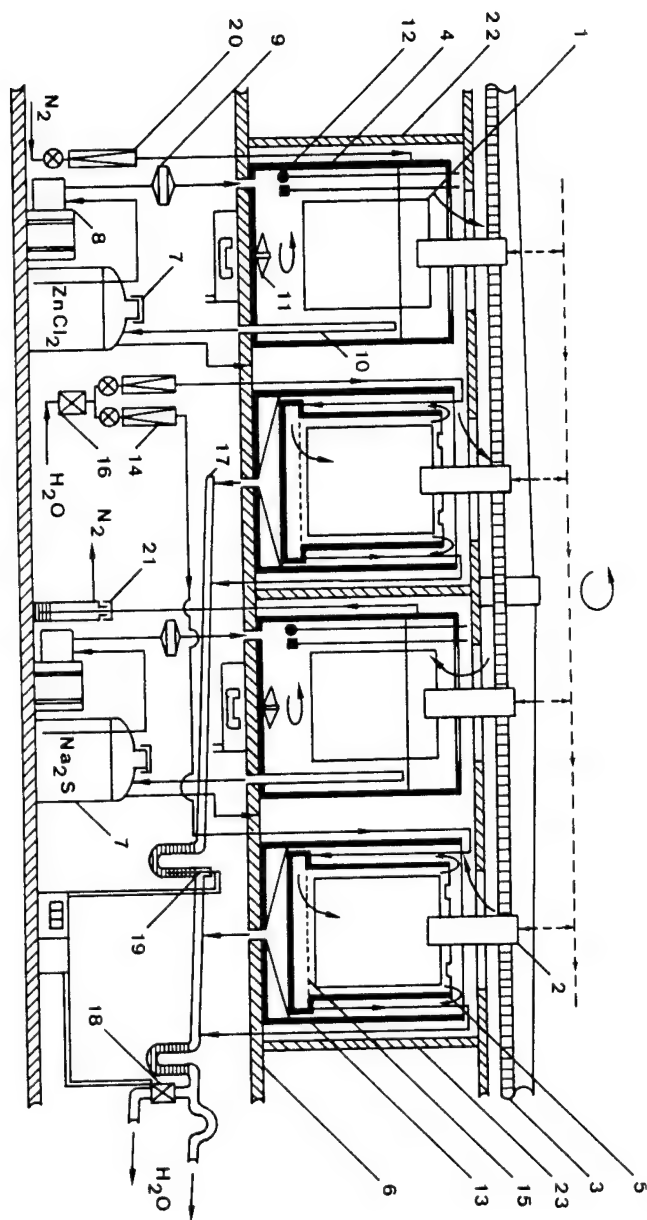
57. Voltammetry of a Au "tri" crystal in 1 mM HSeO_3^- .
58. Cd deposition voltammetry from a mM CdSO_4 solution, on: A) clean Au, B) 1/2 ML of Se, C) full ML of Se.
59. Se structures on the Au low index planes, used as substrate for Cd deposition.
 - A) Au(111) ($\sqrt{3}\times\sqrt{3}$)R 30°-Se, 1/3 coverage.
 - B) Au(100) c(2X2)-Se, 1/2 coverage.
 - C) Au(110) (3X2)-Se, 2/3 coverage.
60. LEED pattern of a Au(111)($\sqrt{3}\times\sqrt{3}$)R 30°-Se.
61. STM micrographs of Au(111) supporting Se atomic layers.
 - A) Just the Au(111)($\sqrt{3}\times\sqrt{3}$)R 30°-Se.
 - B) Au(111)($\sqrt{3}\times\sqrt{3}$)R 30°-Se and some domains of boxes.
62. LEED patterns for CdSe monolayers on Au(111):
 - A) Au(111)($\sqrt{3}\times\sqrt{3}$)R19.1°-CdSe.
 - B) Au(111)(3X3)-CdSe.
63. Proposed structures for CdSe monolayers formed on Au(111):

- A) Au(111)($\sqrt{7}\times\sqrt{7}$)R19.1°-CdSe.
- B) Au(111)(3X3)-CdSe.
64. A) *In-situ* STM image of Se layer formed on Au(111). Some domains of ($\sqrt{3}\times\sqrt{3}$)R30°-Se are present as well as many domains of the Se₈ structure, in mM CdSO₄, at -0.1 V.
- B) The same surface, only at -0.4 V. The hexagonal (3X3) structure (Figure 63B) is evident, as well as small puffs, probably the beginning of a second layer of CdSe.
65. Antiphase domain formation in polar on nonpolar epitaxy. (a) Incomplete pre-layer coverage, (b) odd step height.
- Reproduced from (387), page 1132, with permission from the American Vacuum Society.
66. Auger Spectra: A) Freshly polished, oxidized and contaminated (111)Cd surface of a CdTe crystal; B) (111)Cd surface after a 3 min etch in 1% Br₂/CH₃OH solution; C) Br₂/CH₃OH etched surface after rinse in 1 mM H₂SO₄ at -0.1V; D) (111)Cd surface after electrochemical reduction at -2V in mM H₂SO₄ for 10 min.
- Reproduced from (391) with permission of the Electrochemical Society.
67. LEED patterns: (a) (111)Cd surface after etching, rinsing, and electrochemical reduction. Beam energy: 59 eV. (b) (111)Te surface after etching, rinsing, and electrochemical reduction. Beam energy: 64 eV.
- Reproduced from (391), page 1313, with permission from the Electrochemical Society.

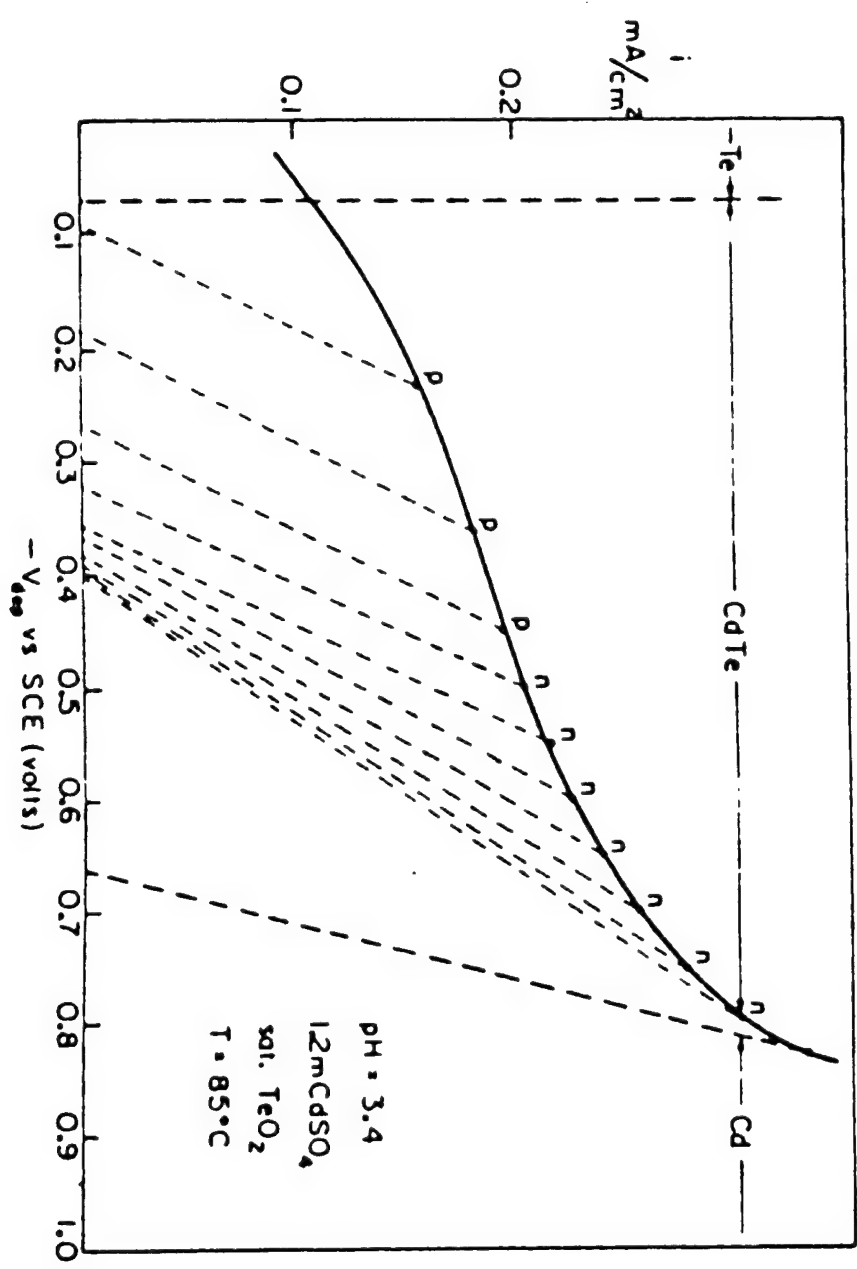
68. Schematic illustrating the electrochemical digital etching process on CdTe(100).
69. AFM images of CdTe(100) surfaces, A) before etching, and B) after 150 cycles of electrochemical digital etching.
70. Voltammograms on an argon ion bombarded, annealed CdTe(100) surface in 50 mM K_2SO_4 , pH = 5.6. A) Reduction from the open circuit potential to -2.0 V. B) Oxidation from the open circuit potential to +0.30 V and reversing to -0.55 V, under illuminated conditions. C) Reduction following B) from open circuit potential to -1.8V and reversing to -0.50 V.
71. Chronoamperograms of ion bombarded, annealed CdTe(100) in 50 mM K_2SO_4 at different oxidative potentials for 5 minutes. A) +0.25 V. B) 0.0 V. C) -0.25 V.
72. Graph showing the charge passed, converted to monolayers, as a function of potential used for oxidation. Total oxidative charge has been separated into two components: transient oxidation and background oxidation. In addition, the subsequent reduction charge for Te is listed as well.



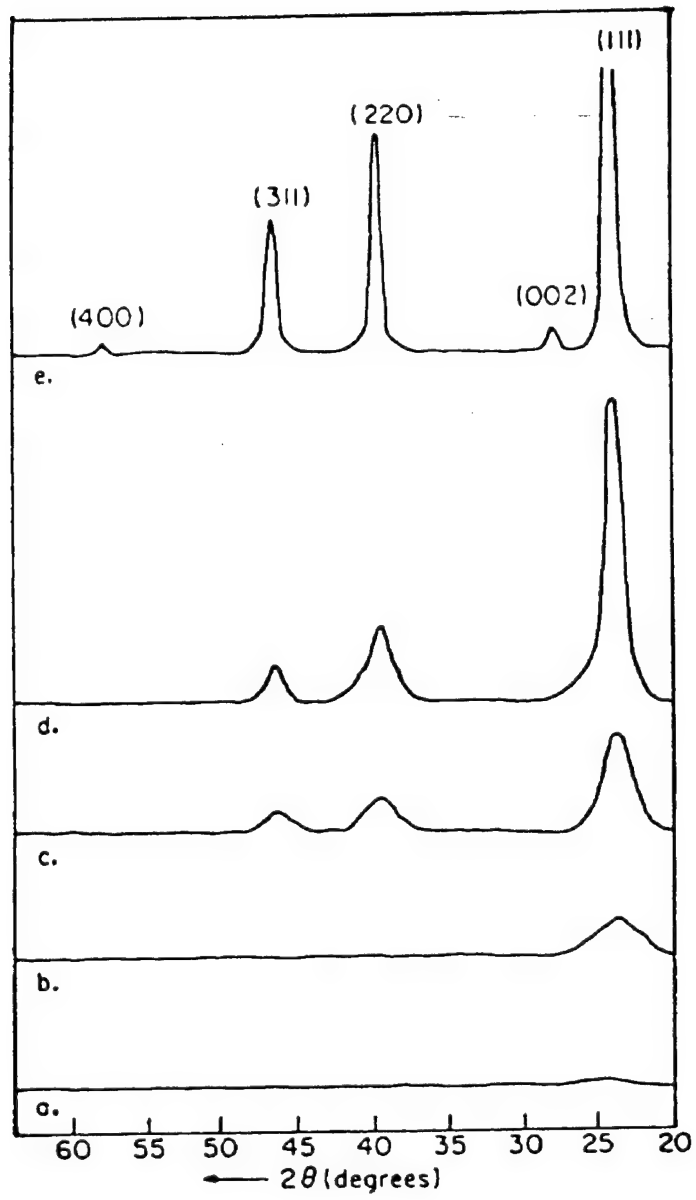
STICKNUB4
Figure 2

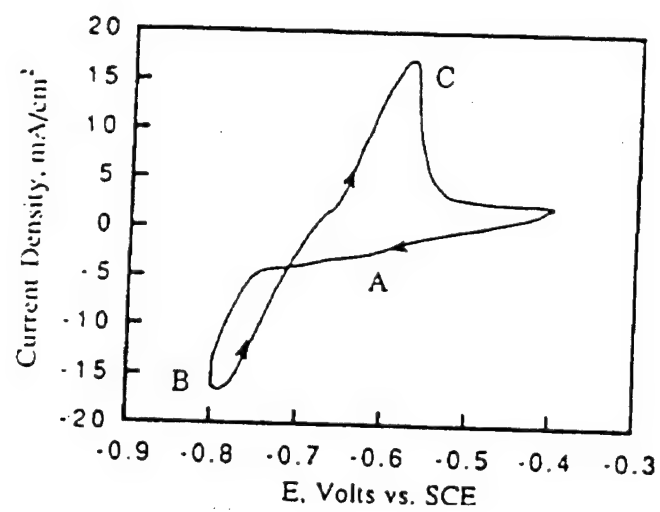


STICKNEY
Figure 3

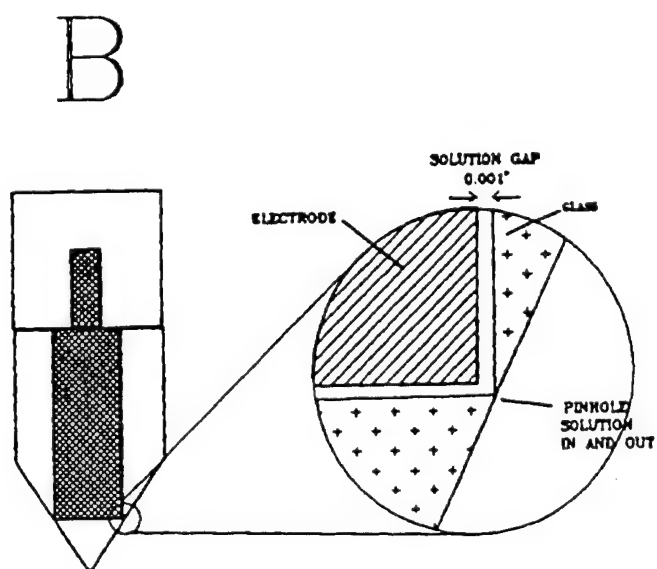
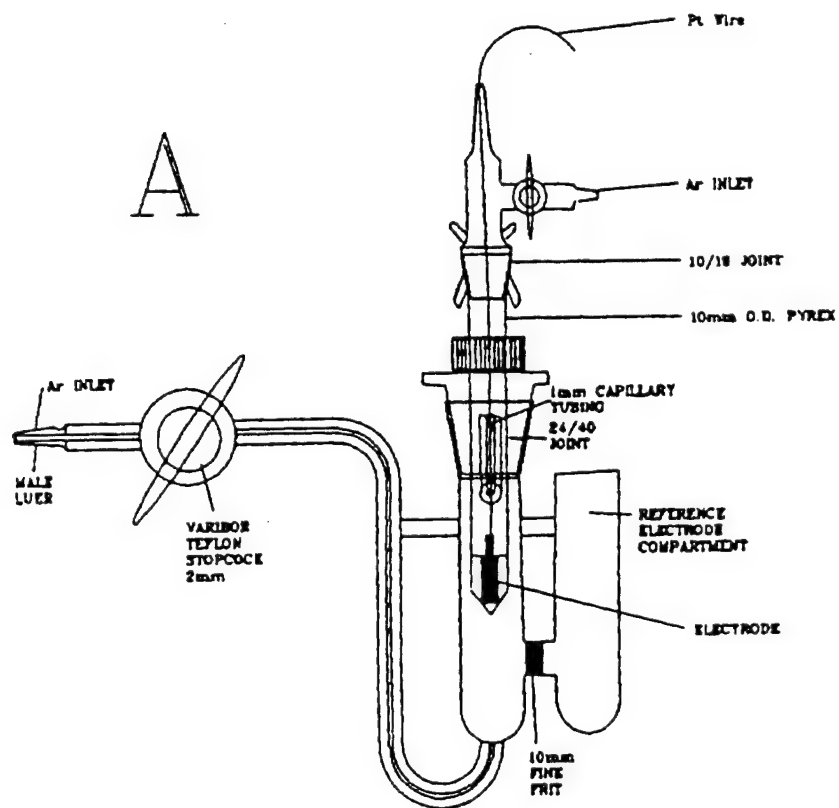


STICKNEY
Figure 4

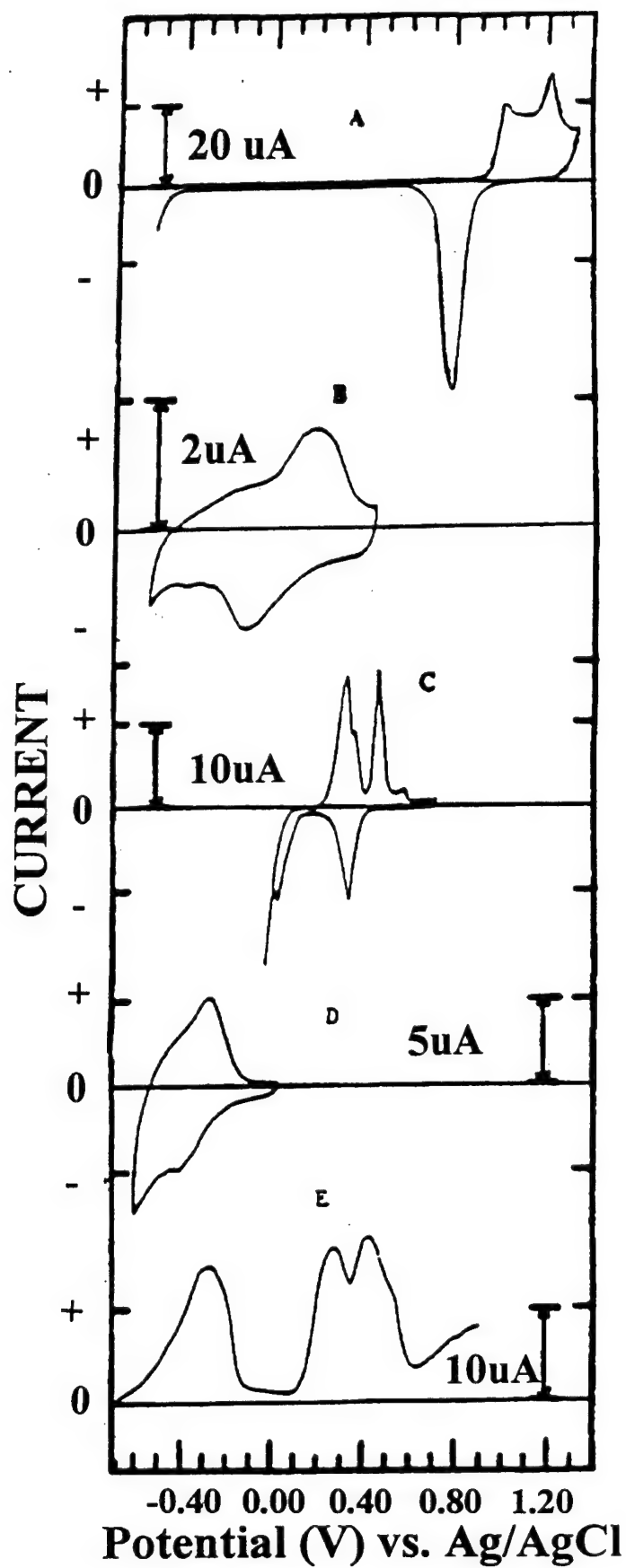




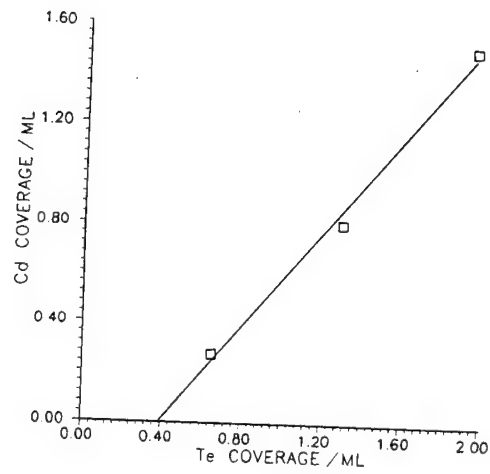
STICKNEY
Figure 6



STICKNEY
Figure 7



STICKNEY
Figure 8



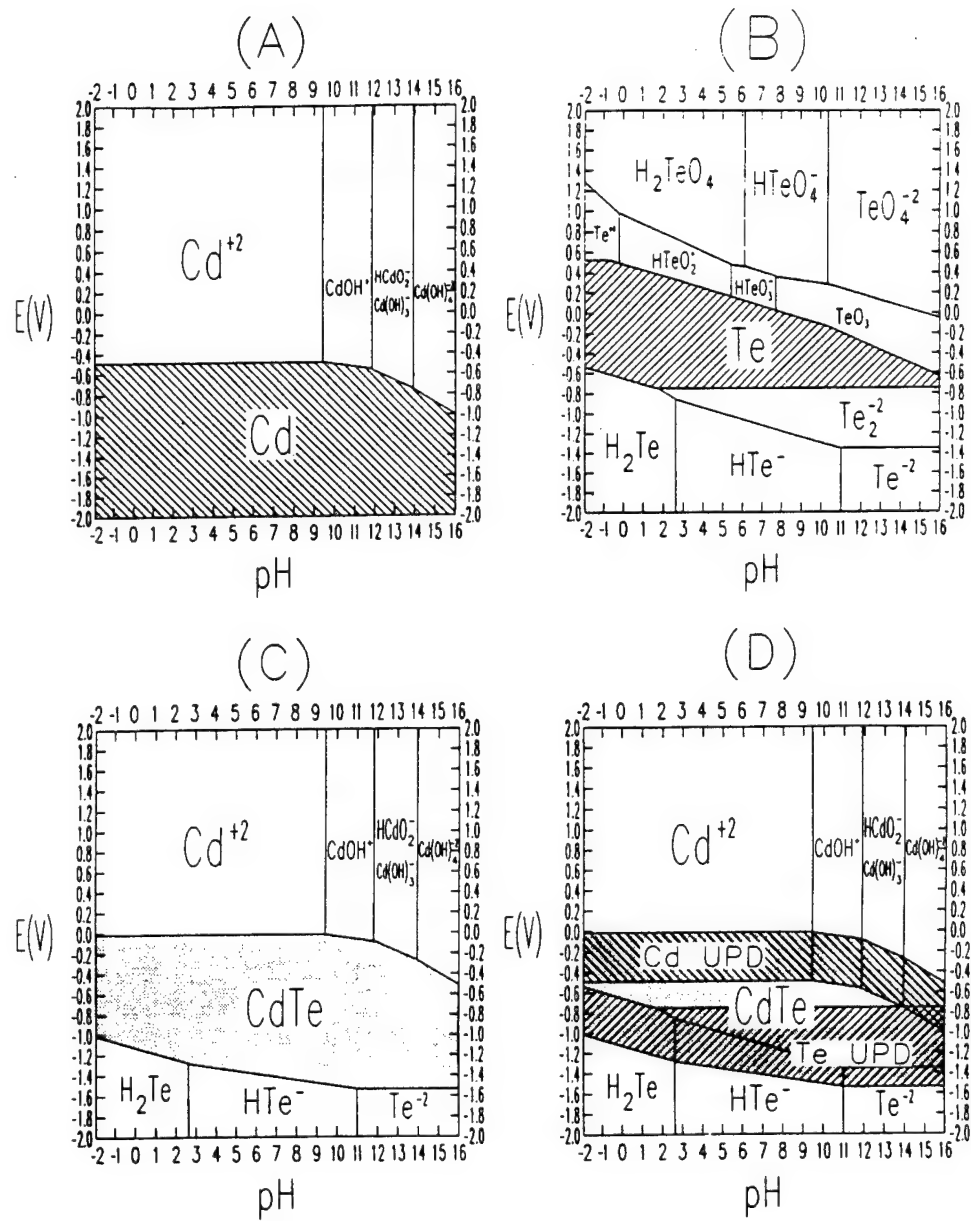
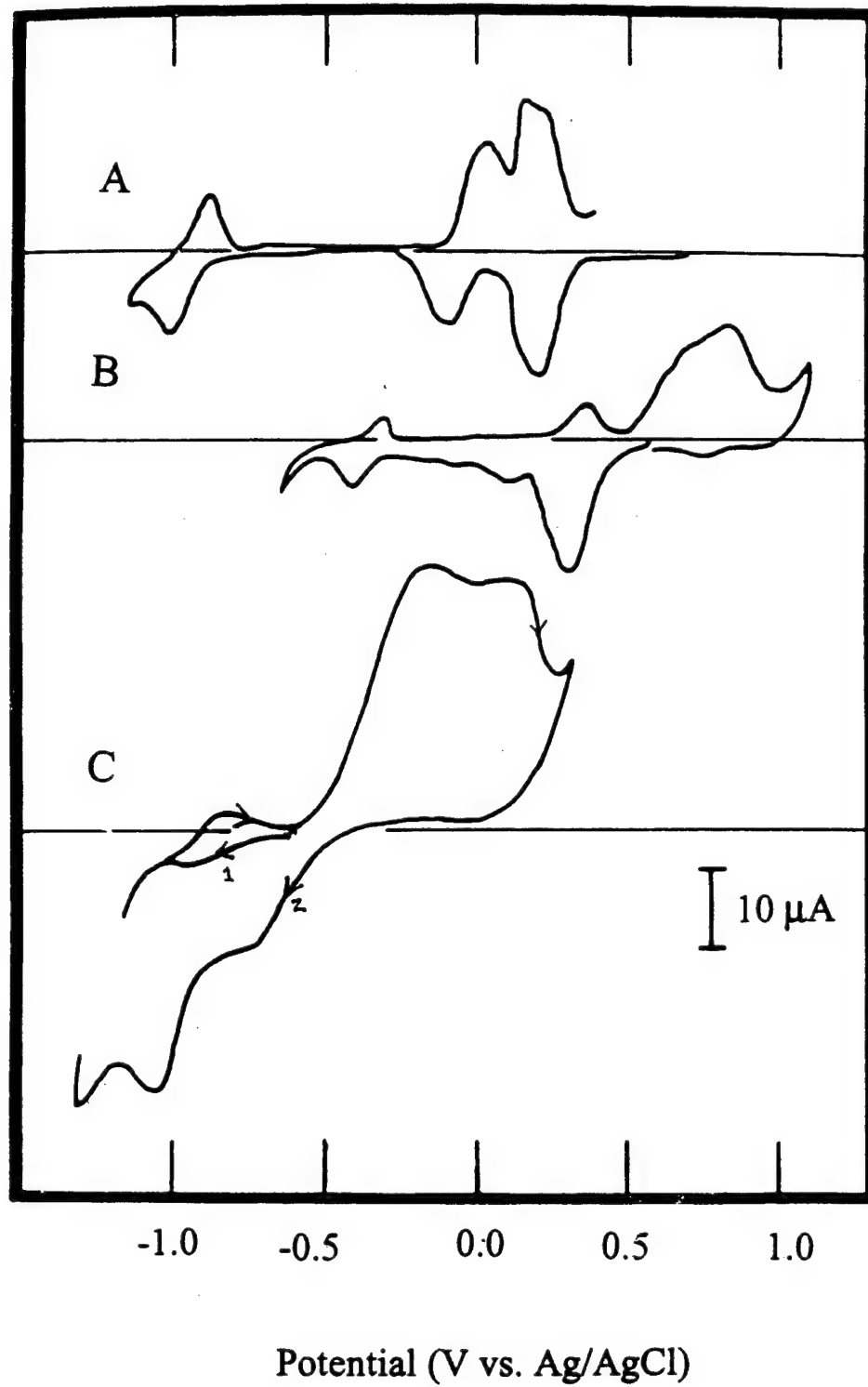
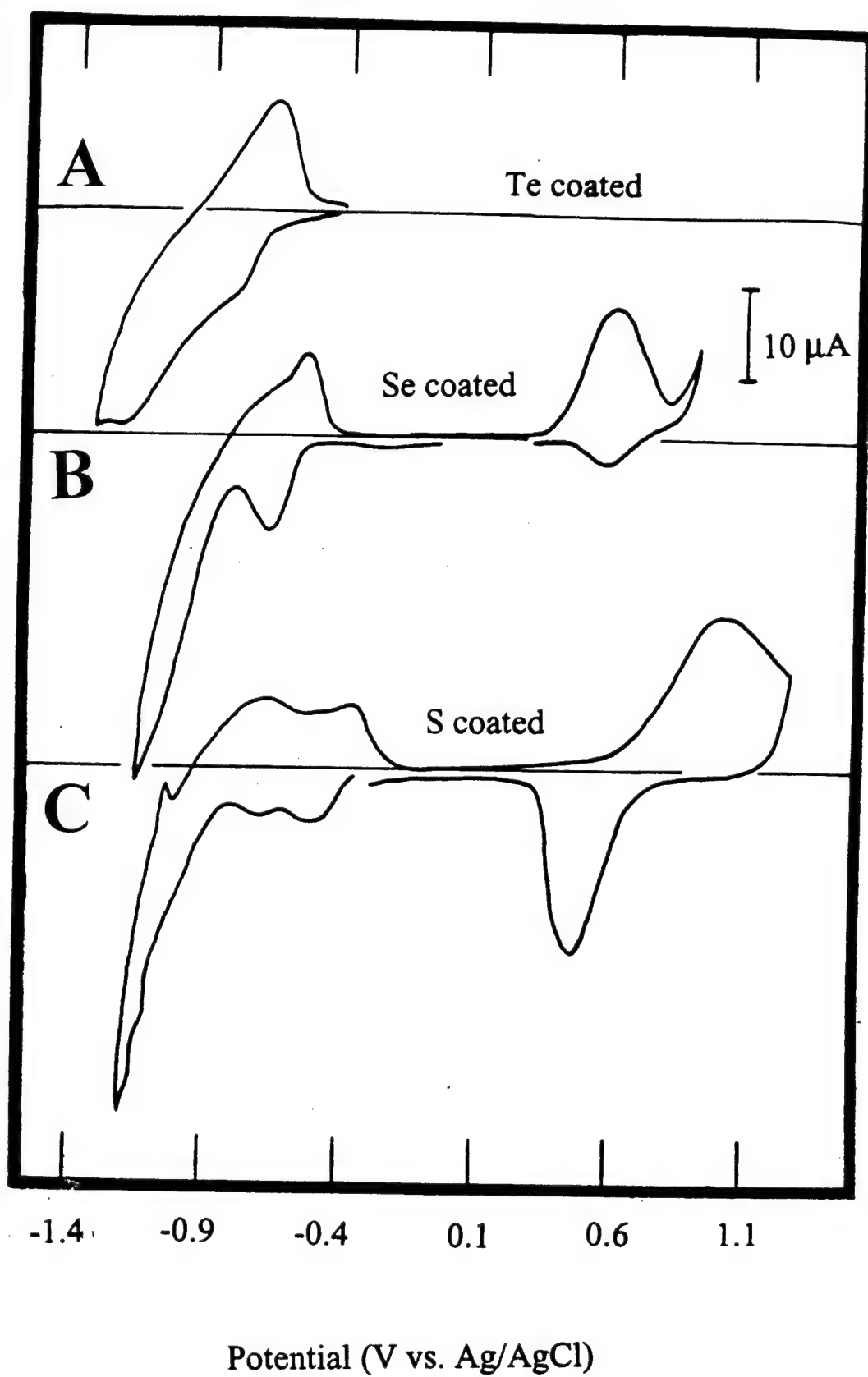


Figure 10
STICKNEY



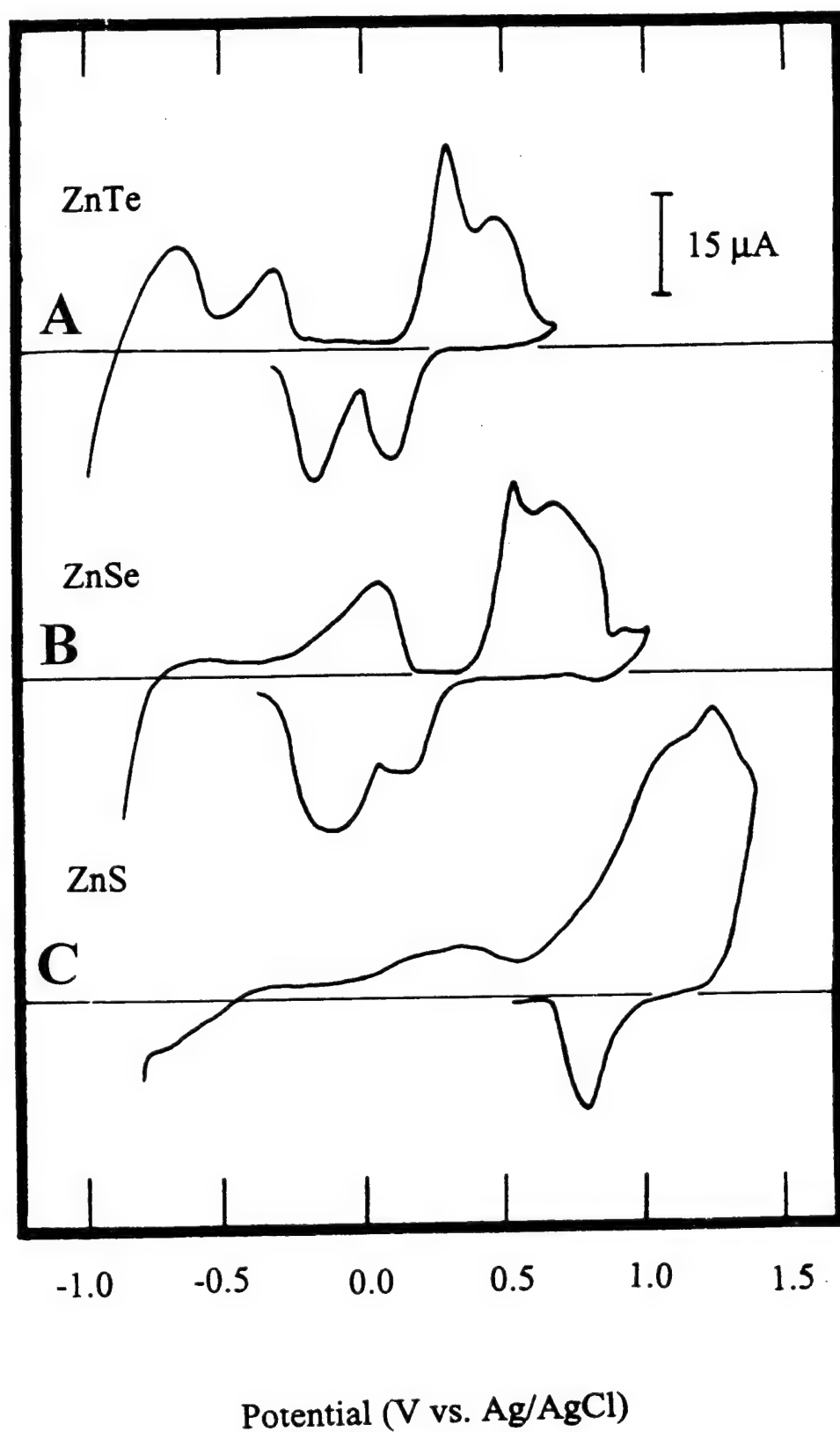


Potential

Solution

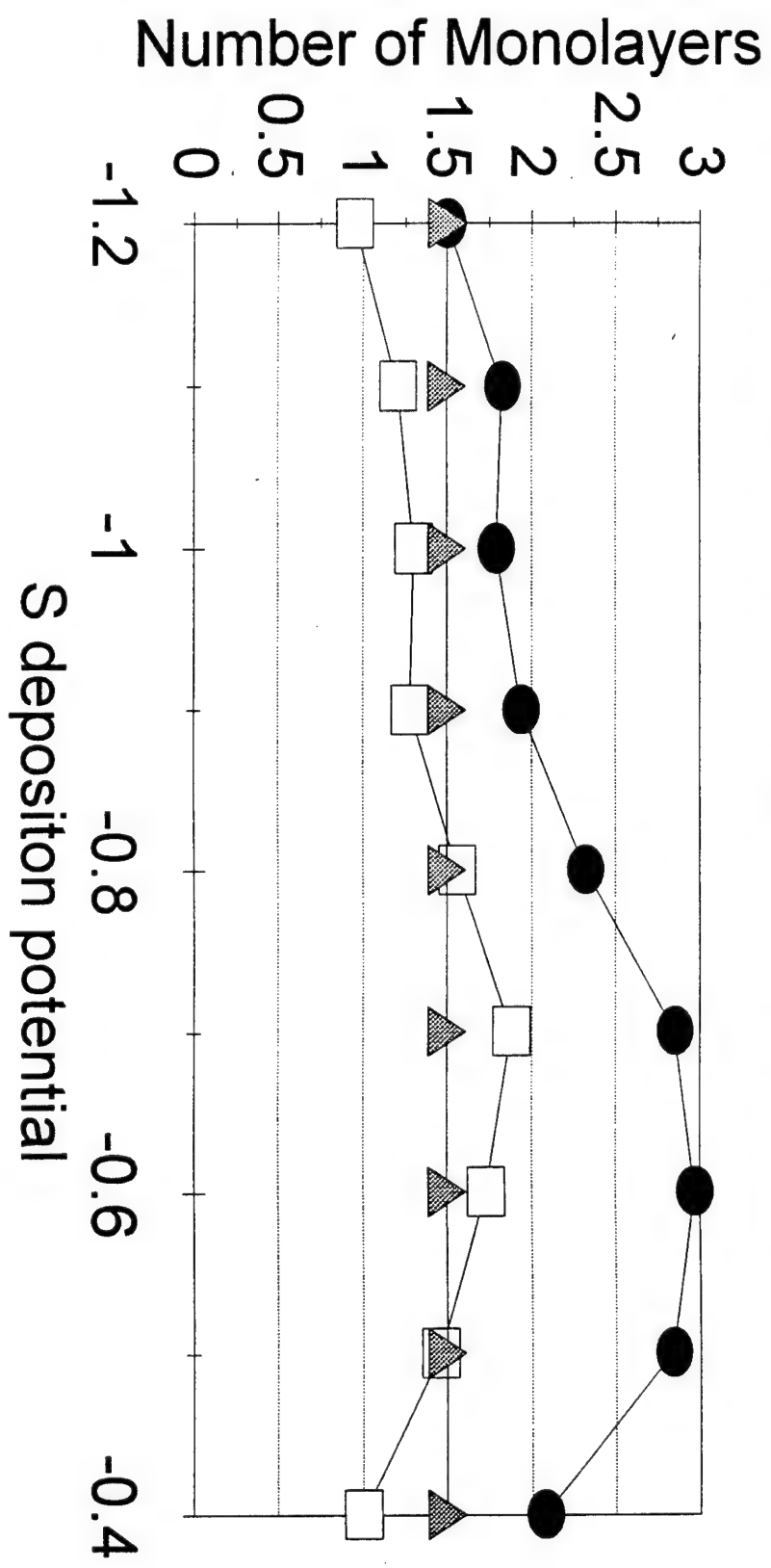
Potential	Solution
	Sb blank
	S
	Zn Blank
	Zn
	H ₂ O
-1.0V	
-0.9V	
O.C.	

Figure 13
STICKNEY



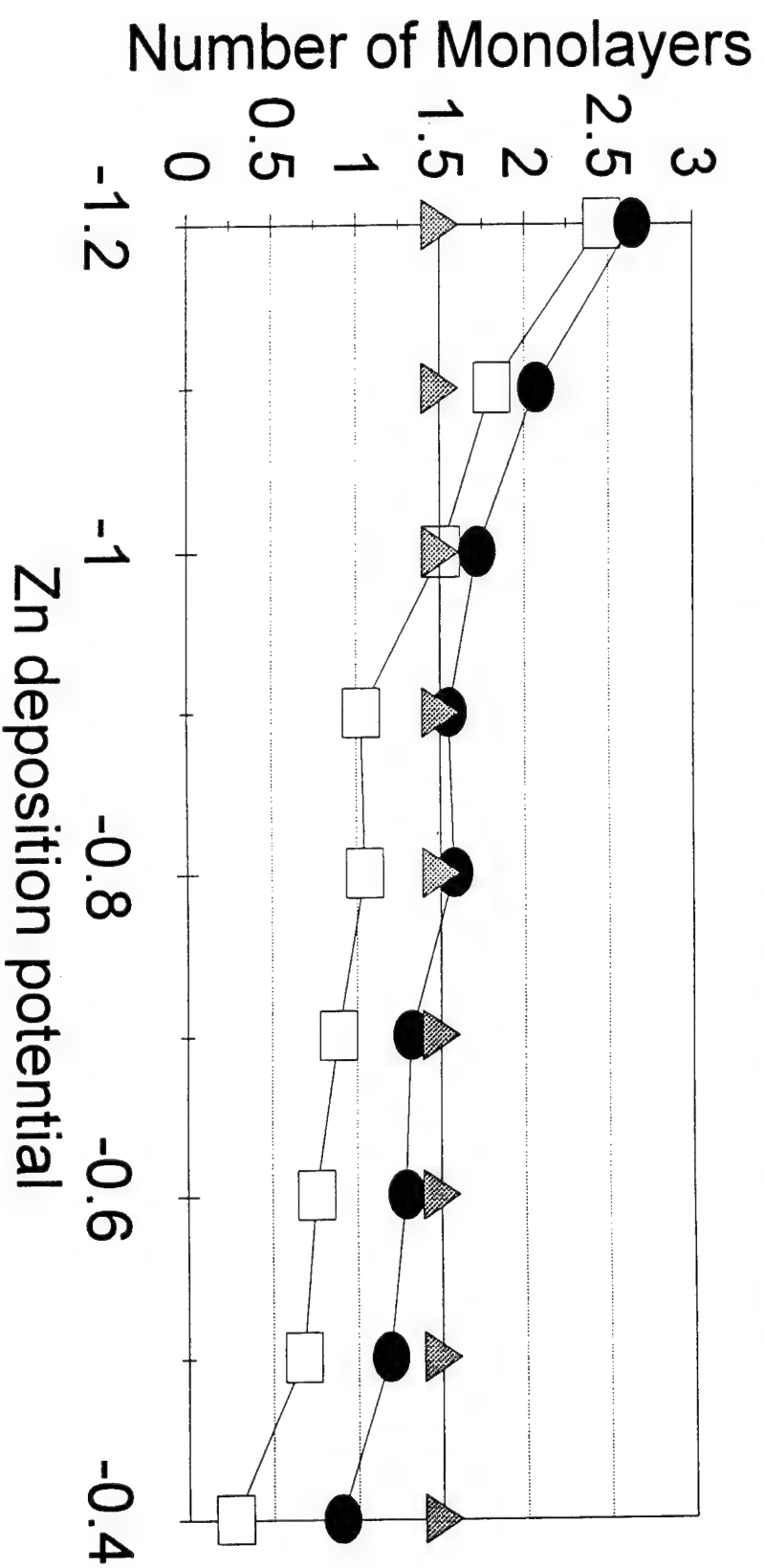
3 Cycles of ZnS deposition

Zn dep. at -0.9V, pH=3.0 strip sol.



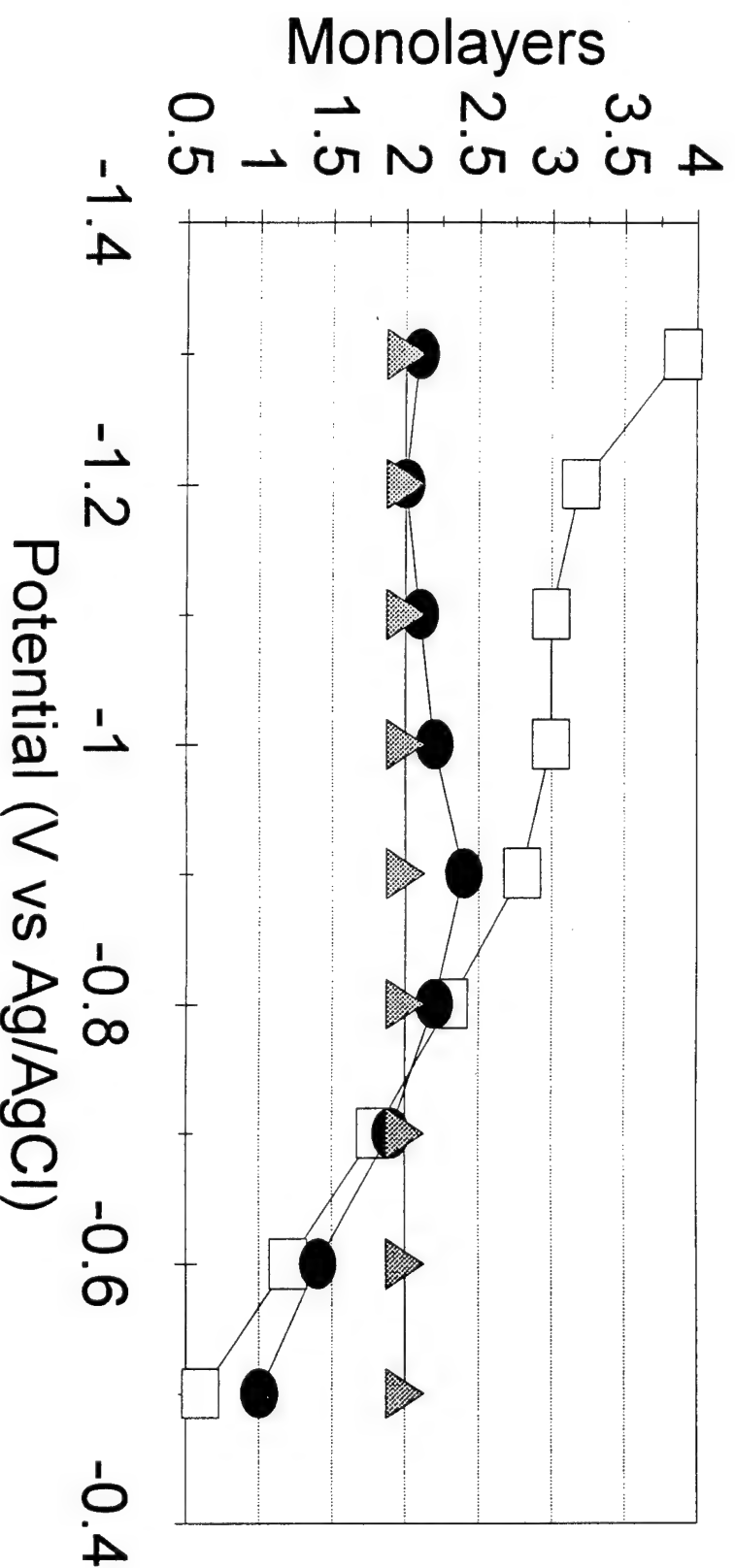
3 Cycles of ZnS Deposition

S deposited at -1.2V, pH=3.0 strip



4 Cycles of ZnSe

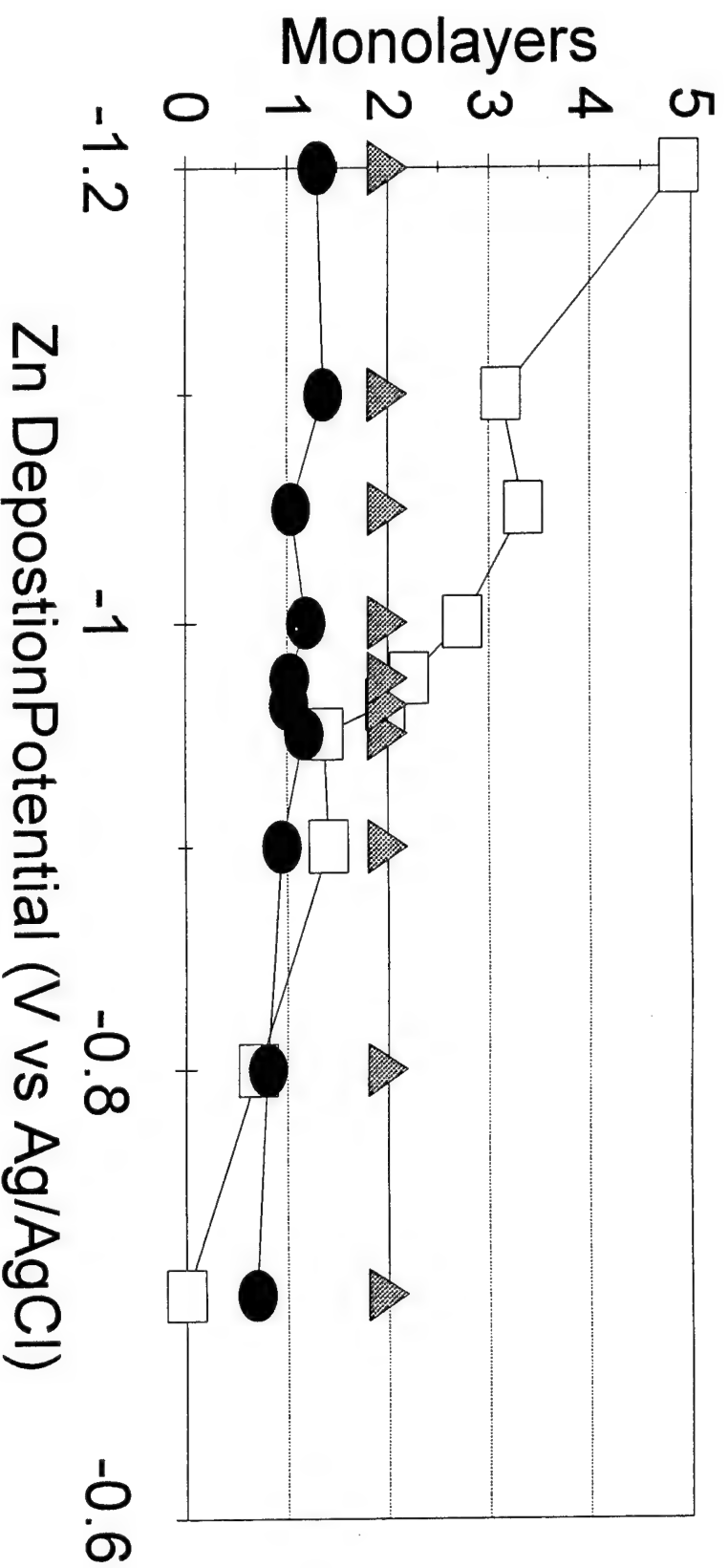
Se dep. at -0.9V, Zn = 2 mM



□ Zinc ● Selenium ▲ Theory

4 ZnTe Cycles

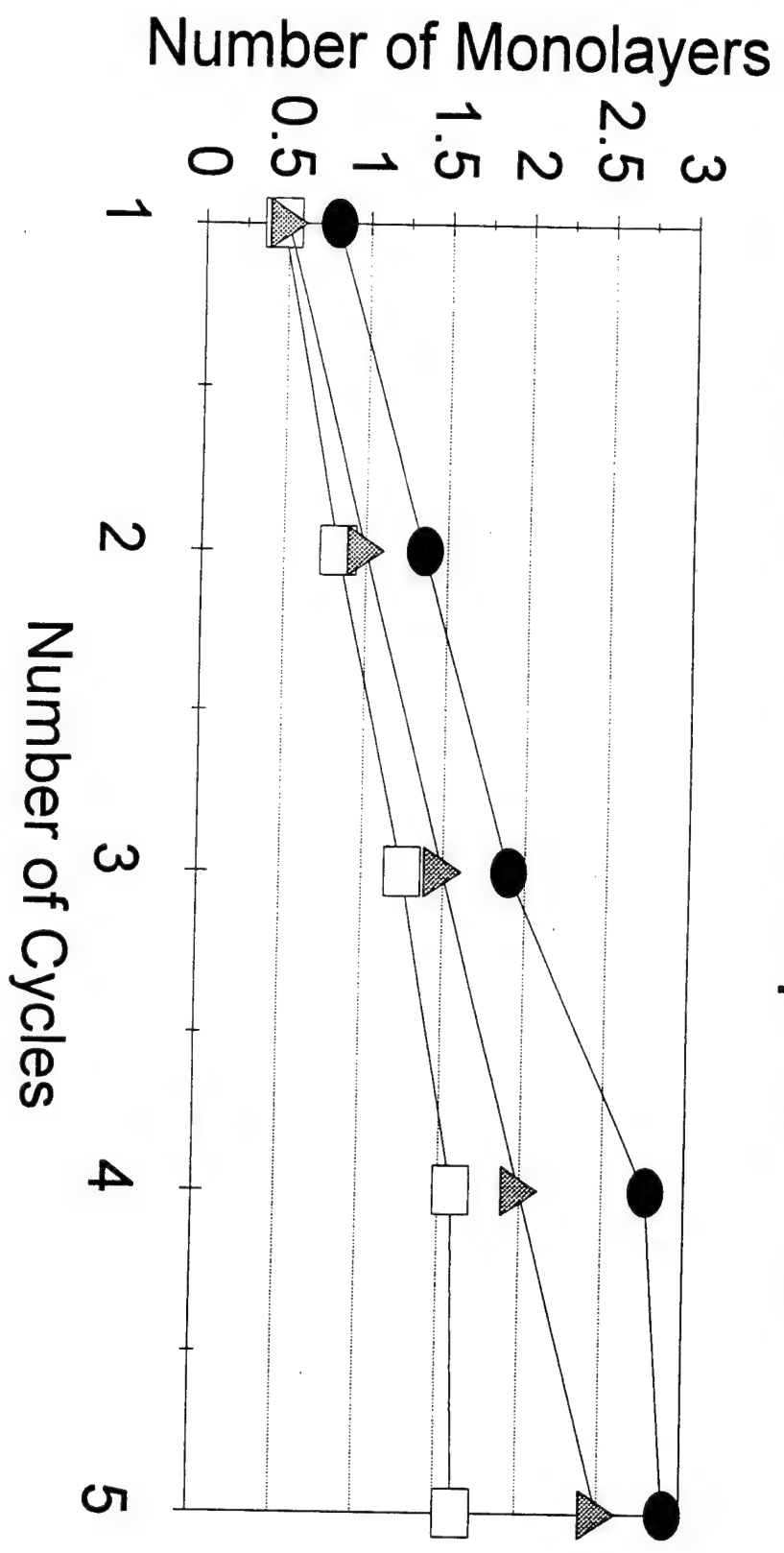
Te dep. at -0.8 V, strip at -1.1 V



□ Zinc ● Tellurium ▲ Theory

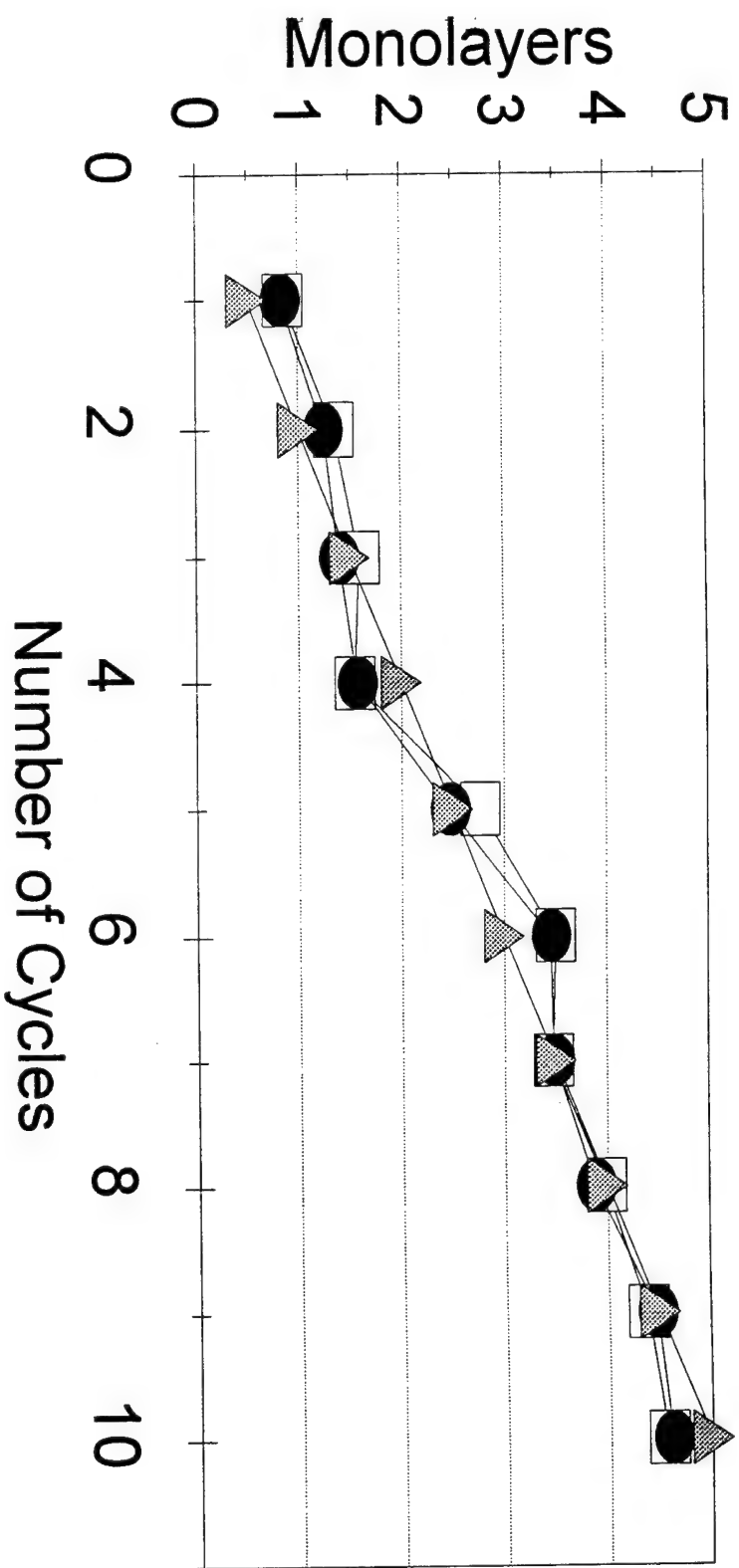
ZnS ECALC Cycles

Zn dep. at -0.9V, S dep. at -1.0V



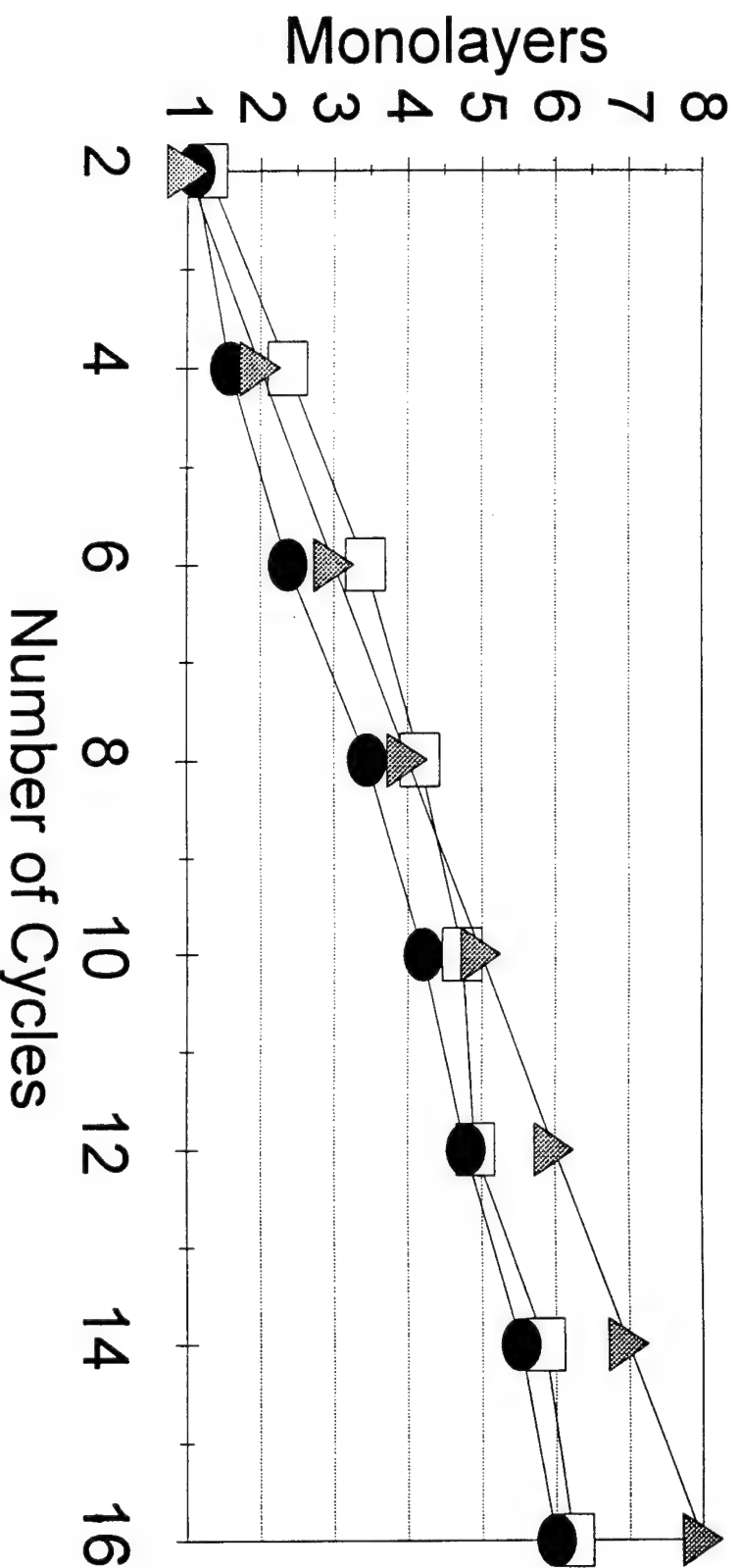
ZnSe ECALC CYCLES

Zn at -0.8V and Se at -0.9V



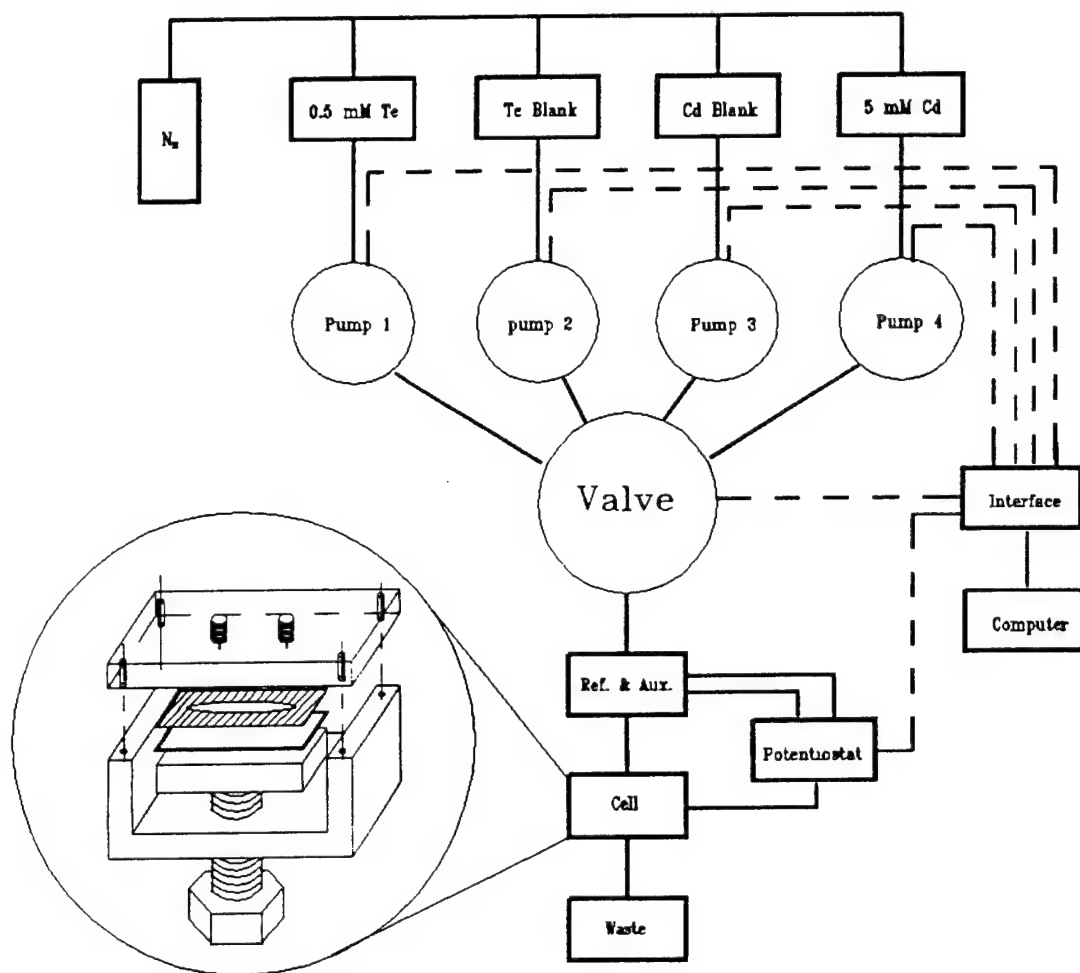
ZnTe ECALC CYCLES

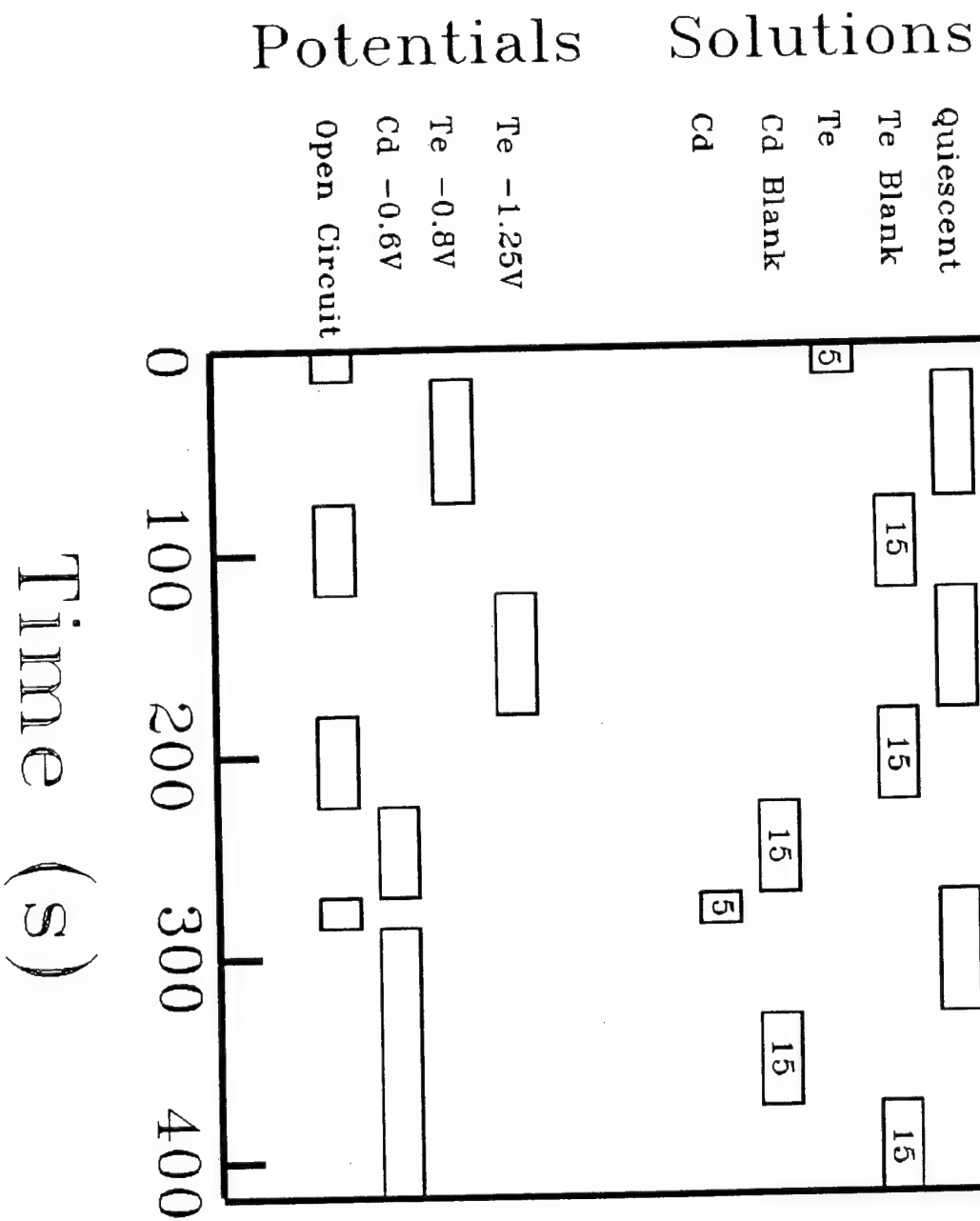
Zn and Te dep. at -1.0V,



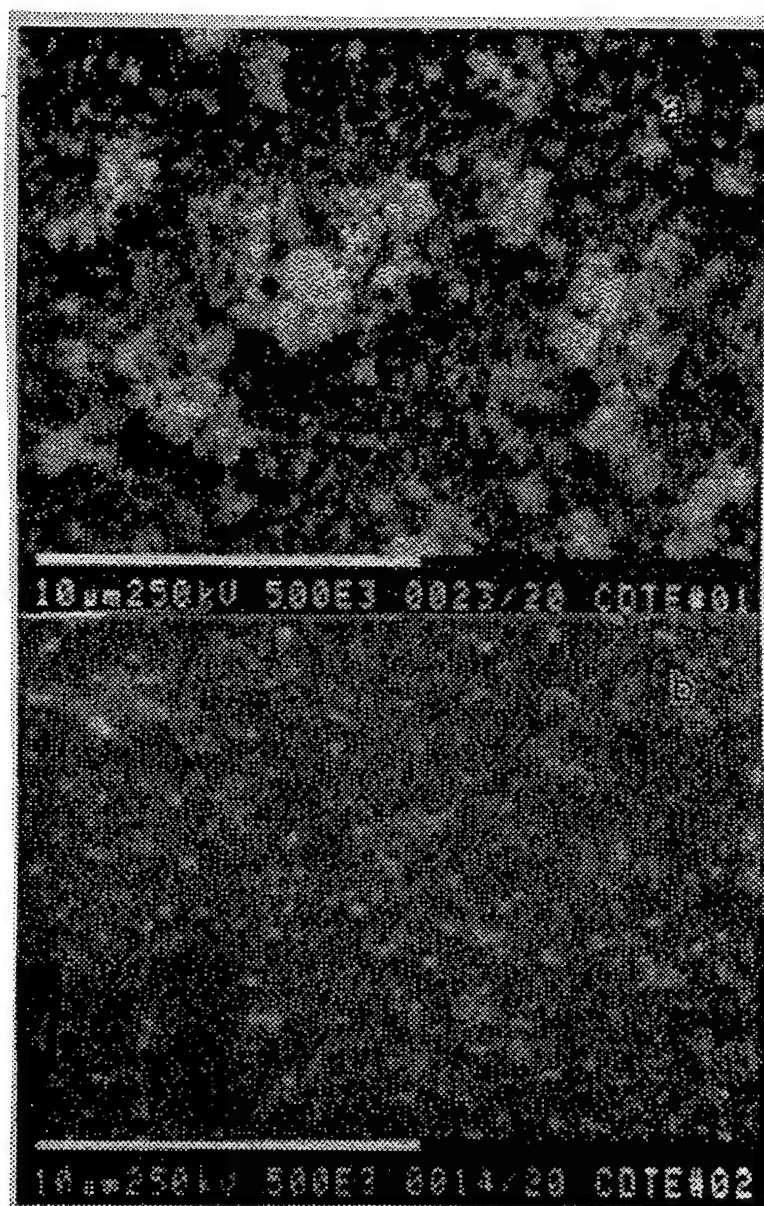
□ Zinc ● Tellurium ▲ Theory

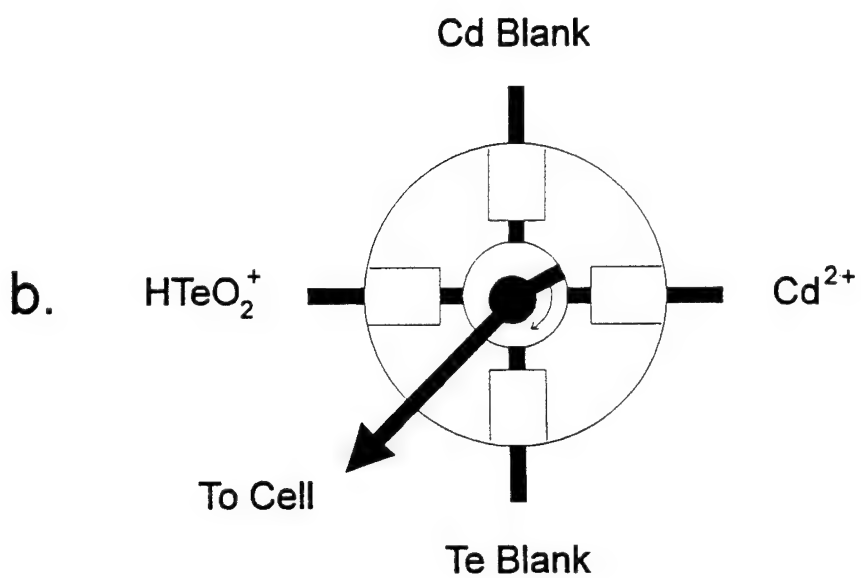
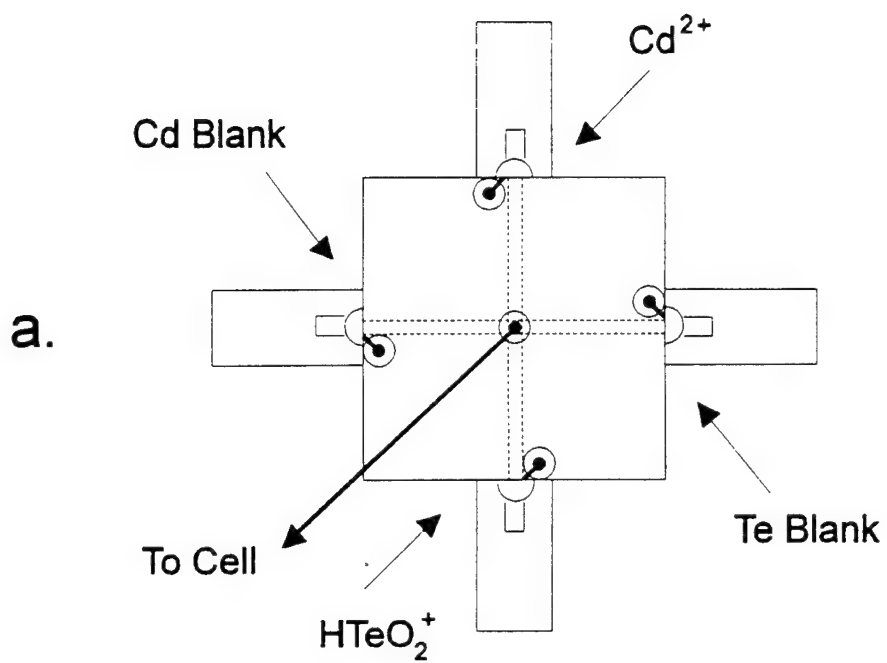
Figure 17
STRUCTURE



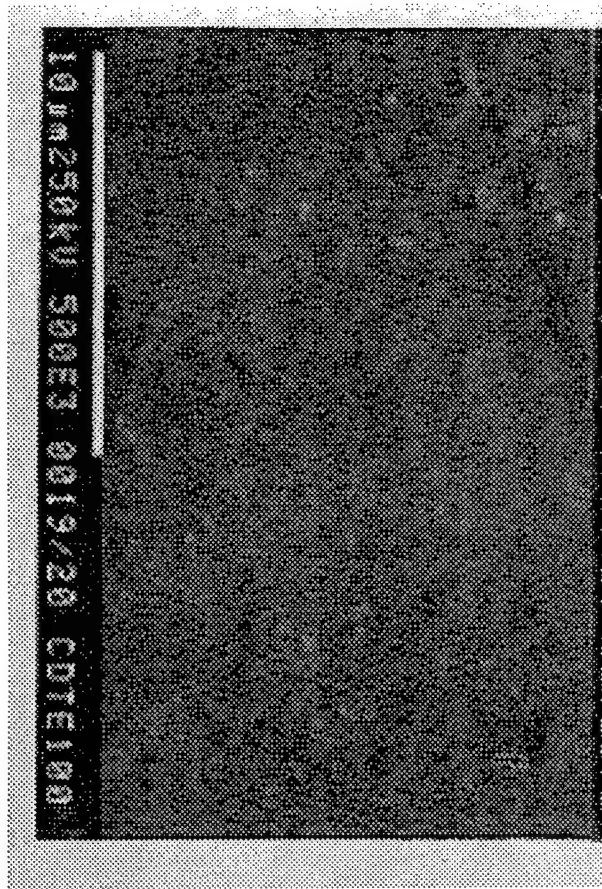


STICKING
Figure 21



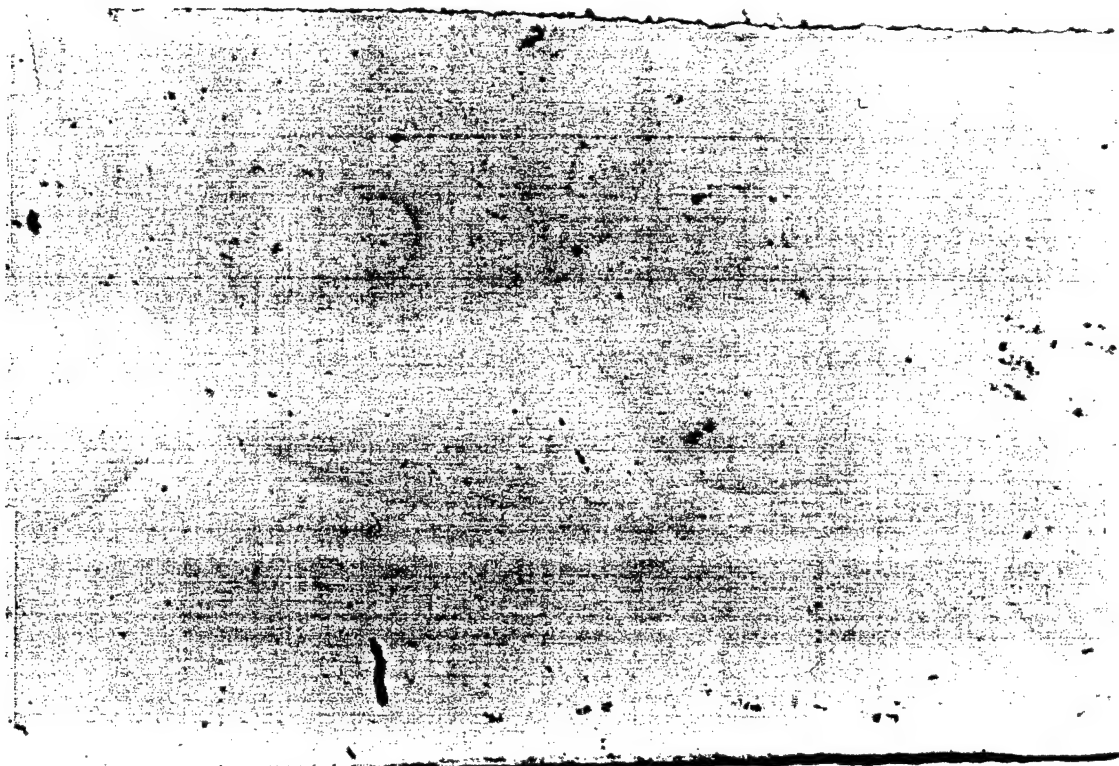


STICKAURY
Figure 23



STILKNBY
Figure 24A,B

A



B

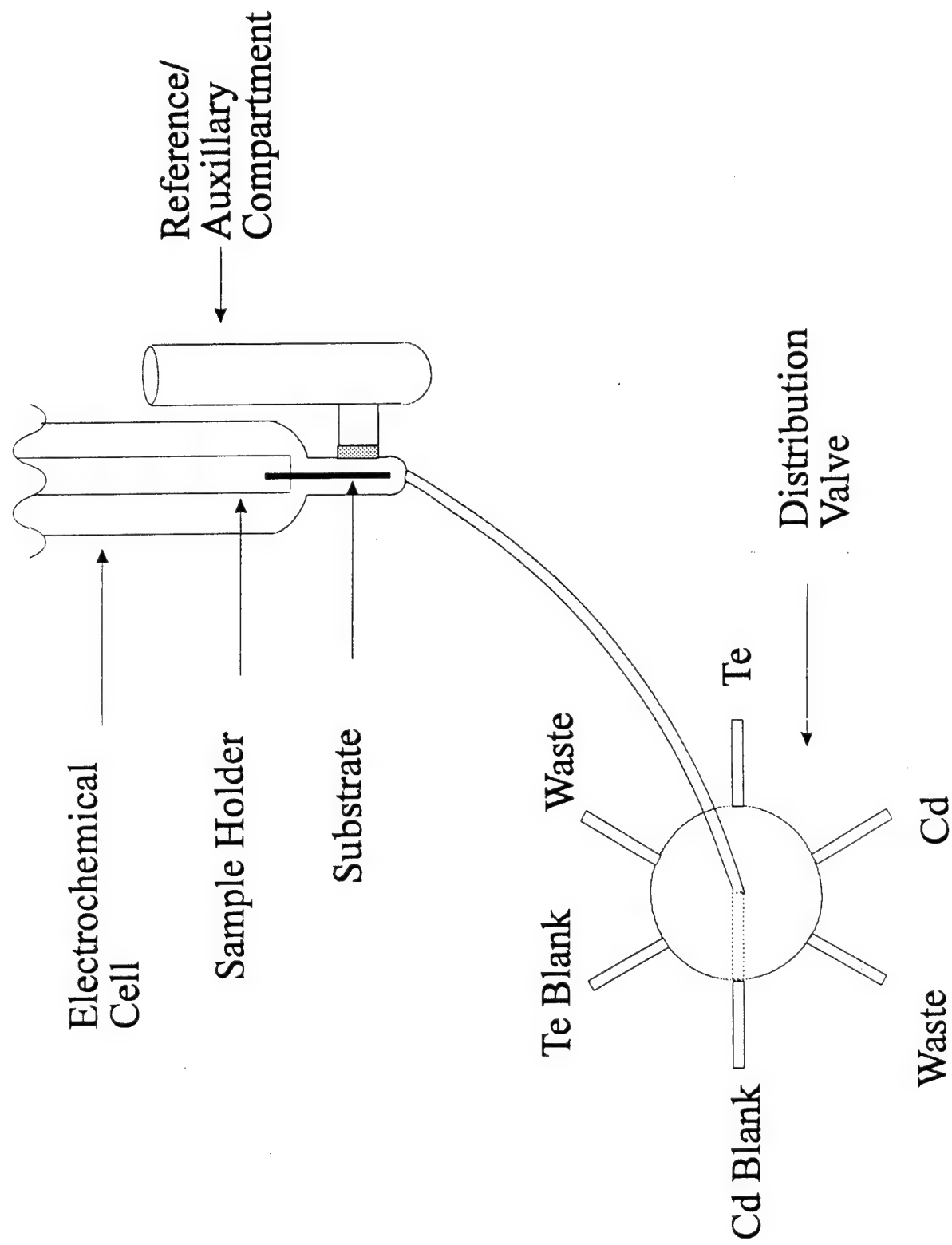


STICKNEY
Figure 24C

C



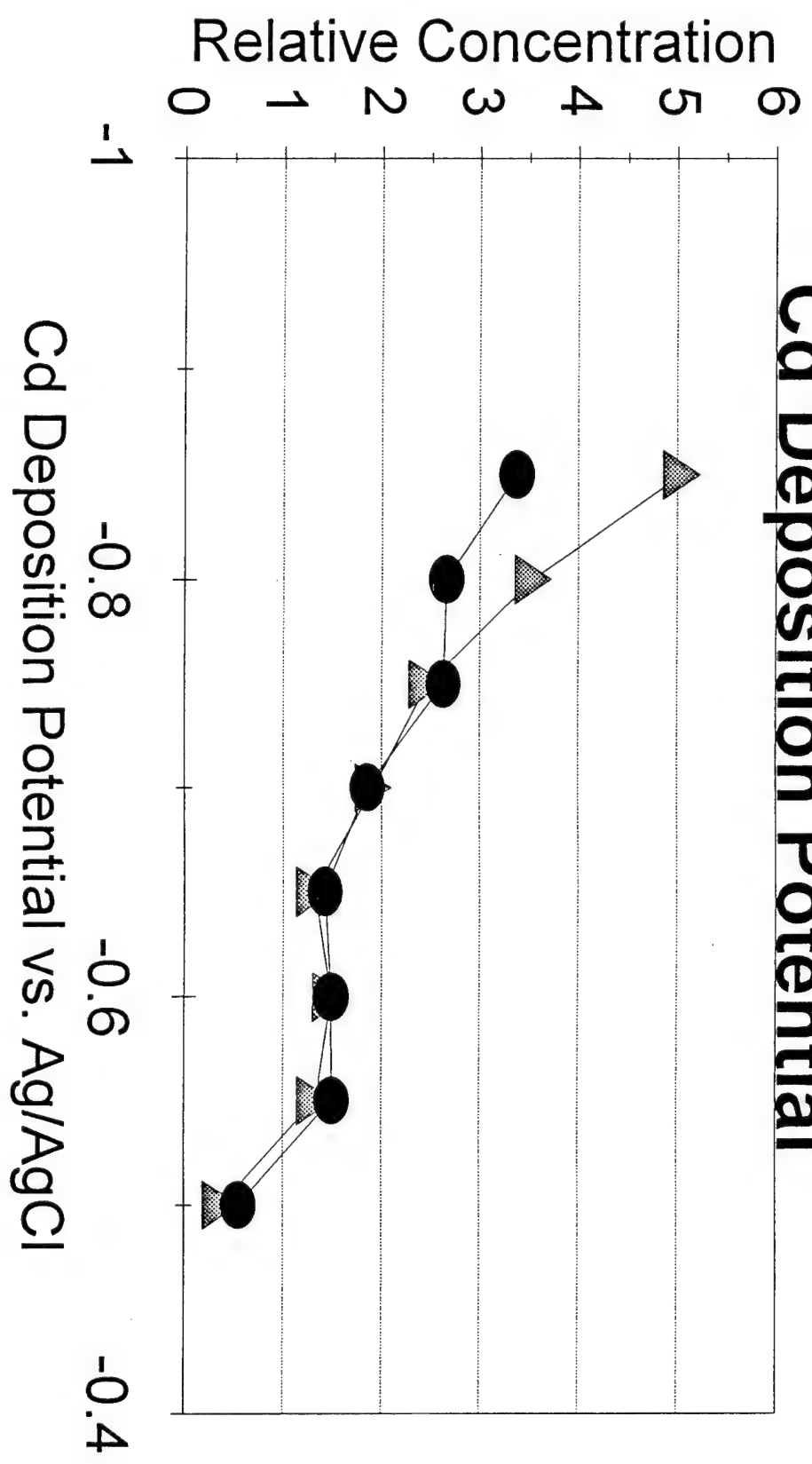
Figure 25



STICKNEY
Figure 26A

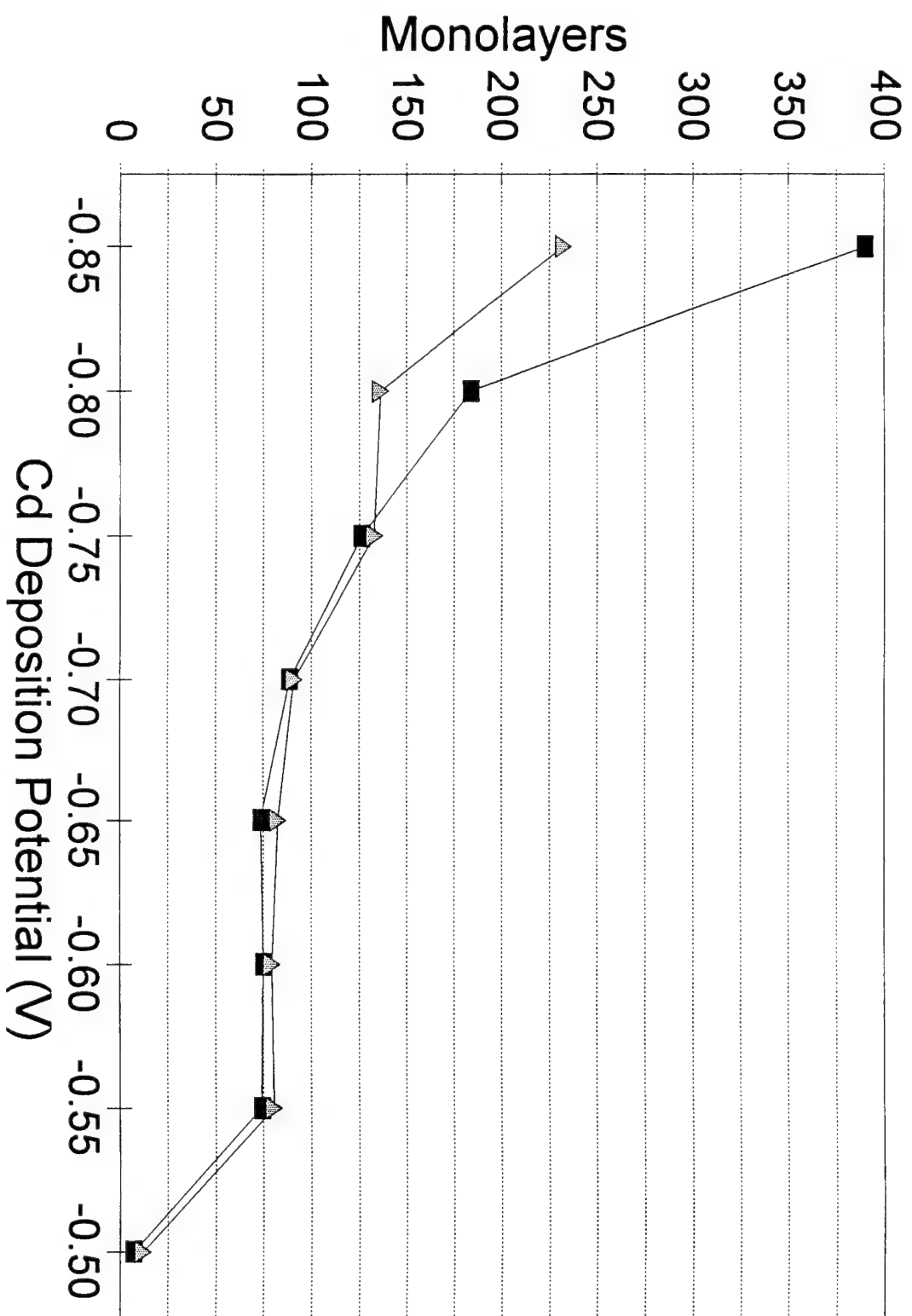
Cd & Te Relative Concentrations Vs.

Cd Deposition Potential

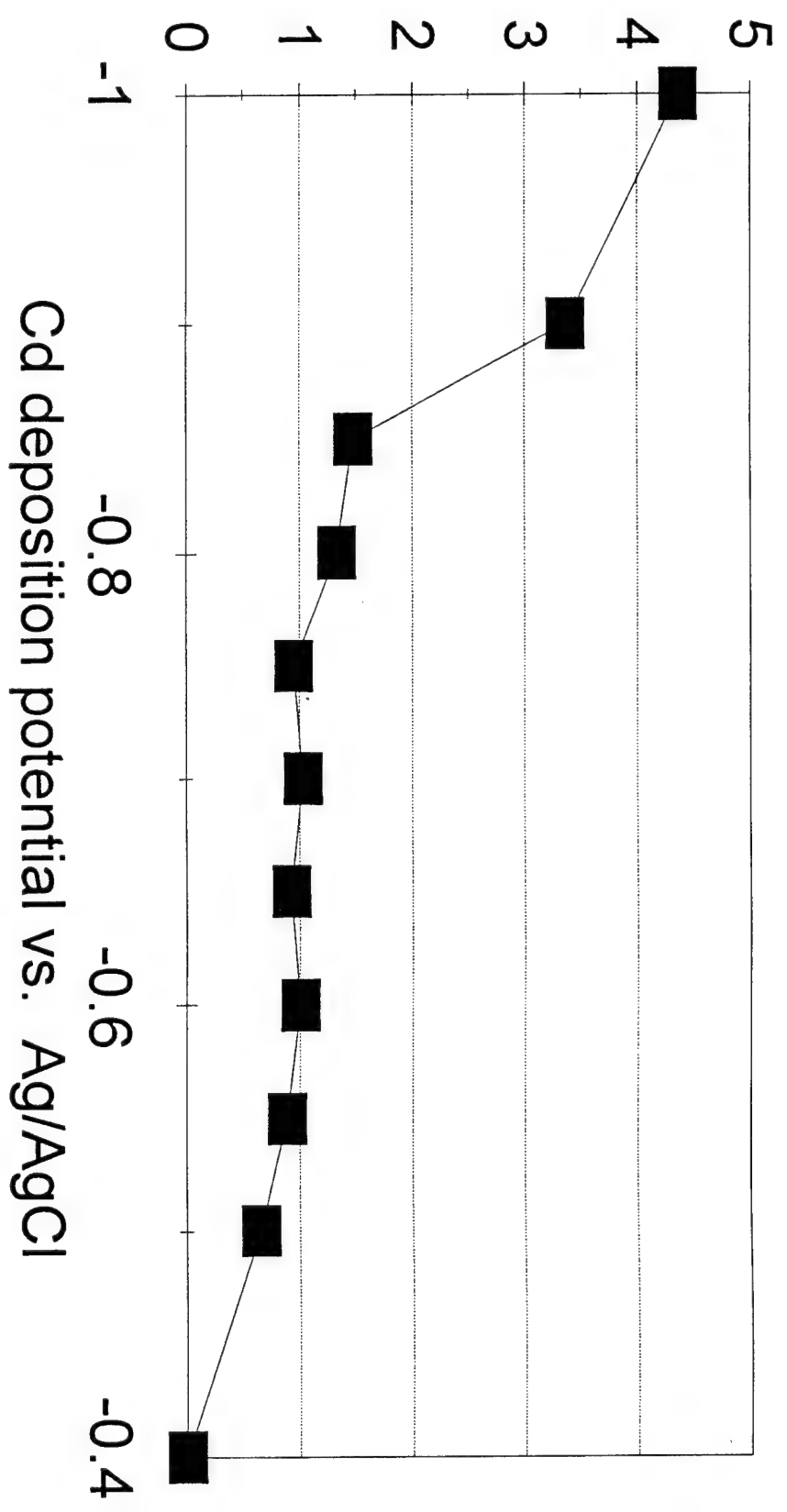


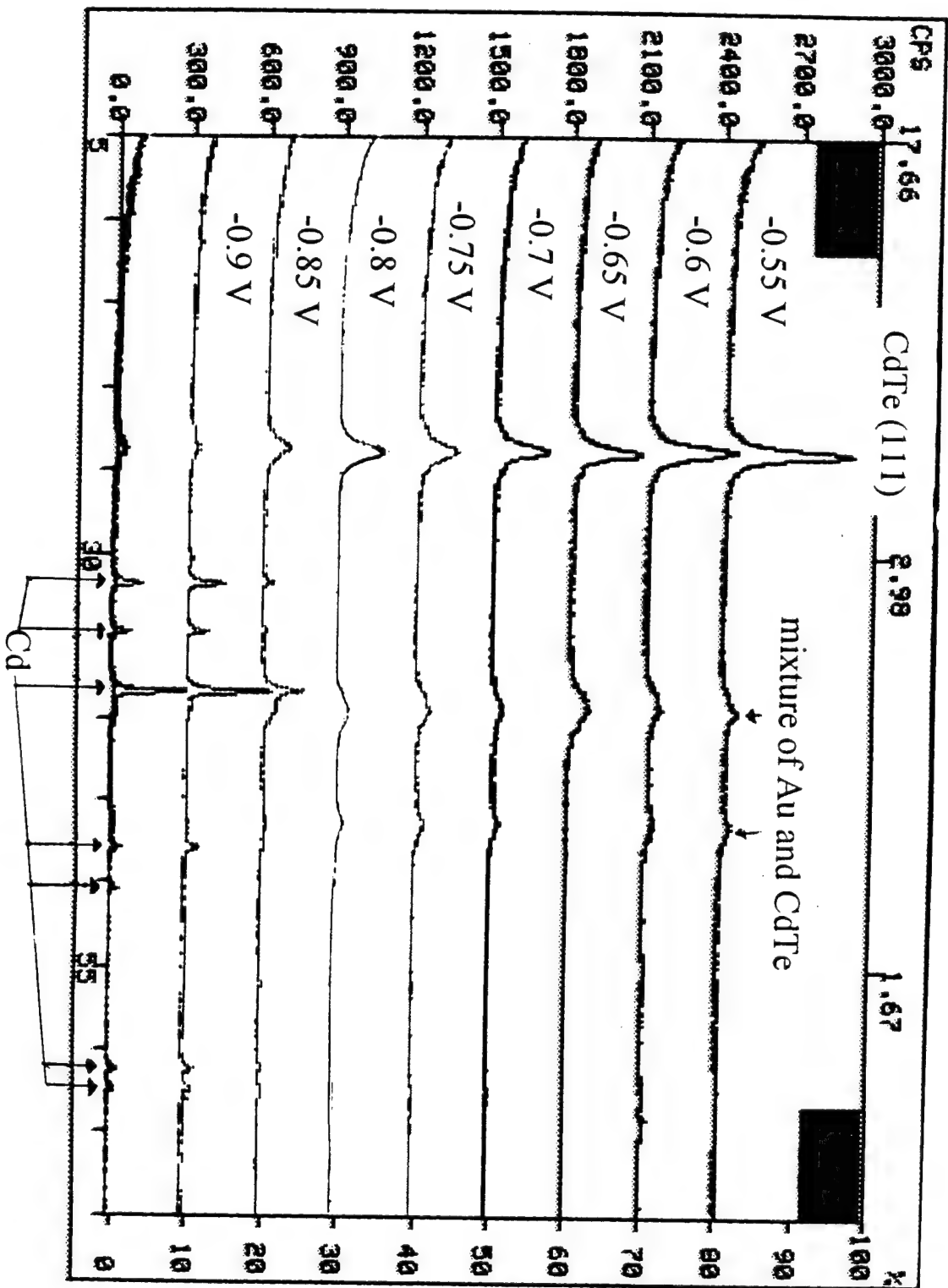
▲ Cd ● Te

FIGURE 26-15
STICKNEY



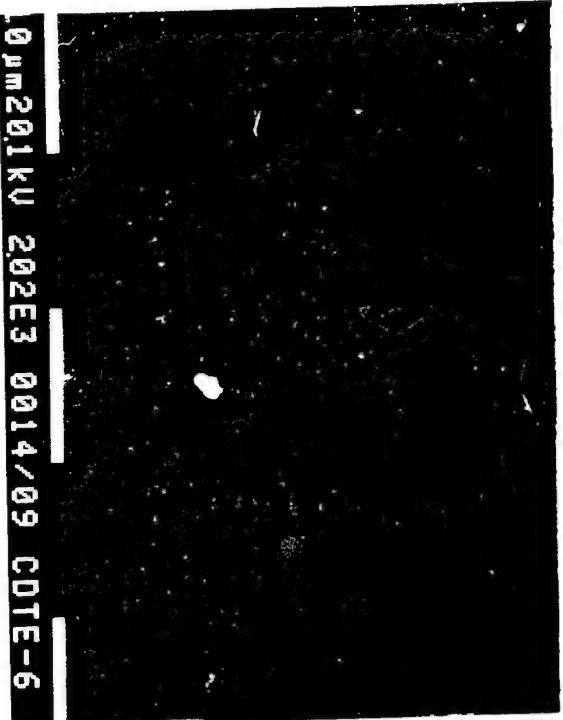
Cd/Te Ratio vs Cd deposition potential



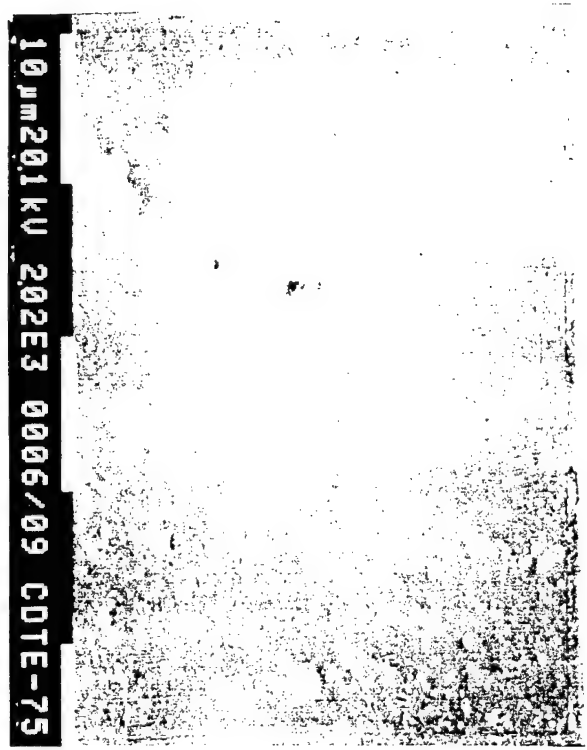




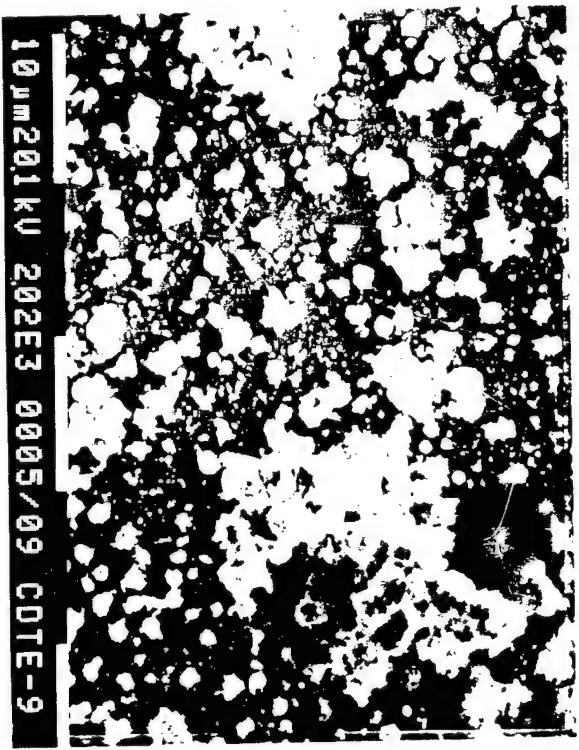
A



B

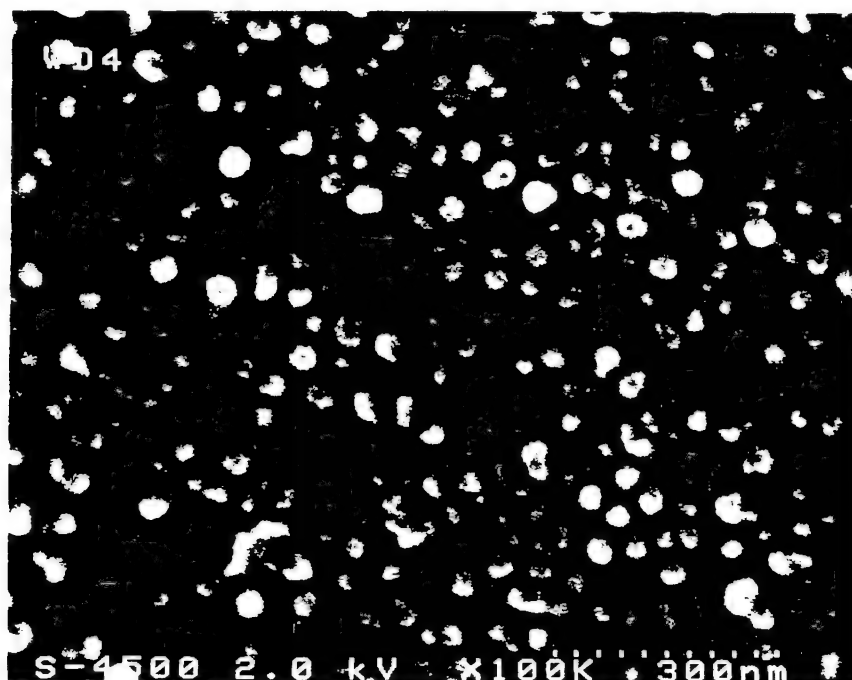


C



D

A



B

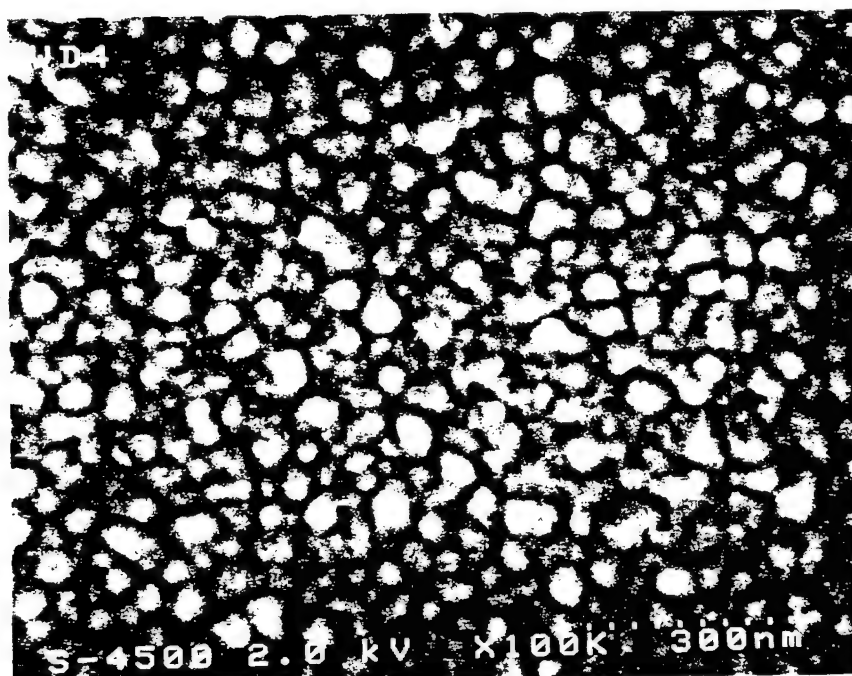
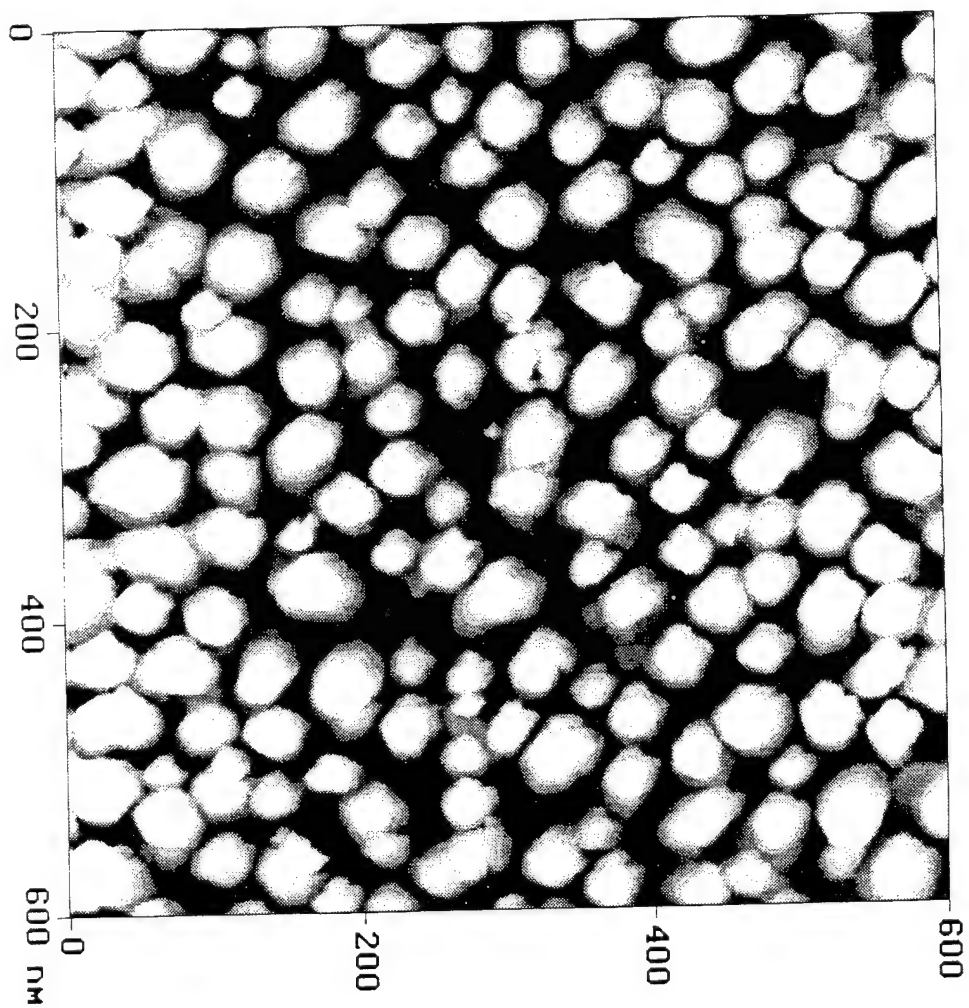
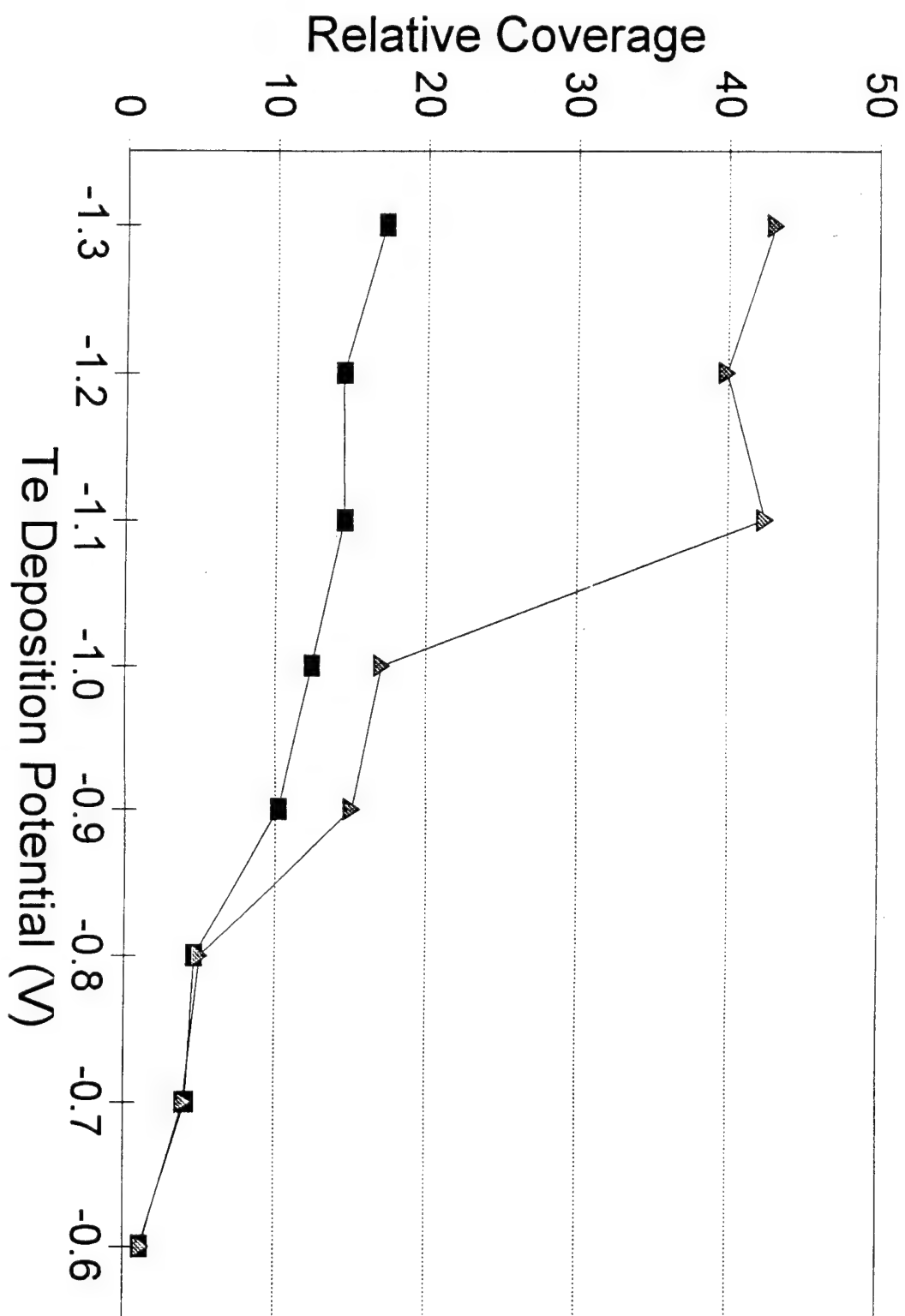
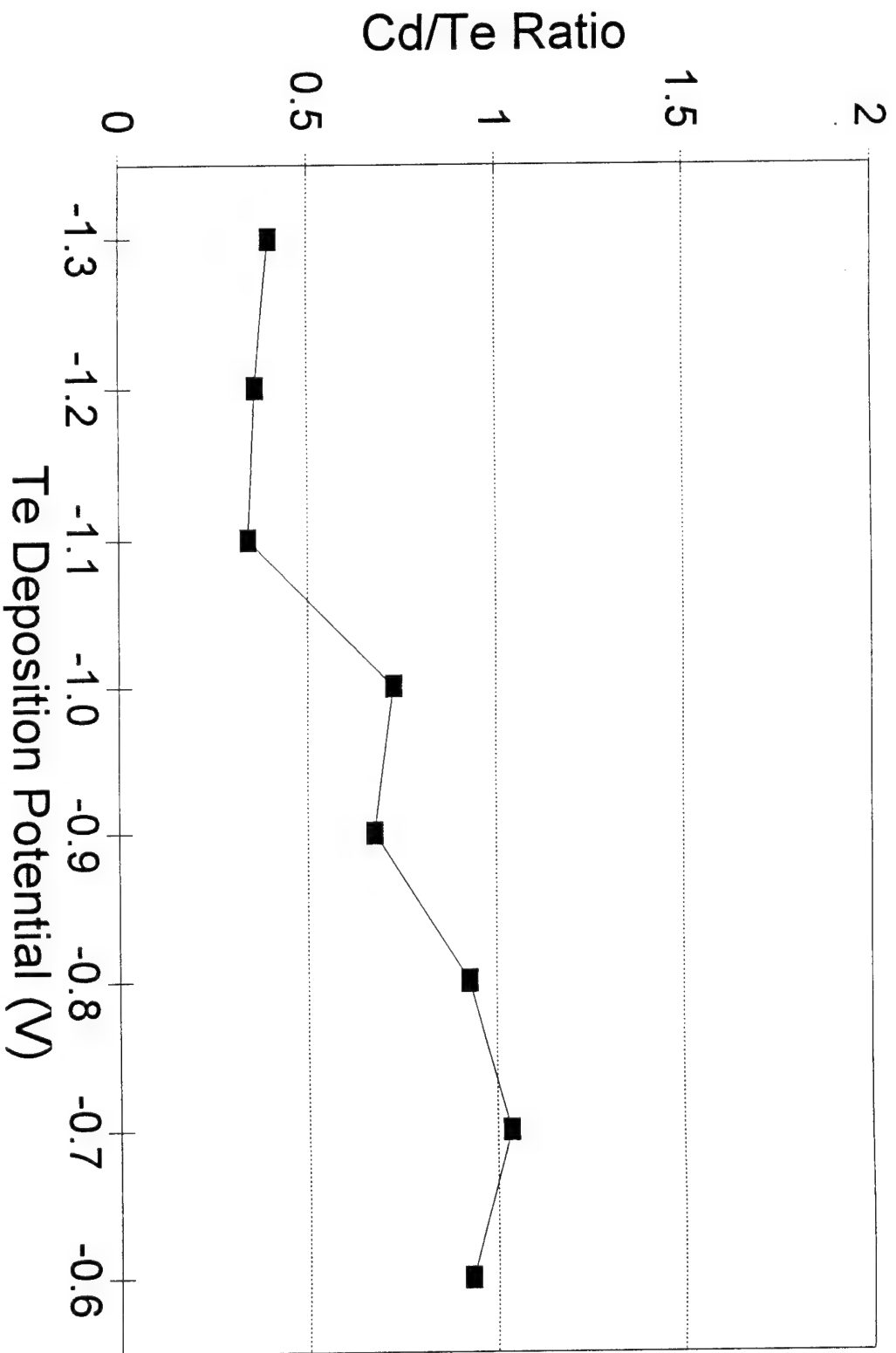
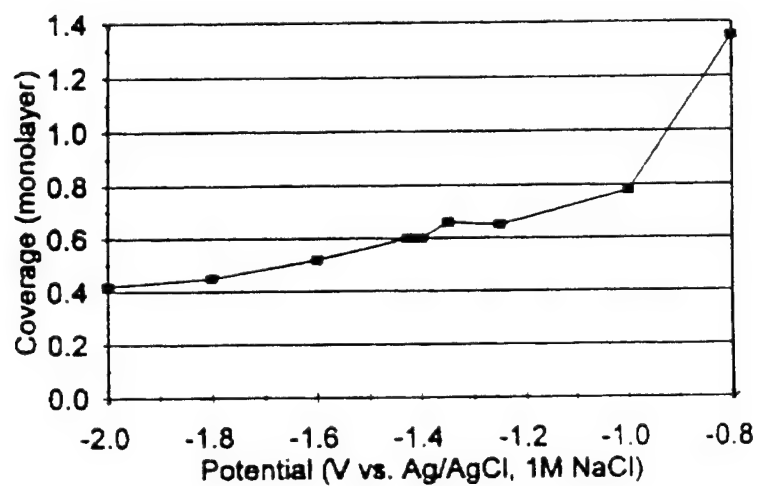


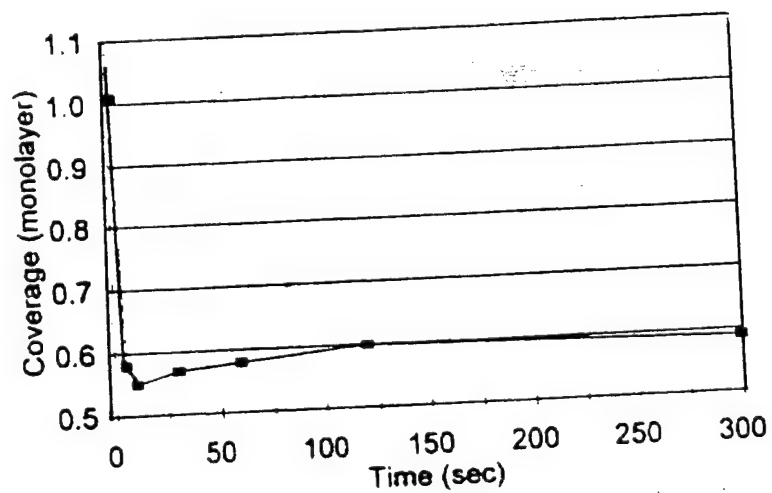
Figure 3)
EMTC K12B4

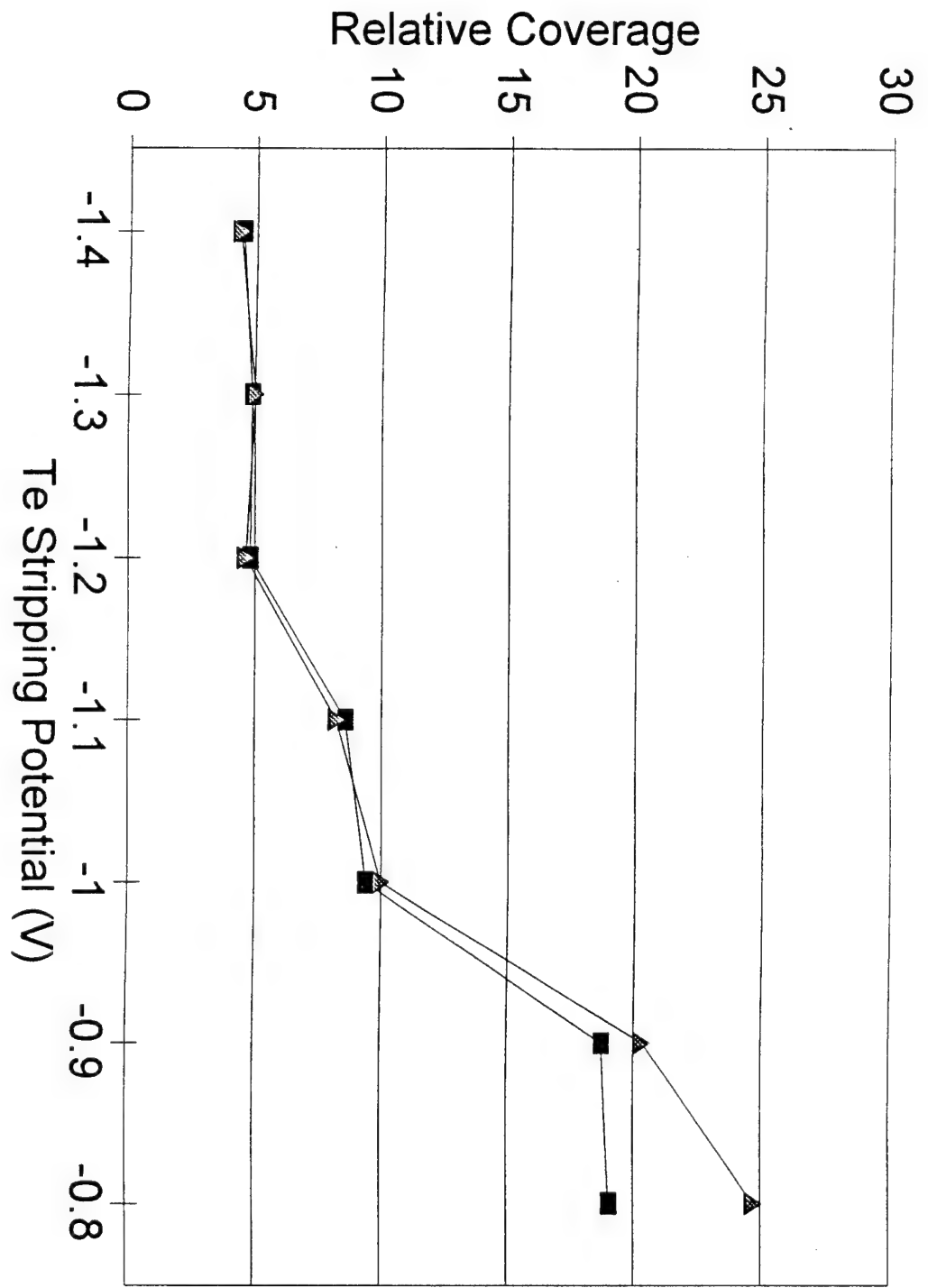




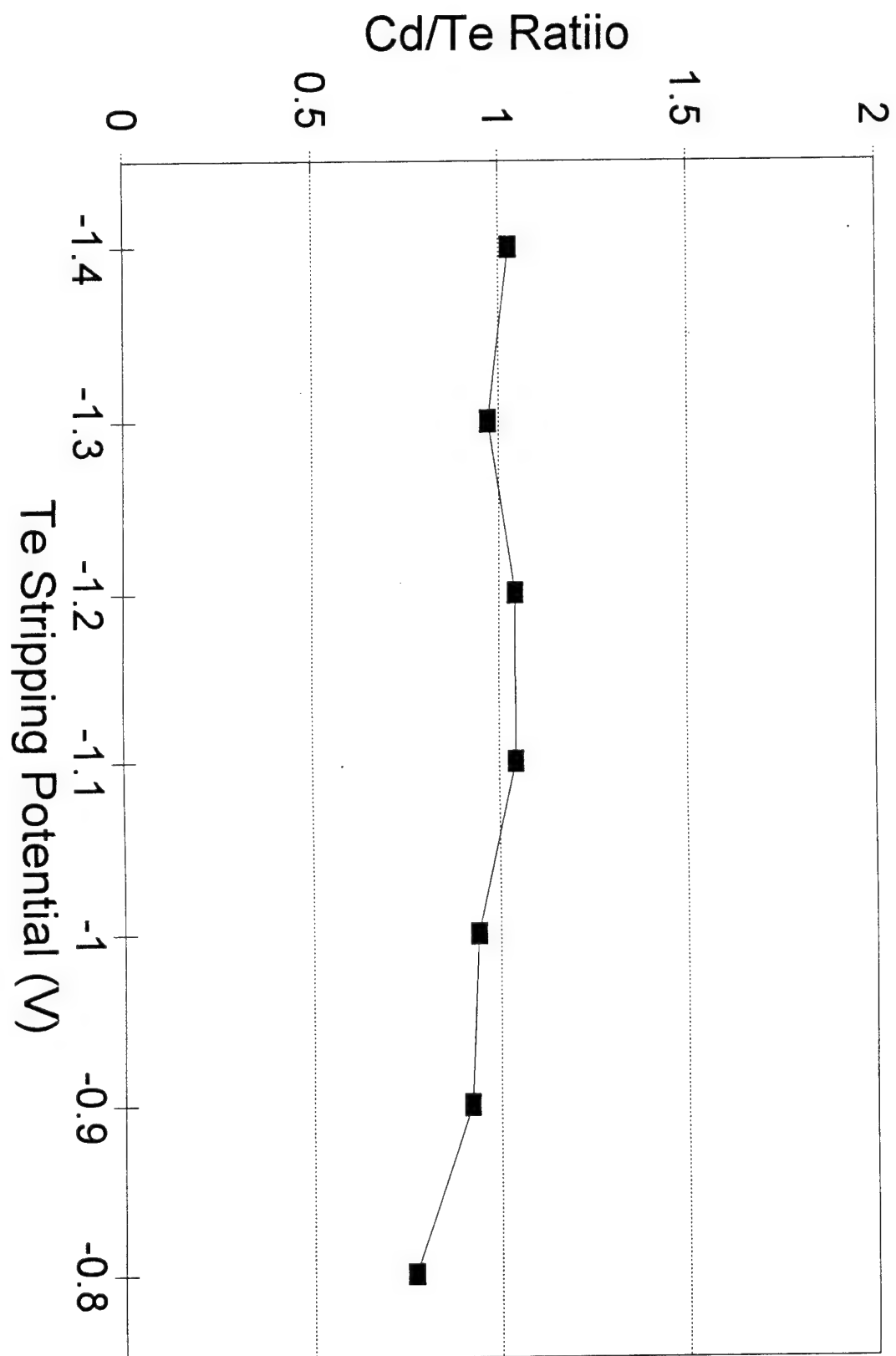




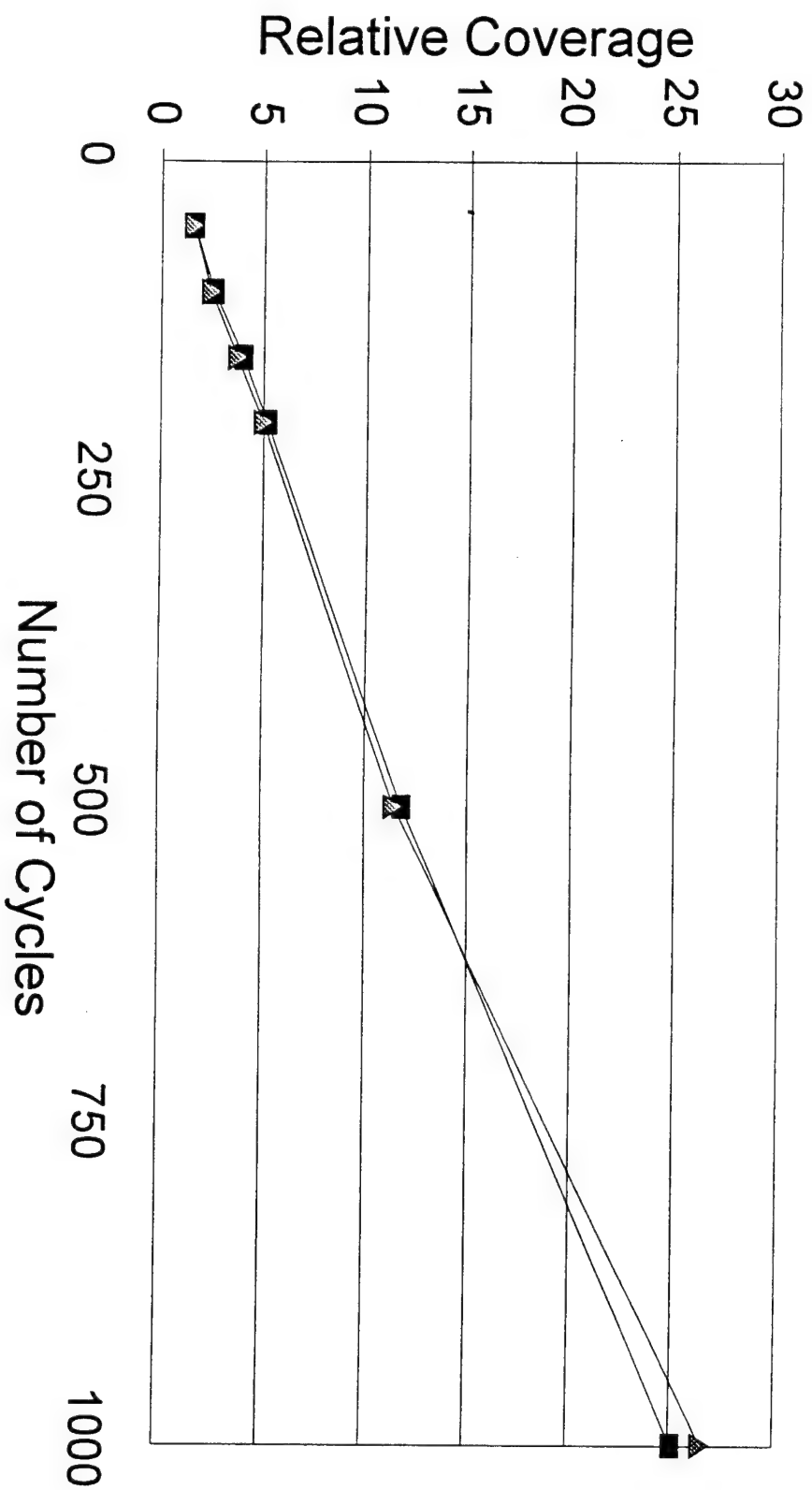




DISCUSSION
Figure 37



Relative Coverage vs. Number of Cycles
Cd @ -0.6V, Te @ -0.8V, Strip @ -1.25V



■ Cd ▲ Te

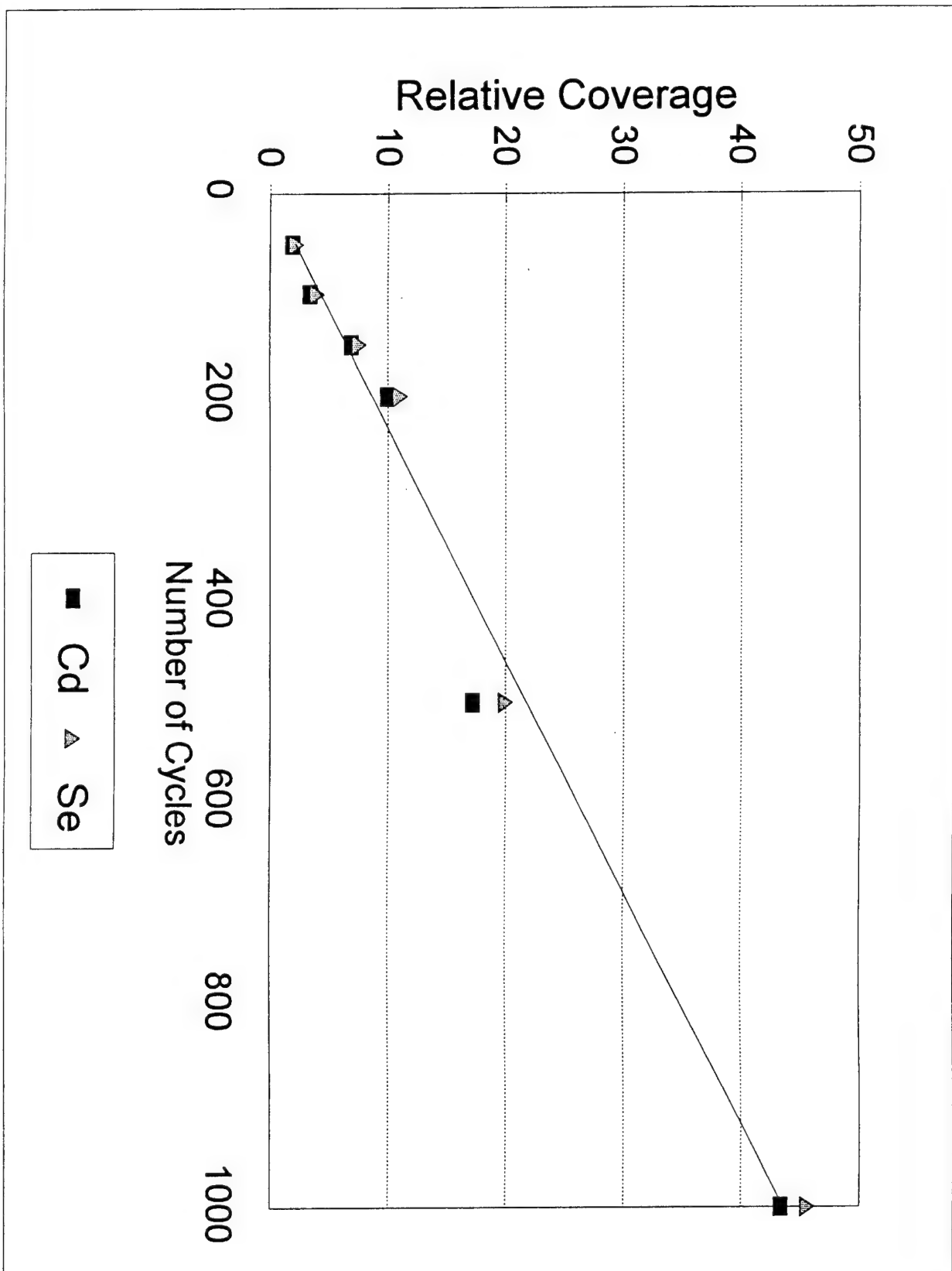
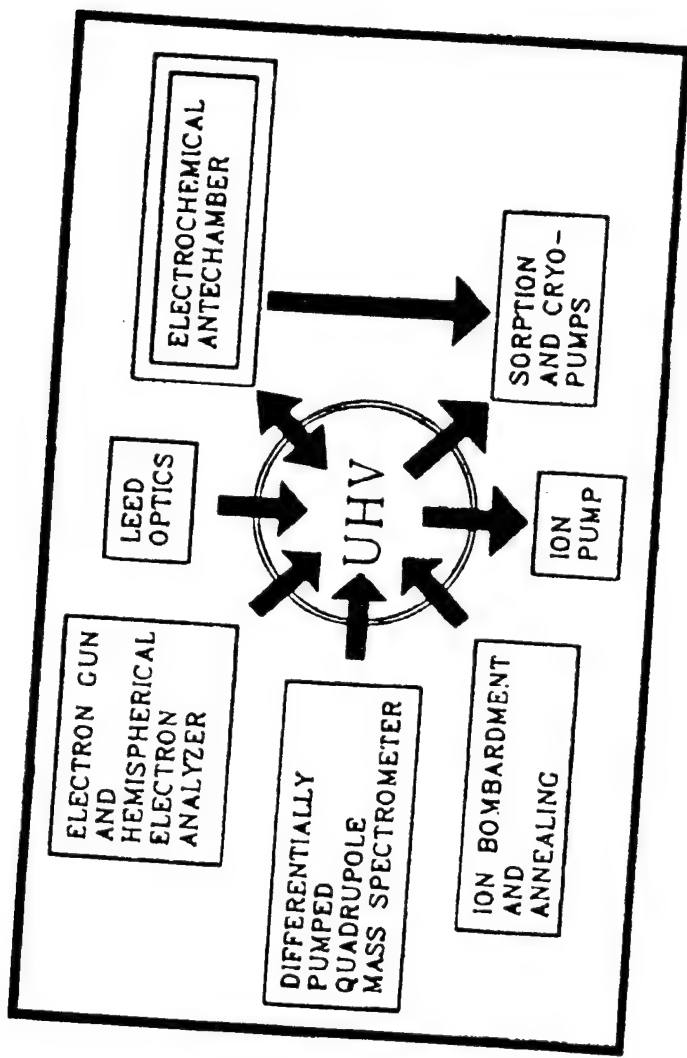
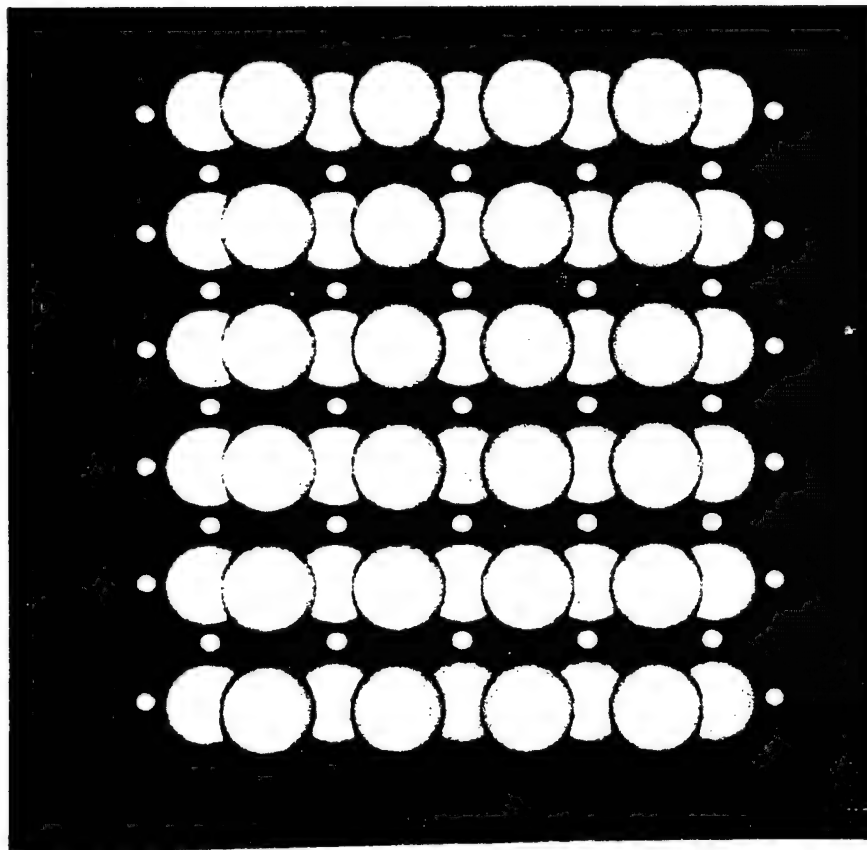
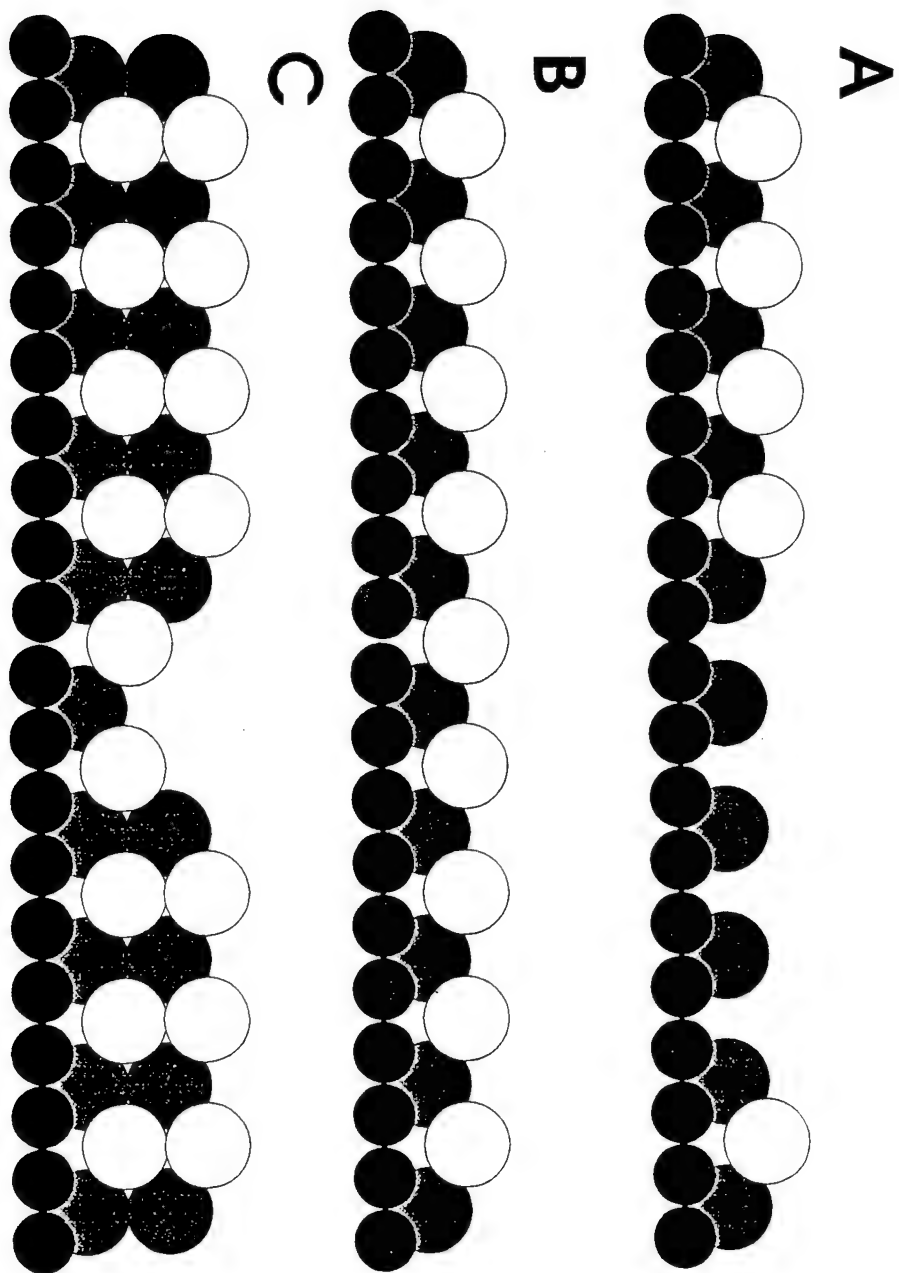
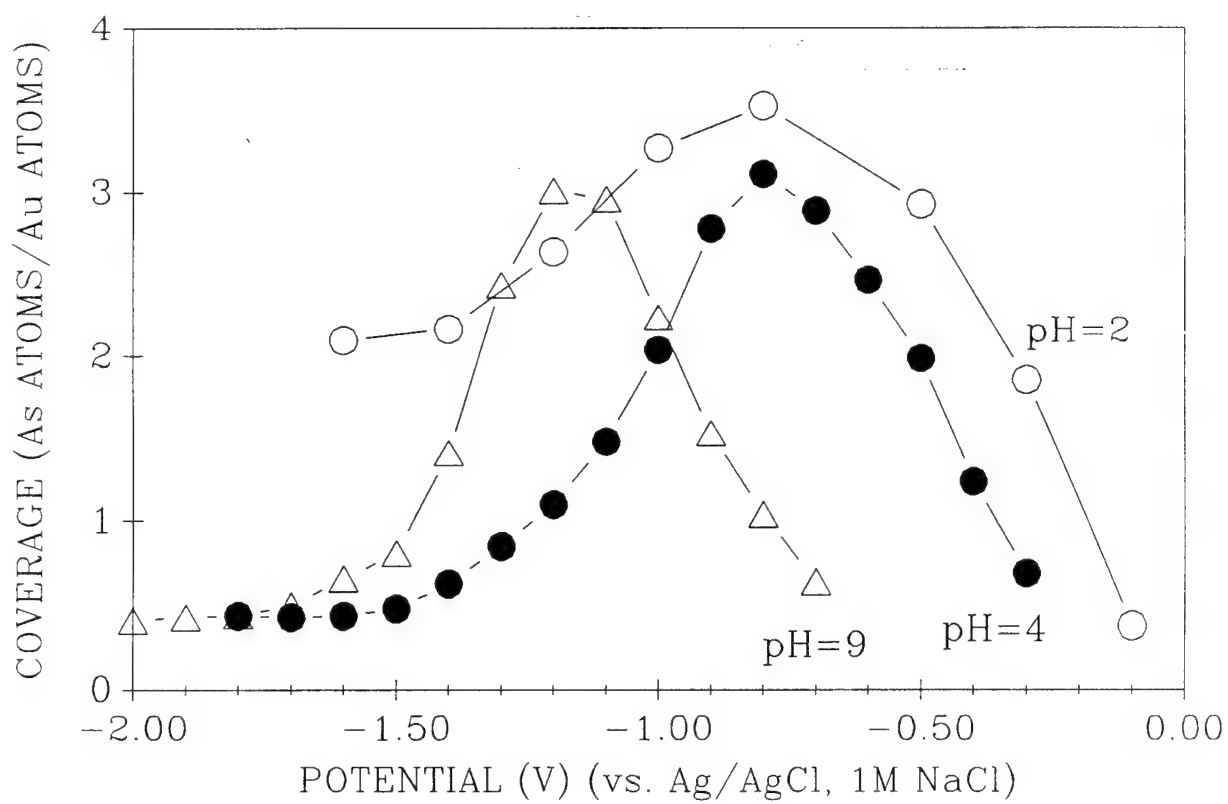


Figure 34
STUCKNEY









KKK 4
Page 43

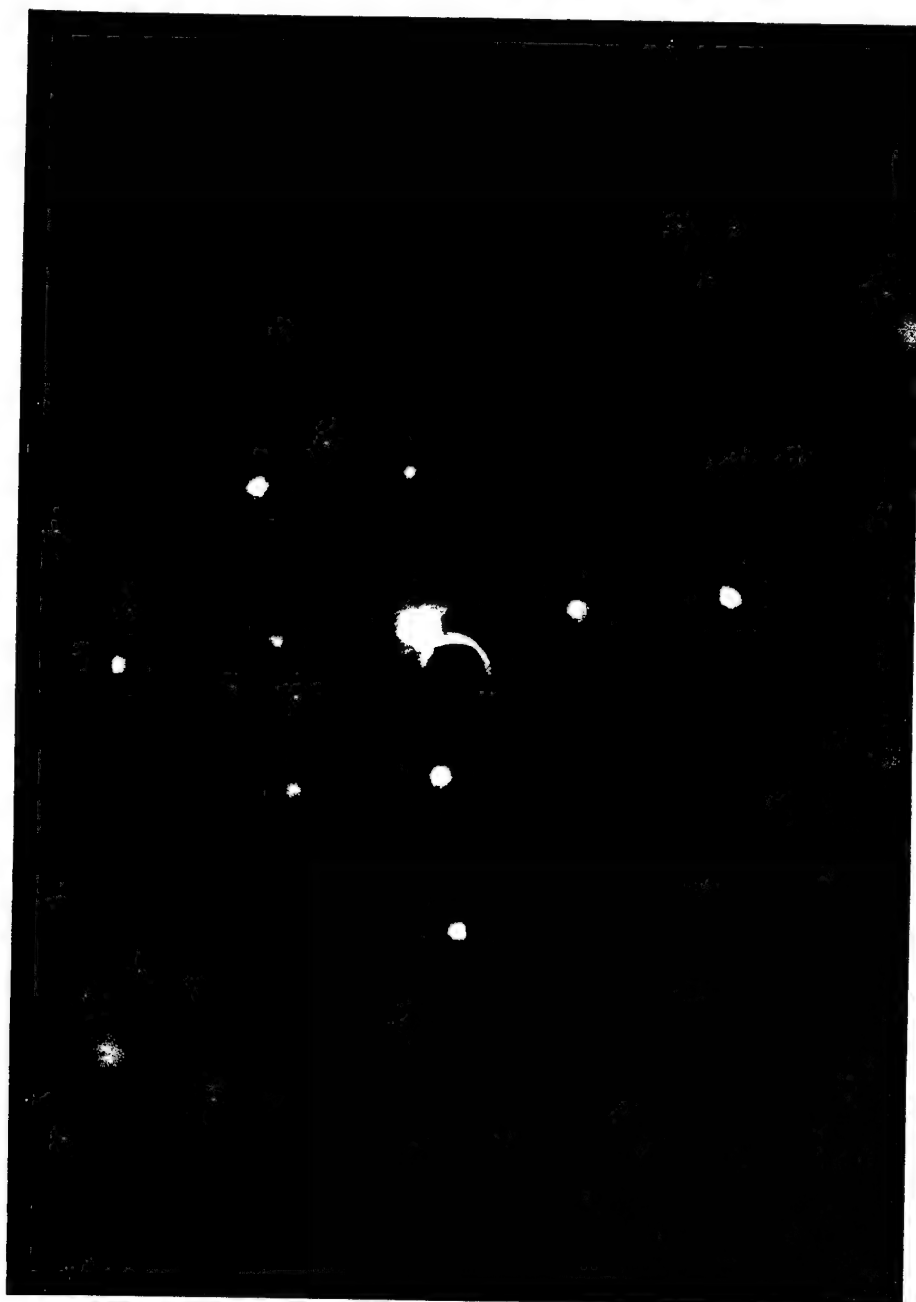
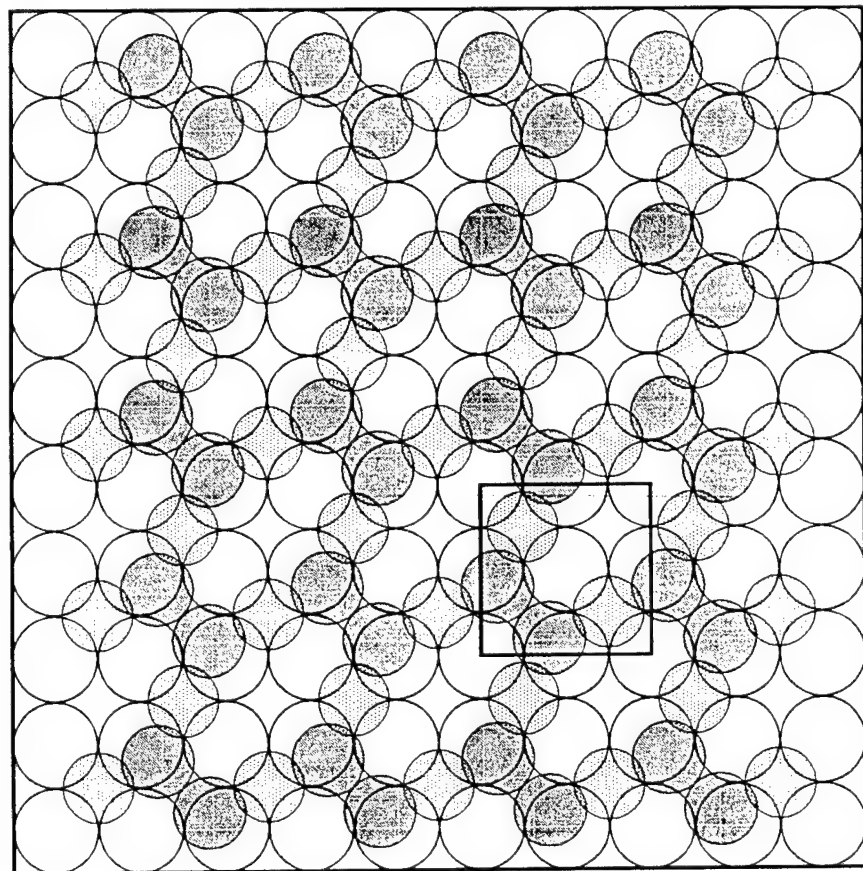


Figure 77
Stillkeny



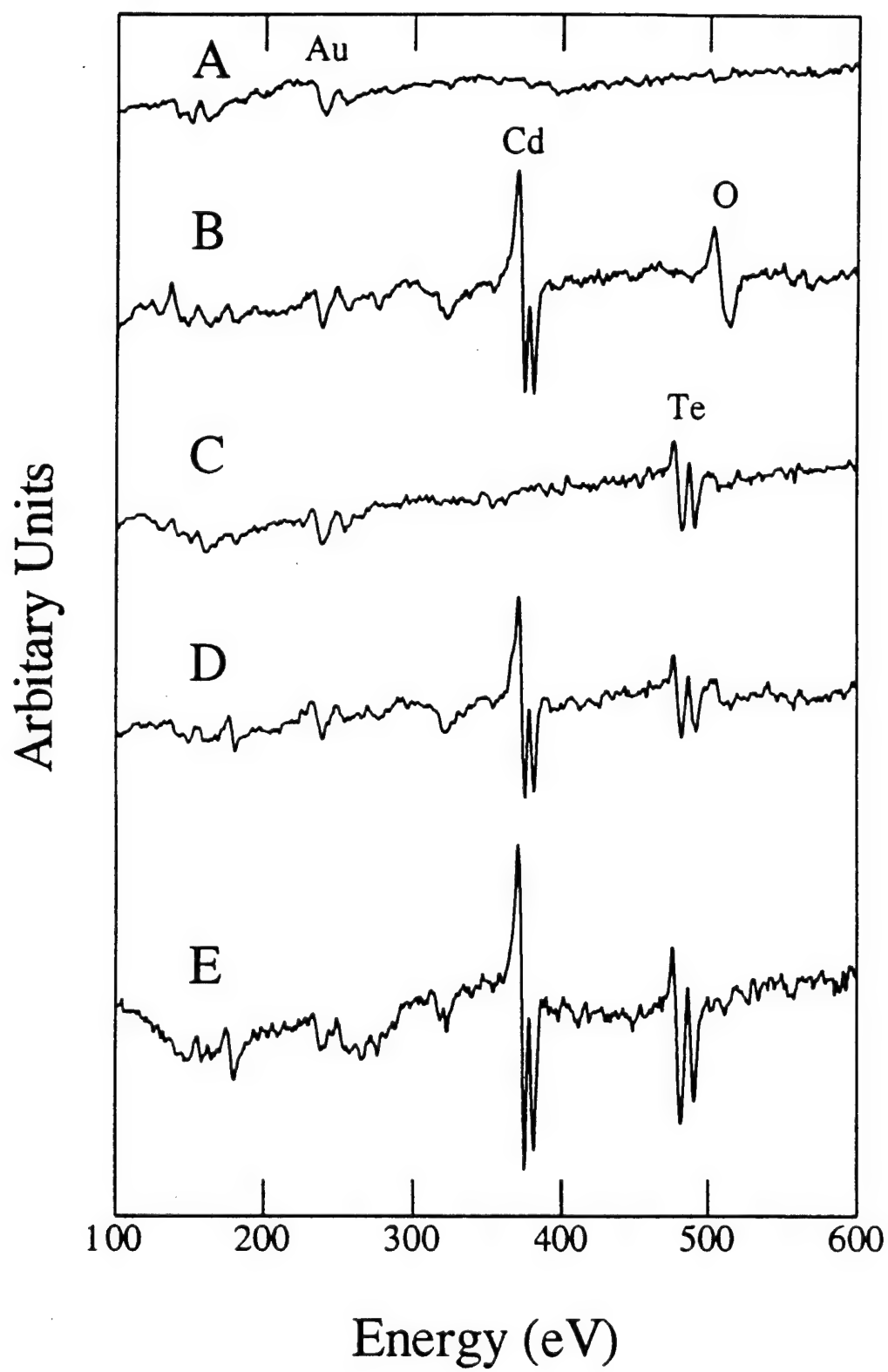
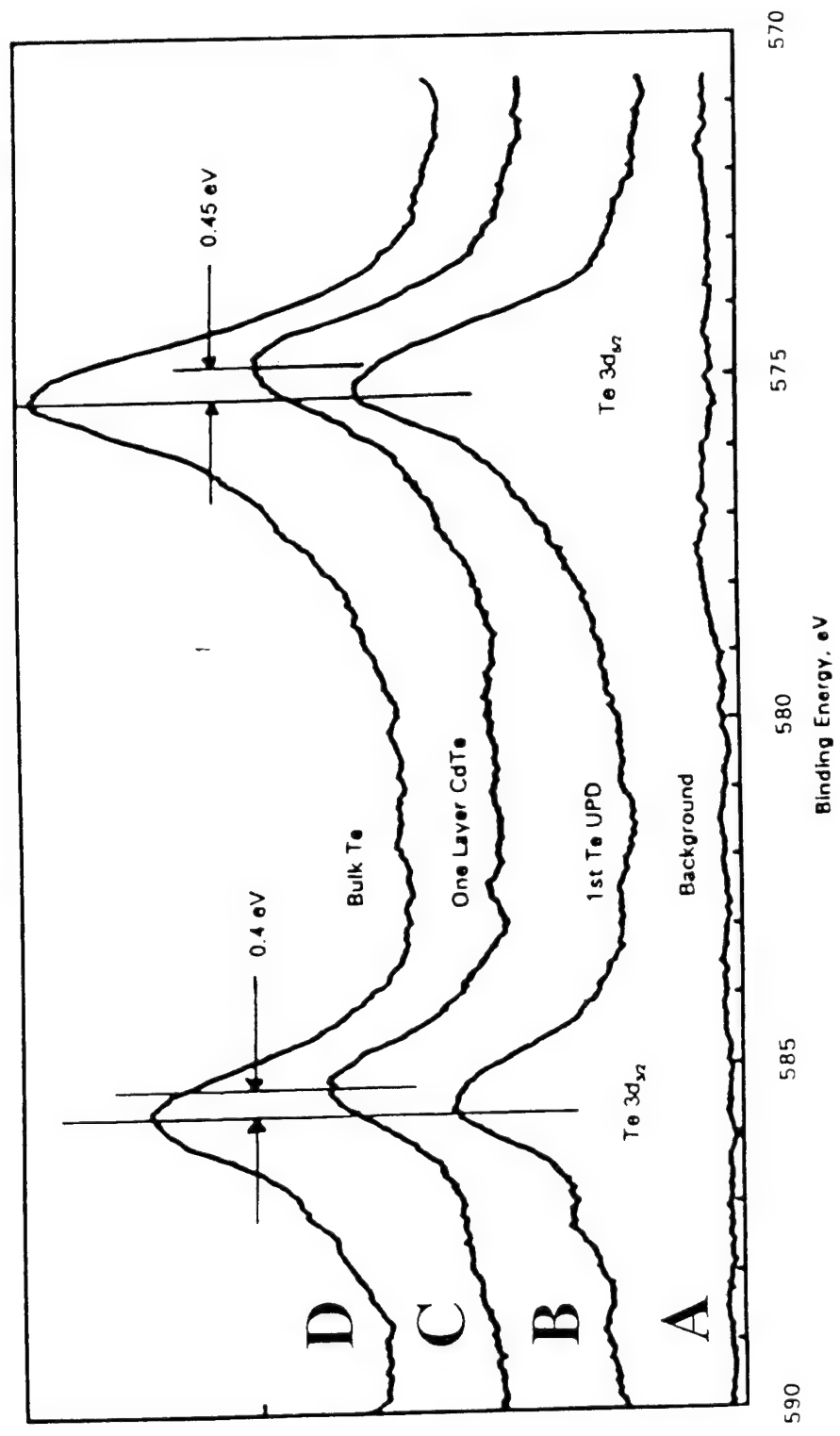
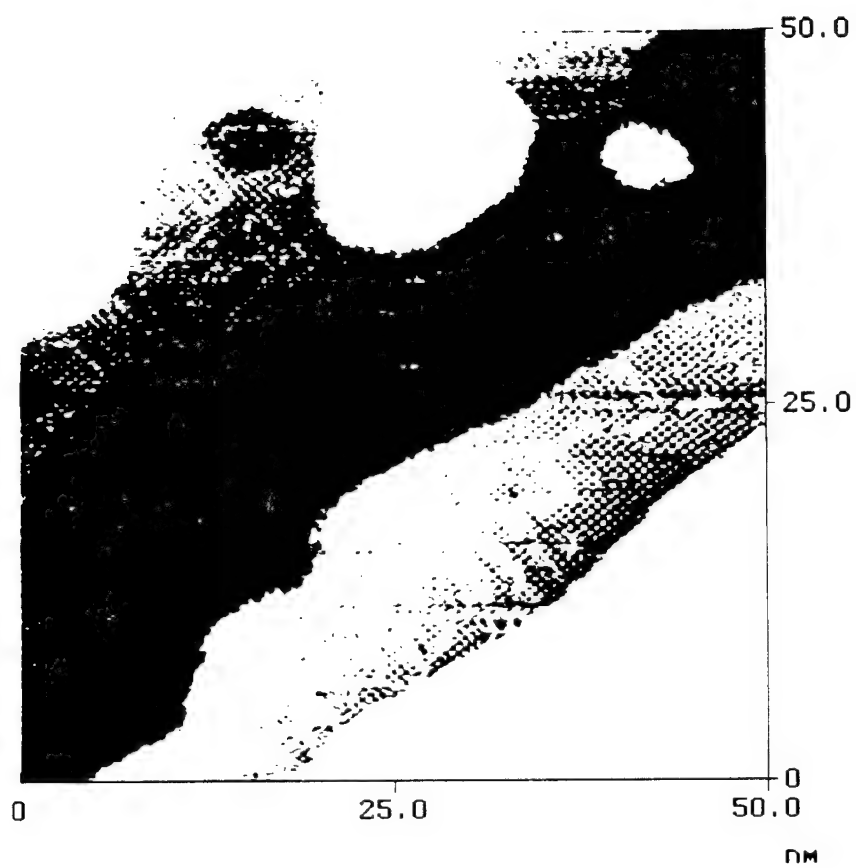


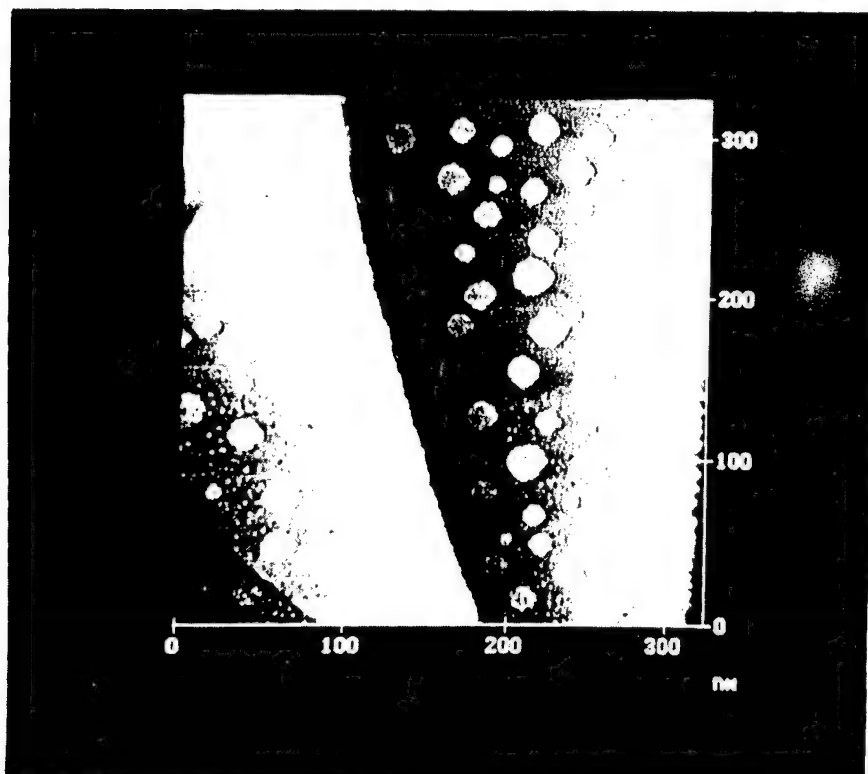
Figure 46
STICKNEY

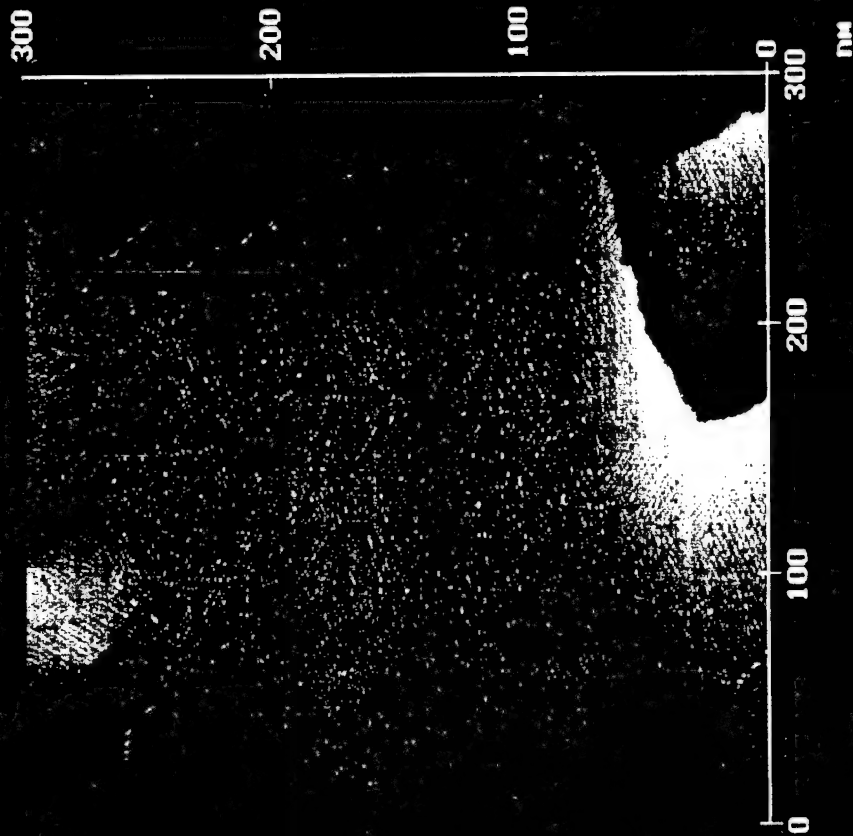


SHICKNEY
Figure 47



STICKNEY
Figure 48

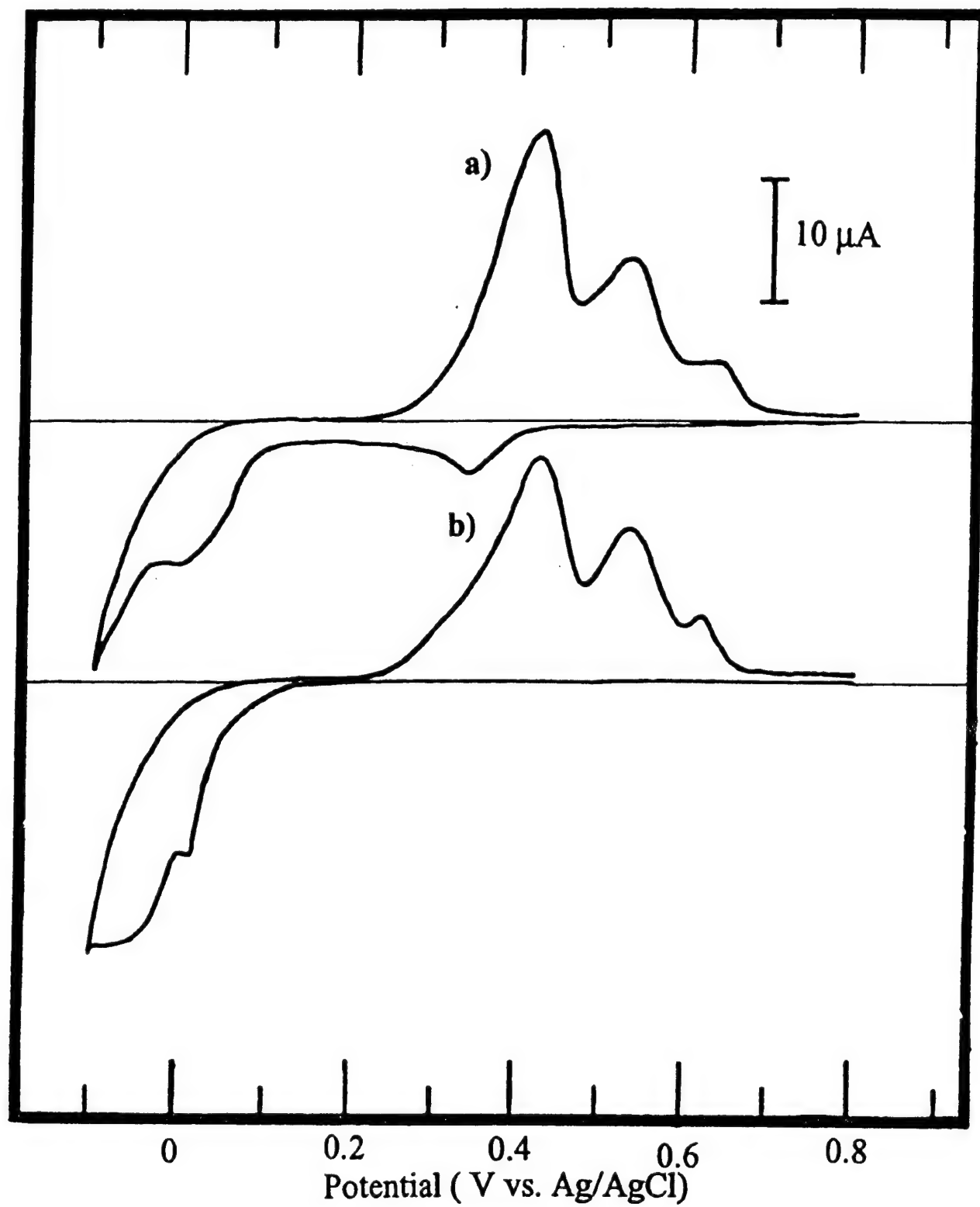


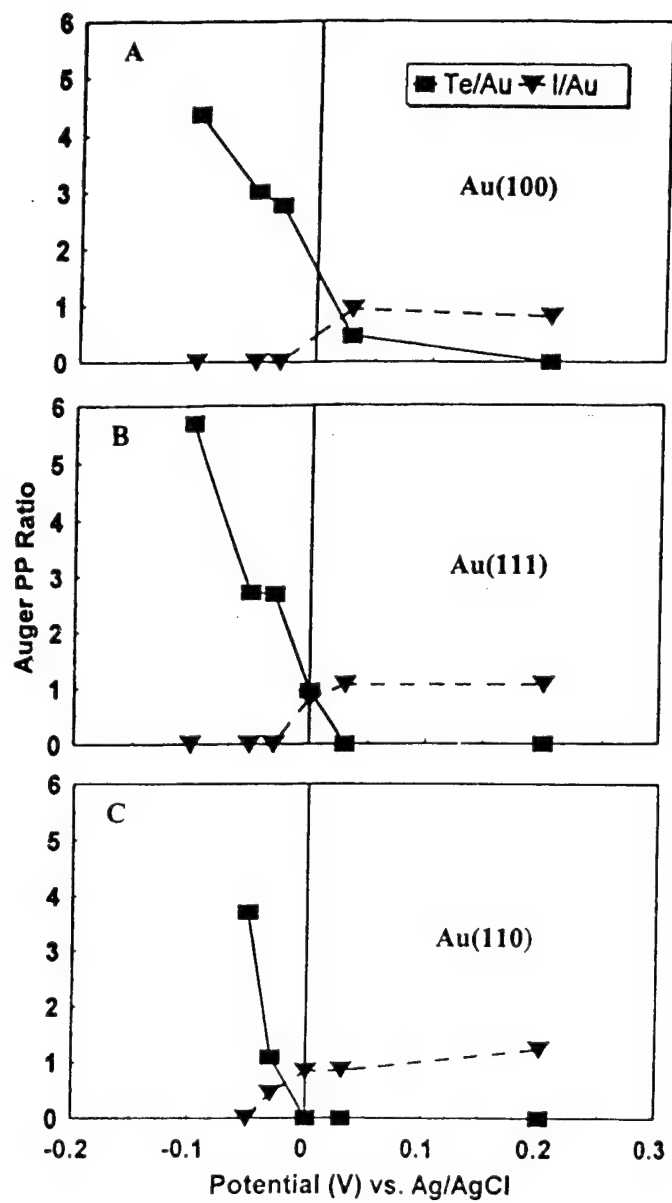


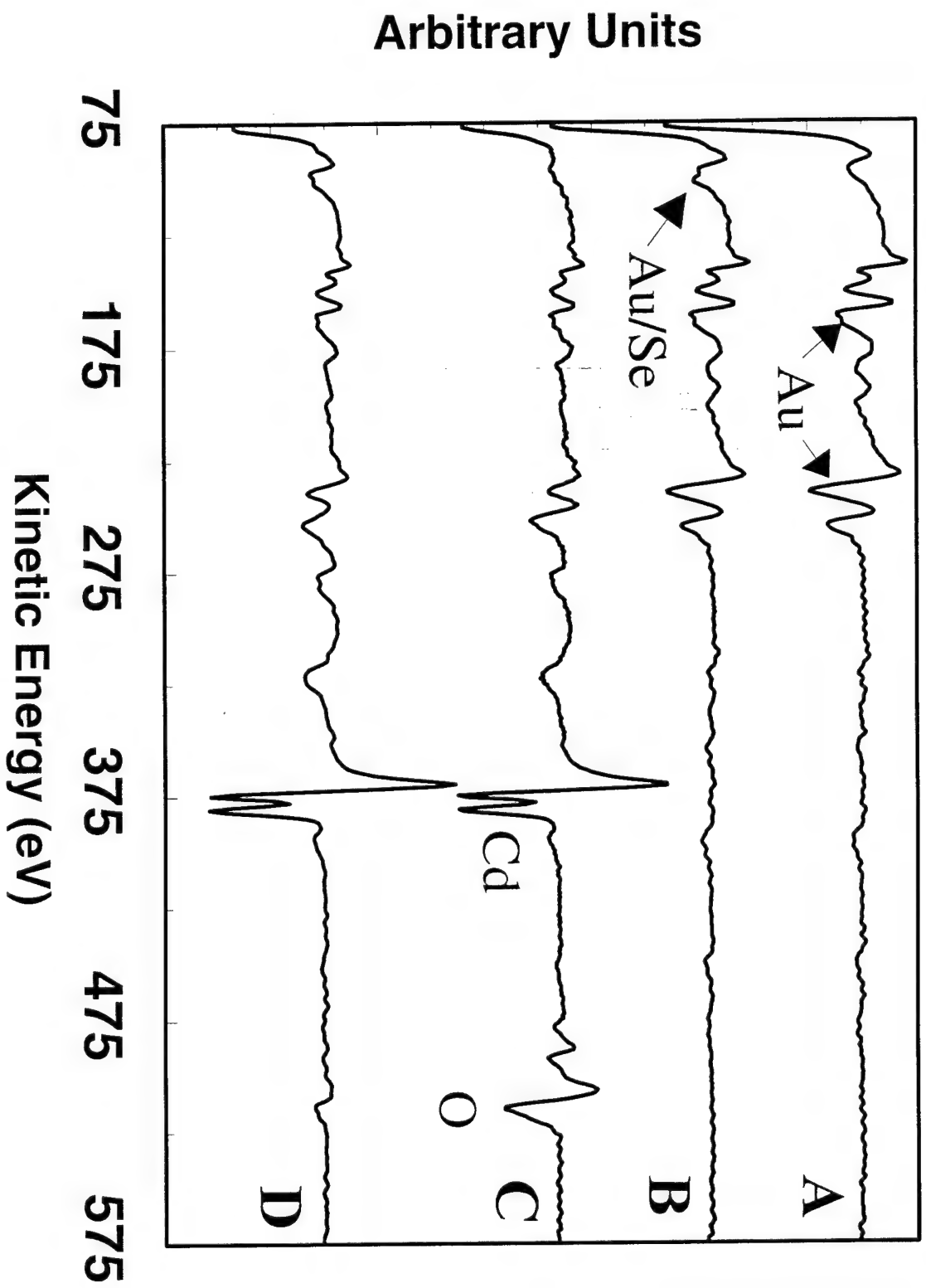
Microscope
Scan size
Setpoint
Bias
Scan rate
Number of samples
Data type
Z range

NSIII STM
300.0 nm
9.0 nA
22.1 mV
7.6 Hz
512
Height
1.6 nm

au100i0.157







STICKNEY
Figure 53A

A.



B.



Figure 53BC

C.

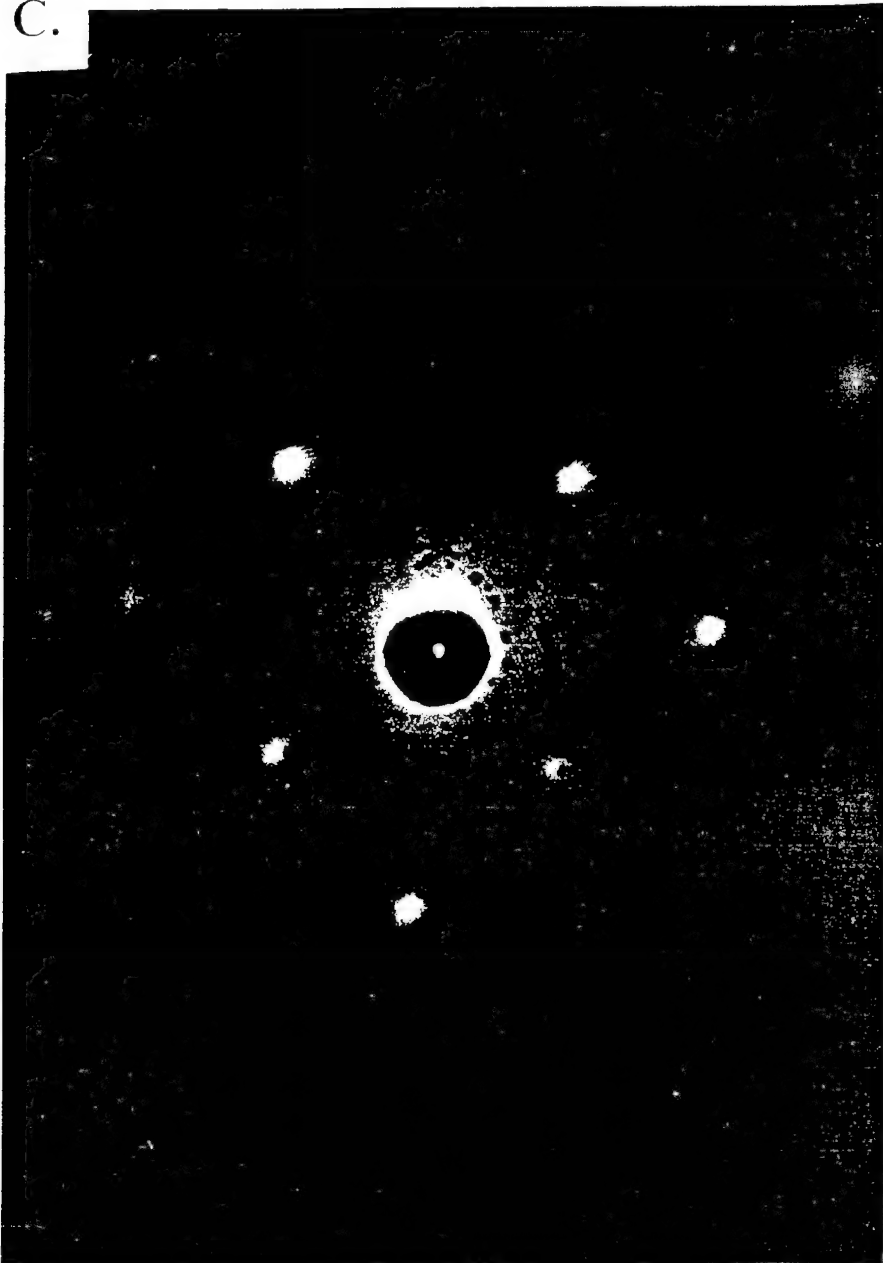
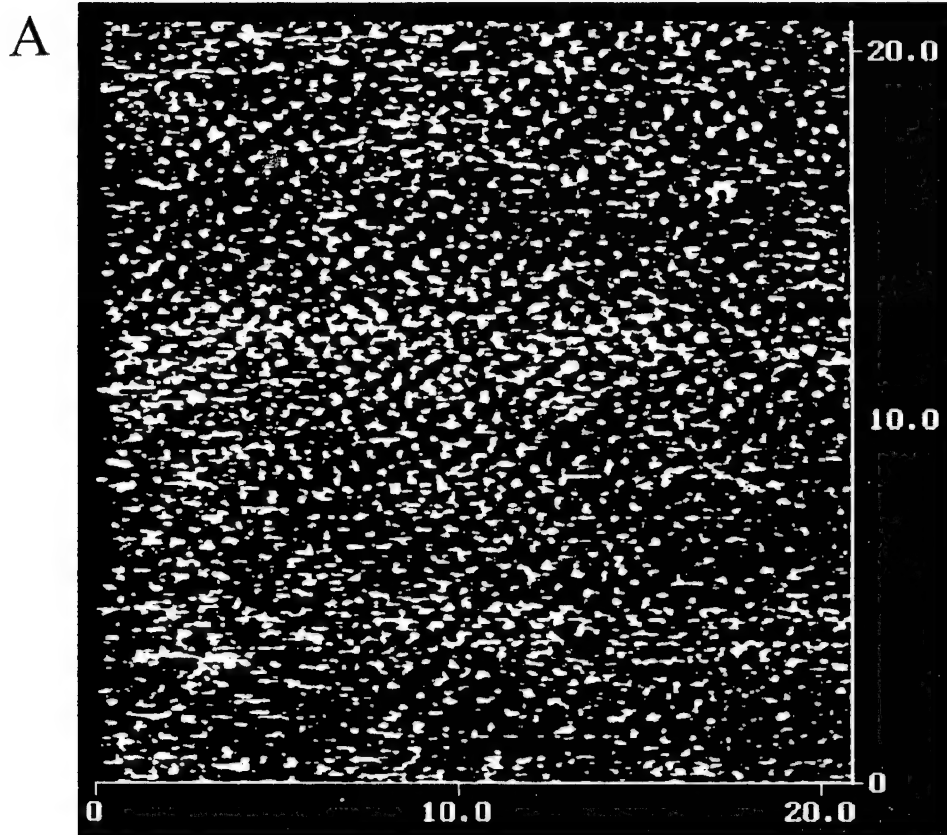


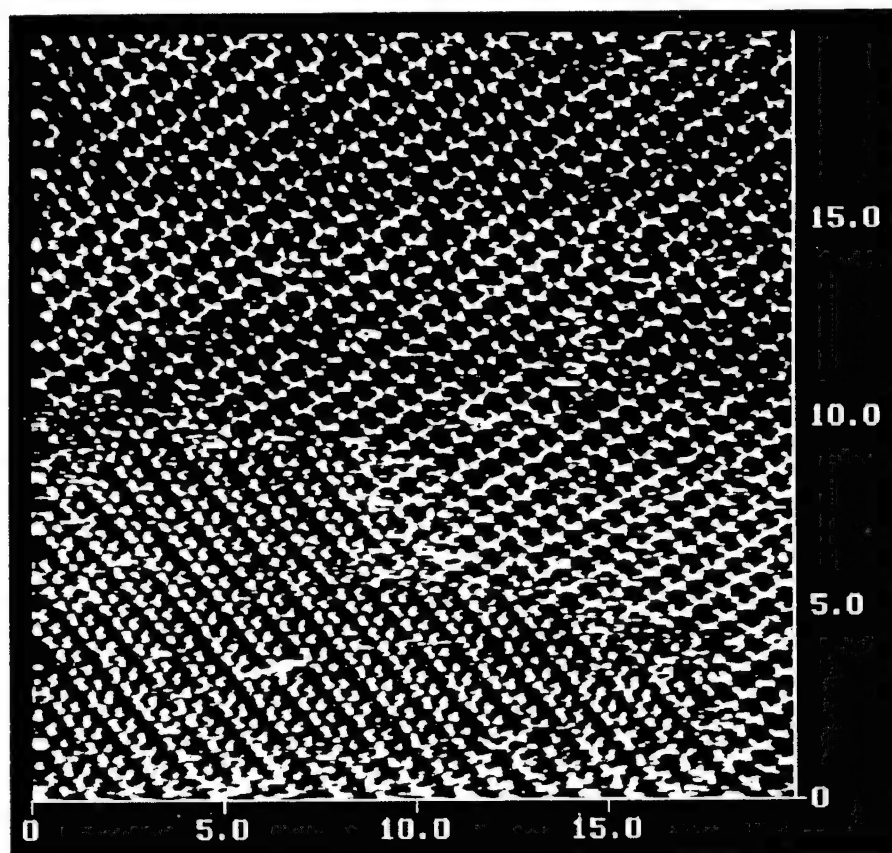
Image 500
STICKNEY

D.

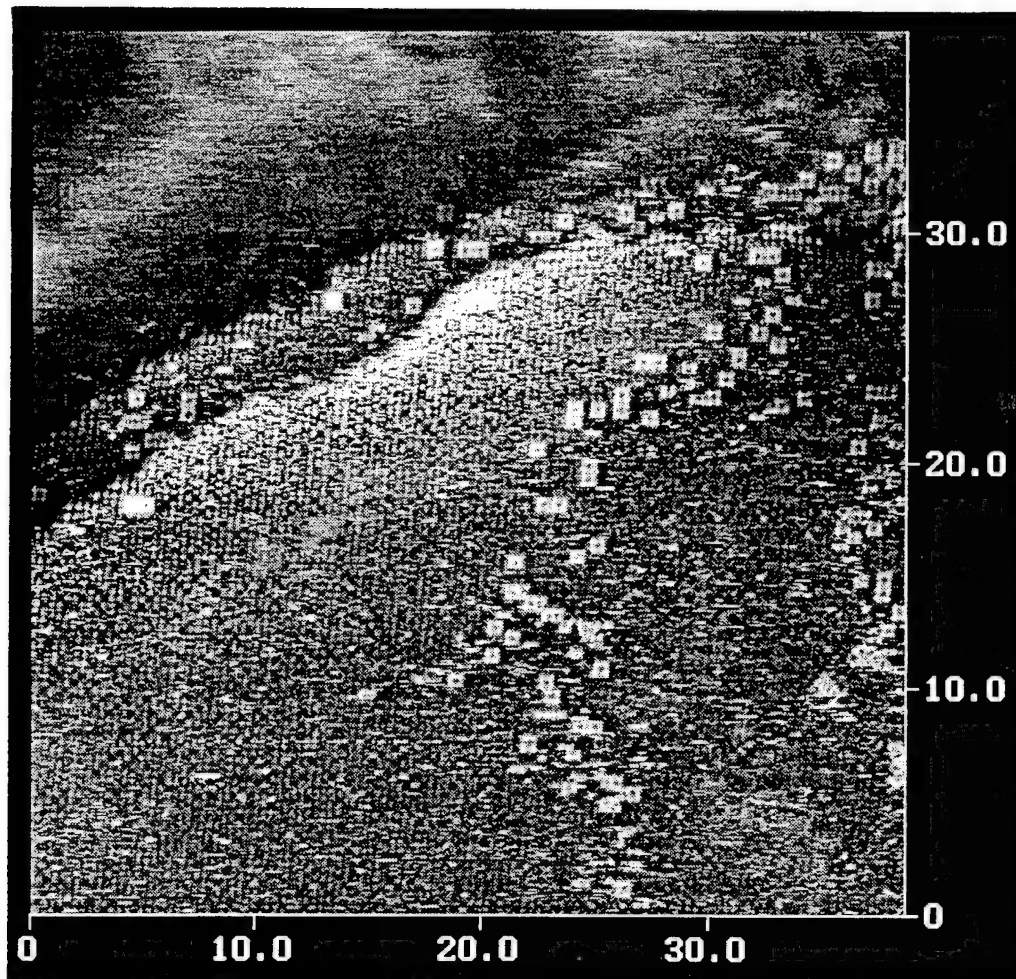




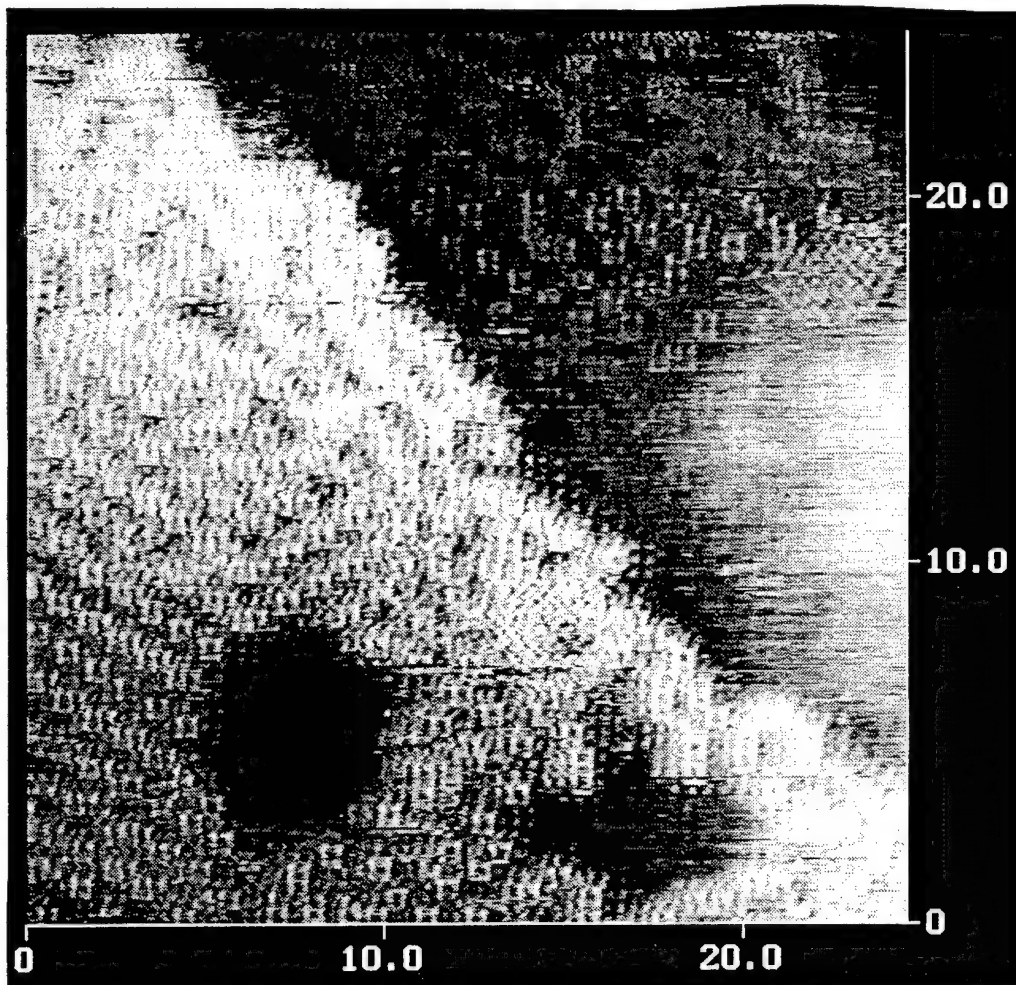
B



C



D



E

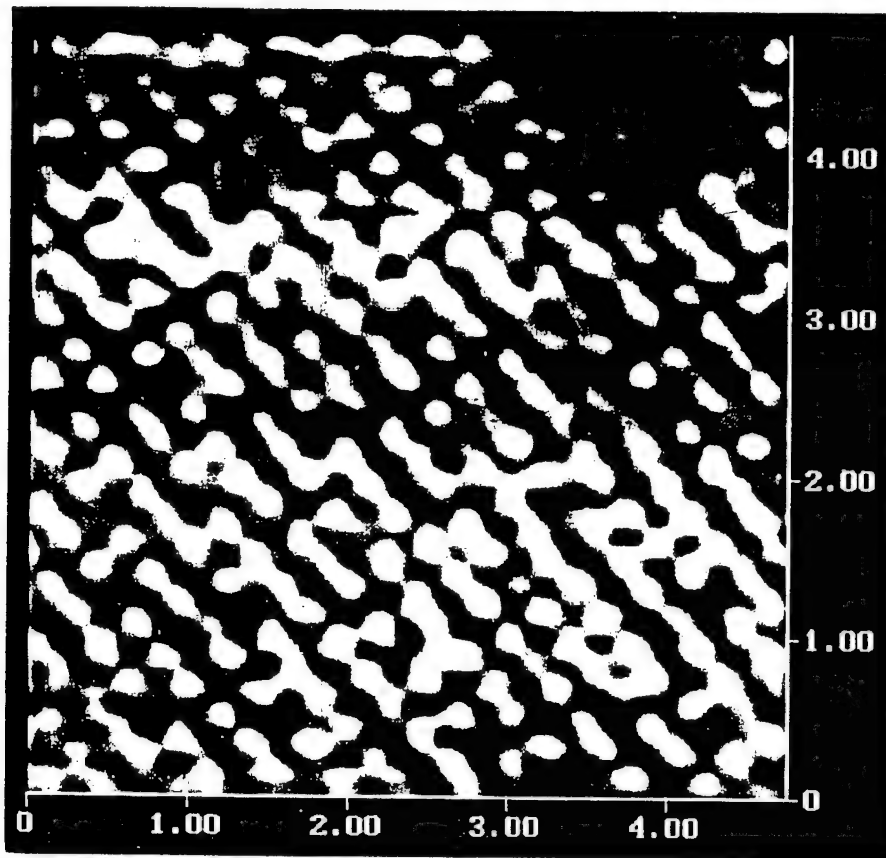
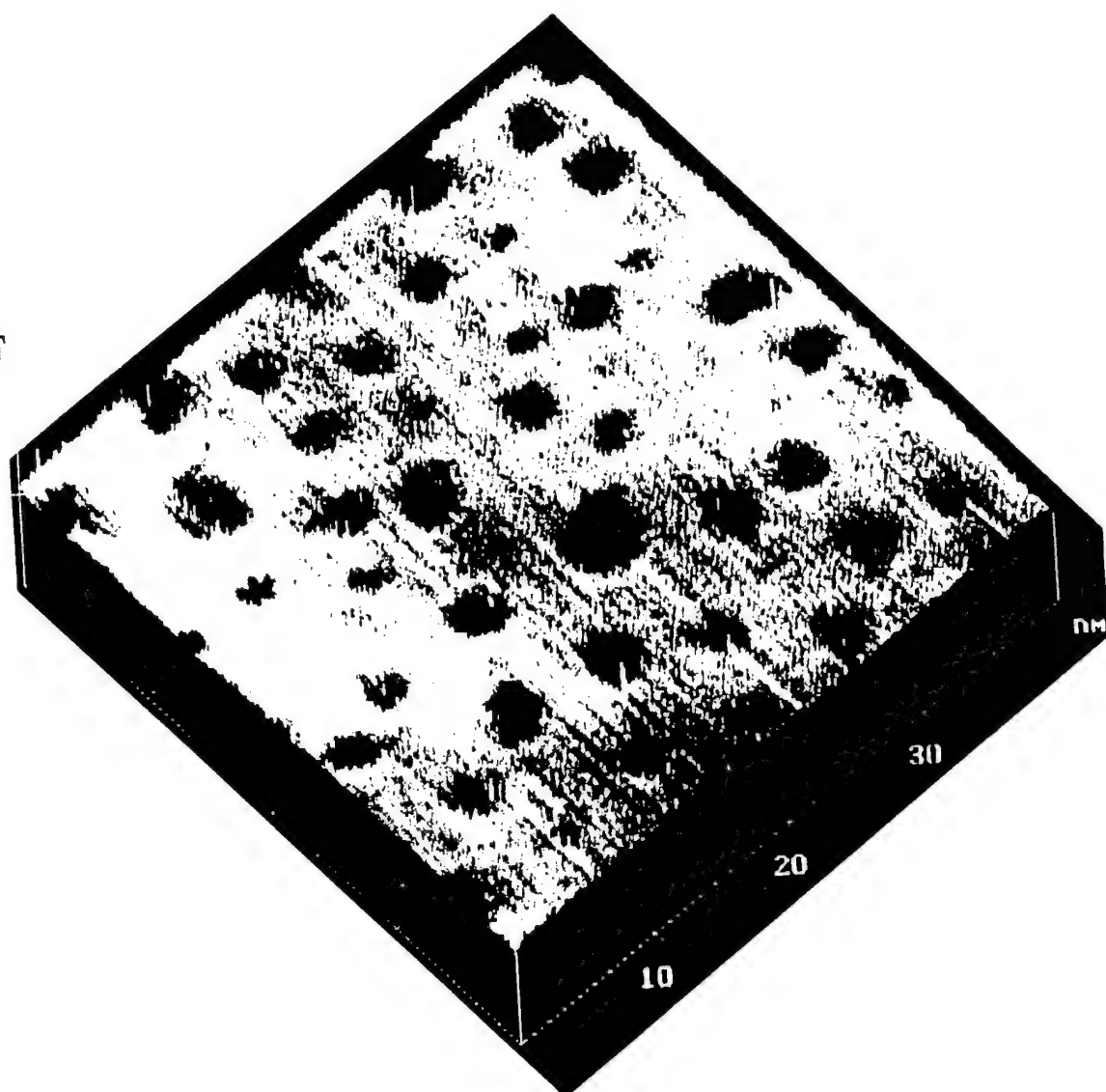
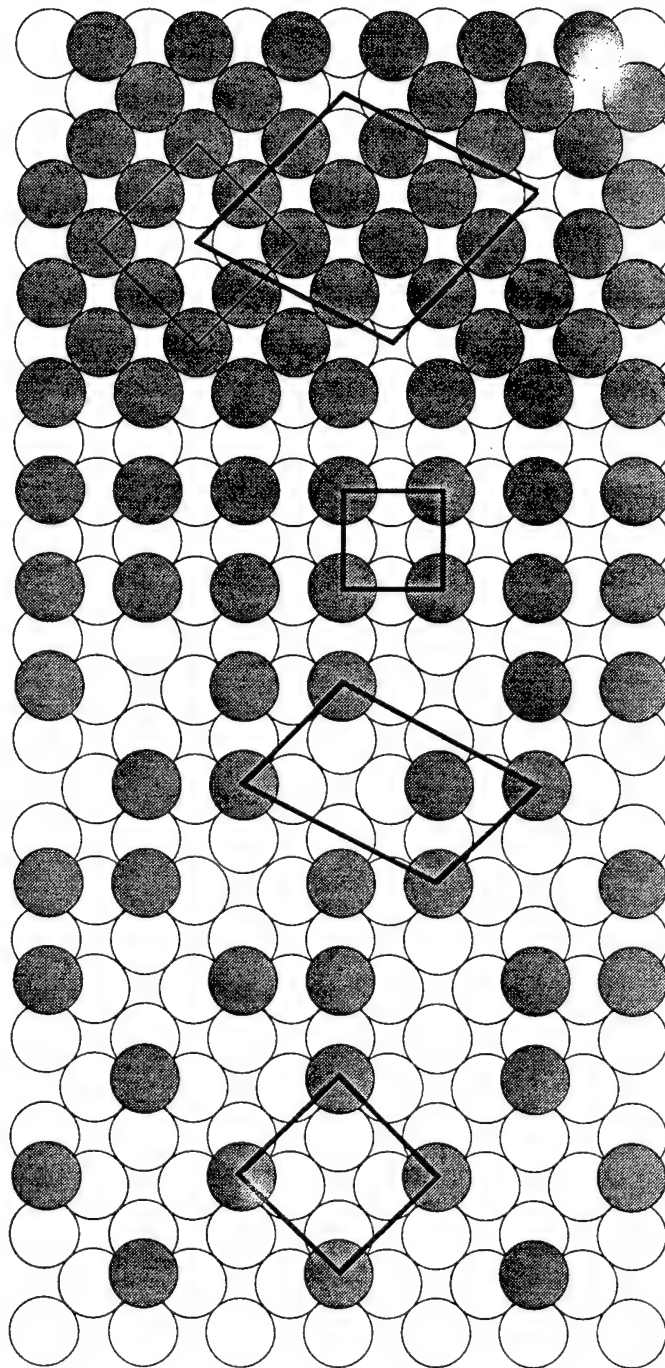
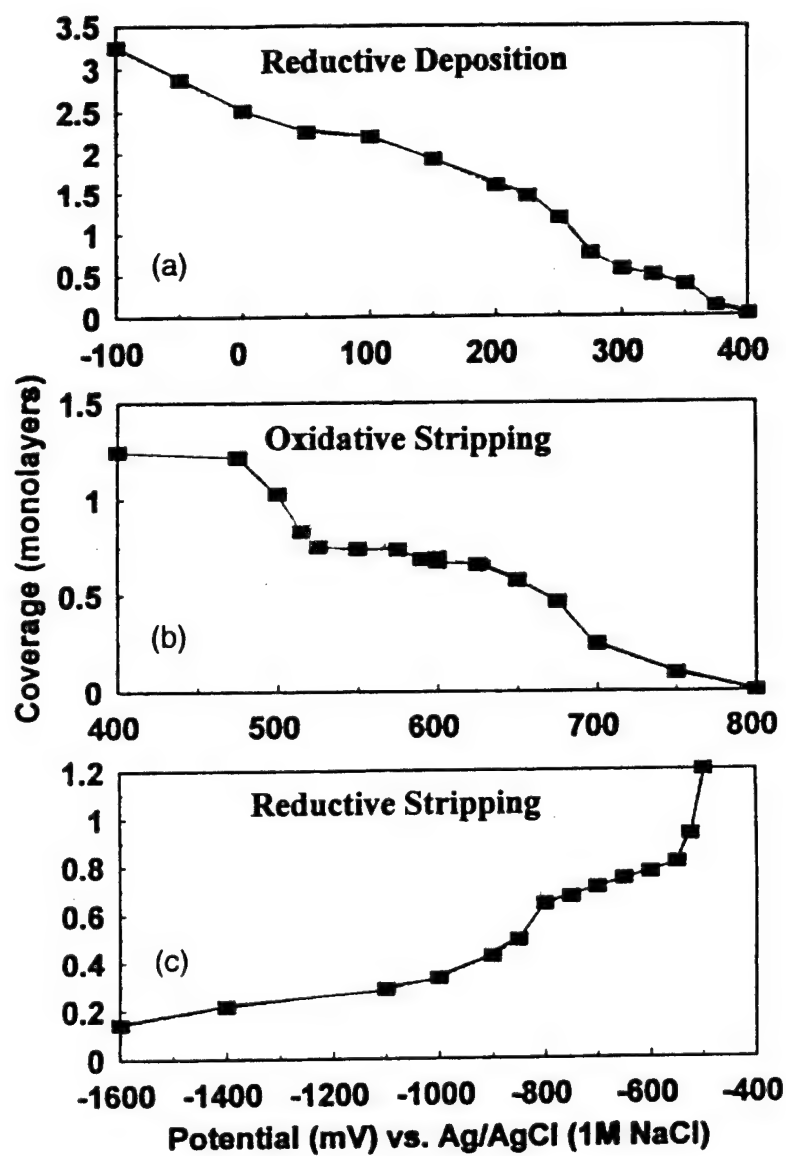


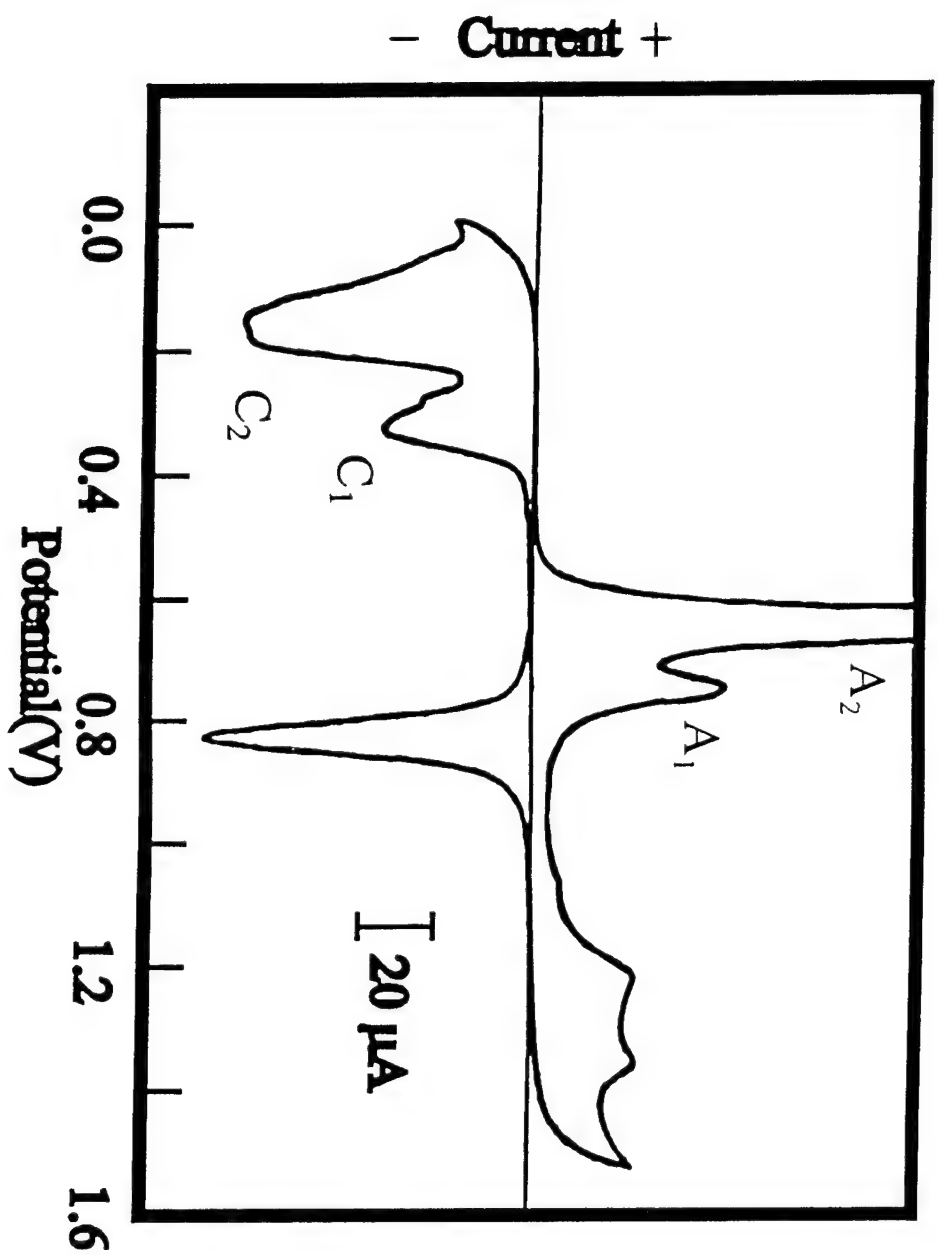
Figure 57F
Stitzkney

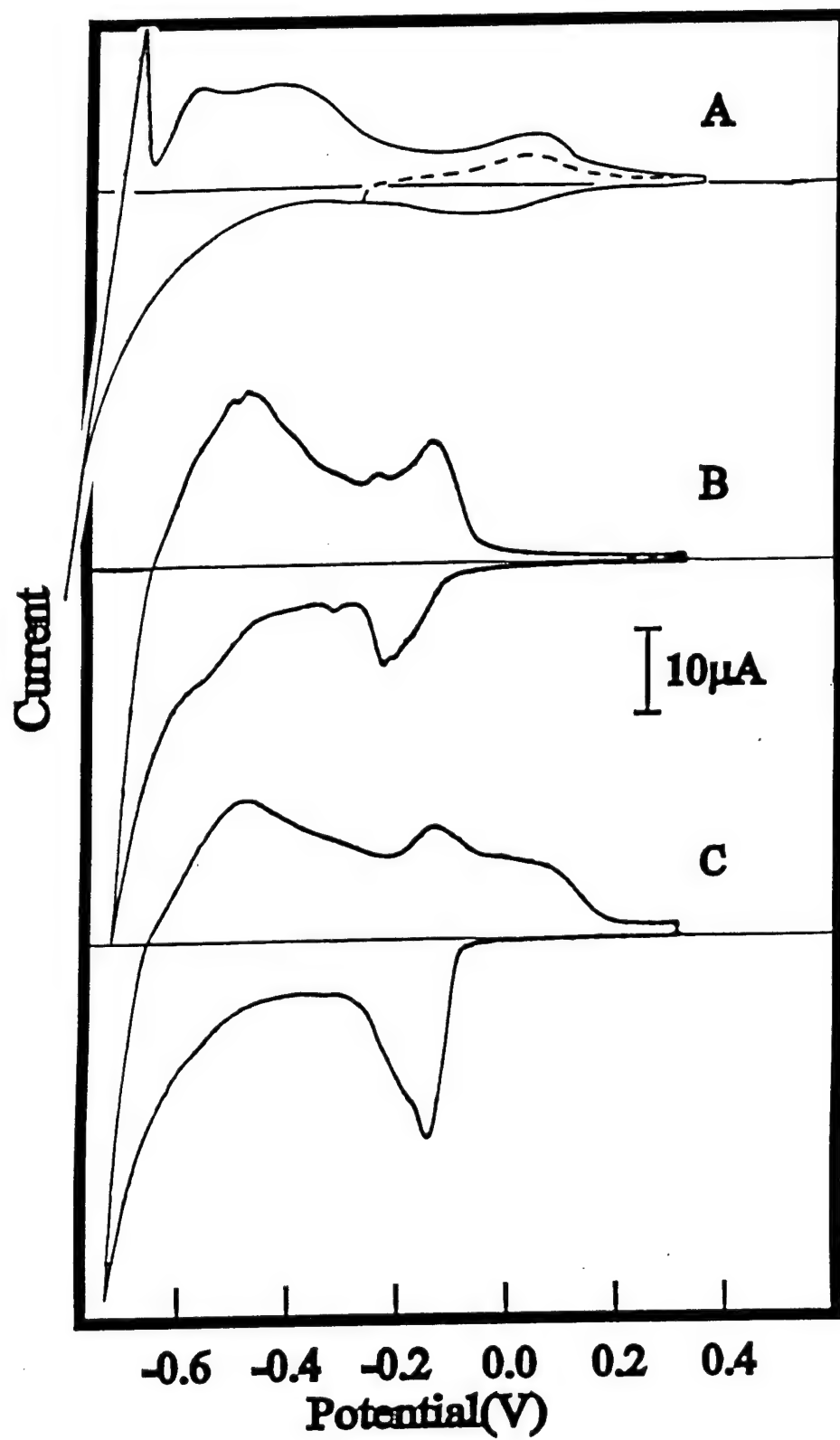
F



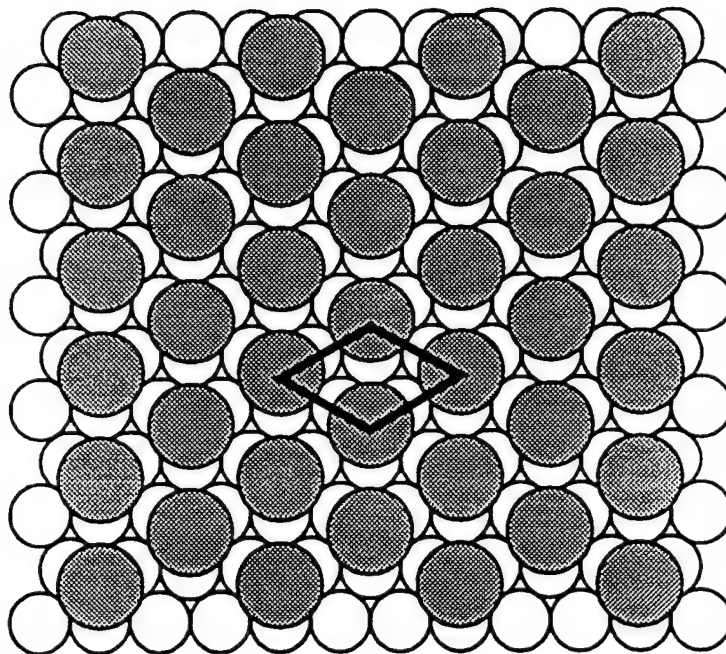








A



B

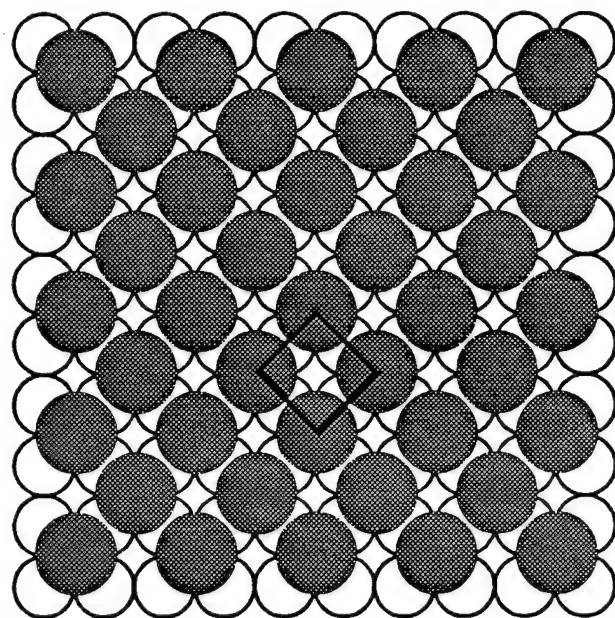
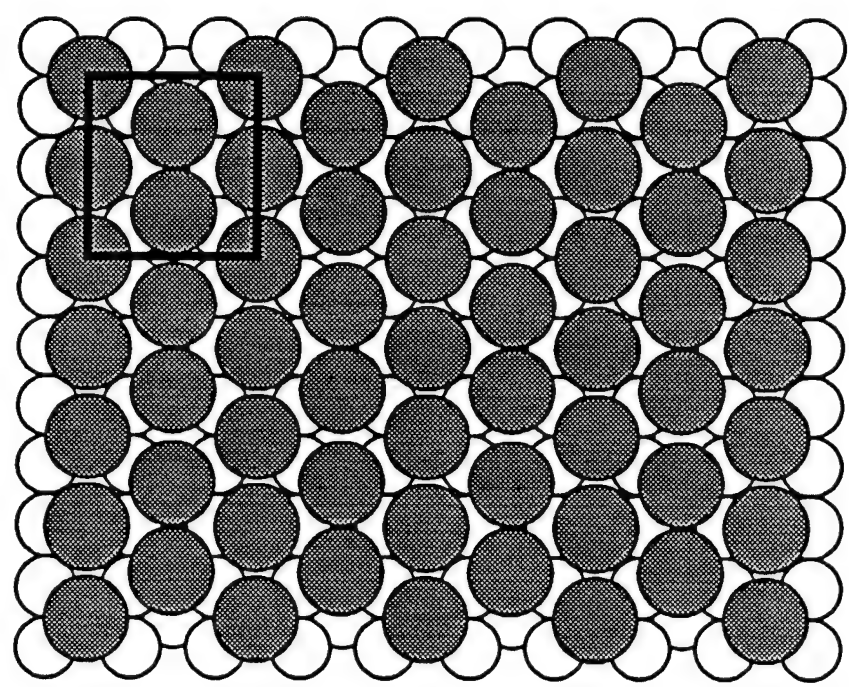
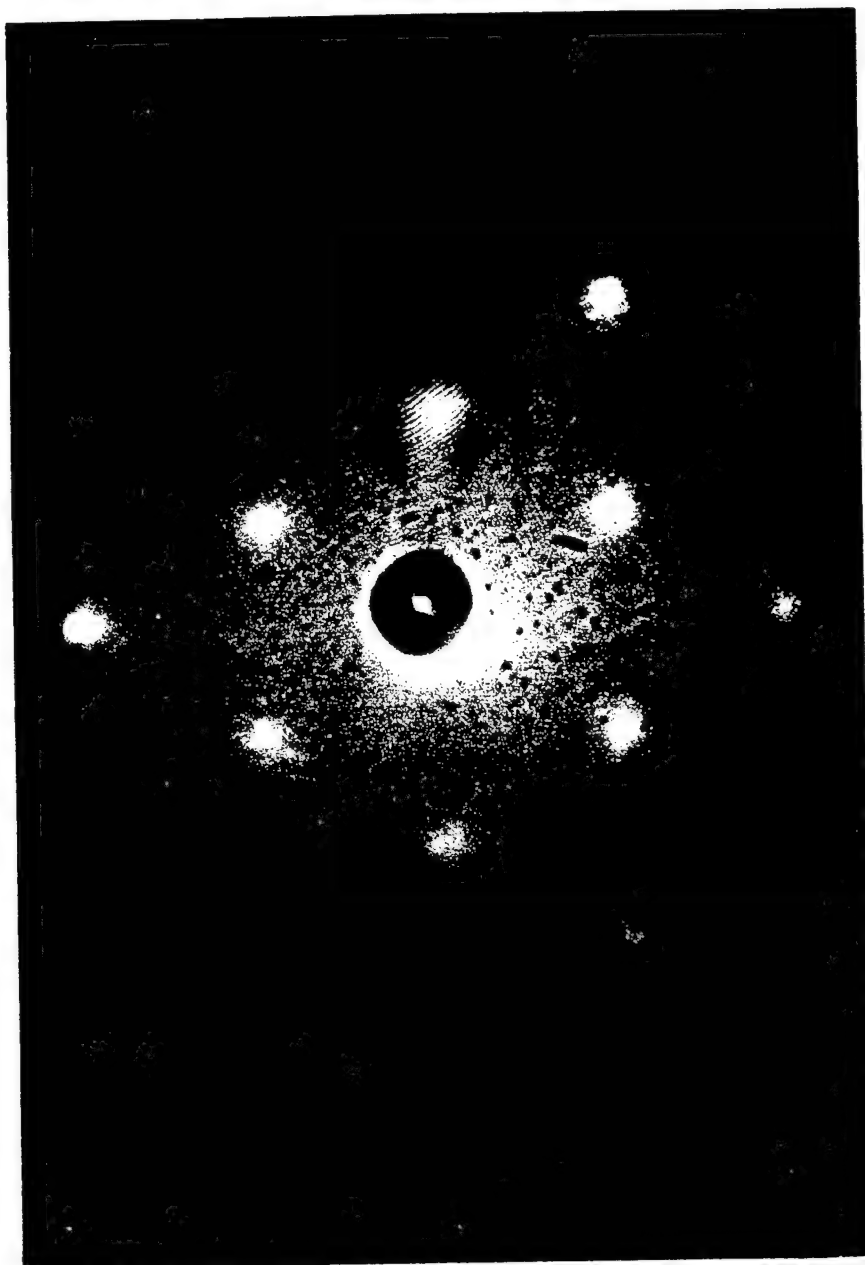


Fig 10
Figure 59C
Stilben

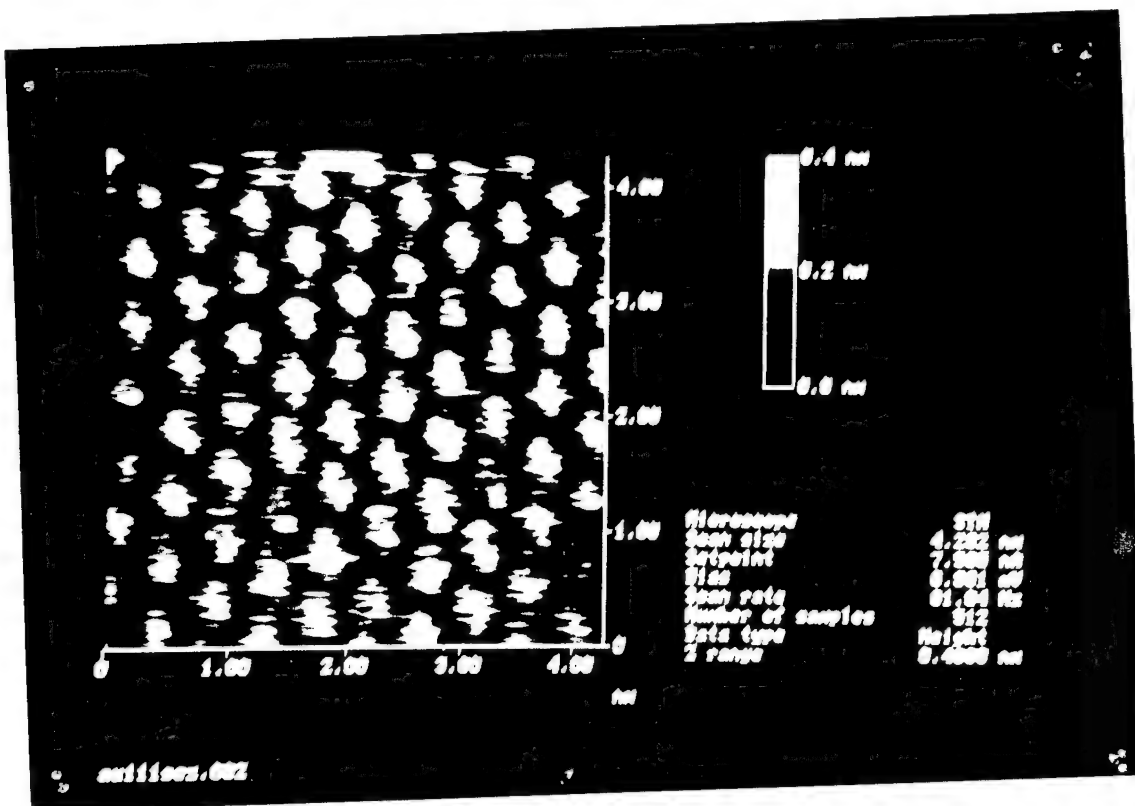
C



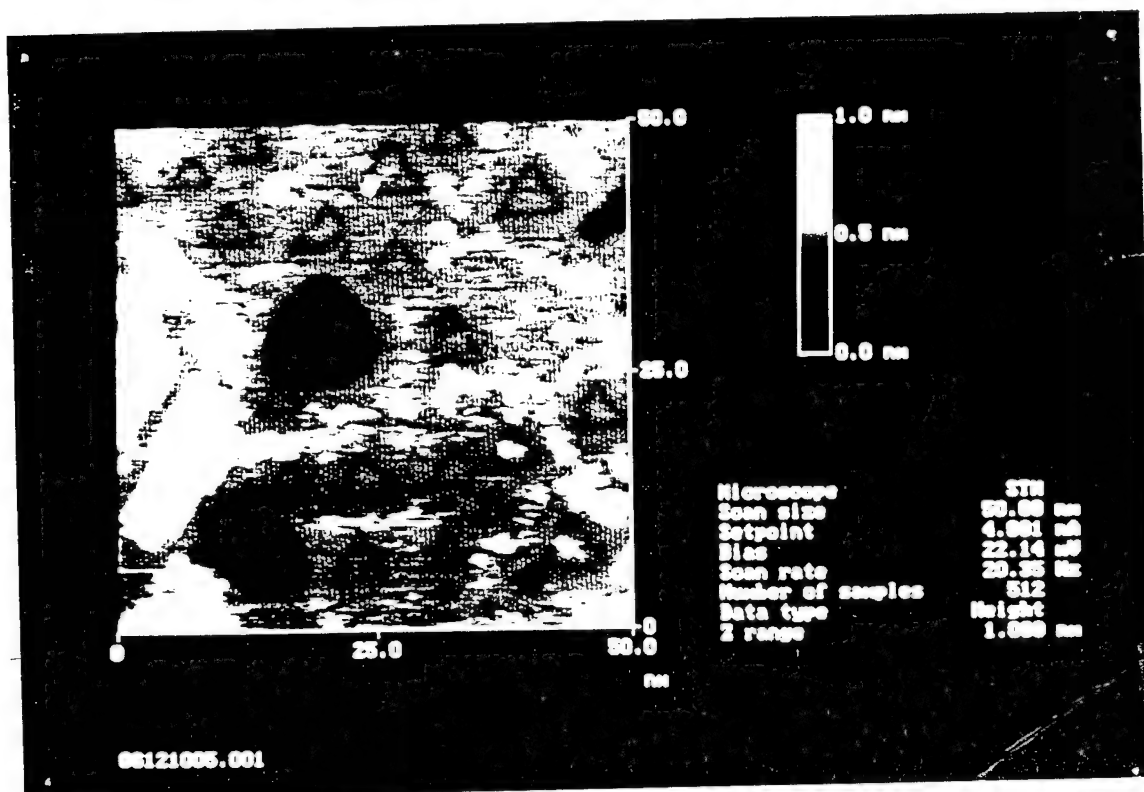


CHV 61

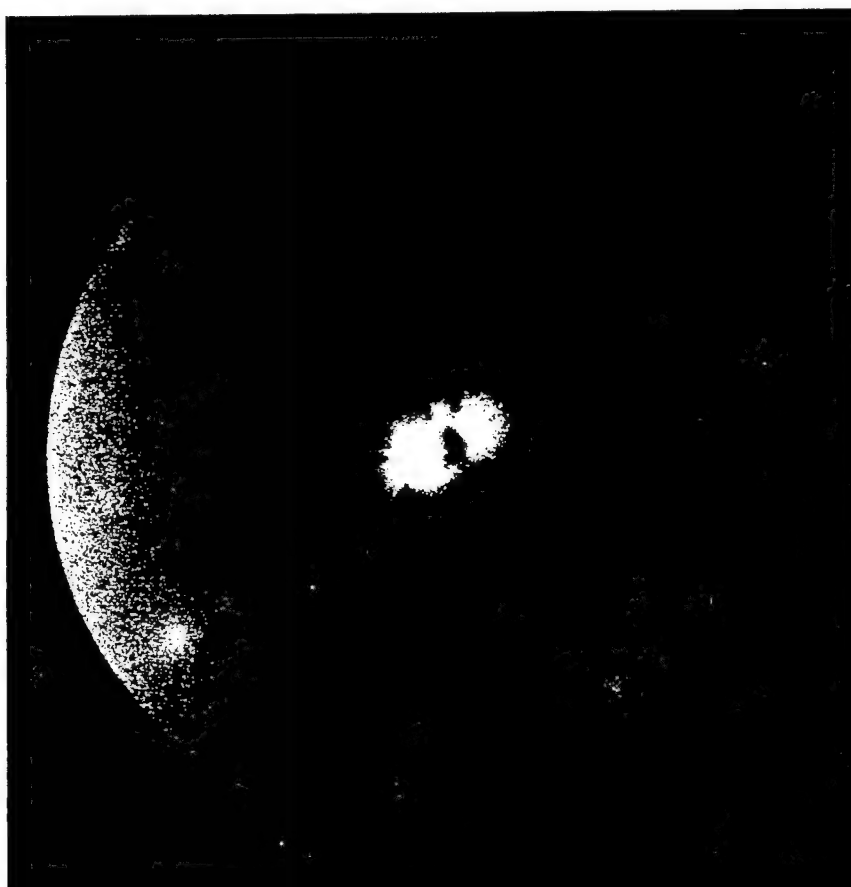
A



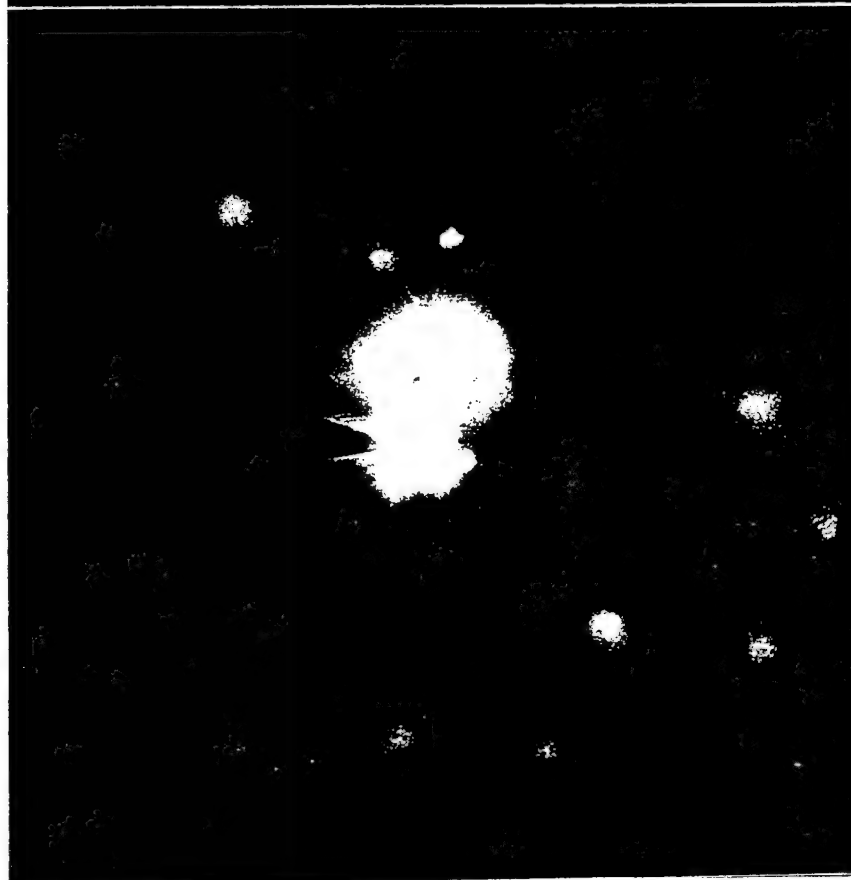
B



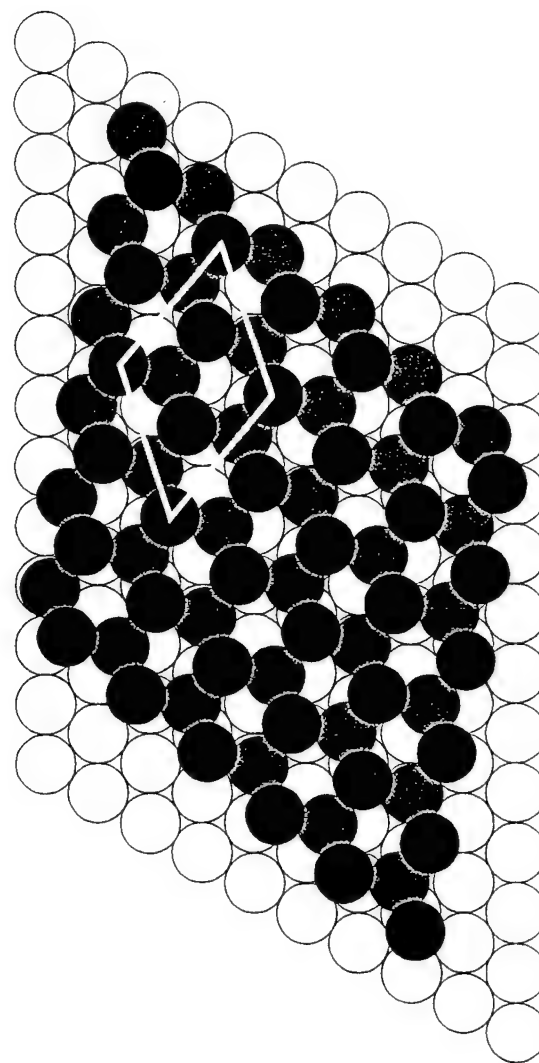
A



B

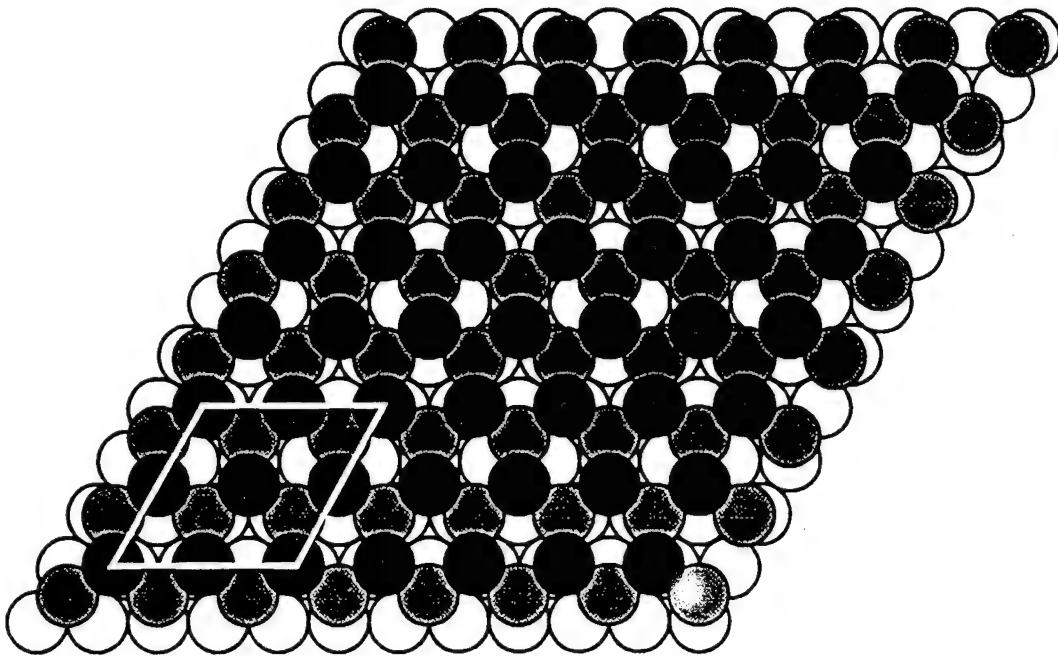


STICK/UBY
Figure 63A

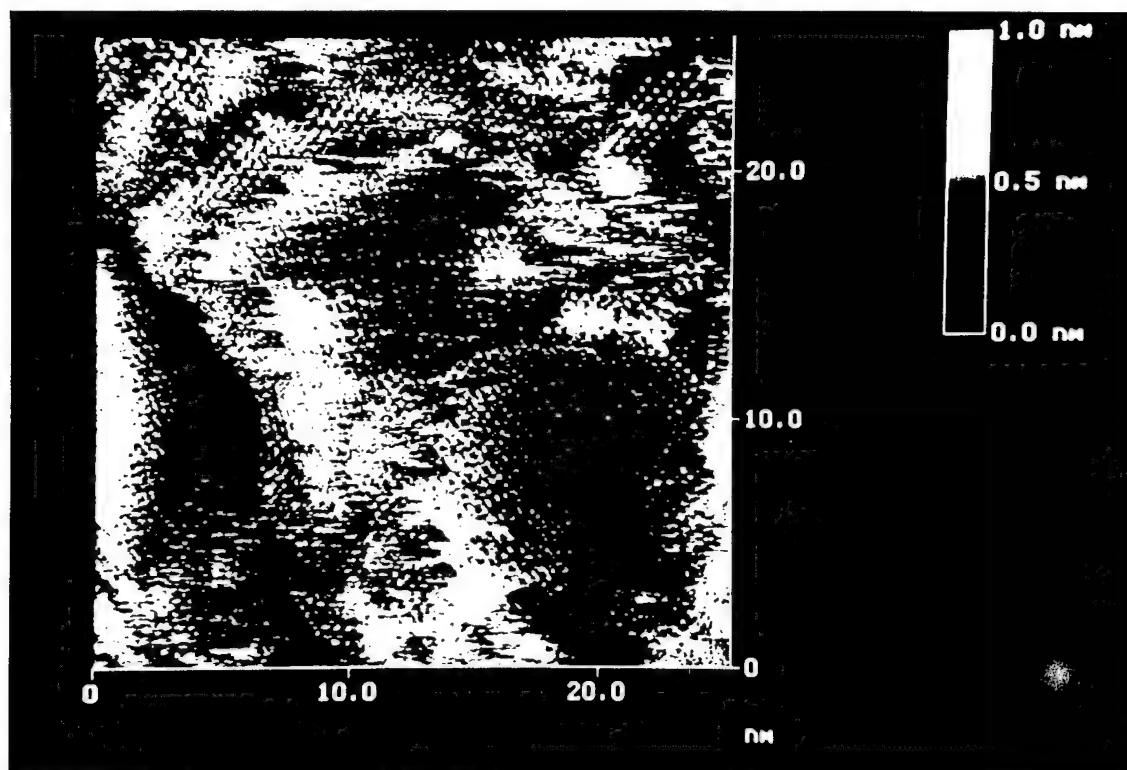


A

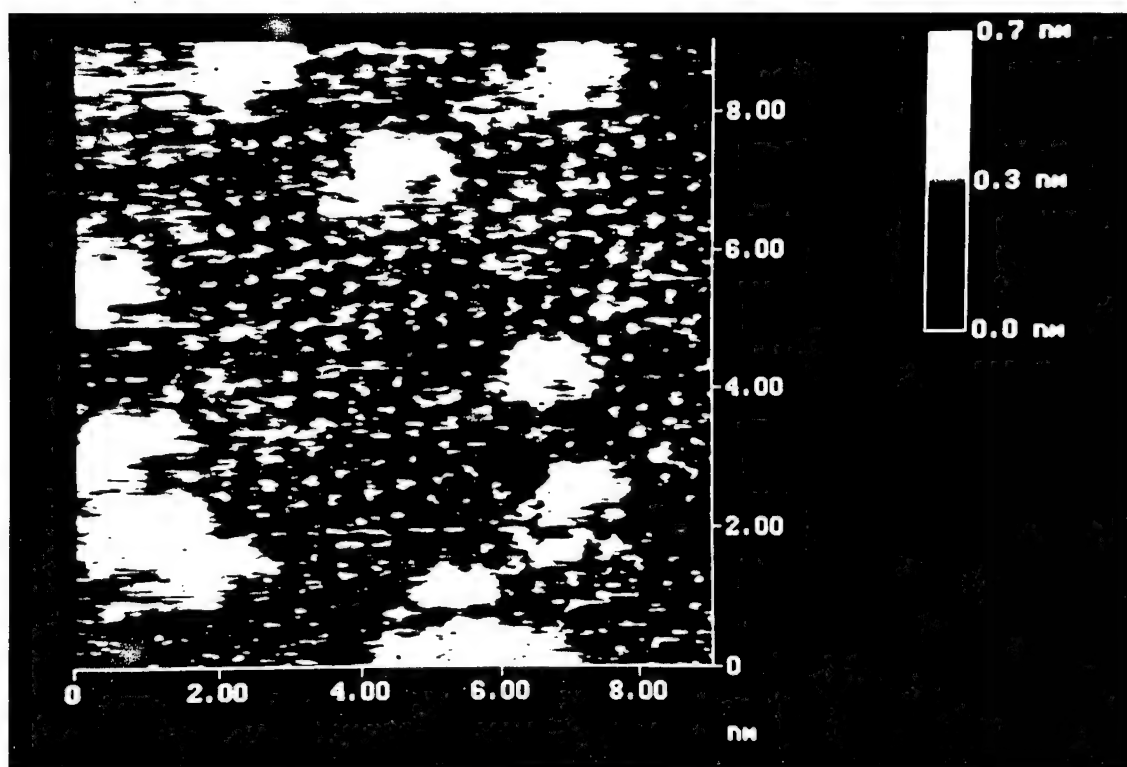
B

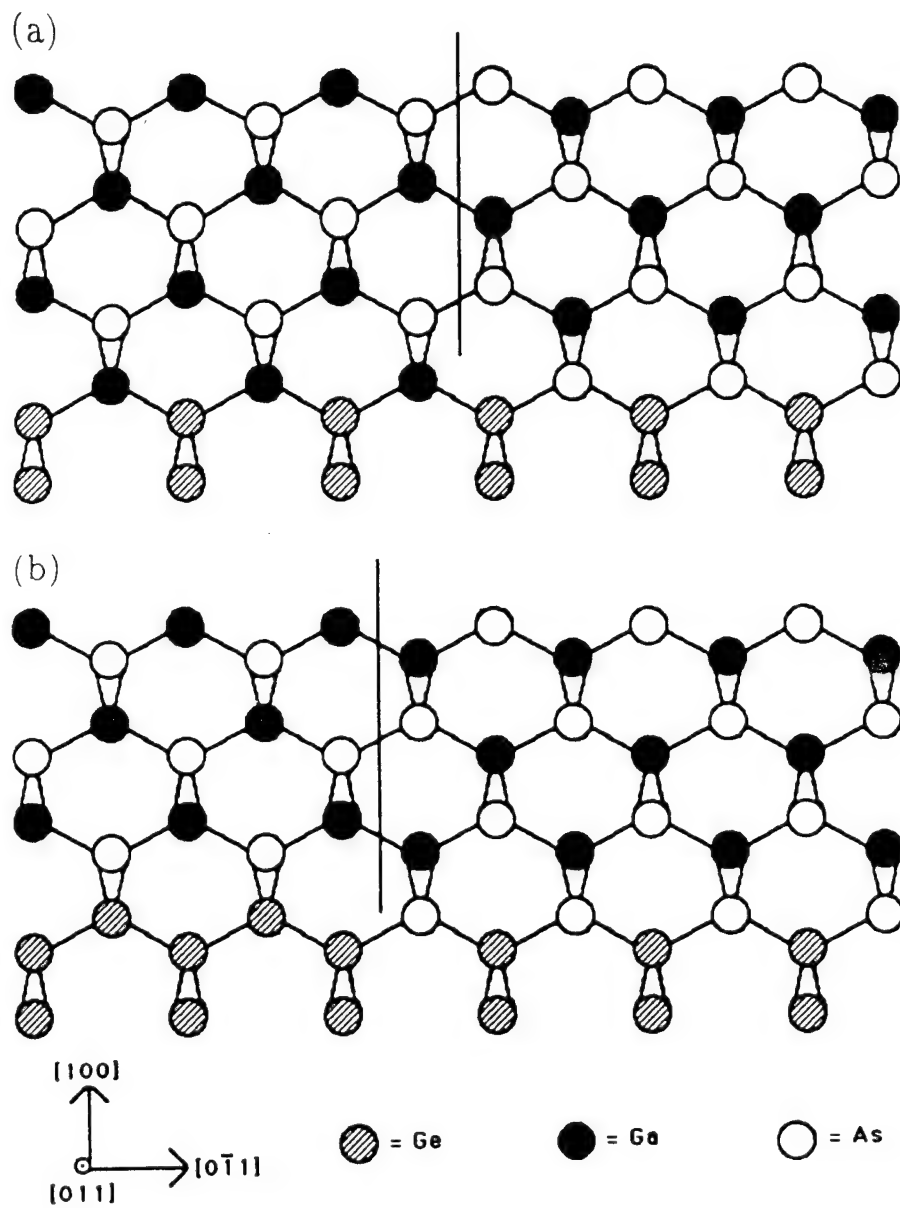


A

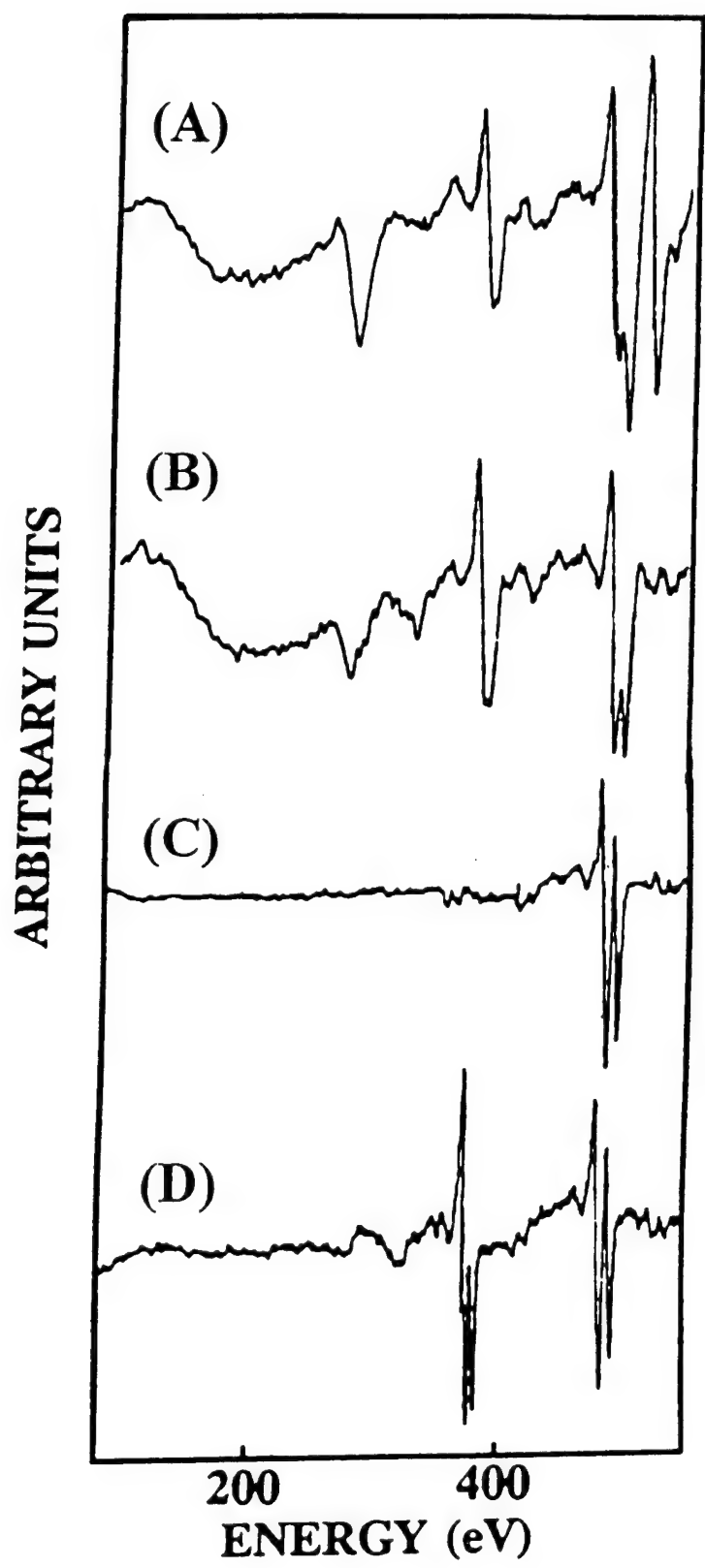


B



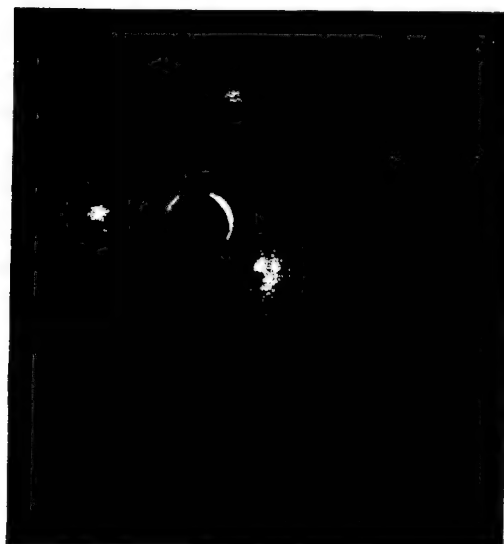


STICKNEY
Figure 66

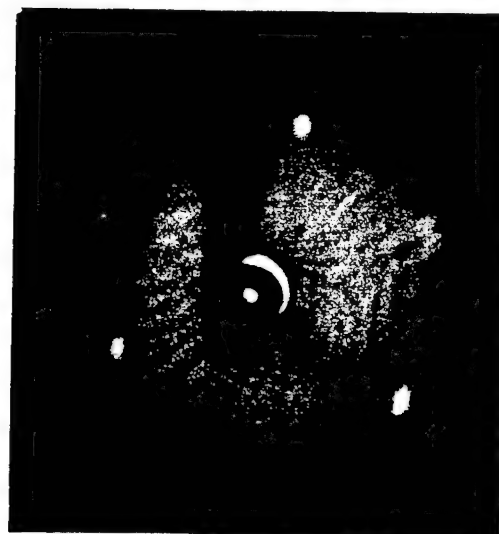


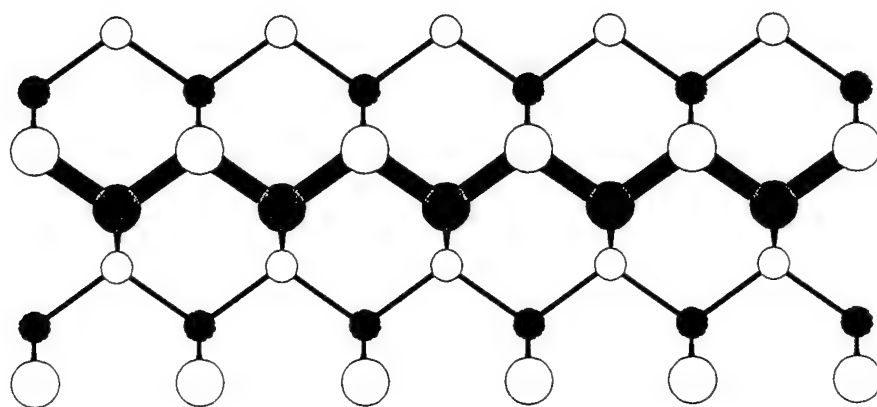
12/20/67
July 67

(A)

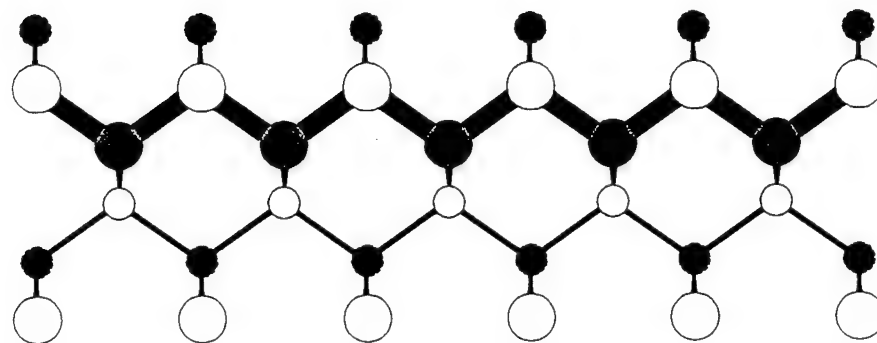


(B)

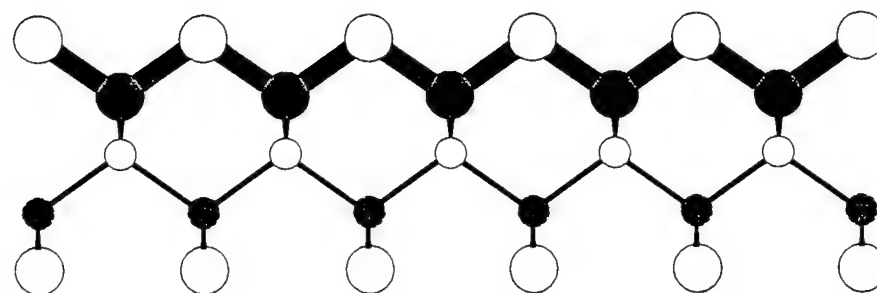
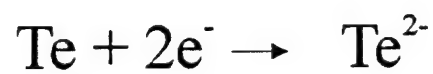




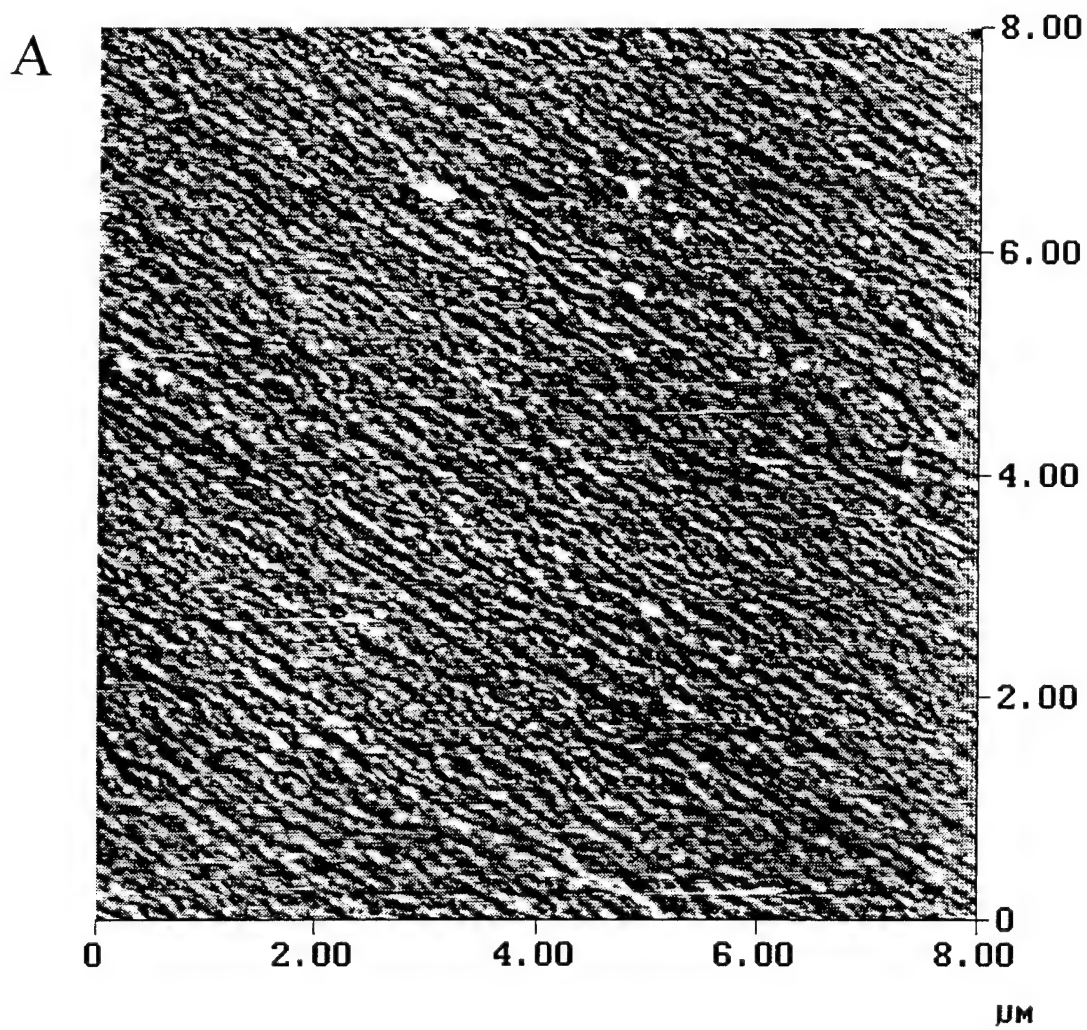
A



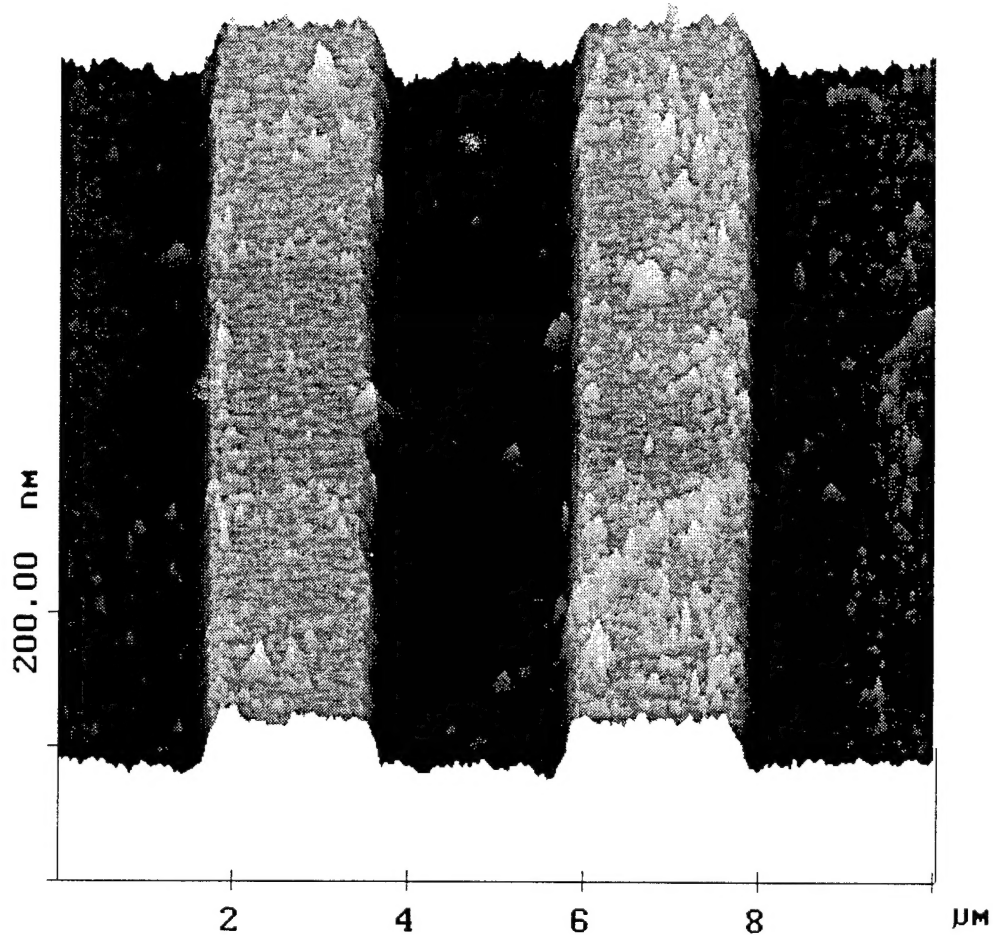
B



C



B



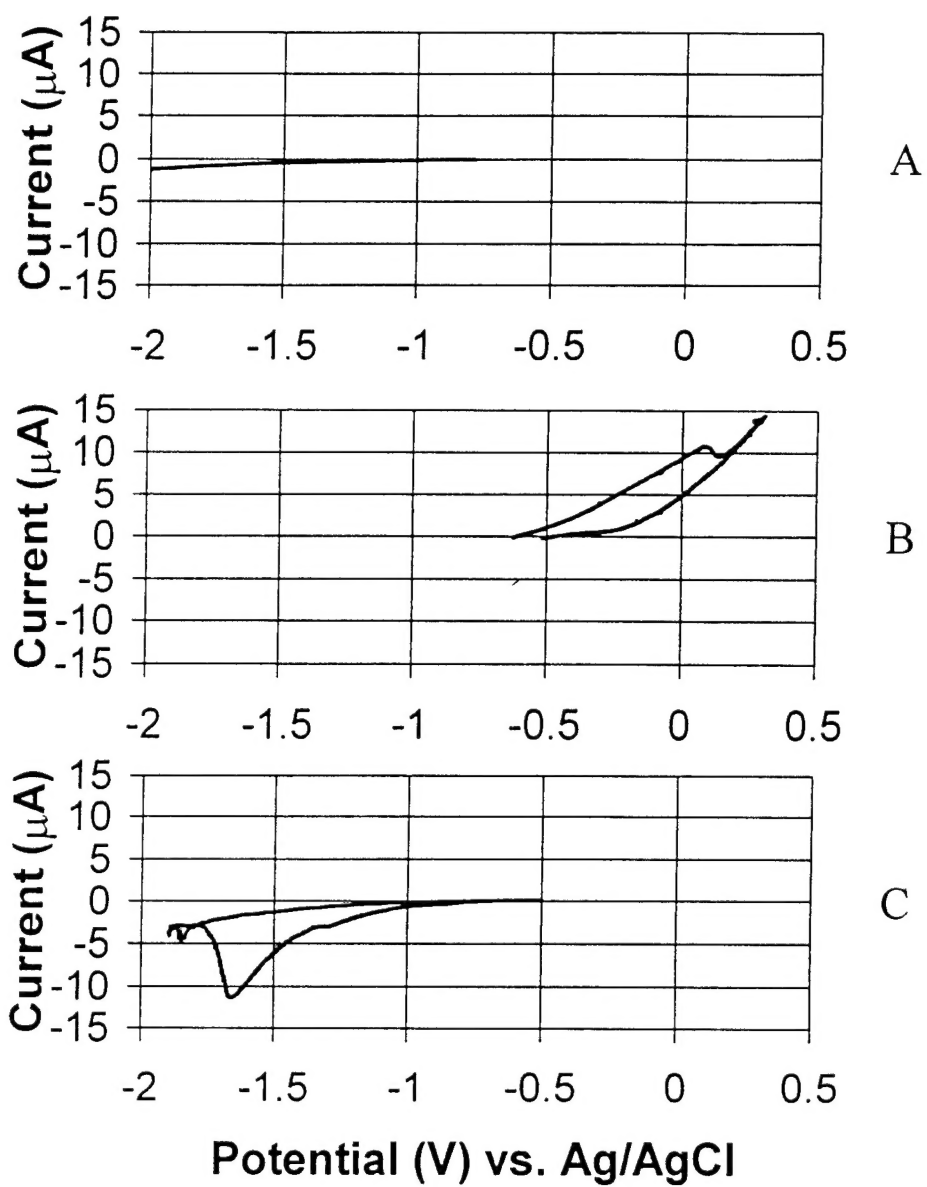


Figure 7/
STICKNEY

